Synthesis and Characterisation of Single-Source Precursors to Metal Chalcogenides and Pnictides

John David Mileham

Supervised by Dr. C. J. Carmalt

Christopher Ingold Laboratories, University College London

This thesis is submitted in partial fulfilment of the requirements for the degree of Doctor of Philosophy (Chemistry)

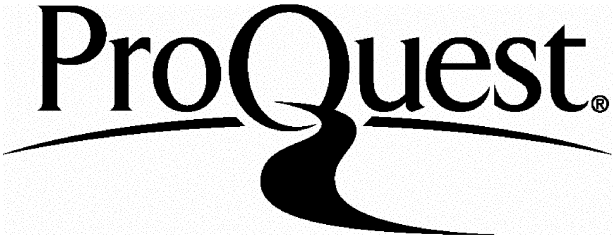

Abstract

This thesis is primarily concerned with the synthesis of group 13 pnictides, group 13 chalcogenides and mixed-metal chalcogenides. The decomposition properties of some of the compounds prepared have also been investigated. **Chapter 1** gives an introduction to techniques used for coating, in particular chemical vapour deposition (CVD). **Chapter 2** is concerned with group 13 pnictides and the synthesis of a number of group 13 silylpnictides are discussed. The properties, preparation procedures and uses of bulk and thin film group 13 pnictides are discussed and the group 13 silylpnictides synthesised so far in the literature. The main synthetic methodologies discussed include dehalosilylation, dealkylsilylation, alkene elimination, salt elimination and adduct formation. The decomposition properties of some of the compounds prepared are investigated by thermal gravimetric analysis and bulk pyrolysis. Vapour-phase deposition studies are carried out in order to test the potential of the group 13 silylpnictides as single-source precursors to the group 13 pnictides. **Chapter 3** discusses the properties, preparation procedures and uses of bulk and thin film aluminium chalcogenides and the aluminium alkoxides and thiolates synthesised so far in the literature. The synthesis of a number of aluminium alkoxides and thiolates is described and the decomposition properties of some of the compounds produced are investigated. Vapour-phase deposition studies are carried out in order to test the potential of the aluminium alkoxides and thiolates as single-source precursors to aluminium oxide and sulfide respectively. **Chapter 4** is concerned with mixed-metal chalcogenides and the synthesis of a number of mixed-metal alkoxide and thiolates is discussed. The decomposition properties of some of these compounds are also investigated.

Index

List of Figures **Page**

Chapter 1

Chapter 2

Chapter 3

Chapter 4

List of Tables **Page**

Chapter 2

Chapter 3

List of Abbreviations

Å	Angstrom
acac	Acetyl acetonate
AES	Auger electron spectroscopy
APCVD	Atmospheric pressure chemical vapour deposition
b.p.	Boiling point
br	Broad
Bu	Butyl
cm	Centimetre
Cp	Cyclopentadiene
Cp*	Pentamethylcyclopentadiene
CVD	Chemical vapour deposition
Cy	Cyclohexyl
δ	Chemical shift (NMR)
d	Doublet
EDXA	Energy dispersive X-ray analysis
Et	Ethyl
eV	Electron volts
g	Gram
h	Hour
^{i}Pr	Isopropyl
IR	Infra-red
LPCVD	Low pressure chemical vapour deposition
m	Multiplet (NMR), medium (IR)
m	Meta
MBE	Molecular beam epitaxy
Me	Methyl
mm	Millimetre
mmol	Millimol
MOCVD	Metal organic chemical vapour deposition
mp	Melting point
nm	Nanometre

NMR	Nuclear magnetic resonance
o	Ortho
OMCVD	Organometallic chemical vapour deposition
OMVPE	Organometallic vapour phase epitaxy
p	Para
Ph	Phenyl
ppm	parts per million
py	Pyridine
q	Quartet
R	Organyl
RBS	Rutherford back scattering
s	Singlet (NMR), strong (IR)
SEM	Scanning electron microscopy
spt	Septet
t	Triplet
^{t}Bu	Tertiary butyl
TGA	Thermal Gravimetric Analysis
thf	Tetrahydrofuran
UV-Vis	Ultra-violet-visable
VPE	Vapour phase epitaxy
vs	Very strong
w	Weak
XPS	X-ray photoelectron spectroscopy
XRD	X-ray diffraction

Acknowledgements

I would like to thank Dr. C. J. Carmalt for her invaluable assistance and advice during the course of my PhD. I would also like to thank Prof. I. P. Parkin for advice on some of the materials work carried out in this study and Dr. Derek Tocher for advice on some of the X-ray crystallography.

I am also very grateful for the assistance of numerous people - Alan Stones, Jill Maxwell, Dave Knapp, Dr. Marianne Odlyha (Birkbeck), Dr. Andrew White (IC), Prof. David Williams (IC), Dr. Derek Tocher and Dr. Jon Steed (KCL) - for making equipment and analysing chemicals.

I would also like to thank all the people who have worked in Lab. 301 for their support and help.

I would like to thank the EPSRC for funding and I would like to acknowledge the support of Epichem Ltd for provision of [$AlH_3(NMe_2Et)$].

Finally, I would like to thank the members of my family for their encouragement, especially my parents and my fiancée, Philippa, without whose support I would not have been able to complete this thesis.

1. Introduction

This thesis is concerned with the synthesis of single-source precursors to technologically important materials. There is considerable interest in preparing thin films of various materials for use in devices. In this chapter, some of the methods which may be used to prepare thin films of materials are discussed. In addition, the use of single-source precursors in chemical vapour deposition (CVD) is described, which is a technique of particular interest for preparing thin films of electronic materials.

There are several routes which may be used to deposit thin films of materials. Solution phase techniques include dip coating, spraying and sol-gel methodology. Increasingly, vapour phase routes are being used to prepare high quality thin films of technologically important materials. A thin film is a solid layer of a material on a surface, usually a few atoms to a few microns in thickness, which has different properties to those of the substrate. The properties of the film are usually significantly different to those of the bulk material.

1.1 Physical vapour deposition

Physical vapour deposition (PVD) is a process which involves laying down a thin solid film by processes such as evaporation, sputtering and sublimation which do not involve gas phase reactions. Molecular beam epitaxy (MBE) is a technique used for forming crystalline films which are lattice matched to the substrate. In MBE, elemental precursors are evaporated and transported by an ultra high vacuum (10^{-10} Torr).[1] This leads to the formation of high purity films as pure elemental sources are used and the ultra high vacuum leads to low concentrations of gases such as O_2. This technique is very precise and single monolayer films may be produced if required. The use of a ultra high vacuum makes the technique very expensive.

1.2 Chemical vapour deposition

Chemical vapour deposition (CVD) is a process which involves depositing a thin solid film from gas phase reactions.[2,3] In general in a CVD reaction, one or more

volatile inorganic or organometallic precursors are transported in the vapour phase, either in a carrier gas or under vacuum, to the reactor chamber. Within the reactor chamber gas phase reactions between the precursor molecules may occur forming intermediate species. These species may be transported to the substrate and adsorption can occur. Surface reactions take place on the heated substrate during which the precursors decompose to form the material of the final film. During decomposition of the precursors volatile byproducts are also formed, which desorb from the substrate and are transported out of the reactor chamber by either the carrier gas or vacuum. The atoms of the film are weakly bound to the substrate, largely through Van der Waals type interactions and are thus free to diffuse. The atoms diffuse across the surface of the film until nucleation occurs by several atoms bonding together, which ultimately leads to growth of the solid film.

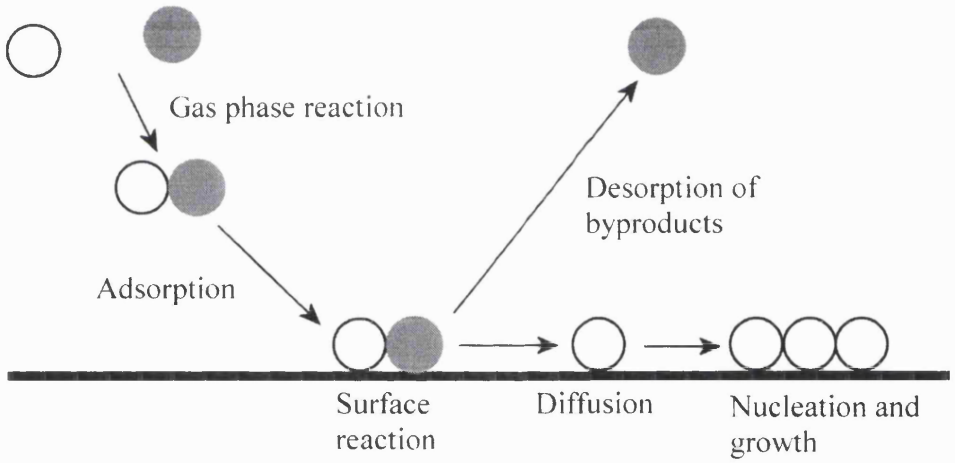

Figure 1.1 Overview of the CVD process

There are various different types of CVD process which are used for laying down thin films. Some of these processes are described below in more detail.

1.2.1 Dual-source chemical vapour deposition

In CVD reactions to form films with simple compositions, for example gallium nitride (GaN), then two precursors are often used (e.g. [Me_3Ga] and NH_3 for GaN). This type of reaction is termed a dual-source reaction and each precursor

contains one of the elements of the final film (i.e. [Me_3Ga] is the gallium source and NH_3 the nitrogen source for GaN).

Dual-source CVD reactions can have a number of problems. It is often hard to control the exact stoichiometry of the final film and films are often inhomogeneous, such that the composition varies over the surface of the film. Usually in a dual-source reaction a large excess of one of the precursors must be present, for example a 1000 fold excess of NH_3 is used in the formation of GaN. These are important factors in the preparation of films for use in electronic devices where small variations in the film are not acceptable. High temperatures are often used in the CVD process, which limits the range of substrates to be deposited on as the substrate must be stable at the temperature used in the reaction. The use of high temperatures also tends to lead to the formation of the thermodynamically stable phase of the material, although other factors, such as the substrate, are also important. Meta-stable phases of materials often have significantly different properties to the thermodynamically stable phase. The precursors used in dual-source CVD are sometimes very reactive, for example [Me_3Ga] is pyrophoric, this leads to problems with handling on a large scale. The precursors may also be toxic, for example NH_3, which also causes problems on a large scale. These problems may be overcome by the use of single-source precursors which is discussed below.

1.2.2 Single-source chemical vapour deposition

Single-source precursors are compounds that contain all the elements of a desired film in one molecule. Often a single-source precursor contains preformed bonds between the elements on the film and sometimes the elements are present in the same stoichiometeric ratio for the final film. This facilitates greater control over the stoichiometry and can lead to films that are very homogeneous. Films with compositions which can not be achieved by conventional dual-source routes can also be prepared.

Single-source precursors often have a number of other advantages over dual-source routes. Single-source precursors are often less reactive and less toxic than conventional precursors which makes handling less of a problem. Lower

temperatures are normally needed for the decomposition of single-source precursors compared to those required in conventional CVD. This leads to a greater range of substrates which may be deposited upon as temperature sensitive substrates may be used. The use of lower substrate temperatures may also lead to the formation of meta-stable phases as opposed to the thermodynamically stable phase which is nearly always formed when high temperatures are used.

If suitable leaving groups are present in a single source precursor then clean decomposition may occur, leading to the formation of films with very low levels of contamination. It is important that the byproducts formed in the CVD process are volatile so that they desorb easily and are transported out of the reactor without decomposition. Important requirements of single-source precursors are that they are volatile and stable in the vapour phase.

1.2.3 Atmospheric pressure chemical vapour deposition

Atmospheric pressure chemical vapour deposition (APCVD) is carried out between atmospheric pressure and 10^{-3} Torr. In this process a carrier gas (for example N_2, Ar) is used to transport the precursors which means that the precursors must be volatile liquids or low melting point solids. The advantages of APCVD are rapid growth rates (2 microns a minute) and the ability to coat large quantities of substrate cheaply as a reactor may be incorporated into a continuous production line.

1.2.4 Low pressure chemical vapour deposition

In low pressure chemical vapour deposition (LPCVD) a partial vacuum (less than 10^{-3} Torr) is used to transport the precursors to the reactor chamber. No carrier gasses are needed although reactive gasses (for example H_2, NH_3) may be added which react with the other precursors. LPCVD apparatus is more expensive that that used in APCVD because a vacuum is used. LPCVD is more time consuming and cannot be used for high volume applications. Less volatile precursors may be used in LPCVD than APCVD as the low pressure used aids volatility.

1.2.5 Metalorganic chemical vapour deposition

Metalorganic chemical vapour deposition (MOCVD), is a dual-source technique that involves the use of a metal source which contains a M-C bond, for example [Me_3Ga]. Organometallic Chemical Vapour Deposition (OMCVD) involves the use of an organometallic compound as a precursor, for example $[Et_2GaNH_2]_3$. Vapour phase epitaxy (VPE) is a CVD process in which an epitaxial film that is crystalline and lattice matched to the substrate is formed. Often VPE processes use either metal organic or organometallic precursors (MOVPE and OMVPE).

1.3 References

1. G. B. Stringfellow, *Rep. Prog. Phys.,* 1982, **45**, 469.
2. M. L. Hitchman & K. F. Jensen, *Chemical Vapour Deposition*, Academic Press, London, 1993.
3. W. S. Rees Jr. Ed, *CVD of Nonmetals,* VCH Publishers, New York, 1996.

2. Group 13 pnictides

2.1 Introduction

Group 13 pnictides (ME where M = Al, Ga, In; E = N, P, As, Sb) exhibit a wide range of electronic and optoelectronic properties.[1] These materials adopt either a cubic (zinc blende) or hexagonal (wurtzite) zinc sulfide structure.[2,3] The thermodynamically stable phase of group 13 nitrides is hexagonal,[4] although they can also adopt a meta-stable cubic structure. Group 13 phosphides and arsenides normally crystallise in a thermodynamically stable cubic phase.[2]

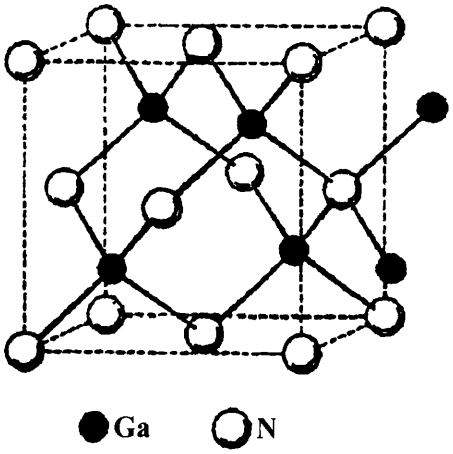

Figure 2.1 The cubic (zinc blende) structure of GaN[3]

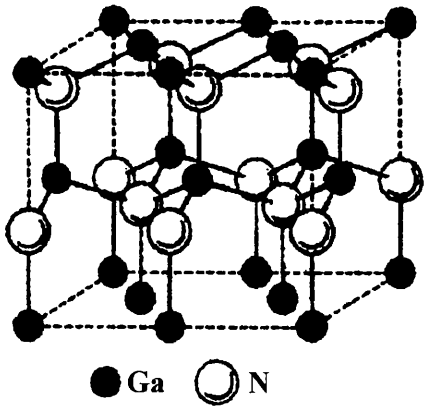

Figure 2.2 The hexagonal (wurtzite) structure of GaN[3]

The cubic (zinc blende) structure, shown for gallium nitride in Figure 2.1, consists of two interpenetrating cubic close packed lattices of, in this case, Ga and N atoms displaced with respect to each other. The atoms are four coordinate, each occupying the tetrahedral sites on the others lattice. The hexagonal (wurtzite) structure, shown for gallium nitride in Figure 2.2, is similar to the cubic structure but consists of two interpenetrating hexagonal close packed layers as opposed to cubic close packed layers.

Group 13 pnictides form a continuous alloy system (InGaE, InAlE and AlGaE where E = N, P, As). In the nitride alloy system the direct band gaps range from 1.9 eV for indium nitride to 6.2 eV for aluminium nitride.[5] These alloy systems are suited to a wide range of applications as the band gap can be tuned to suit the needs of a particular function by altering the stoichiometry of the material.

In this project the synthesis of new single-source precursors to aluminium nitride (AlN), gallium nitride (GaN), indium nitride (InN) and gallium arsenide (GaAs) was attempted and their thermal decomposition properties investigated.

2.1.1 Group 13 nitrides

Group 13 nitrides (AlN, GaN and InN) are well known technologically important materials with a wide range of potential applications. The chemical and physical properties of these materials have been known for a number of years.[6] Their semiconducting properties make them potentially useful for optoelectronic devices in the green, blue and ultraviolet range such as light-emitting diodes or laser diodes.[7] Group 13 nitrides also have various other properties and potential applications, as described below.[8]

Aluminium nitride

Aluminium nitride is of interest because it is a hard and refactory material (hardness between corundum and diamond, melting point 2400 °C), chemically inert and a piezoelectric material with a high acoustic velocity.[9] It also possesses a high intrinsic thermal conductivity[10] and a thermal expansion coefficient similar to that of

silicon and gallium arsenide.[11] Potential uses of AlN include as passive barrier layers, high-frequency acoustic wave devices,[9,12] high temperature windows, protective coatings for high temperature materials[13] and dielectric optical enhancement layers in magneto-optic multilayer structures.[14,15]

Gallium nitride

Interest in GaN is due to its band gap of 3.4 eV,[16] high ballistic electron drift velocity,[16,17] high acoustic velocity,[16,18] and piezoelectric properties.[16,18] Potential applications of GaN include blue,[7] violet-blue,[19] violet and ultra-violet light-emitting diodes,[20] blue semiconductor lasers,[16] photoconductive ultraviolet sensors,[21,22] metal semiconductor field effect transistors,[23] high frequency and microwave power devices[16,17] and acousto-optic applications.[16,18]

Indium nitride

Interest in InN stems mainly from its band gap of 1.9 eV.[24] Potential applications include ohmic contacts in integrated circuits,[25] optoelectronic devices operating in the visible range,[24] low cost solar cells[24] and electrochromic devices.[24]

Nitride Alloys

The continuous alloy system formed by hexagonal group 13 nitrides (InAlN, InGaN, AlGaN) provide excellent materials for band gap engineering. This has lead to extensive use of these materials in electronic applications including violet,[26,27] blue[27,28,29] and blue-green[28] light emitting diodes, heterojunction bipolar transistors,[25] high electron mobility transistors[30] and heterostructure field effect transistors.[31]

2.1.2 Group 13 arsenides

Group 13 arsenides (AlAs, GaAs and InAs) are technologically important materials of particular interest for use in semiconducting applications. Gallium arsenide is used in applications such as infra-red lasers and light emitting diodes.[32]

The continuous alloy system formed by group 13 arsenides (InAlAs, InGaAs, AlGaAs) are excellent materials for band gap engineering.[33] The addition of Al to GaAs leads to the formation of AlGaAs which is used in red or IR light emitting diodes. The alloy $In_{0.53}Ga_{0.47}As$ is lattice matched to indium phosphide (InP) and with a band gap of 0.75 eV is a useful detector for IR applications.

2.1.3 Synthesis of bulk materials by dual-source routes

Group 13 nitrides

Aluminium nitride may be prepared by direct reaction of the elements[34] or by the reaction of aluminium metal with ammonia (NH_3) at high temperatures.[5,35] Gallium nitride may also be prepared by the reaction of gallium metal with NH_3, as summarised in Eq. 2.1.[5,36]

$$2\,Ga + 2\,NH_3 \xrightarrow{600\ ^\circ C} 2\,GaN + 3\,H_2 \quad \textbf{(2.1)}$$

Other gallium sources, for example $[Ga_2O_3]$,[37] $[NH_4]_3[GaF_6]$,[38] gallium halides (e.g. $[GaCl_3]$)[39] and [Ga/Li][40] have been used at temperatures between 900 and 1000 °C. Aerosol-assisted vapour phase synthesis of GaN powder using $[Ga(NO_3)_3]$ and NH_3 at 1000 °C has also been carried out.[41] Preparations using such high temperatures result exclusively in the formation of the thermodynamically stable hexagonal phase of AlN or GaN. To produce the meta-stable cubic phase, lower temperature routes must be used. Although, there has been speculation that the structure of single-source precursors can affect the phase of the material formed. Cubic phase GaN has been prepared at temperatures above 250 °C by the reactions of gallium, gallium iodides or gallium imide-iodides in supercritical ammonia in the presence of NH_4X (where X = Cl, Br, I).[42]

Indium nitride was first prepared using an electrical discharge between indium electrodes through a mixture of liquid NH_3 and liquid nitrogen.[43] Indium nitride is thermally unstable and starts to decompose with loss of N_2 at temperatures below 600 °C, therefore, conventional high temperature synthetic approaches cannot

be used.[3] Indium nitride can be prepared by heating $[NH_4]_3[InF_6]$ in a NH_3 stream.[44] Indium nitride may also be prepared by reducing and nitriding indium oxide, as shown in Eq. 2.2.

$$In_2O_3 + 2\,NH_3 \xrightarrow{630\ ^\circ C} 2\,InN + 3\,H_2O \quad \textbf{(2.2)}$$

Group 13 arsenides

Group 13 arsenides are prepared by direct reaction of the elements at high temperature and in some cases high pressure.

The use of silylpnictides as precursors to arsenides via a dehalosilylation route (i.e. elimination of Me_3SiX) was first demonstrated in 1989.[45] Tris(trimethylsilyl)arsine, $As(SiMe_3)_3$, was reacted with gallium and indium halides to give GaAs and InAs respectively, as shown in Eq. 2.3.

$$[MX_3] + As(SiMe_3)_3 \longrightarrow MAs + 3\,Me_3SiX \quad \textbf{(2.3)}$$

M = Ga, X = Cl or Br; M = In, X = Cl

The metal halide and $As(SiMe_3)_3$ were reacted in solution yielding a coloured solid which was then heated (300 - 500 °C). Gallium arsenide of 96% purity and indium arsenide of 98% purity (by elemental analysis) was produced with low levels of silicon contamination (< 0.7%). It has also been reported that a similar route can be used to prepare AlAs.[46] Recently, InAs of up to 99.96% purity with an average particle size of 90 Å, has been formed from the reaction of $[InCl_3]$ and $As(SiMe_3)_3$.[47] This reaction has since been modified in an attempt to form nanocrystalline GaAs.[48,49] If the reaction between $[GaCl_3]$ and $As(SiMe_3)_3$ was carried out at reflux in quinoline (240 °C) the average particle size was found to be 45 Å × 35 Å (by TEM)[48] and in decane (180 °C) an average particle size of 30 Å was achieved.[49] In addition, GaAs with particles that range in size from 20 to 80 Å has been prepared by the reaction of $[Ga(acac)_3]$ and $As(SiMe_3)_3$ in refluxing triethylene glycol dimethyl ether (216 °C). [50]

2.1.4 Synthesis of bulk materials by single-source routes

The use of single-source precursors for the preparation of group 13 pnictides has two potential advantages. Firstly, materials with the meta-stable cubic structure may be formed. It has been suggested that cubic phase group 13 nitrides have quite different properties to those exhibited by the hexagonal phase.[5] It is thought that the cubic phases of the group 13 nitrides exhibit superior electronic properties and that they may be easier to dope. Secondly, the use of single-source precursors could result in materials with nano-sized particles. The preparation of nanocrystalline group 13 pnictides is of interest because of their unique chemical and electrical properties.[51] It has been observed that the band gap increases with decreasing particle size, this is thought to be due to quantum confinement effects.[52]

Numerous single-source precursors to group 13 pnictides have been investigated over the past 40 years and several comprehensive reviews of this area have been carried out.[1,3-8] In this section, relevant precursors are discussed in detail.

Group 13 nitrides

The preparation of bulk AlN has been reported using the single-source precursors $[Al(NH_2)NH]_x$ (**1**)[8,53] and $[AlH_3\{NMe_3\}_2]$ (**2**).[8,54] Because the pyrolysis of **1** and **2** involved heating the sample at high temperatures in an NH_3 atmosphere it is not clear whether they are true single-source precursors. The single-source precursor $[Cl_2Al\{NH(SiMe_3)\}]_2$ (**3**) is known to yield bulk AlN via the polymeric intermediate $[ClAlNH]_n$ (**4**), as shown in Equations 2.4 and 2.5. [11] In a further study, **3** was isolated and characterised crystallographically.[55] Thermal gravimetric analysis (TGA) of **3** was also carried out and showed weight losses due to the elimination of Me_3SiCl and HCl, which reinforces the proposed reaction pathway.[11]

$$[Cl_2Al\{NH(SiMe_3)\}]_2 \xrightarrow{T > 200\ ^\circ C} [ClAlNH]_n + Me_3SiCl \quad (\mathbf{2.4})$$

$$[ClAlNH]_n \xrightarrow{T > 500\ ^\circ C} AlN + HCl \quad (\mathbf{2.5})$$

Pure hexagonal GaN has been prepared by the thermal decomposition of $[Ga\{N(SiMe_3)_2\}(OSiMe_3)_2(py)]$ (**5**) at temperatures below 350 °C.[56] The first single-source precursor to cubic GaN, namely $[H_2GaNH_2]_3$ (**6**), was prepared by the reaction of $[GaH_3\{NMe_3\}]$ with NH_3.[57] The powder X-ray diffraction patterns of the GaN produced from **6** suggests that the material consists of nanocrystals with a random arrangement of an equal number of cubic and hexagonal planes.[58] This mixed cubic/hexagonal material was found to slowly convert to hexagonal GaN after prolonged heating at 900 °C, with 50% conversion observed after 120 h. Pure cubic GaN could be prepared from **6** by the addition of a small amount of NH_4I, in the presence of NH_3.[59] This process was found to be highly temperature dependent with pure cubic GaN formed between 200 and 350 °C but mixtures of hexagonal and cubic GaN observed over 350 °C. The gallium imide $[Ga(NH_2)_{3/2}]_n$ (**7**), prepared by the reaction of $[Ga(NMe_2)_3]_2$ with NH_3, has been thermally decomposed to form a similar mixed cubic/hexagonal material.[60] A Raman study carried out on materials prepared from **7** confirmed that at high decomposition temperatures the hexagonal phase is dominant.[61] Colloidal GaN quantum dots have also been prepared from **7** by decomposition in trioctylamine at 360 °C and then dispersion of the resulting nanocrystals in a nonpolar solvent.[62] The effect of the precursor route and decomposition temperatures used on the photoluminescence of the GaN produced found that stronger photoluminescence was observed when lower temperatures were used.[63]

Low temperature single-source precursors provide very suitable routes to InN due to the thermal instability of InN at temperatures often used in conventional synthesis. The indium amide $[In(NH_2)_3]$ decomposes at around 200 °C yielding a material which when annealed at 415 °C is identified as crystalline InN.[8] The indium azides, $[R_2InN_3]$ (where R = ^{i}Pr, ^{t}Bu) have been used to prepare crystalline InN in refluxing diisopropylbenzene (b.p. 203 °C).[64] It was found that when H_2NNMe_2 was present in the reaction mixture, polycrystalline InN fibres with diameters around 20 nm and lengths in the range 100 - 1000 nm were produced.

Group 13 arsenides

Relatively few single-source precursors to GaAs powders have been investigated compared with the number used to prepare GaN powders. This is probably due to the success of dual-source routes to nanocrystalline GaAs (see section 2.1.3) which may be altered to produce different particulate sizes and the absence of a meta-stable phase. The first single-source precursor used to form nanocrystalline GaAs powders was the monomeric compound $[(\eta^5\text{-Cp*})_2Ga\{As(SiMe_3)_2\}]$ (**8**).[65] Nanocrystalline GaAs with an estimated average particle size of 60 Å was formed when **8** was reacted with ^{t}BuOH, according to Eq. 2.6.

$$[(\eta^5\text{-Cp*})_2Ga\{As(SiMe_3)_2\}] + 2\,{}^t\text{BuOH} \longrightarrow 2\,\text{GaAs} + 2\,\text{Cp*H} + 2\,{}^t\text{BuOSiMe}_3 \quad (\mathbf{2.6})$$

A polymeric single-source precursor with an As:Cl:Ga ratio of 1:3:2, namely $[AsCl_3Ga_2]_n$ (**9**), decomposes via a novel reaction pathway giving GaAs of 93% purity, according to Eq. 2.7.[66] The decomposition of **9** provides a low temperature route to GaAs with no contamination from group 14 elements which, is important for the preparation of device quality semiconducting materials.

$$1/n\,[AsCl_3Ga_2]_n \xrightarrow{400\ ^\circ\text{C}} \text{GaAs} + GaCl_3 \quad (\mathbf{2.7})$$

Recently the hydride containing complex, $[H_2Ga\{As(SiMe_3)_2\}]_3$ (**10**), has been used to prepare nanocrystalline GaAs with an average particle size of 34 Å, according to Eq. 2.8.[67] Although the thermal instability of the Ga-H bond was expected to enhance the decomposition route shown in Eq 2.8, the final material contained a As:Si ratio of 4.2:1 (by elemental analysis), which was probably due to minor decomposition pathways.[67]

$$[H_2Ga\{As(SiMe_3)_2\}]_3 \xrightarrow[2.\ 450\ ^\circ\text{C}]{1.\ \text{Xylene}/140\ ^\circ\text{C}} 3\,\text{GaAs} + 6\,HSiMe_3 \quad (\mathbf{2.8})$$

2.1.5 Preparation of thin films by dual-source routes

Group 13 nitrides

The CVD of AlN has traditionally been carried out using either an aluminium halide[68,69] or trimethylaluminium[70,71] as the aluminium source and NH_3 as the nitrogen source. High substrate temperatures (typically in excess of 1000 °C) are necessary because of the high thermal stability of NH_3. This leads to a high level of nitrogen vacancies in the deposited film, even when a 2000 fold excess of NH_3 is used. A study into the mechanisms, which lead to nitride growth, found that it occurs by a complex series of reactions.[72] The requirement for very high substrate temperatures seriously limits the choice of substrate. This has led to a need for precursor systems, capable of depositing AlN at lower temperatures, thus increasing the range of substrates that may be coated. One approach is to use different deposition techniques. One of the simplest is photochemical vapour deposition, in which, the gas flow leading into a CVD experiment is irradiated with short wavelength radiation. It has been used to produce thin films of AlN at temperatures between 600 and 950 °C.[73] This technique exploits the reactivity of the photochemically generated radicals allowing lower temperature deposition. Other techniques used to grow AlN films at temperatures between 300 and 700 °C include switched atomic layer epitaxy,[74] electron cyclotron resonance plasma-assisted CVD[75] and reactive sputtering.[12] Another approach is to use a nitrogen source which decomposes at lower temperatures. Hydrazine (N_2H_4) has been used to grow films at temperatures as low as 220 °C, however, its use is limited due to low stability and very high toxicity. Primary amines (e.g. $^tBuNH_2$ and $^iPrNH_2$),[76,77] as well as azides (e.g. Me_3SiN_3),[78] have also been used to prepare thin films of AlN at substrate temperatures between 400 and 600 °C and lower ratios of N:Al. However, the films produced contained high levels of carbon impurity (up to 11%). Molecular beam epitaxy (MBE) and organometallic vapour phase epitaxy (OMVPE) have also been used to prepare thin films of group 13 nitrides and have been reviewed recently.[79]

Like AlN, thin films of GaN have traditionally been prepared by the reaction of either gallium halides[80] or trimethylgallium[5,81] and NH_3 and therefore the same problems of high substrate temperatures (although the temperatures involved are not

as high as for AlN) and large N:Ga ratios are encountered.[82] Lower temperature routes which involve the use of gallium halides and NH_3 have also been investigated.[83] The largest barrier to producing device quality films of GaN is the large lattice mismatch between GaN and the substrates. Films grown on poorly lattice matched substrates are generally polycrystalline island-like with poor morphology and are often cracked due to thermal strain.[3] To overcome the problem of lattice mismatching, buffer layers (such as AlN, SiC)[84] are commonly used. This improves the films crystallinity, morphology, electrical and optical properties. As with AlN films alternative techniques such as electron cyclotron resonance microwave plasma-assisted molecular beam epitaxy[18] and radio frequency reactive sputtering have been used.[85] Alternative gallium[86] and nitrogen sources,[87] have also been used to prepare GaN films at lower temperatures, although, not with as much success as for AlN films.[72]

Growth of high quality InN films is more difficult because of the low decomposition temperature of InN. To overcome this limitation, low substrate temperatures (< 600 °C) and various growth techniques including radio frequency reactive sputtering,[88] microwave-excited MOCVD,[89] laser-assisted CVD[90] and MBE.[91] Thin films of InN have been grown by the use of [$InCl_3$] and NH_3 at substrate temperatures of between 500 and 700 °C.[92]

Group 13 arsenides

Traditionally, GaAs films are prepared by a dual-source CVD reaction involving [Me_3Ga] and AsH_3 with a substrate temperature of 700 °C.[93,94] However, the toxic and pyrophoric nature of the precursors makes them difficult to purify and handle. Carbon contamination in the films deposited can also be a problem. Alternative arsenic sources, including $^tBuAsH_2$ and Et_2AsH, have also been used in CVD processes with [R_3Ga] (where R = Me, Et).[95] It has also been reported that atmospheric pressure CVD of either [$GaCl_3$] or [Me_3Ga] with $As(SiMe_3)_3$ gave thin films of GaAs.[96] Small amounts of oxygen and carbon contamination were reported to have been found in the film, but silicon and chlorine were not detected. Thin films of GaAs may also be prepared by vapour phase epitaxy (VPE)[97] using [Me_3Ga] as the gallium source and AsH_3 as the arsenic source.[98] Alternative arsenic sources,

such as $^{t}BuAsH_2$ have also been used in VPE successfully, with no increase in carbon contamination.[99]

2.1.6 Preparation of thin films by single-source routes

Single-source precursors to group 13 pnictides provide an alternative to the use of high temperatures and toxic precursors, which characterise the dual-source routes. They provide cleaner, safer, lower temperature routes with several additional advantages including greater control over stoichiometry. Several comprehensive reviews have been published[1] and a few examples of precursors described previously are given below.

Group 13 nitrides

The first single-source precursor used to deposit a film of AlN was the aluminium trichloride ammonia complex, $[Cl_3Al(NH_3)_3]$ (**11**), which is formed by the reaction of $[AlCl_3]$ and excess NH_3.[100] Deposition occurred on silicon substrates in the same temperature range as the conventional dual-source route. The single-source method, however, removes the need for large over pressures of NH_3. The aluminium complexes $[HAl(NR_2)_2]_2$ and $[Al(NR_2)_3]_2$ (where R = Me, Et) deposit films of composition $AlC_{1.2}N_{0.4\text{-}0.6}O_{0.06\text{-}0.2}$ at substrate temperatures 300 - 500 °C, which when annealed at 1300 °C form impure AlN.[101] The dialkylaluminium amides $[R_2Al(NH_2)]_3$ (where R = Me (**12**), Et (**13**), ^{i}Bu (**14**) and ^{t}Bu (**15**)) were prepared using the route shown in Eq. 2.9.[102]

$$[Me_3Al] + NH_3 \xrightarrow{RT} [Me_3Al(NH_3)] \xrightarrow{>55\ ^{\circ}C} 1/3\ [Me_2Al(NH_2)]_3 + CH_4 \quad \textbf{(2.9)}$$

The most promising of these compounds is **12** which forms thin films of AlN, with 4 - 5% oxygen impurities, at 400 - 800 °C. A related compound which has been used as a single-source precursor is the adduct $[Me_3Al(NH_3)]$ (**16**), prepared by the reaction of $[Me_3Al]$ and NH_3.[103] Films of AlN prepared from **16** contain 1.5 - 8.9% oxygen and 0.6 - 4.8% carbon impurities, which was explained as being due to dissociation of the adduct.

The first reported single-source precursor to films of GaN was the complex $[Br_3Ga(NH_3)_4]$ (**17**) which was formed by the reaction of molten $[GaBr_3]$ and ammonia.[104] Deposition occurs at substrate temperatures 600 - 750 °C in either an NH_3, Ar or N_2 atmosphere. The single-source precursor, $[Et_2Ga(NH_2)]_3$ (**18**), formed by the reaction of $[Et_3Ga]$ and NH_3, has been used to deposit highly crystalline films of GaN at temperatures above 650 °C.[105] The gallium azide $[Et_2Ga(N_3)]_3$ (**19**) resulted in polycrystalline films of GaN.[106] The optimum substrate temperature was found to be 350 °C, however, films deposited at this temperature contained significant amounts of hydrogen and so had to be annealed at 600 °C. Higher substrate temperatures resulted in greater carbon incorporation and lower temperatures greater oxygen contamination. Recently, the monomeric gallium azide, $[Et_2Ga(N_3)(MeHNNH_2)]$ (**20**), has been prepared.[107] Films of GaN were deposited from **20** at substrate temperatures between 400 - 600 °C and contained less than 0.1% oxygen and carbon (by XPS). The *bis* azide, $[(N_3)_2Ga\{(CH_2)_3NMe_2\}]$ (**21**),[108,109] has also been used as a single-source precursor to films of GaN at substrate temperatures above 500 °C. Low levels of carbon were observed in the films but these could be removed by the addition of very small amounts of NH_3 into the CVD experiment.

Although single-source precursors present a very suitable route to InN at low temperatures, few examples have been reported. The indium azide $[(N_3)In\{(CH_2)_3NMe_2\}_2]$ (**22**)[110] has been prepared and used to deposit thin films of InN at substrate temperatures 350 - 450 °C with no carbon or oxygen contamination detected (by XPS). Indium nitride whiskers could also be grown from **22** by CVD.[111] The only other compound which has been used successfully as a single-source precursor to films of InN is the azide $[Me_2In(\mu\text{-}N_3)]_2$ (**23**).[112] In the CVD of **23**, substrate temperatures 350 - 450 °C were used and films with high levels of carbon and oxygen (*ca.* 11 and 8% respectively by XPS) were obtained.

Gallium arsenide

The first compounds to be proposed as suitable single-source precursors to GaAs were the Lewis acid-base adducts $[(Cl)R_2Ga(AsR'_3)]$ where (R and R' = Me (**24**), Et (**25**)).[113] As predicted, growth of GaAs films from **24** and **25** was achieved.[114,115] The complexes $[(C_6F_5)Me_2Ga(AsEt_3)]$ (**26**) and $[\{(Cl)Et_2GaAsEt_2\}_2CH_2]$ (**27**) have been used as precursors to GaAs in the temperature range 600 - 700 °C and 500 - 625 °C respectively.[116] The effect of varying the substrate temperature on the composition of GaAs films deposited from $[Cl(Me)_2Ga(AsEt_3)]$ (**28**) has been investigated by Auger electron spectroscopy (AES).[117] Precursors of the type $[R_2Ga\{As(^tBu)_2\}]_2$ (where R = Me (**29**)[118] or Et (**30**)[119]) were investigated, but the resulting GaAs films were found to be arsenic deficient. The tris-arsenide $[Ga\{As(^tBu)_2\}_3]$ (**31**) was prepared and found to deposit films of GaAs at a substrate temperature of 480 °C. The resulting GaAs film contained very low levels of carbon contamination which was explained as being due to the absence of direct Ga-C bonds.[120]

A number of precursors to group 13 pnictides have been isolated which incorporate labile silyl leaving groups. Sections 2.1.7 and 2.1.8 describe the range of group 13 silylamines and silylarsenides isolated to date.

2.1.7 Group 13 silylamides

Tris(trimethylsilyl)amine, $N(SiMe_3)_3$ is less reactive than the corresonding silylarsine, $As(SiMe_3)_3$. However, silylamines, of the type $HN(SiR_3)_2$ and $H_2N(SiR_3)$, are stable and have been used in the formation of group 13 silylamides.[121] In the reaction between a metal trihalide $[MX_3]$ and $HN(SiR_3)_2$, two different reactions may occur. The M-X bond may react with the N-H bond leading to the formation of a M-N bond with loss of hydrogen halide, as shown in Eq. 2.10.

$$[MX_3] + HN(SiR_3)_2 \longrightarrow [X_2M\{N(SiR_3)_2\}]_n + HX \quad \textbf{(2.10)}$$

Alternatively, a M-X bond may react with a N-Si bond leading to the formation of a M-N bond with the loss of silyl halide, as shown in Eq. 2.11.

$$[MX_3] + HN(SiR_3)_2 \longrightarrow [X_2M\{NH(SiR_3)\}]_n + R_3SiX \quad \textbf{(2.11)}$$

A similar complication arises in the reaction of silyamines, of the type $HN(SiR_3)_2$, with trialkyl metal. In most cases reactions proceed via a dehalosilylation or dealkylsilylation pathway similar to that shown in Eq. 2.10. The situation is even more complex if alkyl metal halides, of the type $[R_2MX]$ or $[RMX_2]$, are used as a number of products are possible and mixtures may result. If a product which contains two silyl groups attached to the nitrogen is desired then a silylamine, of the type $[M'N(SiMe_3)_2]$ (where M' = Na, Li) is often used, as shown in Eq. 2.12.

$$[MX_3] + [M'N(SiR_3)_2] \longrightarrow [X_2M\{N(SiR_3)_2\}]_n + M'X \quad \textbf{(2.12)}$$

The reaction between $[AlCl_3]$ and $HN(SiMe_3)_2$ has been reported to yield AlN via the intermediates $[Cl_2Al\{NH(SiMe_3)\}]_2$ (**3**) and $[ClAlNH]_n$ (**4**) as discussed in Section 2.1.4.[11] The reaction of $[MX_3]$ and $HN(SiMe_3)_2$ in solution is known to yield the dimeric species $[X_2M\{NH(SiMe_3)\}]_2$ (where M = Al, X = Cl (**3**);[55] M = Ga, X = Cl (**32**)[122] or Br (**33**)).[123] It has been found that **3** is a single-source precursor to AlN. In contrast, no detailed investigation has been reported on the use of **32** as a precursor to GaN. The related complex $[Cl_2Ga\{NMe(SiMe_3)\}]_2$ (**34**) has been prepared by the reaction of $[GaCl_3]$ and $MeN(SiMe_3)_2$. The crystal structure of **32** (Figure 2.3) demonstrated that this compound exists as an amido-bridged dimer with a planar Ga_2N_2 ring at its core. The *trans* isomer was isolated in the solid state but both the *cis* isomer and a trimeric species were reported as being observed in the ^1H NMR. The crystal structures of **3**, **33** and **34** have also been determined and were found to be similar to **32** although the larger size of the bromine atoms prevents formation of the trimeric species in solution.

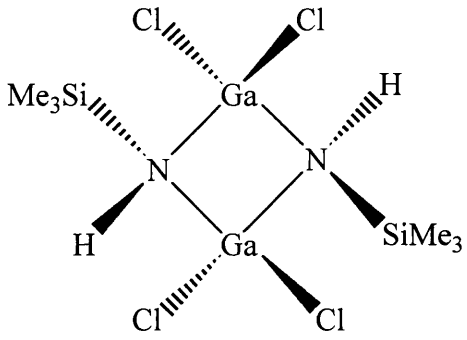

Figure 2.3 Structure of $[Cl_2Ga\{NH(SiMe_3)\}]_2$ (32)

Recently, the monomeric complex $[Cl_2Ga\{NH(SiMe_3)\}(thf)]$ (**35**)[124] has been isolated from a mixture of **32** and $[ZnMe_2]$ (Figure 2.4). It could be assumed that **35** would have a higher volatility than **32** due to its monomeric nature and so may be a more suitable precursor for CVD. However, the presence of a thf moiety in the structure could lead to the inclusion of carbon and oxygen contamination in the GaN films deposited.

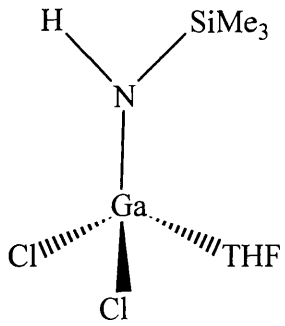

Figure 2.4 Structure of $[Cl_2Ga\{NH(SiMe_3)\}(thf)]$ (35)

The tetrameric complex, $[MeGa(NSiMe_3)]_4$ (**36**), which possesses a cubic Ga_4N_4 core, has been isolated from the reaction of **34** with [MeLi].[125] Interestingly, the corresponding reaction of **33** with [MeLi] resulted in the formation of $[Cl(Me)Ga\{NH(SiMe_3)\}]_2$. The aluminium imido complex $[^tBuAl(NSiMe_3)(thf)]_2$ (**37**) has been obtained by the reaction of $[Li_2N_2(SiMe_3)_2]$ and $[^tBuAlCl_2]$.[126] Removal of the thf molecule from **37** gives $[^tBuAl(NSiMe_3)]_4$, which does not adopt a similar heterocubane structure to **36** but instead consists of three Al_2N_2 rings in a

ladder structure. The dimeric imido complex $[Mes^*Al(NSiPh_3)]_2$ has also been prepared.[127]

If the reaction of $[MCl_3]$ and $HN(SiMe_3)_2$ is carried out at low temperature (-30 °C) in dichloromethane then the adducts $[Cl_3M\{NH(SiMe_3)_2\}]$ (where M = Al (**38**), Ga (**39**)) are formed.[128] It was reported that **38** and **39** decompose in solution at 60 °C with loss of Me_3SiCl to form **3** and **32** respectively. More recently, the reaction of $[AlCl_3]$ and $HN(SiMe_3)_2$ has been carried out in hexane at room temperature and a structural investigation was carried out.[129] It was found that compound **38** adopted the monomeric structure shown in Figure 2.5. The indium adducts, $[Br_3In\{NH(SiMe_3)_2\}]$ (**40**) and $[Br_3In\{NH_2(SiMe_3)\}]$ (**41**) are formed in a 1:3 ratio by heating a solution of $[InBr_3]$ in $HN(SiMe_3)_2$.[130] The crystal structure of **41** was found to be similar to the structure of **38**.

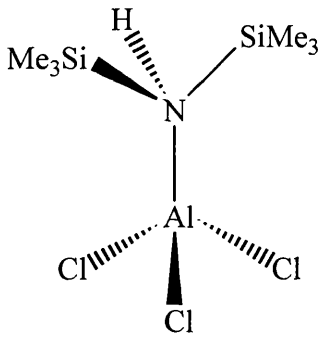

Figure 2.5 Structure of $[Cl_3Al\{NH(SiMe_3)_2\}]$ (38)

The reaction of $[GaCl_3]$ and $[LiN(SiMe_3)_2]$ in hexane has been reported to yield $[Cl_2Ga\{N(SiMe_3)_2\}]_n$ (**42**) although this species was not isolated and analysed.[131] Compound **42** was reacted *in situ* with two equivalents of $[LiOSiMe_3]$ in the presence of pyridine to form $[Ga\{N(SiMe_3)_2\}(Me_3SiO)_2(py)]$ (**43**), which has been used as a single-source precursor to GaN. The reaction of $[InX_3]$ and $[LiN(SiMe_3)_2]$ in either a 1:1 or 1:2 ratio results in the formation of $[X(Me)In\{N(SiMe_3)_2\}]_n$ (where X = Cl (**44**) or Br (**45**)) due to a methyl group transfer from a silyl group to the indium centre.[132] In contrast, the reaction of $[GaCl_3]$ with two equivalents of $[LiN(SiMe_3)_2]$ led to the formation of the expected species $[ClGa\{N(SiMe_3)_2\}_2]$ (**46**).[133] A structural investigation was carried out on **46** which

was found to consist of monomers with a distorted trigonal planar geometry around the gallium centre. The reaction of $[MCl_3]$ with three equivalents of $[LiN(SiMe_3)_2]$ has been found to afford the monomeric species $[M\{N(SiMe_3)_2\}_3]$ (where M = Al (**47**), Ga (**48**) and In (**49**)).[134] Structural studies show that **48**[133] and **49**[135] are similar consisting of a MN_3 trigonal planar skeleton with the silylamide groups arranged in a propeller like fashion around the central metal. The related gallium complex $[Ga\{N(^tBu)SiMe_3\}_3]$ (**50**) has also been prepared by a similar salt elimination reaction.[136] The indium complexes $[In\{NRR'\}_3]$ (where R = ^{t}Bu, R' = $SiMe_3$ (**51**) or $SiMe_2H$ (**52**); R = Ph, R' = $SiMe_3$ (**53**)) have been prepared by salt elimination reactions.[137]

Complexes of the type $[R_2M\{NH(SiR')\}]_2$ (where M = Al, R = Me, R' = Ph_3 (**54**), Et_3 (**55**); R = ^{i}Bu, R' = Ph_3 (**56**), $^tBu_2H$ (**57**);[138] and M = Ga, R = Me, R' = Et_3 (**58**); R = Et, R' = Et_3 (**59**)[139]) have been prepared by the reaction of $[R_3M]$ and $R'SiH_2$ in a 1:1 ratio. These complexes are dimeric with the silyl groups *trans*, as shown in Figure 2.6.

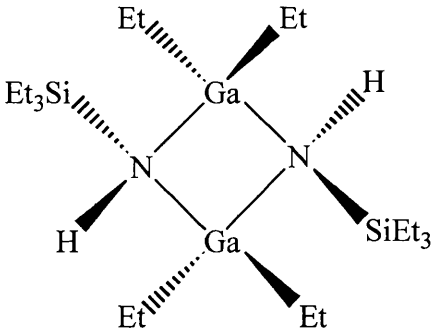

Figure 2.6 Structure of $[Et_2Ga\{NH(SiEt_3)\}]_2$ (59)

The dialkylindium silylamide, $[Me_2In\{N(Me)SiMe_3\}]_2$ (**60**), has been prepared and crystallises with a *trans* structure similar to **54** - **59**.[140] Complexes, of the type $[R_2In\{N(SiMe_3)_2\}]$ (where R = Me (**61**)[141] and Et (**62**)[142]), were prepared by salt elimination routes, as summarised in Eq. 2.13. Structural studies carried out on **61** revealed it has a dimeric structure (Figure 2.7).

$$[R_2InCl] + [LiN(SiMe_3)_2] \xrightarrow[R = Me, Et]{} [R_2In\{N(SiMe_3)_2\}] + LiCl \quad \textbf{(2.13)}$$

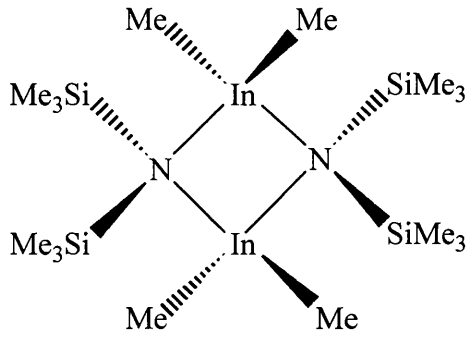

Figure 2.7 Structure of $[Me_2In\{N(SiMe_3)_2\}]_2$ (61)

The dimethylaluminium silylamide $[Me_2Al\{N(SiMe_2H)_2\}]_2$ (**63**) has been prepared by reaction of $[Me_3Al]$ with $HN(SiMe_2H)_2$.[143] Compound **63** possesses a similar dimeric structure to **61** (Figure 2.7). The related complex $[Me_2Al\{NH(SiMe_3)\}]_2$ (**64**) has been prepared by the reaction of $[Me_2AlCl]$ and an excess of $HN(SiMe_3)_2$.[144] The reaction of $[MeAlCl_2]$ and $HN(SiMe_3)_2$ was found to yield $[Cl(Me)Al\{NH(SiMe_3)\}]_2$ (**65**).[144] Both **64** and **65** were found to have the expected dimeric structure. The monomeric complex $[Me_2Al\{N(Si^tBu_2Me)(Si^tBu_2Ph)\}]$ has been prepared by the reaction of $[Me_3Al]$ and $N(Si^tBu_2)(Si^tBu_2Ph)$ via a methyl group transfer from the aluminium to a silicon, as shown in scheme 2.1.

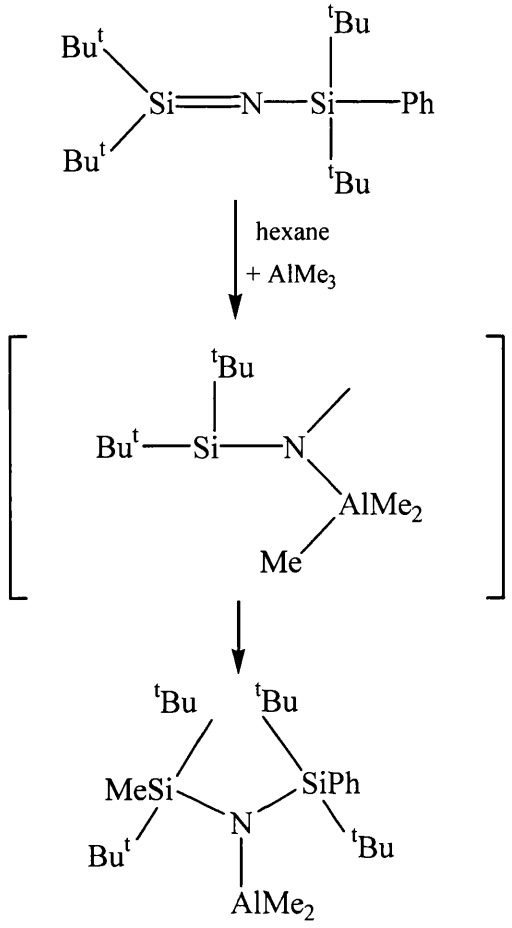

Scheme 2.1

2.1.8 Group 13 silylarsenides

Two gallium silylarsenides have been used as precursors to GaAs. The complex $[(\eta^5\text{-Cp*})_2Ga\{As(SiMe_3)_2\}]$, formed by the reaction of $[(\eta^5\text{-Cp*})_2GaCl]_2$ and $[LiAs(SiMe_3)_2]$, summarised in Eq. 2.14, has been chemically converted into GaAs by reaction with ^{t}BuOH (as described in 2.1.4).[65]

$$[(\eta^5\text{-Cp*})_2GaCl]_2 + 2\ As(SiMe_3)_3 \longrightarrow 2\ [(\eta^5\text{-Cp*})_2Ga\{As(SiMe_3)_2\}] + 2\ Me_3SiCl \quad \textbf{(2.14)}$$

The trimeric species $[H_2Ga\{As(SiMe_3)_2\}]_3$, which was prepared by the reaction of $[H_3Ga(NMe_3)]$ and $As(SiMe_3)_3$ (see Eq. 2.15), has been used to prepared nanocrystalline GaAs.[67]

$$[H_3Ga(NMe_3)] + As(SiMe_3)_3 \longrightarrow 1/3\,[H_2Ga\{As(SiMe_3)_2\}]_3 + Me_3SiH + NMe_3 \quad \textbf{(2.15)}$$

A range of group 13 silylarsenides have also been prepared, some of which have been used as single-source precursors to metal arsenides. The aluminium silylarsenides $[Me_2Al\{As(SiMe_3)_2\}]_3$ (**66**)[145] and $[Et_2Al\{As(SiMe_3)_2\}]_2$ (**67**),[146] have been synthesised and structurally characterised. Monomeric species have been formed from the reaction of either **66** or **67** with equimolar amounts of 4-(dimethylamino)-pyridine (dmap) to form $[R_2Al\{As(SiMe_3)_2\}\{dmap\}]$ (**68**).[147] Although $[R_3M]$ (where R = Me, Et) reacts directly with $As(SiMe_3)_3$ to give GaAs, complexes of the type $[R_2Ga\{As(SiMe_3)_2\}]_2$ (where R = ^{t}Bu (**69**), [148] Ph (**70**),[149] CH_2CMe_3 (**71**),[150] CH_2SiMe_3 (**72**),[151]) have been prepared by a salt elimination route, shown in Eq. 2.16.

$$[R_2GaCl] + [LiAs(SiMe_3)_2] \longrightarrow 1/2\,[R_2Ga\{As(SiMe_3)_2\}]_2 + LiCl \quad \textbf{(2.16)}$$

The corresponding indium complexes $[R_2In\{As(SiMe_3)_2\}]_2$ (where R = Ph (**73**),[152] CH_2CMe_3 (**74**)[153] and CH_2SiMe_3 (**75**)[154]) have also been prepared by similar routes. The mixed bridged monomeric species $[R_2Ga\{As(SiMe_3)_2\}Ga(R)_2X]$ (X = Cl, R = ^{t}Bu (**76**),[148] Ph (**77**),[155] CH_2CMe_3 (**78**),[150] CH_2SiMe_3 (**79**);[151] X = Br, R = Ph (**80**)) have been synthesised and structurally characterised. Complexes of the type $[R_2In\{As(SiMe_3)_2\}In(R)_2Cl]$ (where R = CH_2CMe_3 (**81**)[153] and R = CH_2SiMe_3 (**82**)[154]) have also been isolated. It is not thought that mixed bridged complexes of this type would be suitable as single-source precursors due to the non-stochiometric ratio of M:As.

2.2 Results and discussion

2.2.1 Synthetic strategies for group 13 pnictides

Five main synthetic methodologies were attempted in order to prepare group 13 silylamides, as described below.

(1) Dehalosilylation (i.e. elimination of R_3SiX) by direct reaction of a silylamine or silylarsine and a group 13 metal halide (e.g. $[GaCl_3]$). The driving force for this reaction is the formation of the trialkylsilyl halide. As discussed in 2.1.7, a number of products may form when *bis* silylamines are used in a reaction as either the silyl group or the hydrogen atom could be involved in the reaction.

(2) Dealkylsilyation (i.e. elimination of R_4Si) by direct reaction of a silylamine and an alkyl group 13 complex (e.g. $[Me_2GaCl]$ or $[Et_3Ga]$). A tris silylamine (e.g. $N(SiMe_3)_3$) may be used, as shown in Eq. 2.17. The driving force for these reactions is formation of the tetraalkylsilane.

$$[R'_3M] + N(SiR_3)_3 \longrightarrow 1/n\,[R_2MN(SiR_3)_2]_n + Me_3SiR' \quad \textbf{(2.17)}$$

(3) Elimination of an alkane by direct reaction of a *bis* silylamine (e.g. $HN(SiMe_3)_2$) and a alkyl group 13 complex (e.g. $[Et_3Al]$), as shown in Eq. 2.18.

$$[R'_3M] + HN(SiR_3)_2 \longrightarrow 1/n\,[R'_2MN(SiR_3)_2]_n + R'H \quad \textbf{(2.18)}$$

(4) Salt metathesis using alkali metal salts of the silylamine (e.g. $[LiN(SiMe_3)_2]$) and the metal halide, as shown in Eq. 2.19. The driving force for this reaction is the high lattice energy of the co-formed alkali metal halide.

$$[MX_3] + [LiN(SiR_3)_2] \longrightarrow 1/n\,[X_2MN(SiR_3)_2]_n + LiX \quad \textbf{(2.19)}$$

(5) Adduct formation by direct reaction of a silylamine and a metal halide or alkyl metal complex as shown in Eq. 2.20.

$$[MX_3] + HN(SiR_3)_2 \longrightarrow [X_3M\{NH(SiR_3)_2\}] \quad \textbf{(2.20)}$$

2.2.2 Synthesis of group 13 metal silylamides by dehalosilylation reactions

As discussed in section 2.1, the aluminium and gallium silylamides $[X_2M\{N(SiMe_3)_2\}]_2$ (where M = Al, X = Cl (**3**);[55] M = Ga, X = Cl (**32**),[122] Br(**33**)[123]) have been characterised and the thermal decomposition of **3** to give AlN has been described. These complexes were prepared by the reaction of $[MX_3]$ and one equivalent of $HN(SiMe_3)_2$ in refluxing ether.

In this study compounds **32** and **33** were prepared using a modified synthesis in which the reaction of $[MX_3]$ and $HN(SiMe_3)_2$ was carried out in CH_2Cl_2 either at -78 °C or room temperature. The reaction of gallium halides and a range of substituted silylamines (e.g. $HN(SiMe_2H)_2$ and $HN(SiMe_2Ph)_2$) was also carried out. The isolation of monomeric gallium silylamides was also attempted by the use of a Lewis base using a similar method to that used in the preparation of monomeric aluminium and gallium silylantinamides.[147]

2.2.3 Reaction of $[GaCl_3]$ and $HN(SiMe_3)_2$

Compound **32** was prepared using the modified synthesis, described above, in order to study the decomposition properties of this complex. After work-up colourless crystals were obtained by cooling a concentrated CH_2Cl_2 solution to -20 °C. Analytical and spectroscopic data indicated the colourless crystals were $[Cl_2Ga\{NH(SiMe_3)\}]_2$ (**32**). The ^1H NMR of **32** was carried out in $CDCl_3$ and shows peaks at 0.40 and 0.53 ppm corresponding to the trimethylsilyl protons of the *cis* and *trans* dimers. This corresponds well to the peaks observed in the CD_2Cl_2 spectrum of **32** reported by Nutt *et al.*[122] The infra-red spectrum of **32** was recorded and compared with the literature values. Peaks were observed at 3205 cm^{-1} and 1130 cm^{-1}, which are assigned to the presence of N-H. Peaks due to the Ga-N (535 cm^{-1} and 500 cm^{-1}) and Ga-Cl (405 cm^{-1}) bonds are also observed in the spectrum.

2.2.4 Reaction of $[GaCl_3]$ and $HN(SiMe_2Ph)_2$

The reaction of $[GaCl_3]$ and one equivalent of $HN(SiMe_2Ph)_2$ in CH_2Cl_2 was carried out at -78 °C. After work-up and cooling to -20 °C colourless crystals were

obtained. Recrystallisation from ether at -20 °C afforded colourless X-ray quality crystals in 63% yield. Analytical and spectroscopic data showed the crystals to be $[Cl_2Ga\{NH(SiMe_2Ph)\}]_2$ (**83**), as shown in Eq. 2.21.

$$2\,[GaCl_3] + 2\,HN(SiMe_2Ph)_2 \longrightarrow [Cl_2Ga\{NH(SiMe_2Ph)\}]_2 + 2\,Me_2PhSiCl \qquad (\mathbf{2.21})$$

The melting point (104 - 107 °C) is lower than that reported for **32** (153 °C).[122] Ideally, for CVD precursors, a lower melting point is desirable as this indicates that the compound may have a higher volatility.

The ^1H NMR spectrum of **83** was carried out in CD_2Cl_2 and is shown in Figure 2.8. Two peaks (0.78 ppm and 0.82 ppm) due to the methyl groups attached to the silicon are clearly visible in a 1:1 ratio. The occurrence of two peaks suggests the presence of a *cis-trans* dimer equilibrium in solution. The ^1H NMR of spectrum of **32** in CD_2Cl_2 shows only peaks assigned to *cis-trans* equilibrium, although the spectrum recorded in toluene-d_8 (by Nutt *et. al.*)[122] also shows peaks due to a dimer-trimer equilibrium. The ^{13}C NMR spectrum of **83** shows two peaks which are due to these methyl groups as would be expected as well as the expected peaks due to the aryl carbons. The ^1H NMR spectrum of **83** also shows peaks due to the N-H proton (at 2.41 ppm) and the aromatic protons of the phenyl group (7.00 - 7.39 ppm). The infra-red spectra of **83** shows two peaks at 3213 cm^{-1} and 1116 cm^{-1} corresponding to those expected for the N-H bond.

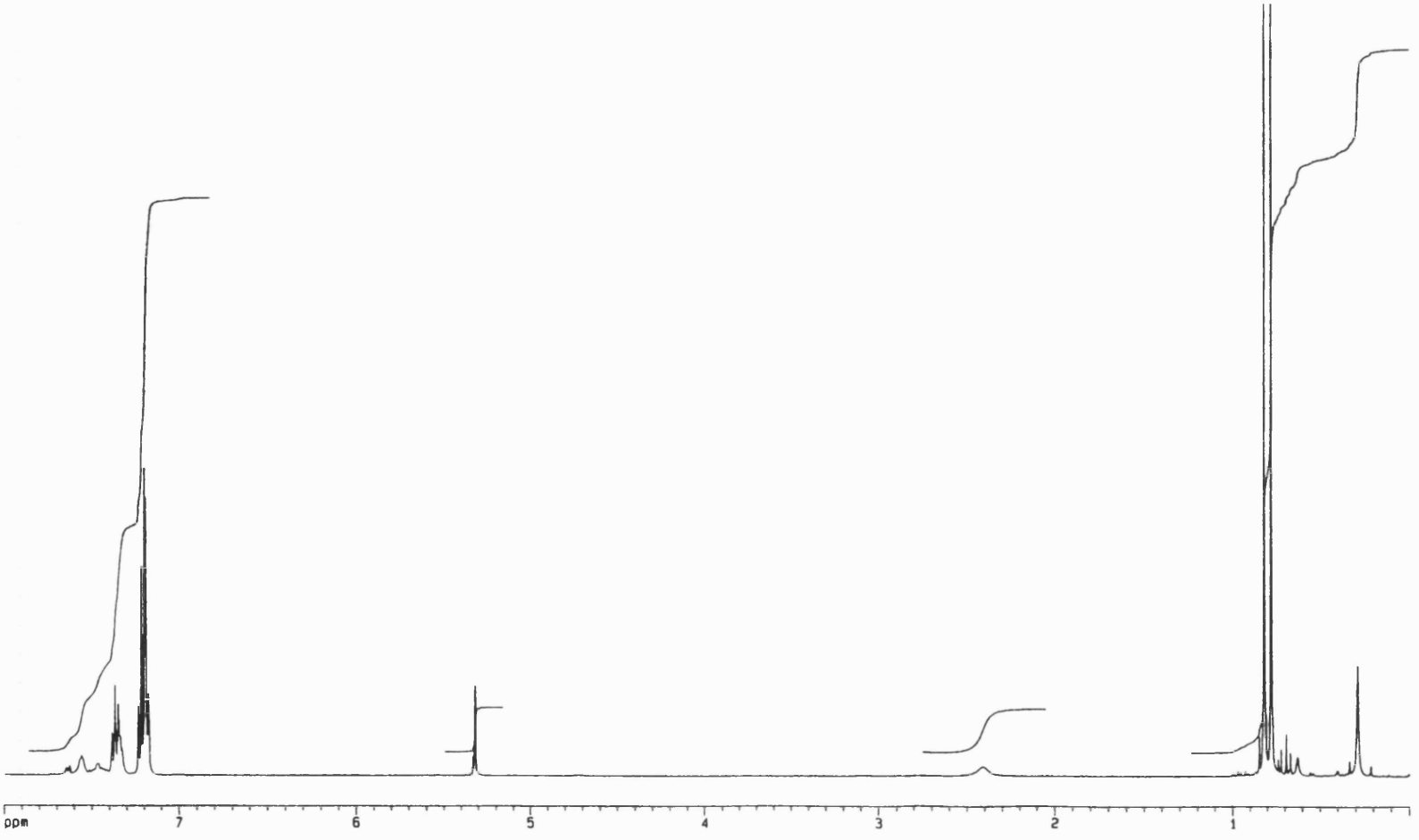

Figure 2.8 ^{1}H NMR spectrum of $[Cl_2Ga\{NH(SiMe_2Ph)\}]_2$ (83)

2.2.5 X-ray structure of $[Cl_2Ga\{NH(SiMe_2Ph)\}]_2$ (83)

The structure of **83** was confirmed by X-ray crystallography, the results of which are shown in Figure 2.9; selected bond lengths and angles are given in Table 2.1. Tables of all the bond lengths, angles and crystallographic data for **83** and all subsequent structures presented in this thesis are given in the appendix. The X-ray crystallographic study confirms the structure to consist of centrosymemetric dimers, which contain a planar Ga_2N_2 ring at their core and *trans* dimethylphenylsilyl groups (Figure 2.9). The bond lengths and angles in **83** are virtually identical to those determined for **32**, which was established by Nutt *et al.*[122] The Ga_2N_2 ring is almost square with the Ga'-N-Ga and N'-Ga-N angles being within statistical significance 90°. The nitrogen bridge is, however, slightly asymmetric with the Ga-N distance being 1.988(4) Å and the Ga-N' distance 1.968(3) Å. The structure of **32** shows a similar asymmetry in the bridging nitrogen. The N-Si bond is the same as that observed in **32** although this is significantly longer than in some alkyl substituted complexes, for example, $[Cl(Me)Ga\{NH(SiMe_3)\}]_2$ (N-Si 1.744 Å)[156] and $[Me_2Ga\{N(SiMe_2H)_2\}]_2$ (av. N-Si 1.770 Å).[123]

Table 2.1 Selected bond lengths (Å) and angles (°) for $[Cl_2Ga\{NH(SiMe_2Ph)\}]_2$ (83)

Ga–N'	1.968(3)	Ga–N	1.988(4)
Ga–Cl(1)	2.1380(13)	Ga–Cl(2)	2.1540(14)
Ga–Ga'	2.8033(9)	Si–N	1.801(4)
Si–C(2)	1.852(5)	Si–C(1)	1.852(5)
Si–C(8)	1.897(3)	N–Ga'	1.968(3)
N'–Ga–N	89.74(14)	N'–Ga–Cl(1)	115.86(11)
N–Ga–Cl(1)	110.55(11)	N'–Ga–Cl(2)	110.73(11)
N–Ga–Cl(2)	114.88(11)	Cl(1)–Ga–Cl(2)	113.12(6)
N–Si–C(2)	109.5(2)	Si–N–Ga	120.1(2)
Si–N–Ga'	127.2(2)	Ga'–N–Ga	90.26(14)

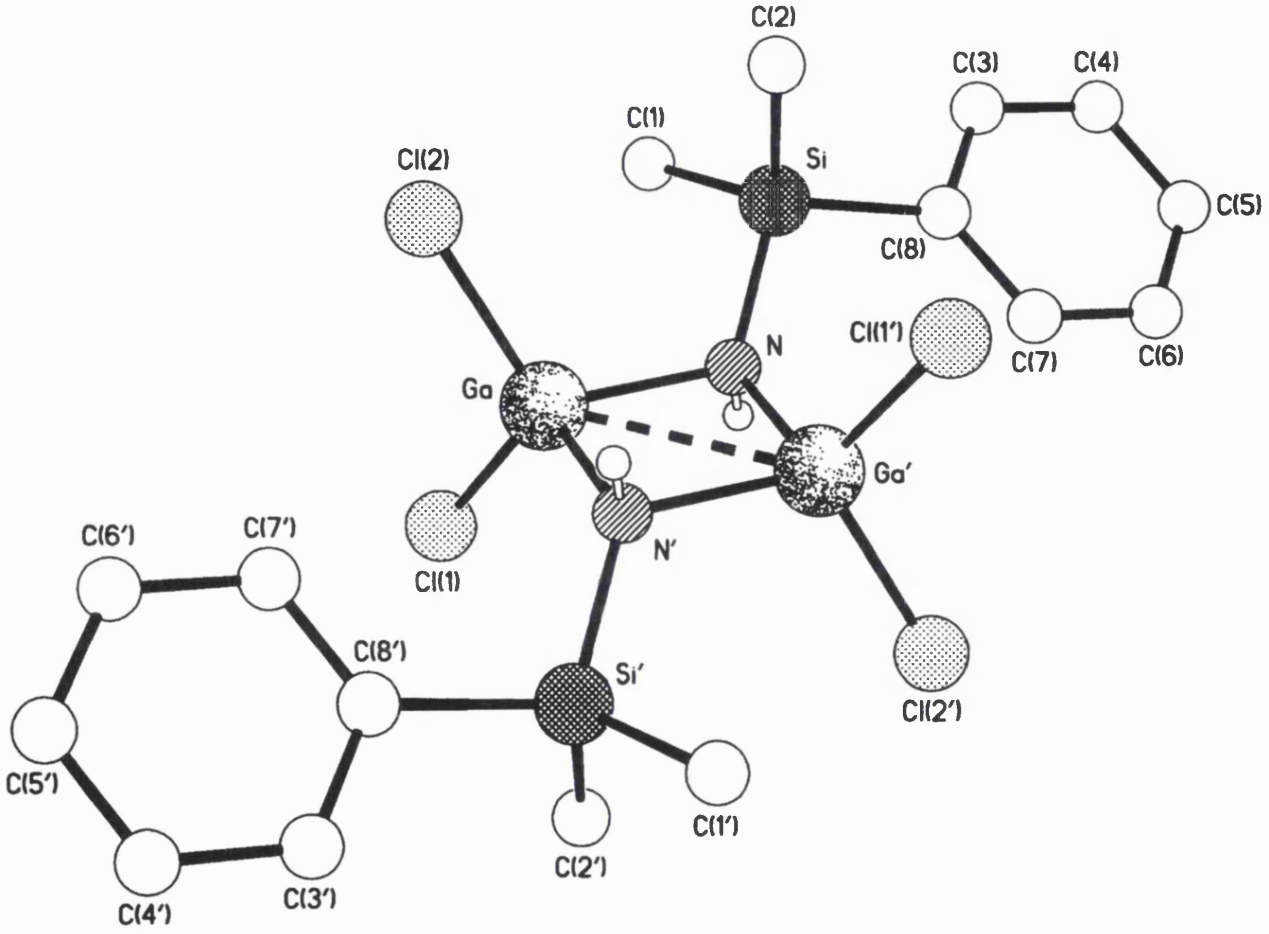

Figure 2.9 X-ray structure of $[Cl_2Ga\{NH(SiMe_2Ph)\}]_2$ (83)

2.2.6 Reaction of $[GaCl_3]$ and $HN(SiMe_2H)_2$

The reaction of $[GaCl_3]$ and $HN(SiMe_2H)_2$ was carried out at room temperature in CH_2Cl_2. After work-up a white oil was obtained. On standing at room temperature for 1 week colourless crystals and a grey solid were formed, suggesting that decomposition had occurred. A small quantity of the crystals were isolated and analysis suggested that a mixture of decomposition products had been formed and that the expected product $[Cl_2Ga\{NH(SiMe_2H)\}]_n$ had not been formed. This suggests that the white oil may be the desired product but that this is not stable at room temperature and has decomposed.

2.2.7 Reaction of $[GaCl_3]$ and $HN(^tBu)SiMe_3$

The reaction between $[GaCl_3]$ and $NH(^tBu)SiMe_3$ was carried out in refluxing diethyl ether to ensure that one product was formed (lower temperatures resulted in a mixture of products). After work-up colourless crystals suitable for X-ray analysis were obtained in 63% yield by cooling to -20 °C. Analytical and spectroscopic data showed the crystals to be $[Cl_2Ga\{NH(^tBu)\}]_2$ (**84**), as shown in Eq. 2.23.

$$2\,[GaCl_3] + 2\,HN(^tBu)SiMe_3 \longrightarrow [Cl_2GaNH(^tBu)]_2 + 2\,Me_3SiCl \quad (\mathbf{2.23})$$

The ^1H NMR of **84** shows three singlets due to the ^tBu group protons in a 4:4:1 ratio and three peaks due to the NH in the same ratio. This suggests that a *cis-trans* equilibrium exists in solution accounting for the two major sets of peaks and a dimer-trimer equilibrium also exists which accounts for the minor peak. The %N found in the sample was less than that expected and is thought to be due to the formation of GaN during the analytical process. This is observed in other silylamides which have been prepared.

2.2.8 X-ray structure of $[Cl_2Ga\{NH(^tBu)\}]_2$ (84)

The structure of **84** was confirmed by X-ray crystallography, the results of which are shown in Figure 2.10; selected bond lengths and angles are given in Table

2.2. The structure of **87** was found to consist of centrosymmeteric dimers with a planar Ga_2N_2 ring and *trans tert*-butyl groups. The bond lengths and angles are similar to those found in **83** except that the bridging nitrogen atoms are not asymmetric. The Ga_2N_2 ring is not square with the Ga(A)-N-Ga angle being 93.18(10)° and N-Ga-N(0A) 86.82(10)°. The Ga-Ga(A) distance (2.8695(8) Å) is also significantly longer than that in **83** (2.803 Å). Each gallium has severely distorted tetrahedral geometry (Cl(2)-Ga-Cl(1) 110.26(4)°, N-Ga-N(0A) 86.82(10)°, N-Ga-Cl(1) 109.89(8)°).

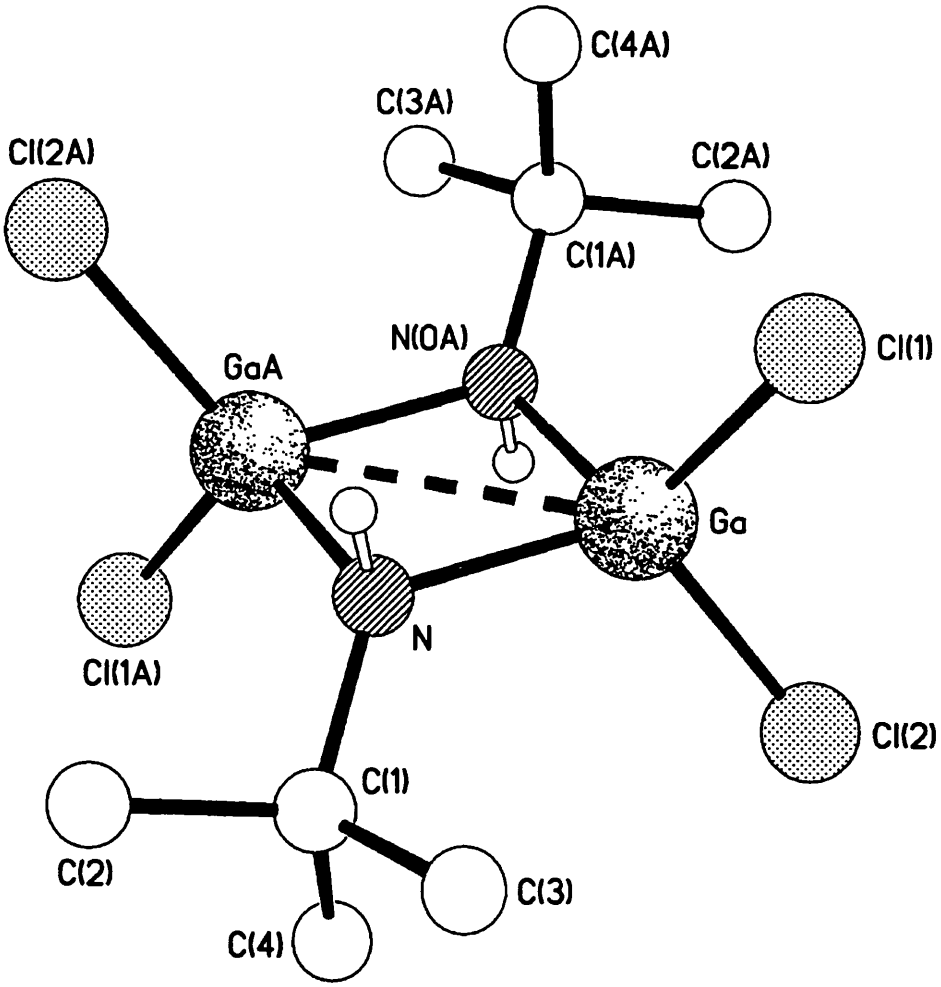

Figure 2.10 X-ray structure of $[Cl_2Ga\{NH(^tBu)\}]_2$ (84)

Table 2.2 Selected bond lengths (Å) and angles (°) for $[Cl_2Ga\{NH(^tBu)\}]_2$ (84)

Ga-N(0A)	1.973(2)	N-C(1)	1.516(4)
Ga-N	1.977(2)	Ga(A)-N	1.973(2)
Ga-Cl(2)	2.1408(9)	C1-C(4)	1.518(4)
Ga-Cl(1)	2.1579(9)	C1-C(3)	1.524(5)
Ga-Ga	2.8695(8)	C1-C(2)	1.526(5)
N-Ga-N(0A)	86.82(10)	Cl(2)-Ga-Cl(1)	110.26(4)
N(0A)-Ga-Cl(2)	110.33(8)	C(1)-N-Ga(A)	125.4(2)
N-Ga-Cl(2)	118.81(8)	C(1)-N-Ga	124.3(2)
N(0A)-Ga-Cl(1)	119.44(8)	Ga(A)-N-Ga	93.18(10)
N-Ga-Cl(1)	109.89(8)	C(4)-C(1)-C(3)	110.8(3)

2.2.9 Reaction of $[GaBr_3]$ and $HN(SiMe_3)_2$

The reaction between $[GaBr_3]$ and $HN(SiMe_3)_2$ was carried out using the method described in section 2.2.2. After work-up a white microcrystalline powder was obtained. The expected product, $[Br_2Ga\{NH(SiMe_3)\}]_2$ (**33**), appears to have been formed during the reaction and although the analytical data shows a small variation from that expected. The small discrepancy may be due to the presence of a small amount of solvent (of crystallisation) or contamination by minor products formed during the reaction. The ^1H NMR of **33** (CD_2Cl_2) shows four peaks due to the protons of the methyl groups, this is in contrast to the two peaks reported in the literature (when carried out in toluene-d_8).[123] However, the ^1H NMR for related compounds is highly dependant on the concentration of the solution and the NMR solvent used.[122,123] These peaks may be due to the presence of *cis-trans* and dimer-trimer equilibia in solution. A peak assigned to the NH proton (3.08 ppm) is observed, in contrast to the ^1H NMR reported in the literature.[123] The ^{13}C NMR spectrum of **33** also shows four peaks, which are assigned to the methyl groups. The infra-red spectrum was recorded and compared with the literature values.[123] The peaks due to the N-H bond (at 3193 and 1129 cm^{-1}) correspond well to the published values (3195 and 1131 cm^{-1}).

2.2.10 Reaction of $[InCl_3]$ and $HN(SiMe_3)_2$

The reaction of $[InCl_3]$ and $HN(SiMe_3)_2$ was carried out in ether at room temperature over a period of days. After work-up and cooling to -20 °C a white powder was obtained in 34% yield. Analytical and spectroscopic data showed this powder to be $[Cl_2In\{NH(SiMe_3)\}]_n$ (**85**), as shown in Eq. 2.23.

$$[InCl_3] + HN(SiMe_3)_2 \longrightarrow 1/n\,[Cl_2InNH(SiMe_3)]n + Me_3SiCl \quad (\mathbf{2.23})$$

The ^1H NMR of **85** shows two peaks (at 0.34 and 0.40 ppm) which are due to the protons of the trimethylsilyl groups. The integrals show that the peak at 0.40 ppm represents the major trimethylsilyl environment. These two peaks may arise from either a *cis-trans* or a dimer-trimer equilibrium occurring in solution. Related indium compounds reported previously suggest that the compound would be dimeric in the solid state with a *trans* arrangement of the silyl groups. The elemental analysis for **85** suggests that there is some solvent (ether) present in the powder obtained. The ^1H NMR confirms the presence of ether showing a 1:4 ratio of solvent to product.

2.2.11 Reaction of $[GaCl_3]$ and $N(SiMe_3)_3$ in CH_2Cl_2

The reaction of $[GaCl_3]$ and 1 equivalent of $N(SiMe_3)_3$ in CH_2Cl_2 at -78 °C resulted, after work-up, in a light brown oil. Colourless crystals suitable for X-ray analysis were obtained by dissolving the oil in the minimum amount of CH_2Cl_2 and cooling to -20 °C. Analytical and spectroscopic data showed the crystals to be $[MeGaCl_2]_2$ (**86**), as shown in Eq. 2.24.

$$[GaCl_3] + N(SiMe_3)_3 \longrightarrow [MeGaCl_2]_2 \quad (\mathbf{2.24})$$

The analytical data shows a small discrepancy with that expected for **86**, this is thought to arise from the difficulty of separating the crystalline material from the light brown oil. The ^1H NMR of **86** shows a number of peaks in the region 0.42 - 0.62 ppm corresponding either to impurities (from the oil) or the formation of isomers in solution (e.g. $[MeGaCl_2]$ and $[MeGaCl_2]_3$). The exchange of a chlorine

attached to a group 13 metal for a methyl group from a silyl group is not unexpected. The synthesis of a number of organogallium halides by reaction of [$GaCl_3$] and silyl complexes (for example Me_4Si, $[Me_2SiO]_4$, $(Me_3Si)_2O$) has been reported.[157] The structure of **86** was predicted by Weidlen as consisting of centrosymmetric dimers.[158]

2.2.12 X-ray structure of $[MeGaCl_2]_2$ (86)

The structure of **86** was determined by X-ray crystallography, the results of which are shown in Figure 4.11; selected bond lengths and angles are given in Table 2.3. The dimeric structure of $[MeGaCl_2]_2$ was confirmed by an X-ray crystallographic study which shows it to be centrosymmetric with the [$MeGaCl_2$] units linked by bridging chlorine atoms. This is similar to the analogous aluminium compound $[MeAlCl_2]_2$ which also has a dimeric structure.[159] The Ga_2Cl_2 ring is planar and nearly square (Cl(2')-Ga-Cl(2) 88.89(6)° and Ga'-Cl(2)-Ga 91.11(6)°) with a uniform Ga-Cl(2) bond length of 2.3324(12) Å. As expected the terminal Ga-Cl(1) bonds (2.1547(19) Å) are shorter than the bonds between the gallium and the bridging chlorine atoms (2.3324(12) Å). The gallium atoms adopt a severely distorted tetrahedral geometry shown by the Cl(2')-Ga-Cl(2) angle which is significantly reduced from tetrahedral at 88.89(6)° and the C(1)-Ga-Cl(1) angle which is larger than tetrahedral at 127.0(3)°. The packing of molecules of **86** is a classic cubic close-packed arrangement with hexagonal layers of molecules stacked in an ABCABC fashion, as shown in Figure 2.12. The interlayer separation is 5.82 Å.

Table 2.3 Selected bond lengths (Å) and angles (°) for $[MeGaCl_2]_2$ (86)

Ga(1)-C(1)	1.928(7)	Ga(1)-Cl(2)	2.3324(12)
Ga(1)-Cl(1)	2.1547(19)	Ga(1)-Cl(2')	2.3324(12)
C(1)-Ga(1)-Cl(1)	127.0(3)	Cl(1)-Ga(1)-Cl(2)	103.83(4)
C(1)-Ga(1)-Cl(2)	113.17(17)	Cl(2')-Ga(1)-Cl(2)	88.89(6)
Ga(1')-Cl(2)-Ga(1)	91.11(6)		

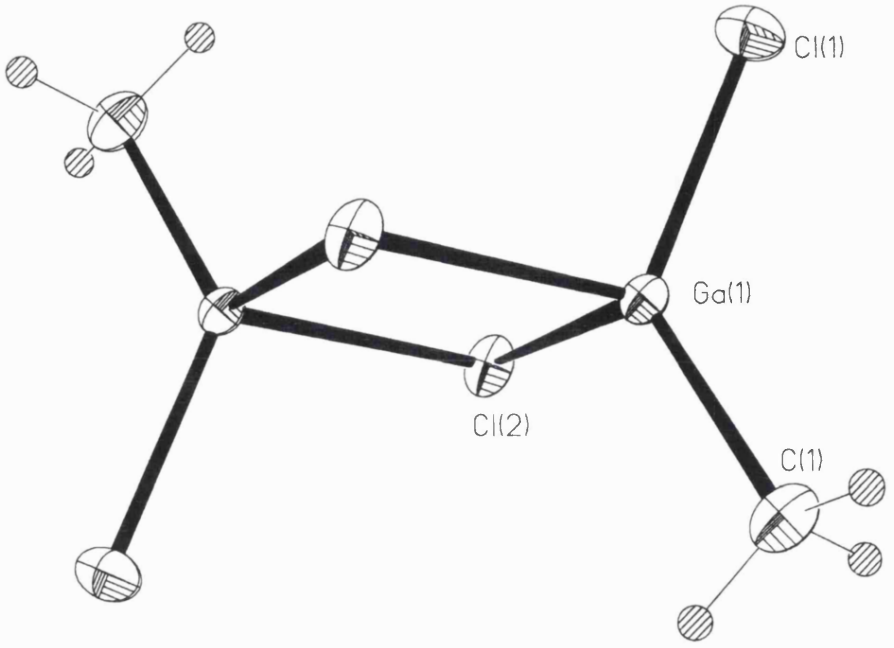

Figure 2.11 X-ray structure of $[MeGaCl_2]_2$ (86)

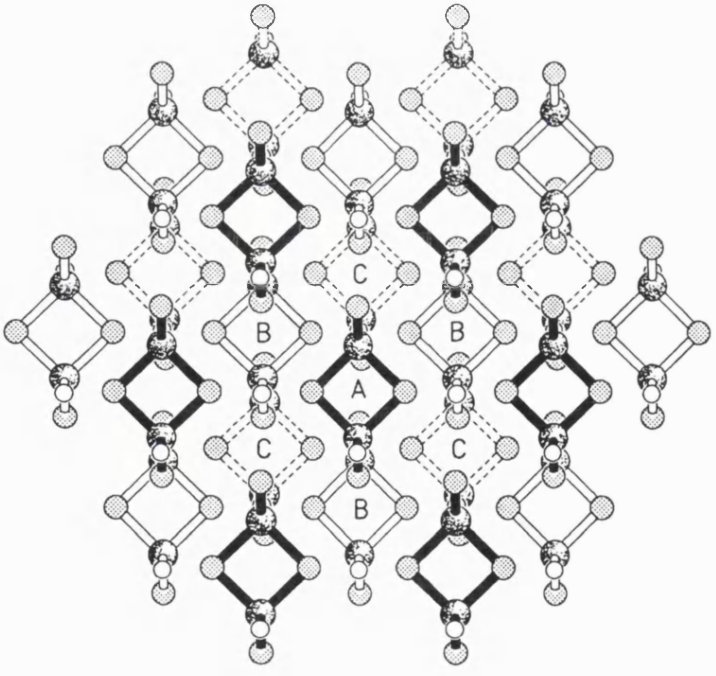

Figure 2.12 The packing of molecules of $[MeGaCl_2]_2$ (86) showing the ABC sequence layers

2.2.13 Reaction of $[GaCl_3]$ and $N(SiMe_3)_3$ in hexane

The reaction of $[GaCl_3]$ and $N(SiMe_3)_3$ was carried out in hexane at room temperature. After work-up a white powder was obtained. On standing for 24 hours a colourless oil had formed. Over time large colourless needles formed, the analytical data for which, suggested a mixture of $[MeGaCl_2]$ and $[Me_2GaCl]$ in a 1:1 ratio. An X-ray crystallographic study was carried out and suggested that a polymer of the type $[(MeGaCl_2)(Me_2GaCl)]_n$, with a linear chlorine bridged chain structure, had been formed. However, it was not possible to fully resolve the structure.

2.2.14 Reaction of $[GaCl_3]$, $HN(SiMe_3)_2$ and 3,5-$Me_2C_5H_3N$

In an attempt to prepare a monomeric gallium silylamide, the reaction of $[GaCl_3]$, $HN(SiMe_3)_2$ and 3,5-$Me_2C_5H_3N$ was carried out at -78 °C in CH_2Cl_2. It was hoped that the 3,5-lutidine would coordinate to the gallium and stabilise a monomeric species. After work-up and cooling to -20 °C colourless crystals were obtained. Analytical and spectroscopic data showed these to be $[Cl_3Ga(NC_5H_3Me_2\text{-}3,5)_2]$ (**87**), as shown in Eq. 2.25.

$$[GaCl_3] + HN(SiMe_3)_2 + 2\,NC_5H_3Me_2 \longrightarrow [GaCl_3(NC_5H_3Me_2\text{-}3,5)_2] \quad \textbf{(2.25)}$$

The $HN(SiMe_3)_2$ has not been involved in the reaction, however, it is volatile and easily removed during work-up of the reaction. The anticipated product, $[Cl_2Ga\{NH(SiMe_3)\}(NC_5H_3Me_2)]$, was not formed.

2.2.15 Reaction of $[Cl_2GaNH(SiMe_3)]_2$ and 3,5-$Me_2C_5H_3N$

As the direct reaction of $[GaCl_3]$, $HN(SiMe_3)_2$ and 3,5-$Me_2C_5H_3N$ failed to yield a monomeric gallium silylamide, the reaction between $[Cl_2Ga\{NH(SiMe_3)\}]_2$ (**32**) and 3,5-$Me_2C_5H_3N$ was carried out in diethyl ether. After work-up and cooling to -20 °C, large colourless crystals formed. Analytical data showed that compound **87** had formed. The mechanism for the formation of **87** is unknown and any side products were not isolated. The ^1H NMR spectrum of **87** is shown in Figure 2.13.

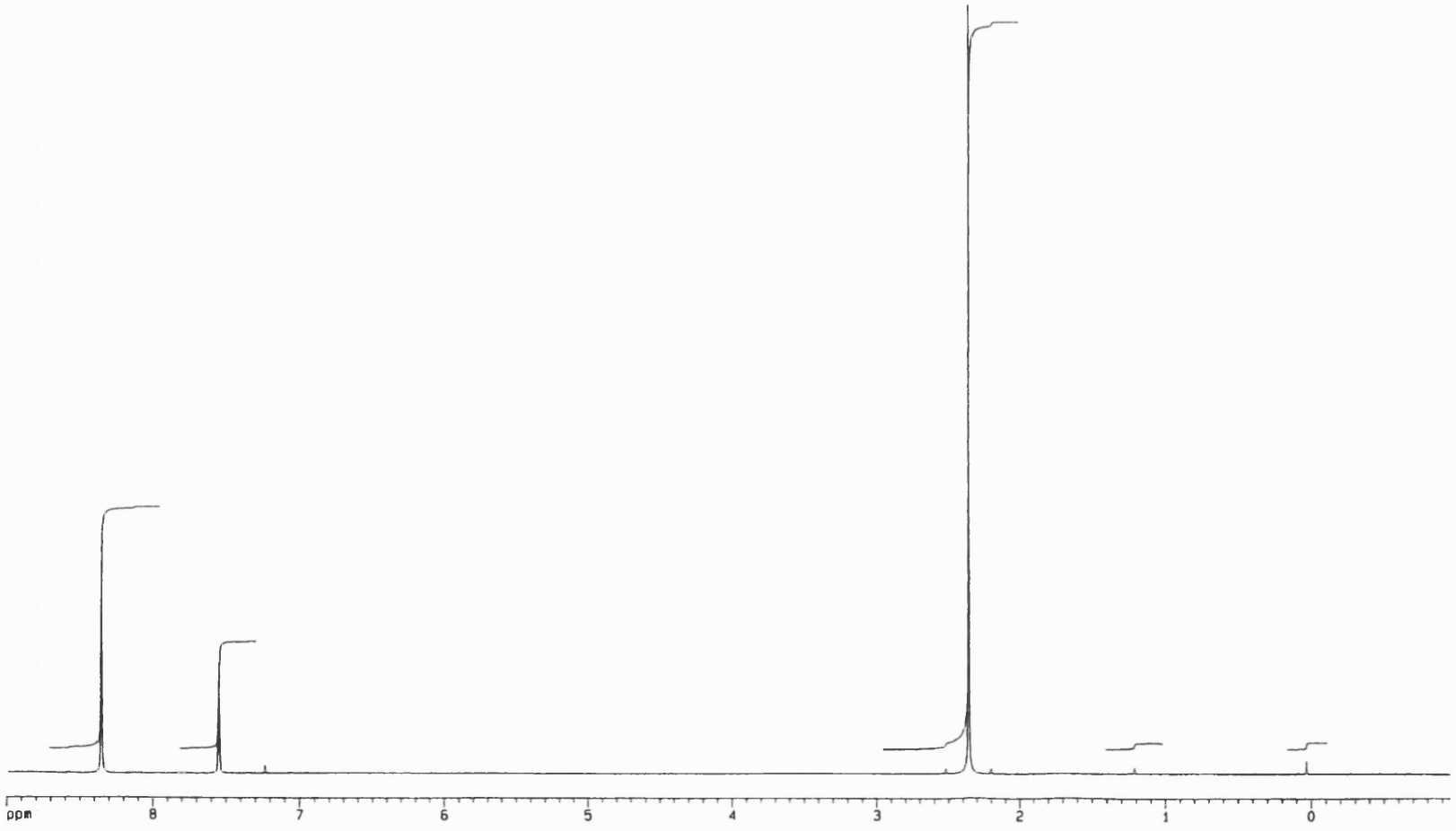

Figure 2.13. ^{1}H NMR spectrum of [$Cl_3Ga(NC_5H_3Me_2$-3,5)$_2$] (87)

2.2.16 Synthesis of group 13 silylamides by dealkylsilaytion reactions

Precursors containing alkyl groups attached to the metal show potential as precursors to metal pnictides. The synthesis of aluminium and gallium silylamides was attempted by the reaction of $[R_3M]$ or $[R_2MCl]$ and silylamines with loss of $[R_4Si]$.

2.2.17 Reaction of $[Me_2AlCl]$ and $HN(SiMe_2H)_2$

The reaction of $[Me_2AlCl]$ and $HN(SiMe_2H)_2$ was carried out in CH_2Cl_2 at -78 °C. The solvent was removed *in vacuo* leaving a colourless oil. Standing the oil at room temperature for one week resulted in the formation of colourless crystals, which were suitable for X-ray analysis. Analytical and spectroscopic data showed the crystals to be $[Cl(Me)Al\{NH(SiMe_2H)\}]_2$ (**88**) according to Eq. 2.26.

$$2\,[Me_2AlCl] + 2\,HN(SiMe_2H)_2 \longrightarrow [Cl(Me)Al\{NH(SiMe_2H)\}]_2 + Me_3(H)Si \quad (\mathbf{2.26})$$

The ^1H NMR spectrum of **88** shows peaks due to the methyl group, the silyl group and the NH in the expected ratio. The methyl groups attached to the silicon are diastereotopic which gives reise to two peaks of equal intensity.

2.2.18 X-ray structure of $[Cl(Me)Al\{NH(SiMe_2H)\}]_2$ (88)

The structure of **88** was confirmed by X-ray crystallography, the results of which are shown in Figure 2.14; selected bond lengths and angles are given in Table 2.4. Each dimer has at its core an almost square, planar Al_2N_2 ring. The trimethylsilyl groups are arranged in a *trans* fashion. The bond lengths and angles are virtually identical to those published for $[Cl(Me)Al\{NH(SiMe_3)\}]_2$ (**65**).[144] Unlike the structure of **83** the bridging nitrogen atoms are symmetric. Each aluminium is four coordinate adopting a distorted tetrahedral geometry (N(0A)-Al-N 89.22(13)°, C(1)-Al-Cl 117.08(12), N-Al-C(1) 115.48(14)).

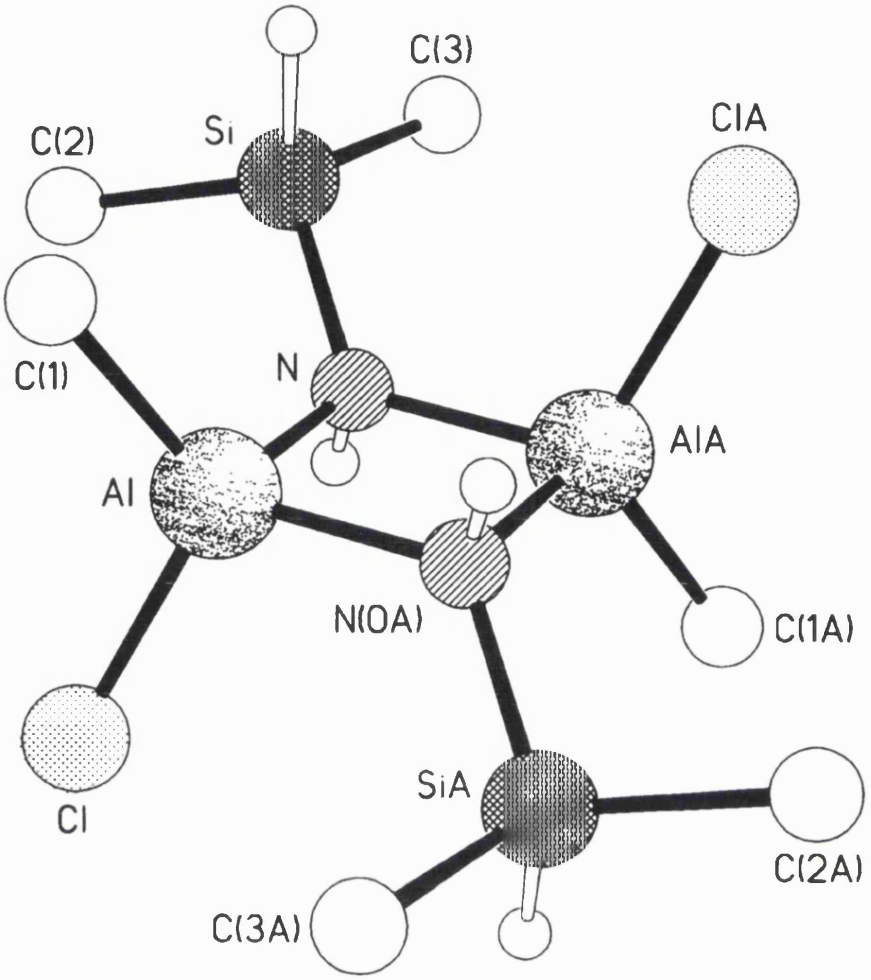

Figure 2.14 X-ray structure of $[Cl(Me)Al\{NH(SiMe_2H)\}]_2$ (88)

Table 2.4 Selected bond lengths (Å) and angles (°) for $[Cl(Me)Al\{NH(SiMe_2H)\}]_2$ (88)

Al-N(0A)	1.920(3)	Al-Cl	2.1357(14)
Al-N	1.924(3)	Al-Al(A)	2.737(2)
Al-C(1)	1.971(3)	N-Si	1.773(3)
N(0A)-Al-N	89.22(13)	C(1)-Al-Cl	117.08(12)
N(0A)-Al-C(1)	113.58(15)	Si-N-Al(A)	126.3(2)
N-Al-C(1)	115.48(14)	Si-N-Al	119.1(2)
N(0A)-Al-Cl	110.70(10)	Al(A)-N-Al	90.78(13)
N-Al-Cl	107.35(11)		

2.2.19 Reaction of $[Et_3Al]$ and $N(SiMe_3)_3$

The reaction of $[Et_3Al]$ and $N(SiMe_3)_3$ was carried out in CH_2Cl_2 at room temperature. The solvent was removed yielding a colourless liquid. Spectroscopic data on the product is inconclusive and suggests that either $[Et_2Al\{N(SiMe_3)_2\}]_n$ or the adduct $[Et_3Al\{N(SiMe_3)_3\}]$ has formed. The ^1H NMR of the liquid shows only one peak due to the protons of the trimethylsilyl groups at 0.20 ppm. A quartet (at 0.33 ppm) and a triplet (at 1.10 ppm) due to the Al-Et groups are observed with a 2:3 ratio of integrals. The ratio of trimethylsilyl protons to ethyl protons is 9:5, which is the expected ratio for both species. The sharpness and the observance of only one set of peaks for each environment suggests that one product has been formed exclusively. The infra-red spectrum does not resolve which product has been formed. A peak due to Al-N bond in the adduct would be expected at around 530 cm^{-1} (when compared with $[Cl_3Al\{NH(SiMe_3)_2\}]$) may be observed at 545 cm^{-1} however this may be due to the trimethylsilyl groups.[129] Elemental analysis, which might confirm the nature of the product form, could not be carried out as the sample is liquid.

2.2.20 Synthesis of group 13 silylamides by alkane elimination

An alternative route for the preparation of group 13 silylamides is alkane elimination. This route is particularly useful for the preparation of complexes with two alkyl groups attached to the metal by the reaction of trialkyl metal complexes (e.g. $[Et_3Ga]$) with *bis* silylamines.

2.2.21 Reaction of $[Et_3Al]$ and $HN(SiMe_2H)_2$

The reaction of $[Et_3Al]$ and $HN(SiMe_2H)_2$ was carried out in CH_2Cl_2 at -78 °C. Evolution of a colourless gas was observed on addition of the silylamine. After work-up, a white crystalline solid was obtained in 85% yield. Recrystallisation from CH_2Cl_2 afforded colourless plates, which proved to be unsuitable for X-ray analysis. However, analytical and spectroscopic data showed the white powder was $[Et_2Al\{N(SiMe_2H)_2\}]_n$ (**89**), as shown in Eq. 2.27. The related reaction of $[Me_3Al]$ and $HN(SiMe_2H)_2$ is known to yield the dimeric species $[Me_2Al\{N(SiMe_2H)_2\}]_2$. Therefore, **89** is the expected product of the reaction of $[Et_3Al]$ and $HN(SiMe_2H)_2$.

$$[Et_3Al] + HN(SiMe_2H)_2 \longrightarrow [Et_2Al\{N(SiMe_2H)_2\}]_n + EtH \quad (\mathbf{2.27})$$

Although the analytical data shows a closer fit to $[Et_2Al\{NH(SiMe_2H)\}]_n$, the ^1H NMR (Figure 2.15) of **89** and infra-red data showed that this species could not be the major product of the reaction. The yield suggests **89** is the product of the reaction as the yield would be 116% if the product were $[Et_2Al\{NH(SiMe_2H)\}]_n$.

2.2.22 Spectroscopic data for $[Et_2Al\{N(SiMe_2H)_2\}]_n$ (89)

The ^1H NMR spectrum (Figure 2.15) of **89** shows peaks due to the ethyl groups attached to the aluminium and the silyl groups. The integrals show the ratio of silyl groups to ethyl groups to be 1:1 as would be expected if **89** was the major product from the reaction. The ^1H NMR also shows small amounts of impurity may be present in the product, this would explain the discrepancy in the analytical data. In addition, no peaks due to N-H protons were observed. The infra-red spectrum also supports the formation of **89** as opposed to any other product. The main feature of the spectrum is the absence of any peaks due to N-H bonds.

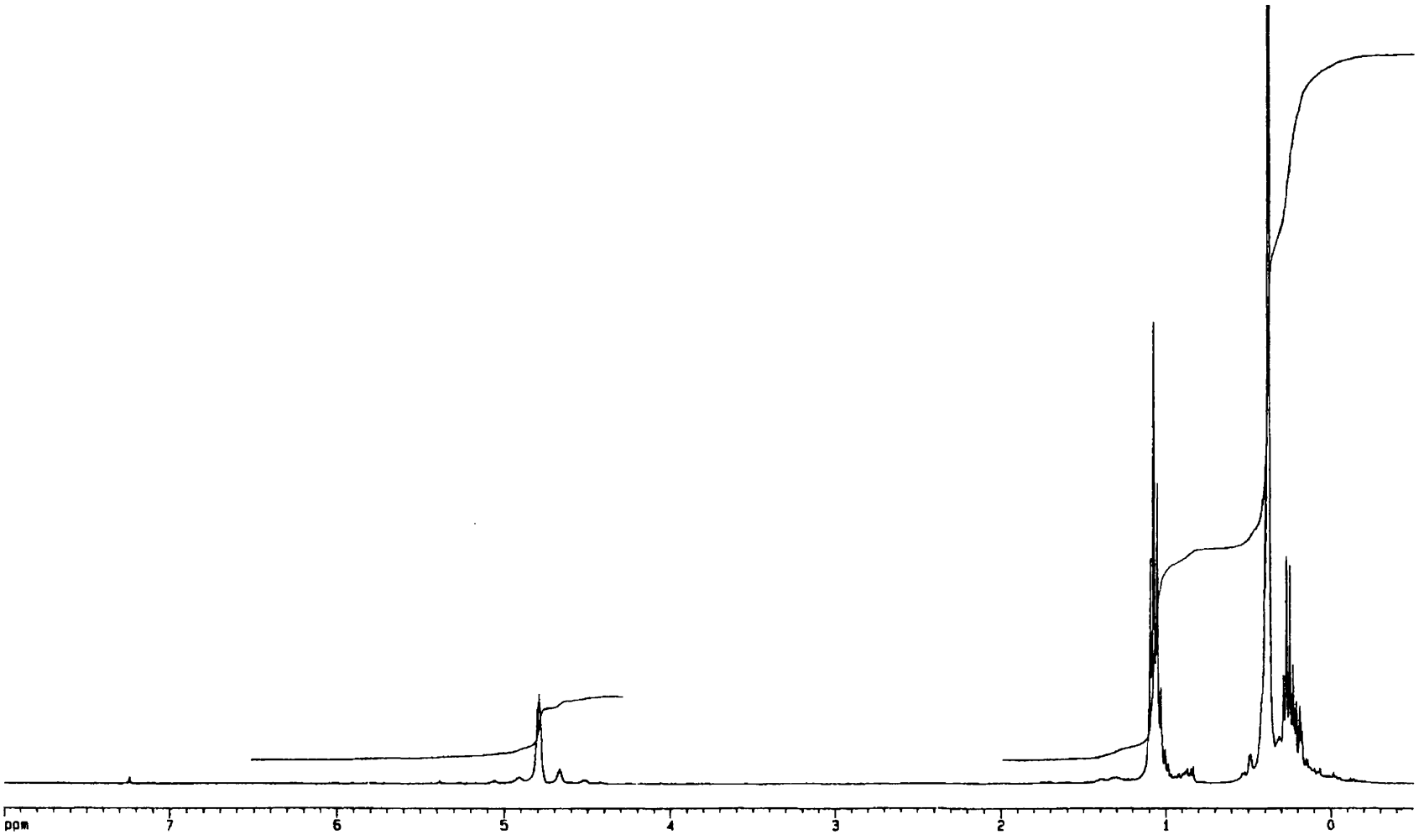

Figure 2.15 ^{1}H NMR spectrum of $[Et_2Al\{N(SiMe_2H)_2\}]_n$ (89)

2.2.23 Reaction of $[Et_3Al]$ and $HN(SiMe_3)_2$

The reaction of $[Et_3Al]$ and $HN(SiMe_3)_2$ was carried out using the method described in section 2.2.17. After work-up a colourless liquid was isolated. Spectroscopic data showed that this liquid was similar to the product of the reaction of $[Et_3Al]$ and $N(SiMe_3)_3$ (see section 2.2.17). This suggests that the product formed from both reactions is $[Et_2Al\{N(SiMe_3)_2\}]_n$ (**90**) as would be expected. The ^1H NMR and infra-red spectra are almost identical for the two complexes, the only major difference being that the spectrum from the product of the reaction with $HN(SiMe_3)_2$ contains minor peaks which suggest that a second product (e.g. $[Et_2Al\{NH(SiMe_3)\}]_n$) may have been formed in small amounts. On standing at room temperature for several weeks colourless crystals formed. An X-ray crystallographic study was carried out and it was found that the crystals were not **90** but were $[(EtO)EtAl\{N(SiMe_3)_2\}]_2$ (**91**). Compound **91** is probably formed by the decomposition of **90** in the presence of small amounts or oxygen of water.

2.2.24 X-ray structure of $[(EtO)EtAl\{N(SiMe_3)_2\}]_2$ (91)

The structure of **91** was confirmed by X-ray crystallography, the results of which are shown in Figure 2.16; selected bond lengths and angles are shown in Table 2.5. Compound **91** is dimeric with the OEt groups bridging the two aluminium atoms with one ethyl group and one $N(SiMe_3)_2$ group attached to each aluminium. The aluminium adopts a distorted tetrahedral geometry (AlA-O-Al 100.5(2)°, O-Al-N(0A) 117.5(2)°). The $N(SiMe_3)_2$ groups are arranged in a *trans* fashion across the Al_2O_2 ring. The Al-C(3) bond length (1.970(6) Å) corresponds well with the Al-C bond length observed in **88** (1.971(3) Å).

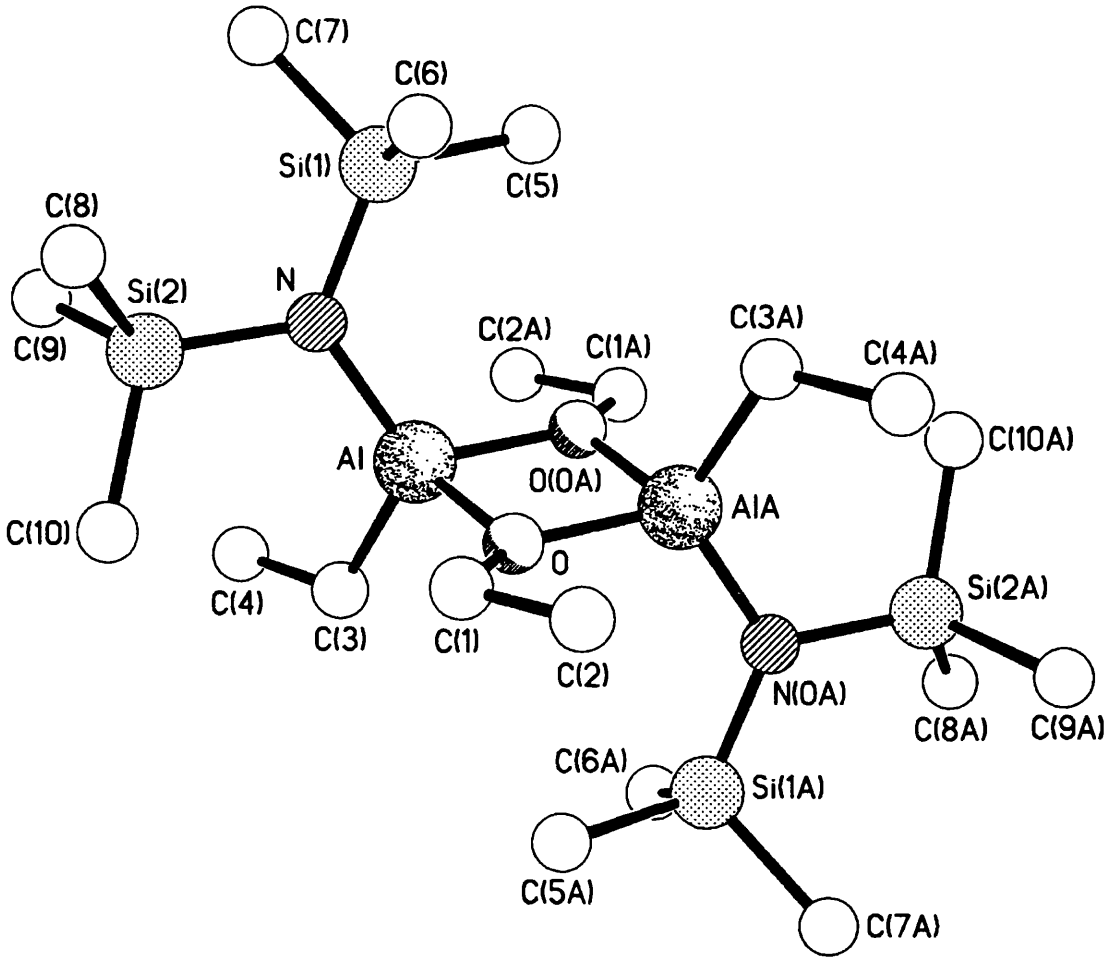

Figure 2.16 X-ray structure of $[(EtO)EtAl\{N(SiMe_3)_2\}]_2$ (91)

Table 2.5 Selected bond lengths (Å) and angles (°) for $[(EtO)EtAl\{N(SiMe_3)_2\}]_2$ (91)

Al-O(0A)	1.836(3)	Al-AlA	2.835(3)
Al-N	1.840(4)	Si(1)-N	1.726(5)
Al-O	1.852(3)	O-C(1)	1.458(6)
Al-C(3)	1.970(6)	O-AlA	1.836(3)
O-Al-N(0A)	117.5(2)	N-Al-C(3)	121.7(2)
O-Al-O(0A)	79.5(2)	O-Al-C(3)	110.3(2)
N-Al-O	111.1(2)	O(0A)-AlA-Al	39.97(10)
O(0A)-Al-C(3)	108.8(2)	N-AlA-Al	122.3(2)
O-AlA-Al	39.57(10)	C(3)-Al-AlA	115.8(2)
AlA-O-Al	100.5(2)	C(1)-O-AlA	131.8(3)
Si(1)-N-Al	125.1(2)	C(1)-O-Al	125.2(3)
Si(2)-N-Al	117.2(3)		

2.2.25 Reaction of $[Et_3Ga]$ with $N(SiMe_3)_3$

The reaction of $[Et_3Ga]$ and $N(SiMe_3)_3$ was carried out in refluxing ether. This reaction yielded after work-up a colourless liquid. Spectroscopic data shows that the liquid is a mixture of $[Et_3Ga\{N(SiMe_3)_3\}]$ and $[Et_2Ga\{N(SiMe_3)_2\}]_n$. The ^1H NMR data shows multiple environments for the ethyl group protons. The ^{13}C NMR shows two environments for each of the ethyl group carbon atoms, indicating two species are present. If the species $[Et_2Ga\{N(SiMe_3)_2\}]_n$ had been formed, then a dimer-trimer equilibrium may occur, however, the difference in the chemical shifts is larger than would be expected for such an equilibrium. Furthermore, the ^{13}C chemical shifts of the $SiMe_3$ groups suggest that both $[Et_3Ga\{N(SiMe_3)_3\}]$ and $[Et_2Ga\{N(SiMe_3)_2\}]_n$ have been formed. The two peaks observed in the ^{13}C NMR spectra at 1.0 ppm and 3.8 ppm correspond well with peaks reported in the literature as due to an adduct (0.56 ppm - $[Cl_3Al\{NH(SiMe_3)_2\}]$)[129] and a complex in which there is a formal M-N bond between the metal and the nitrogen (2.92 ppm -

$[Me_2Al\{NH(SiMe_3)\}]_2$).[144] The infra-red spectra shows peaks which may be due to either of the products.

2.2.26 Synthesis of group 13 silylamides by salt elimination routes

Salt elimination routes, involving the reaction of a group 13 halide and the alkali metal salt of a silylamine ($[MN(SiMe_3)_2]$ M = Li, Na) may be used to prepare group 13 silylamides. This route is particularly useful for the synthesis of a *bis* silylamide as the starting amide does not contain hydrogen attached to the nitrogen atoms. The salt elimination reactions which were attempted are described below.

2.2.27 Reaction of $[GaCl_3]$ and $[LiN(SiMe_3)_2]$

The reaction between $[GaCl_3]$ and $[LiN(SiMe_3)_2]$ was reported by Barry *et al.* to yield $[Cl_2Ga\{N(SiMe_3)_2\}]_n$, although this species was not isolated and characterised.[131] Carrying out the reaction of $[GaCl_3]$ and $[LiN(SiMe_3)_2]$ under the same conditions led to the isolation of a white or cream coloured oil. Spectroscopic studies carried out on this oil suggest a complex mixture of products is formed. A small quantity (ca. 6% yield) of orange crystals was isolated from this mixture. Analytical data showed these crystals to be the expected product of the reaction $[Cl_2Ga\{N(SiMe_3)_2\}]_n$ (**42**). Altering the reaction conditions did not lead to the isolation of **42** in a higher yield.

2.2.28 Reaction of $[GaCl_3]$ and $[LiN(SiMe_2Ph)_2]$

$[LiN(SiMe_2Ph)_2]$ was prepared by the reaction of $[^nBuLi]$ and $HN(SiMe_2Ph)_2$, as shown in Eq. 2.28.

$$[^nBuLi] + HN(SiMe_2Ph)_2 \longrightarrow [LiN(SiMe_2Ph)_2] + {}^nBuH \quad \textbf{(2.28)}$$

The addition of $[LiN(SiMe_2Ph)_2]$ (*in situ*) to a stirred solution of $[GaCl_3]$ at -78 °C afforded, after work-up, colourless crystals suitable for X-ray analysis. Analytical and spectroscopic data showed these crystals to be $[Cl(Ph)Ga\{N(SiMe_2Ph)_2\}]_2$ (**92**), as shown in Eq. 2.29.

$$[GaCl_3] + [LiN(SiMe_2Ph)_2] \longrightarrow [Cl(Ph)GaN(SiMe_2Ph)_2]_2 \quad (\mathbf{2.29})$$

The ^1H and ^{13}C NMR spectra of **92** show two peaks which is casued by the methyl groups which are attached to the silicon being diastereotopic. Formation of **92** involves the transfer of a phenyl group from a silicon to a gallium atom. Although this transfer is unexpected, transfer of a phenyl group in preference to a methyl group is not, this preference having been demonstrated by Schimidaur *et al.* by the reaction of Me_3PhSi and $[GaCl_3]$ resulting in the formation of $[PhGaCl_2]$.

2.2.29 X-ray structure of $[Cl(Ph)Ga\{N(SiMe_2Ph)_2\}]_2$ (92)

The structure of compound **92** was confirmed by X-ray crystallography, the results of which are shown in Figure 2.17; selected bond lengths and angles are given in Table 2.6. The compound consists of a slightly folded (by ca. 13° around the Cl···Cl vector) Ga_2Cl_2 ring. The bond lengths and angles of the Ga_2Cl_2 ring are very similar to those observed in $[Cy_2Ga(\mu\text{-}Cl)]_2$ (Cy = cyclohexyl), having a transannular Ga-Ga separation of 3.411(1) Å compared with 3.38 Å in the cyclohexyl species.[160] The gallium atoms are four coordinate with a extremely distorted tetrahedral geometry. The N-Ga-Cl angles are substantially enlarged from tetrahedral being 130.0(1)° and 132.9(1)° at Ga(1) and Ga(2) respectively. This enlargement is substantially greater than those observed in **83** where the Cl(1)-Ga-Cl(2) angle is only 113.12(6)°. The compound is chlorine bridged as opposed to nitrogen bridged because the lone pair which forms the bond to the second gallium atom attracted towards the electron withdrawing silicon atoms. This forces the nitrogen atom to adopt a three coordinate trigonal planar geometry as opposed to the tetrahedral geometry usually adopted by a nitrogen bridge in compounds such as **83**.

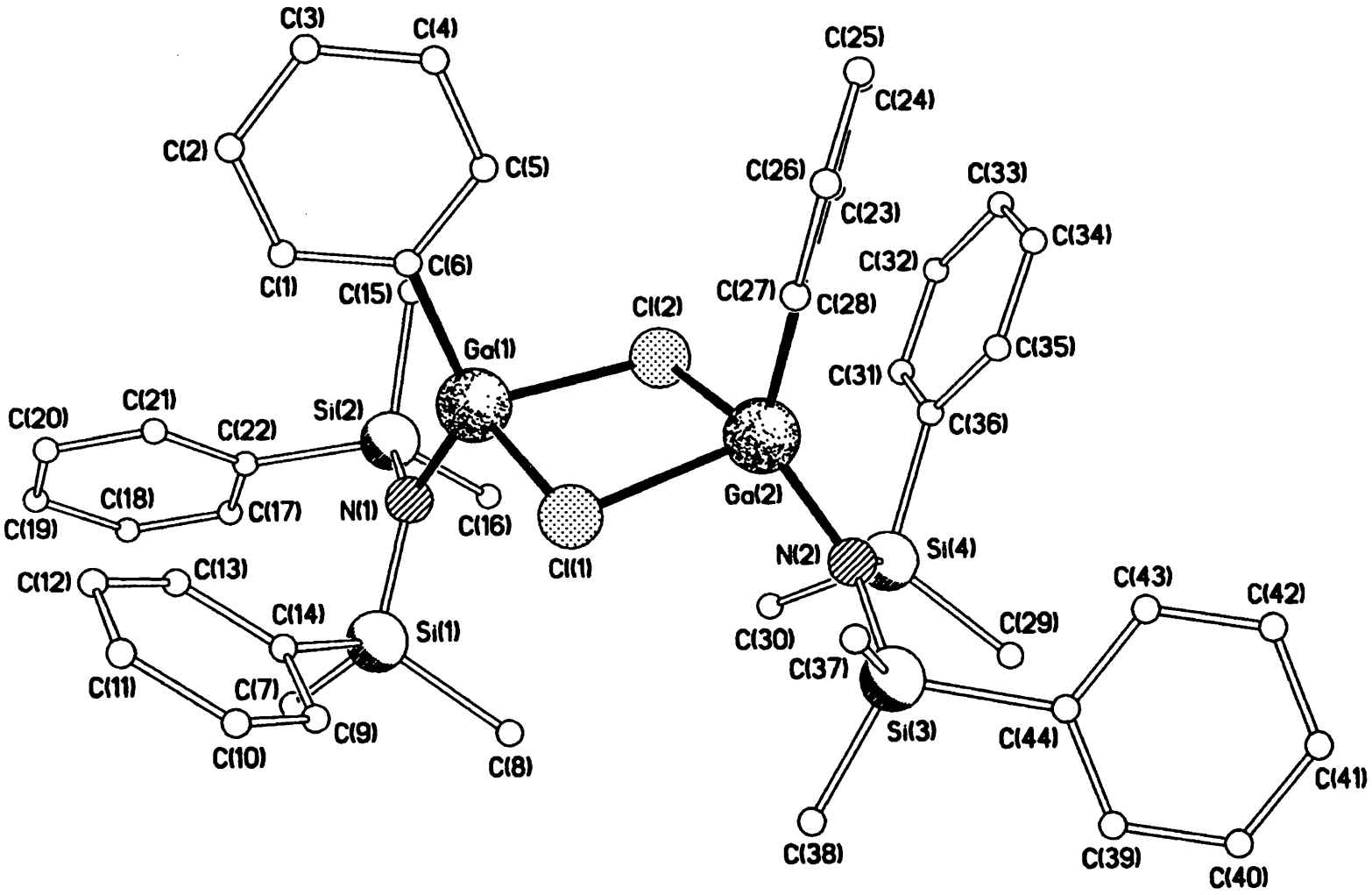

Figure 2.17 X-ray structure of $[Cl(Ph)Ga\{N(SiMe_2Ph)_2\}]_2$ (92)

Table 2.6 Selected bond lengths (Å) and angles (°) for $[Cl(Ph)Ga\{N(SiMe_2Ph)_2\}]_2$ (92)

Ga(1)-Ga(2)	2.3587(9)	Ga(1)-Cl(2)	2.3813(8)
Ga(1)-N(1)	1.850(3)	Ga(1)-C(6)	1.952(2)
Ga(2)-Cl(1)	2.4025(8)	Ga(2)-Cl(2)	2.3651(9)
Ga(2)-N(2)	1.846(2)	Ga(2)-C(28)	1.957(2)
Si(1)-N(1)	1.739(3)	Si(2)-N(1)	1.738(3)
Si(3)-N(2)	1.738(3)	Si(4)-N(2)	1.740(3)
N(1)-Ga(1)-C(6)	130.04(11)	N(1)-Ga(1)-Cl(1)	111.27(9)
C(6)-Ga(1)-Cl(1)	105.73(9)	N(1)-Ga(1)-Cl(2)	106.62(8)
C(6)-Ga(1)-Cl(2)	107.12(7)	Cl(1)-Ga(1)-Cl(2)	87.89(3)
N(2)-Ga(2)-(28)	132.93(11)	N(2)-Ga(2)-Cl(2)	109.80(9)
C(28)-Ga(2)-Cl(2)	103.97(7)	N(2)-Ga(2)-Cl(1)	106.68(9)
C(28)-Ga(2)-Cl(1)	106.76(7)	Cl(2)-Ga(2)-Cl(1)	87.25(3)
Ga(1)-Cl(1)-Ga(2)	91.50(3)	Ga(2)-Cl(2)-Ga(1)	91.87(3)

2.2.30 Synthesis of group 13 silylamine adducts

Adducts of group 13 halides and silyamines may be formed by the reaction of the appropriate complexes in hexane at room temperature. The insoluble adduct is isolated as a precipitate in good yield. This method was used by Jansen *et al* for the preparation of $[Cl_3Al\{NH(SiMe_3)_2\}]$.[129]

2.2.31 Reaction of $[GaCl_3]$ and $HN(SiMe_3)_2$ in hexane

The reaction of $HN(SiMe_3)_2$ with $[GaCl_3]$ was carried out as described above (section 2.2.30). After work-up, a white powder was isolated in 90% yield. Analytical and spectroscopic data showed that the adduct $[Cl_3Ga\{NH(SiMe_3)_2\}]$ (**39**) had formed, as shown in Eq. 2.30.

$$[GaCl_3] + HN(SiMe_3)_2 \longrightarrow [Cl_3Ga\{NH(SiMe_3)_2\}] \quad (\mathbf{2.30})$$

2.2.32 X-ray structure of $[Cl_3Ga\{NH(SiMe_3)_2\}]$ (39)

The structure of **39** was predicted by Wiberg in 1966, on the basis of infra-red data as monomeric.[128] The structure of **39** was confirmed by X-ray crystallography, the results of which are shown in Figure 2.18; selected bond lengths and angles are given in Table 2.7. The structure of **39** is disordered giving rise to two molecules A and B in which the position of the nitrogen atom is common. The structure consists of a monomeric adduct, the geometry at the gallium atom being distorted tetrahedral, similar to that observed in $[Cl_3Al\{NH(SiMe_3)_2\}]$ (**38**). The Ga-N bond length (2.007(4) Å) is significantly longer than the Ga-N bond length observed in $[Cl(Ph)Ga\{N(SiMe_2Ph)_2\}]_2$ (**92**) (1.850(3) Å). The Ga-N bond length is also significantly longer than the Al-N bond length observed in **38** (1.939(3) Å). The other bond lengths and angles are comparable in both structures.

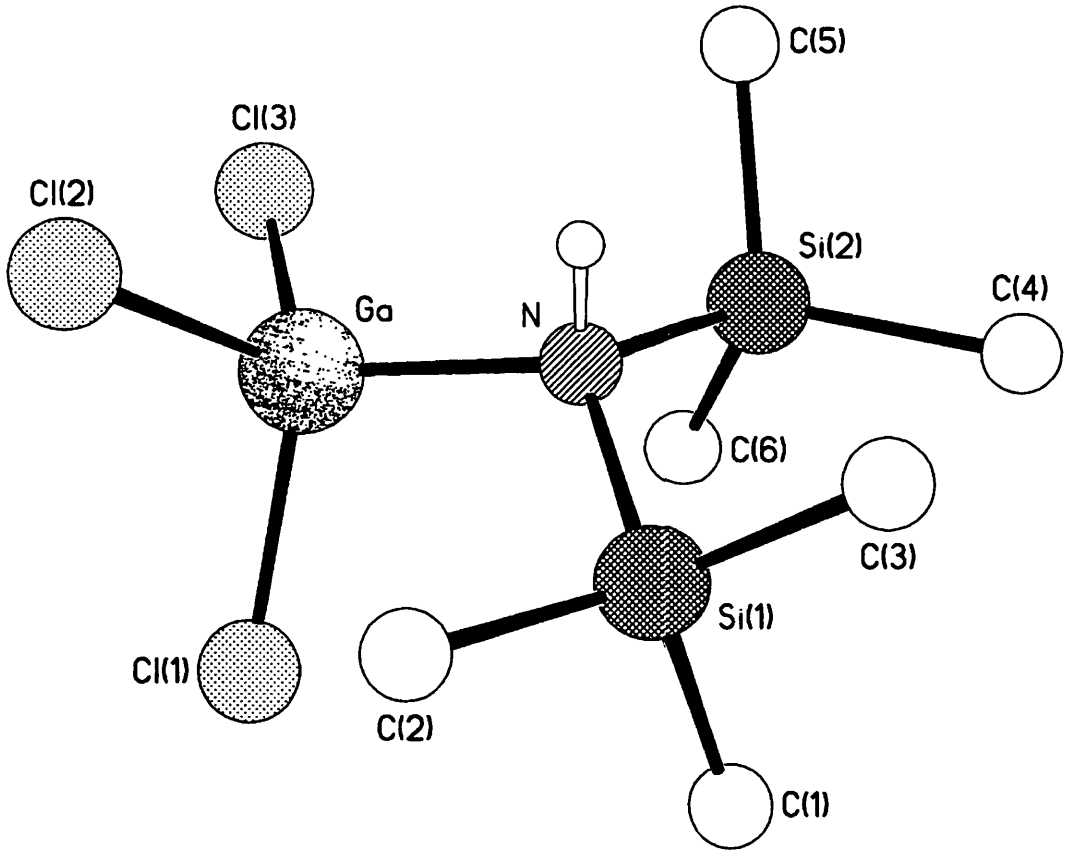

Figure 2.18 X-ray structure of $[Cl_3Ga\{NH(SiMe_3)_2\}]$ (39)

Table 2.7 Selected bond lengths (Å) and angles (°) for $[Cl_3Ga\{NH(SiMe_3)_2\}]$ (39)

	A	B
N-Si(1)	1.841(5)	1.776(14)
N-Si(2)	1.842(4)	1.87(2)
N-Ga	2.007(4)	2.059(11)
Ga-Cl(3)	2.099(3)	2.12
Ga-Cl(1)	2.170(2)	2.12
Ga-Cl(2)	2.187(2)	2.16
N-Ga-Cl(3)	115.1(2)	108.0(4)
N-Ga-Cl(1)	106.63(13)	108.9(5)
Cl(3)-Ga-Cl(1)	112.2(2)	111.8
N-Ga-Cl(2)	107.52(14)	108.5(4)
Cl(3)-Ga-Cl(2)	106.02(14)	109.7
Cl(1)-Ga-Cl(2)	109.24(14)	110.0
N-Ga-Cl(3)	115.1(2)	108.0(4)
N-Ga-Cl(1)	106.63(13)	108.9(5)
N-Ga-Cl(2)	107.52(14)	108.5(4)

2.2.33 Reaction of $[GaCl_3]$ and $HN(SiMe_2Ph)_2$ in hexane

The reaction between $[GaCl_3]$ and $HN(SiMe_2Ph)_2$ was carried out in a similar manner to that described in 2.2.30. After work-up, a white powder was obtained in 93% yield. Analytical and spectroscopic data showed that $[Cl_3Ga\{NH(SiMe_2Ph)_2\}]$ (**93**) had formed, as shown in Eq. 2.31.

$$[GaCl_3] + HN(SiMe_2Ph)_2 \longrightarrow [Cl_3GaNH(SiMe_2Ph)_2] \quad \textbf{(2.31)}$$

The infra-red spectrum was recorded and shows peaks due to N-H at 3115 cm^{-1} and 1117 cm^{-1} which are at slightly lower wavenumbers than those reported for compound **39** (3138 and 1135 cm^{-1}).[128] This may be due to differences in the Ga-N

bond strength in compounds **39** and **93** due to a small difference in the Lewis base strengths of the nitrogen in $HN(SiMe_3)_2$ and $HN(SiMe_2Ph)_2$.

2.2.34 Reaction of $[GaCl_3]$ and $HN(SiMe_2H)_2$ in hexane

The reaction between $[GaCl_3]$ and $HN(SiMe_2H)_2$ was carried out in hexane and as expected a white powder was formed. It would be expected that $[Cl_3Ga\{NH(SiMe_2H)_2\}]$ (**94**) resulted, however, the powder was not stable at room temperature and decomposed to form colourless crystals and a grey coloured material after 24 hours. This result is not unexpected as the product of the same reaction carried out in CH_2Cl_2 decomposed after one week (see section 2.2.6).

2.2.35 Reaction of $[GaCl_3]$ and $HN(^tBu)SiMe_3$ in hexane

The reaction between $HN(^tBu)SiMe_3$ and $[GaCl_3]$ was carried out in hexane at room temperature. After work-up a white powder was isolated in 79% yield. Analytical and spectroscopic data showed the white powder to be $[Cl_3Ga\{NH(^tBu)(SiMe_3)\}]$ (**95**), as shown in Eq. 2.32.

$$[GaCl_3] + HN(^tBu)(SiMe_3) \longrightarrow [Cl_3GaNH(^tBu)(SiMe_3)] \quad (\mathbf{2.32})$$

The analytical data showed reasonable agreement with that calculated for **95** with the slightly low %C probably due to small amounts of contamination from other products, which may be formed during the reaction (such as $[Cl_2Ga\{NH(^tBu)\}]_2$). The melting point was found to be 126 °C which is in good agreement with $[Cl_3Ga\{NH(SiMe_3)_2\}]$ (**39**) (126 - 128 °C).[128] The narrow melting point range indicates that compound **95** is the major species formed in the reaction. The infra-red spectrum shows the major peak due to N-H at 3152 cm^{-1}, which is also in good agreement with the value published for **39**. [128]

2.2.36 Reaction of [$GaBr_3$] and $HN(SiMe_3)_2$ in hexane

The reaction of [$GaBr_3$] and $HN(SiMe_3)_2$ was carried out using the method described in section 2.2.30. After work-up, a white powder was obtained in 56% yield. Analytical and spectroscopic data showed this powder to be [$Br_3Ga\{NH(SiMe_3)_2\}$] (**96**), as shown in Eq. 2.33.

$$[GaBr_3] + HN(SiMe_3)_2 \longrightarrow [Br_3Ga\{NH(SiMe_3)_2\}] \quad (\mathbf{2.33})$$

The melting point was determined as 113 - 115 °C, which is lower than **39**. It would be expected that the melting point of **96** would be higher because of the increased mass of the molecules. This suggests that the intermolecular interactions between the molecules in **96** are weaker than those in **39**. The infra-red spectrum was recorded and showed the peaks at 3141 and 1116 cm^{-1}, again indicating the presence of a N-H bond.

2.2.37 Reaction of [$GaBr_3$] and $HN(SiMe_2Ph)_2$

The reaction of [$GaBr_3$] and $HN(SiMe_2Ph)_2$ was carried out as described in 2.2.30. Work-up yielded a white powder in 77% yield. Analytical and spectroscopic data showed that [$Br_3Ga\{NH(SiMe_2Ph)_2\}$] (**97**) had formed, as shown in Eq. 2.34.

$$[GaBr_3] + HN(SiMe_2Ph)_2 \longrightarrow [Br_3GaNH(SiMe_2Ph)_2] \quad (\mathbf{2.34})$$

The analytical data is in good agreement with that calculated for **97** and the melting point, which was determined as 108-109 °C, was similar to compound **96**. As would be expected, the infra-red spectrum showed the peaks due to N-H at 3155 and 1116 cm^{-1}.

2.2.38 Reaction of [$GaBr_3$] and $HN(^tBu)SiMe_3$

The reaction of [$GaBr_3$] and $HN(^tBu)SiMe_3$ was carried out as described in 2.2.29. Analytical and spectroscopic data showed the resulting white powder to be

$[Br_3Ga\{NH(^tBu)(SiMe_3)\}]$ (**98**) which was formed in 65% yield. The analytical data corresponded reasonably to the calculated data for **98** although the %C found was slightly low, which could be due to formation of other products. The infra-red spectrum showed the peak due to the N-H bond at 3145 cm^{-1}. Unexpectedly, it was found that the compound decomposed without melting below 230 °C. This suggests that the compound may not be volatile or very stable in the vapour phase and so unsuitable for use in CVD.

2.2.39 Reaction of $[Me_2AlCl]$ and $HN(SiMe_2Ph)_2$

The reaction of $[Me_2AlCl]$ and $HN(SiMe_2Ph)_2$ was carried out as described in section 2.2.30. After work-up and cooling to -20 °C colourless crystals suitable for X-ray crystallography were obtained. Spectroscopic data indicated that the species $[Cl_2(Me)Al\{NH(SiMe_2Ph)_2\}]$ (**99**) had been formed. X-ray crystallography showed the crystals to consist of a mixture of **99** and $[Cl(Me)_2Al\{NH(SiMe_2Ph)_2\}]$ (**100**) in approximately a 2:1 ratio. The ^1H NMR spectrum shows two different $AlCH_3$ environments are present in solution. Three peaks are observed due to the dimethylsilyl protons and numerous peaks are observed due to the phenyl group. The expected product of the reaction $[Cl(Me)Al\{NH(SiMe_2Ph)\}]_2$ (**101**) does not appear to have been formed in the reaction. The formation of **100** is straight forward, however the formation of **99** is more complex and involves the exchange of one of the methyl groups attached to the aluminium with a chlorine atom. To the best of our knowledge an exchange of this nature occurring in a reaction between an aluminium complex and a silylamine is unprecedented. This exchange may explain the low yield of the reaction. To confirm that **99** is a major product of the reaction it would be necessary to repeat the reaction and analyse the product formed.

2.2.40 X-ray structure of $[Cl_2(Me)Al\{NH(SiMe_2Ph)_2\}]$ (99)

The structure of **99** was determined by X-ray crystallography and is shown in Figure 2.19, selected bond lengths and angles for **99** are given in Table 2.8. The structure was found to consist of 80% $[Cl_2(Me)Al\{NH(SiMe_2Ph)_2\}]$ (**99**) and 20% $[Cl(Me)_2Al\{NH(SiMe_2Ph)_2\}]$ (**100**), although only the structure of **99** could be determined with reasonable accuracy. The structure also shows disorder at C(1) and

Cl(2) with positions C(1') and Cl(2') being those of the disordered structure. Compound **99** is monomeric, the Al-N bond length (2.001(2) Å) is significantly longer than the Al-N bond length observed in $[Cl_3Al\{NH(SiMe_3)_2\}]$ (**38**) (1.939(3) Å).[129] The geometry at the aluminium is distorted tetrahedral (N-Al-Cl(1) 103.77(8)°) which is comparable to the geometry observed in **38**.

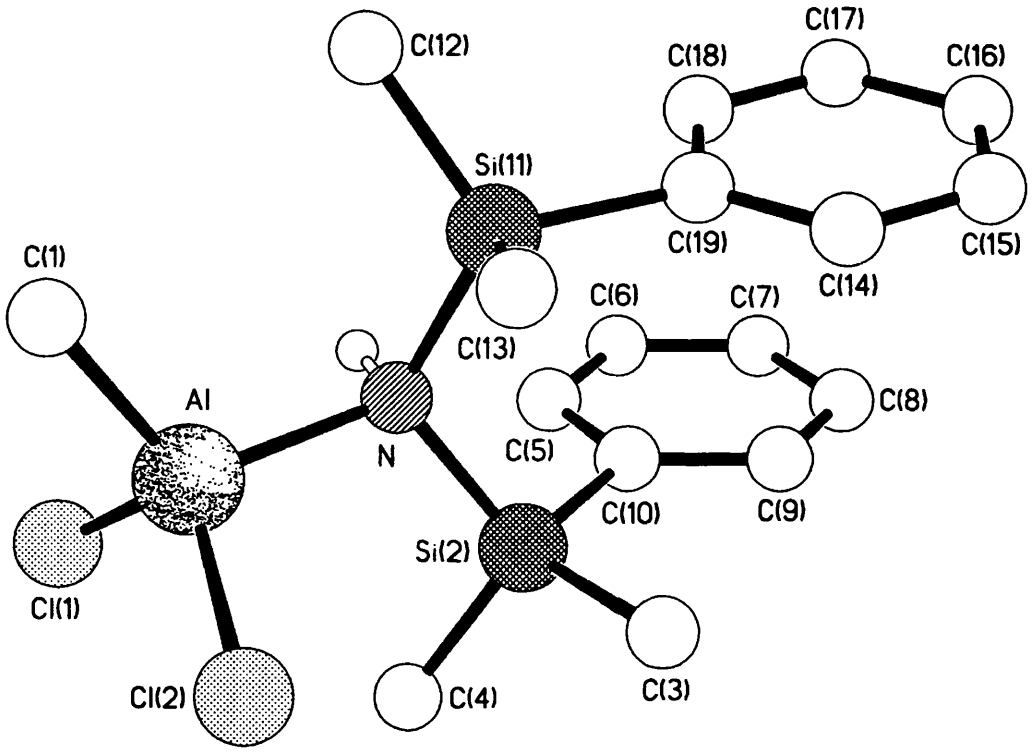

Figure 2.19 X-ray structure of $[Cl_2(Me)Al\{NH(SiMe_2Ph)_2\}]$ (99)

Table 2.8 Selected bond lengths (Å) and angles (°) for $[Cl_2(Me)Al\{NH(SiMe_2Ph)_2\}]$ (99)

Al-C(1)	1.932(4)	Al-C(1')	1.959(5)
Al-N	2.001(2)	Al-Cl(2)	2.101(2)
Al-Cl(2')	2.118(4)	Al-Cl(1)	2.1708(12)
N-Si(11)	1.835(2)	N-Si(2)	1.836(2)
Si(2)-C(4)	1.848(3)	Si(2)-C(3)	1.850(3)
Si(2)-C(10)	1.883(2)	Si(11)-C(12)	1.847(3)
Si(11)-C(13)	1.851(3)	Si(11)-C(19)	1.889(2)
C(1)-Al-N	117.1(4)	C(1')-Al-N	111.9(6)
C(1)-Al-Cl(2)	110.3(3)	N-Al-Cl(2)	107.21(13)
C(1')-Al-Cl(2')	110.9(6)	N-Al-Cl(2')	111.7(3)
C(1)-Al-Cl(1)	108.2(3)	C(1')-Al-Cl(1)	112.7(7)
N-Al-Cl(1)	103.77(8)	Cl(2)-Al-Cl(1)	109.98(12)
Cl(2')-Al-Cl(1)	105.6(4)		

2.2.41 Synthesis of group 13 silylarsenides

The reaction of $[GaCl_3]$ and $As(SiMe_3)_3$ is known to yield GaAs. However, it would be interesting to isolate a gallium silylamide which may act as a single source precursor to GaAs. Thus, reactions of $[GaCl_3]$ and $As(SiMe_2R)_3$ (where R = Ph, ^tBu) were investigated. The compounds $As(SiMe_2Ph)_3$ and $As(SiMe_2{}^tBu)_3$ were prepared by literature routes.[161,162]

2.2.42 Reaction of $[GaCl_3]$ and $As(SiMe_2Ph)_3$

The reaction of $[GaCl_3]$ and $As(SiMe_2Ph)_3$ was carried out at -78 °C in CH_2Cl_2. A cream coloured precipitate formed which was removed by filtration through Celite. The resulting orange coloured solution was cooled to -20 °C and an orange coloured powder had formed after 1 week. Analytical and spectroscopic data showed that $[Cl_2Ga\{As(SiMe_2Ph)_2\}]_n$ (**102**) had formed (Eq. 2.35).

$$[GaCl_3] + As(SiMe_2Ph)_3 \longrightarrow [Cl_2GaAs(SiMe_2Ph)_2] + Me_2PhSiCl \quad (\mathbf{2.35})$$

The analytical data is in good agreement with the values calculated for **102** although the %C observed was slightly lower than expected. This may be due to contamination by other products formed during the reaction. The ^1H NMR shows several peaks which are due to methyl group protons and a wide multiplet due to the phenyl group protons. This suggests that either the solution behaviour of **102** is complex or a number of different products have been formed. The low yield of the reaction (33%) suggests that other products have been formed during the reaction which were not isolated. The precipitate formed could be an insoluble product such as $[ClGa\{As(SiMe_2Ph)\}]_n$.

2.2.43 Reaction of $[GaCl_3]$ and $As(SiMe_2{}^tBu)_3$

The reaction of $[GaCl_3]$ and $As(SiMe_2{}^tBu)_3$ was carried out using the procedure described in 2.2.41. However, on cooling overnight a dark brown precipitate formed. This suggests that decomposition had occurred.

2.3 Decomposition studies

In this section the potential of group 13 silylpnictides as precursors to thin films and bulk materials is explored. The decomposition pathways of some of the precursors, whose preparation was described in section 2.2, were explored by Thermal Gravimetric Analysis (TGA). The compounds $[Cl_2Ga\{NH(SiMe_3)\}]_2$ (**32**), $[Cl_3Ga\{NH(SiMe_3)_2\}]$ (**39**), $[Cl_2Ga\{HN(SiMe_2Ph)\}]_2$ (**83**), $[Et_2Al\{N(SiMe_2H)_2\}]_n$ (**89**) and $[Cl_2Ga\{As(SiMe_2Ph)_2\}]_n$ (**102**) were pyrolysed under a number of conditions to ascertain their suitability as single-source precursors to bulk group 13 pnictides. Vapour-phase deposition studies of **39** and **89** were carried out in order to assess the ability of silylamides to produce thin films. The films produced were analysed in an attempt to determine the phase of the material produced and the amount of contamination present.

2.3.1 Thermal Gravimetric Analysis

Initial investigations into the suitability of using the compounds prepared as precursors to group 13 pnictides involved obtaining TGA. Typically, a known amount (approximately 10 mg) of the sample was heated from 20 to 500 °C in a sealed aluminium pan under N_2 at a uniform rate of 10 °C per minute. Before the heating is carried out a small pinhole is made in the lid of the pan to allow the gaseous decomposition products to escape. During the experiment, N_2 is flowed across the pan to avoid oxidation of the sample and to remove any gaseous byproducts. By measuring the weight of the pan during the experiment a graph of weight against temperature may be plotted. Any weight losses and the temperature they occur at are obtained, which in turn gives information on the decomposition pathway. Therefore, the temperature required for decomposition of the precursor to occur is also identified (if <500 °C). This is important data if the precursor is to be considered for use in CVD. A compound should not decompose at too high a temperature or the range of substrates, which may be deposited upon, is limited. Decomposition at too low a temperature is also a problem as the compound must be stable at the temperatures required to transport it in the vapour phase to avoid decomposition before the substrate.

2.3.2 Decomposition properties of $[X_2Ga\{NHR\}]_n$

The synthesis of the potential precursors $[X_2Ga\{NHR\}]_n$ (where X = Cl, R = $SiMe_3$ (**32**), $SiMe_2Ph$ (**83**), ^tBu (**84**); X = Br, R = $SiMe_3$ (**33**)) was discussed in section 2.2. The decomposition properties of these compounds were measured using TGA and compared. The decomposition of $[X_2Ga\{NH(SiMe_3)\}]_2$ (where X = Cl (**32**), Br (**33**) (shown in Fig. 2.20)) are clean and show total weight losses of 52% and 67% respectively. This does not indicate that decomposition to GaN has occurred by 500 °C (where the total weight loss would be 63% and 74% respectively). However, these results suggest that decomposition to form GaN may occur at slightly above 500 °C as shown by the fact that both samples are still losing weight at 500 °C (shown by the downward slope in the TGA). The TGA of **32** and **33** indicate that a two step decomposition process is occurring. The first step occurs in the temperature range 175 - 300 °C for **32** and 160 - 220 °C for **33** and involves a weight loss of 47%

for both compounds. This suggests that the complexes are decomposing with loss of $XSiMe_3$ to form a material of the type $[XGaNH]_n$ (calculated weight losses X = Cl, 47%; X = Br, 48%), as shown in Eq. 2.36.

$$[X_2Ga\{NH(SiMe_3)\}]_2 \longrightarrow 2/n\,[XGaNH]_n + 2\,XSiMe_3 \quad \textbf{(2.36)}$$

The loss of HX to form GaN, which is the second step in the decomposition pathway, is calculated to be 16% (X = Cl) and 25% (X = Br), as shown in Eq. 2.37. The overall weight losses therefore show that not all the HX is lost and that distinct steps are not observed in the temperature ranges, therefore the steps occur in overlap.

$$[XGaNH]_n \longrightarrow n\,GaN + 2\,HX \quad \textbf{(2.38)}$$

Recently, the imido species $[ClGaNH]_n$ (n = 1-4, 6) has been computationally investigated as an intermediate in the decomposition of the adduct $[Cl_3Ga\{NH_3\}]$ to give GaN.[163] In this investigation the authors concluded that HCl would be a poor leaving group when compared with H_2 or CH_4, due to the strong Ga-Cl bond compared with Ga-H and Ga-C bonds.

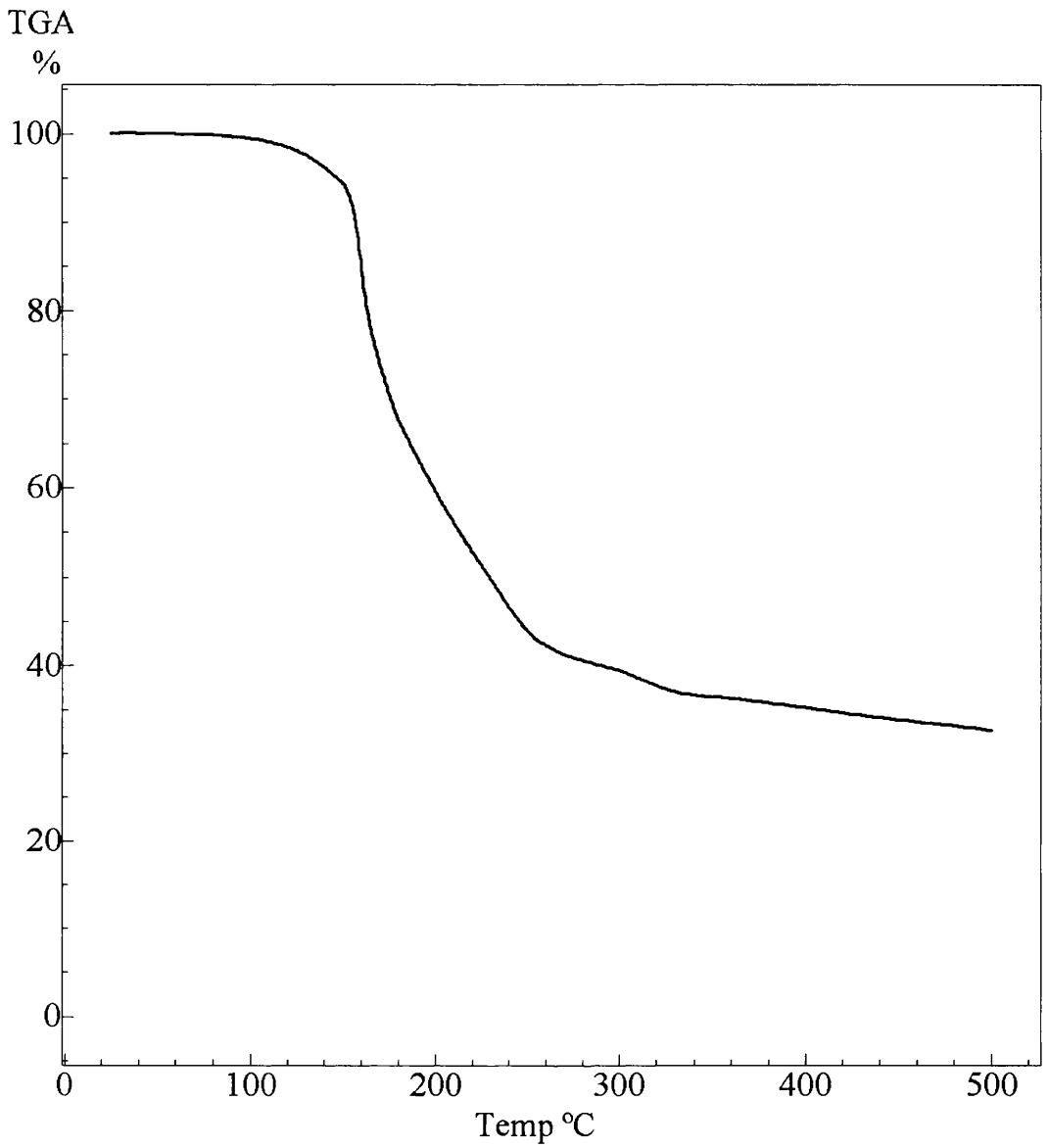

Figure 2.20 TGA of $[Br_2Ga\{NH(SiMe_3)\}]_2$ (33)

The TGA of $[Cl_2Ga\{NH(SiMe_2Ph)_2\}]_2$ (**83**) shows a total weight loss of 70% which is close to the calculated total weight loss of 71%. If a similar decomposition pathway to that suggested for **32** was followed then such complete decomposition would not be expected as the first step would form a material of composition $[ClGaNH]_n$. The two observed weight losses (44% and 26%) do not correspond with those expected (59% and 13%). This suggests that an alternative decomposition pathway is taking place or that more than one decomposition process may occur.

The TGA of $[Cl_2Ga\{NH(^tBu)\}]_2$ (**84**) shows two distinct weight losses between 160 - 280 °C (55%) and 310 - 450 °C (12%), which suggests that complete decomposition may have occurred. The total weight loss is therefore 67%, which is slightly greater than the calculated total weight loss to GaN (61%). This may be due to minor quantities of the sample subliming during the TGA or to a small error in recording the initial mass. The decomposition of **84** does not appear to follow a similar route to the decomposition of **32** because $[ClGaNH]_n$ would be formed as the result of the first step and this species would not be expected to decompose below 500 °C. However, the ^tBu group has the ability to leave via a β-hydride elimination pathway and therefore a different decomposition route may be followed. Groups which undergo β-hydride elimination (e.g. Et, ^tBu) are often used in single-source precursors due to their ability to undergo clean decomposition at low temperature.

The decomposition properties of $[Cl_2In\{NH(SiMe_3)\}]_n$ were not determined in this study. This was because it would not be expected that the precursor would decompose below 500 °C (compared with **32**) and InN is thermally unstable at 500 °C which may lead to misinterpretation of the results.

2.3.3 Decomposition properties of $[Et_2Al\{N(SiMe_2H)_2\}]_n$

The decomposition properties of $[Et_2Al\{N(SiMe_2H)_2\}]_n$ (**89**) were determined by TGA and the results are shown in Figure 2.21. The decomposition of **89** is clean and shows a total weight loss of 79% starting at 40 °C and finishing at 500 °C. The calculated total weight loss to form AlN is 81% and given the accuracy of the TGA used (*ca.* 2%) this indicates AlN is formed at temperatures below 500 °C. There are no obvious features in either the TGA or the first derivative (a measure of change in weight against time) to suggest that two distinct decomposition steps occur. Therefore, no information is given on the decomposition route. Decomposition may occur with loss of two equivalents of $HSiMe_2Et$ or via a more complex β-hydride decomposition pathway.

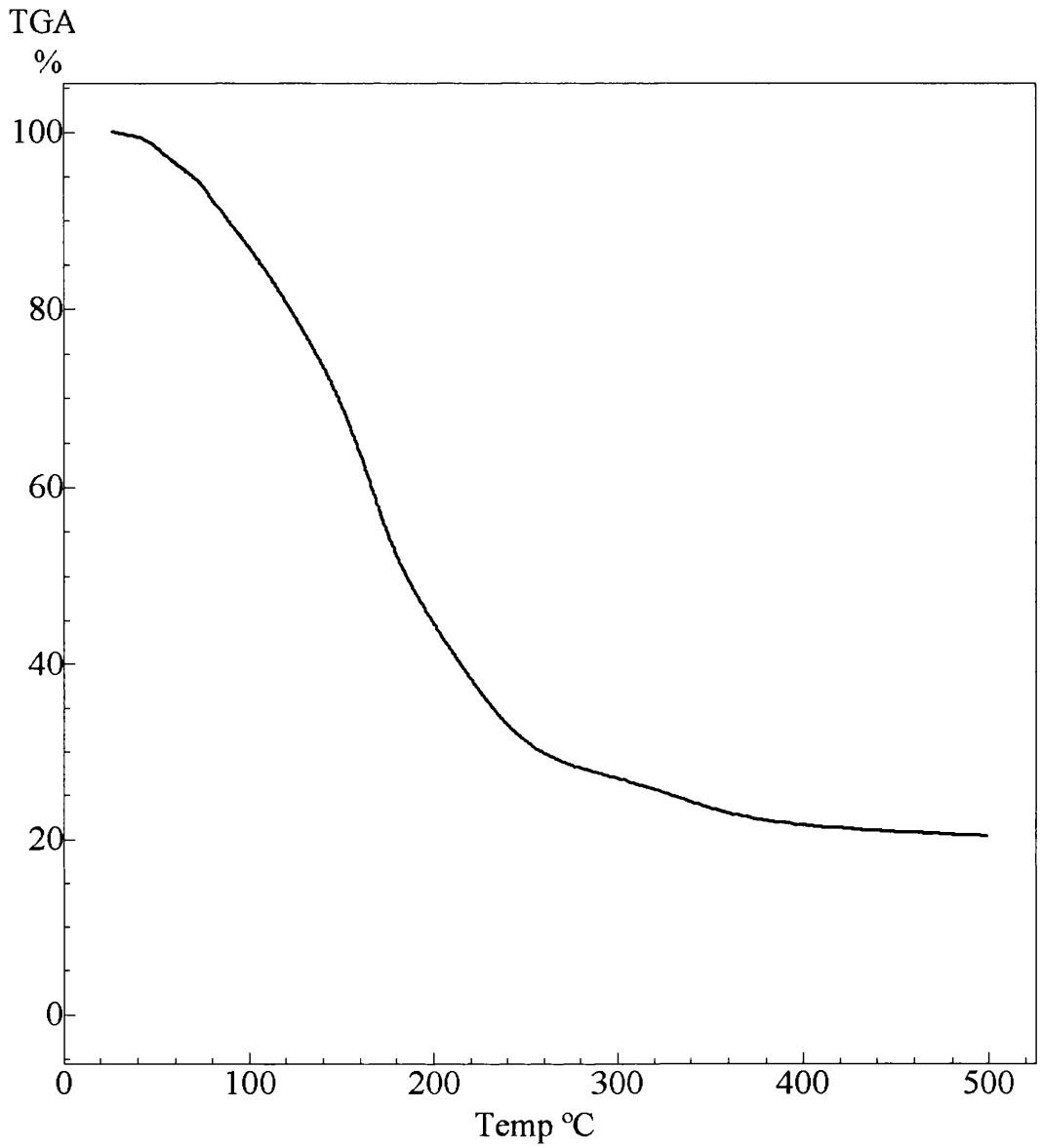

Figure 2.21 TGA of $[Et_2Al\{N(SiMe_2H)_2\}]_n$ (89)

2.3.4 Decomposition of $[X_3Ga\{NH(R)R'\}]$

The synthesis of the adducts $[X_3Ga\{NH(R)R'\}]$ (where X = Cl, Br, R = R' = $SiMe_3$, $SiMe_2Ph$; X = Cl, Br, R = ^tBu, R' = $SiMe_3$) is described in section 2.2. In this section the decomposition properties of these adducts is described and compared to the decomposition properties of the related complexes $[X_2Ga\{NHR\}]_n$ (described in 2.3.2). The TGA obtained for $[Br_3Ga\{NH(SiMe_3)_2\}]$ (**96**) is shown in Figure 2.22.

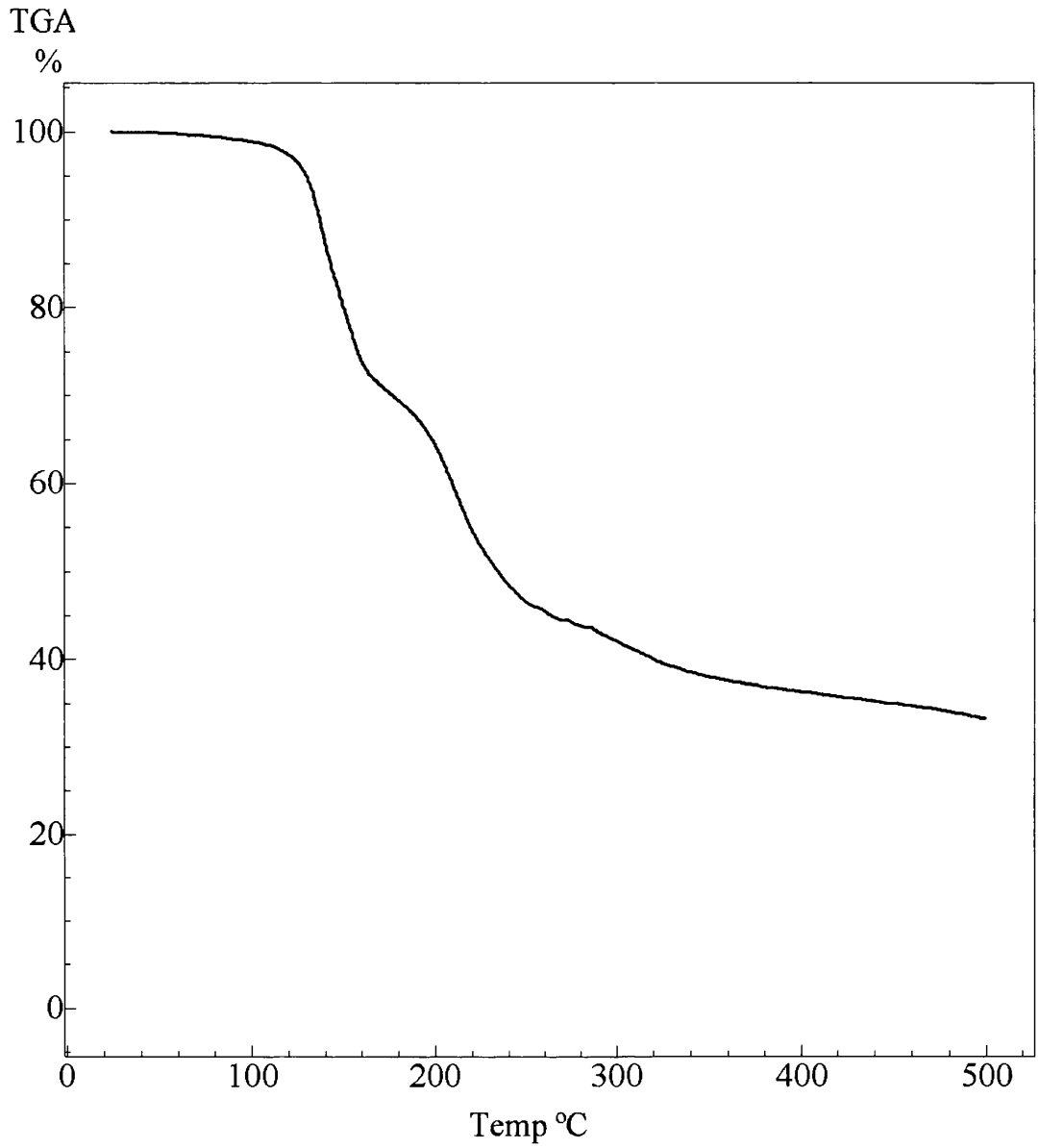

Figure 2.22 TGA of $[Br_3Ga\{NH(SiMe_3)_2\}]$ (96)

The decomposition of $[X_3Ga\{NH(SiMe_3)_2\}]$ (where X = Cl (**39**), Br (**96**)) is clean and shows total weight losses of 71% and 65% respectively. Complete decomposition to GaN has not taken place instead the material $[XGaNH]_n$ has been formed. The TGA of $[X_3Ga\{NH(SiMe_3)_2\}]$ show two weight losses (see Figure 2.22) of approximately equal size (31% where X = Cl and 32% where X = Br), each corresponding to the loss of a $XSiMe_3$ group (calculated as 32% and 33% respectively). These weight losses occur in the temperature range 120 - 400 °C and result in the formation of $[XGaNH]_n$.

The TGA of $[Cl_3Ga\{NH(SiMe_2Ph)_2\}]$ (**93**) shows an overall weight loss of 82% which corresponds to the weight loss expected (81%) if complete decomposition occurs. As was suggested for $[Cl_2Ga\{NH(SiMe_2Ph)\}]_2$ (**83**), the decomposition pathway for **93** is different to that followed by compounds **39** and **96**. The TGA of $[Br_3Ga\{NH(SiMe_2Ph)_2\}]$ (**97**) shows an overall weight loss of 69% which indicates that complete decomposition has not occurred. These results suggest that, in contrast to **93**, decomposition of **97** occurs via a similar pathway to $[X_3Ga\{NH(SiMe_3)_2\}]$ where two equivalents of $Me_2PhSiBr$ are lost followed by loss of HBr. The weight loss of 69% corresponds well with the calculated weight loss for removal of two equivalents of $Me_2PhSiBr$ (72%).

The TGA of $[Cl_3Ga\{NH(^tBu)SiMe_3\}]$ (**95**) shows an overall weight loss of 53% which unexpectedly does not correspond with complete decomposition to GaN, as might be suggested by the decomposition of $[Cl_2Ga\{NH(^tBu)\}]_2$ (**84**). Two weight losses are observed at temperatures between 60 - 140 °C (20%) and 150 - 300 °C (33%). These correspond with the loss of butene (18%) and $ClSiMe_3$ (34%). Butene would be one of the expected products if a decomposition pathway involving β-hydride elimination occurred. The TGA of $[Br_3Ga\{NH(^tBu)SiMe_3\}]$ (**98**) (see Figure 2.23) shows a total weight loss of 81%, indicating that complete decomposition has occurred (calculated as 81%). Four weight losses are visible in the TGA but the derivative shows that the first two weight losses are overlapping. Therefore, the size of the weight losses cannot be determined accurately and no useful information on the mechanism of the decomposition can be obtained. The final weight loss suggests that butene is being formed which would be expected if the decomposition occurred via a β-hydride mechanism.

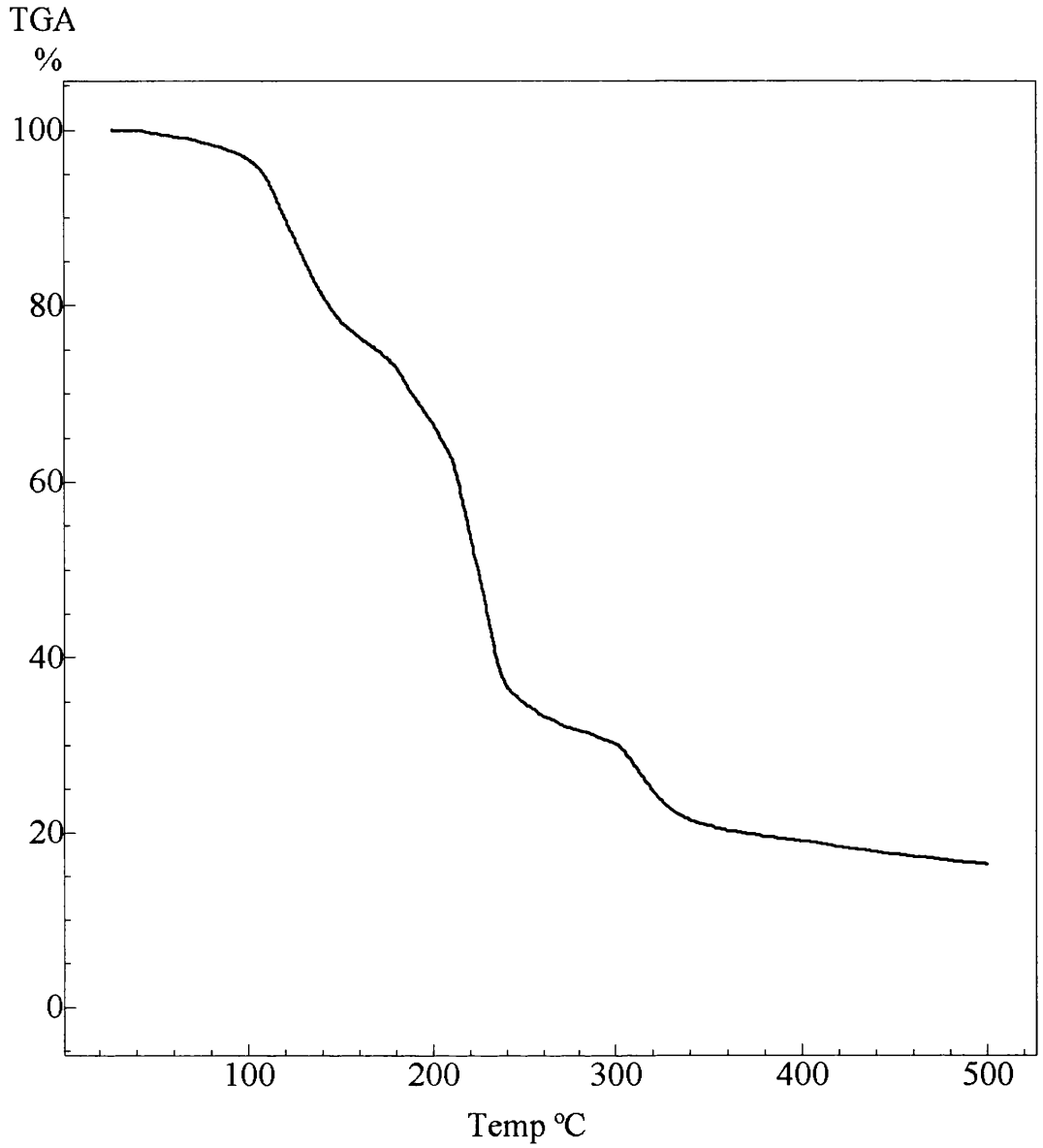

Figure 2.23 TGA of $[Br_3Ga\{NH(^tBu)SiMe_3\}]$ (95)

2.3.5 Decomposition of $[Cl_2Ga\{As(SiMe_2Ph)_2\}]_n$

The decomposition properties of $[Cl_2Ga\{As(SiMe_2Ph)_2\}]_n$ (**102**) were investigated by TGA and the results are shown in Figure 2.24. The total weight loss for **102** is 67%, which indicates that complete decomposition to GaAs has occurred (calculated 70%). Only one weight loss is observed corresponding with the loss of two equivalents of $Me_2PhSiCl$. The temperature range in which decomposition

occurred was between 80 °C and 360 °C which suggests that **102** may be a good low temperature precursor to GaAs.

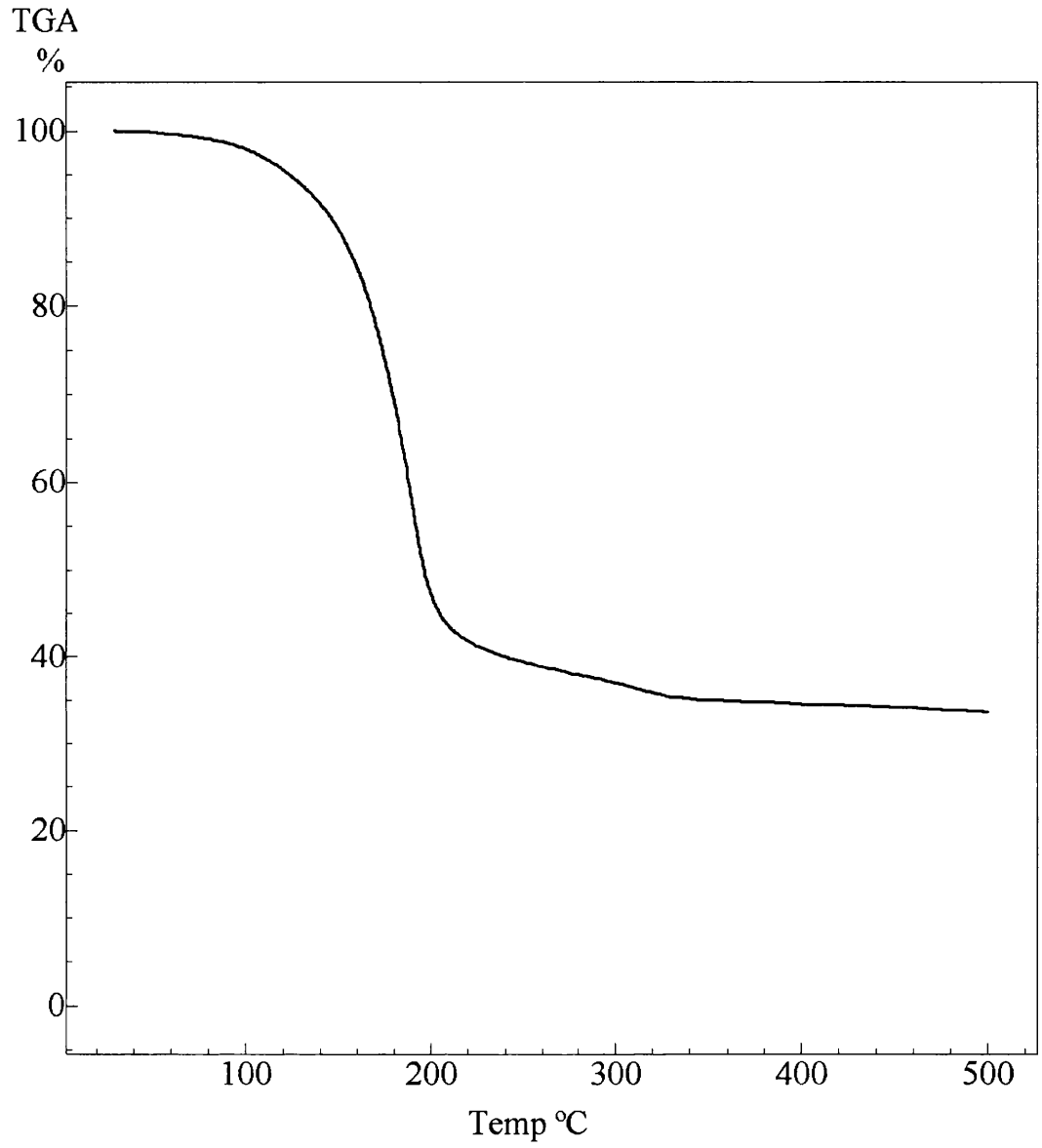

Figure 2.24 TGA of $[Cl_2Ga\{As(SiMe_2Ph)_2\}]_n$ (102)

2.3.6 Preparation of bulk group 13 pnictides

Given the results obtained from TGA, pyrolysis studies were carried out on $[Cl_2Ga\{NH(SiMe_3)\}]_2$ (**32**), $[Cl_2Ga\{NH(SiMe_2Ph)\}]_2$ (**83**), $[Cl_3Ga\{NH(SiMe_3)_2\}]$ (**39**) and $[Cl_2Ga\{As(SiMe_2Ph)_2\}]_n$ (**102**) in order to assess whether bulk gallium

pnictides could be made from these compounds. The experimental procedure adopted is described in section 2.4.

2.3.7 Bulk decomposition of gallium silylamides

Initial attempts to prepare bulk GaN involved the pyrolysis of **32** under a N_2 atmosphere. To minimise loss of the precursor due to vaporisation, the sample was loaded into an ampoule which was then placed in a pre-heated oven. The results of pyrolysis carried out over a range of temperatures are shown in Table 2.9.

Table 2.9. Analytical and powder XRD data for the decomposition of $[Cl_2Ga\{NH(SiMe_3)\}]_2$ (32) at different temperatures

Temperature °C	%C	%H	%N	%Cl	Appearance	Powder XRD
350	2.84	2.37	9.13	24.05	White	-
450	1.36	0.33	7.92	-	Pale grey	Amorphous
500	0.41	0.56	12.17	24.27	Grey	Amorphous
550	0.24	0.88	10.24	-	Grey	Amorphous
650	0.42	0.42	11.87	15.91	Pale yellow	Weakly crystalline
750	0.41	0.54	12.43	16.11	Yellow	Mixture - cubic
850	1.91	0.81	13.39	5.24	Yellow	Mixture - hexagonal

Pyrolysis of **32** between 350 and 500 °C gave rise to amorphous samples which were found to contain low levels of carbon and high levels of chlorine (by elemental analysis). From the TGA of **32** the formation of $[ClGaNH]_n$ was proposed which corresponds with the high %Cl obtained (H, 0.84%; Cl, 29.50%). If $[ClGaNH]_n$ is air sensitive this may lead to an inaccuracy in the determination of the amount of chlorine present (determination of %Cl involves handling the sample in air). At decomposition temperatures between 650 and 750 °C the amount of chlorine

was found to be lower (~10%) although it is still significant indicating that incomplete decomposition has taken place. The powder X-ray diffraction (XRD) patterns recorded for the samples heated to 750 and 850 °C indicate that a material similar to that prepared by Gladfelter *et al* from $[H_2GaNH_2]_3$ is obtained.[58] These materials appear to adopt a structure which consists of a random arrangement of cubic and hexagonal layers of GaN. The diffraction pattern for the sample pyrolysed at 750 °C is shown in Figure 2.25 along with the calculated pattern for cubic GaN, and shows that the cubic phase is dominant. The sample which was pyrolysed at 850 °C had a significantly lower chlorine content than those decomposed at lower temperatures. The powder XRD pattern for the material obtained at 850 °C is shown in Figure 2.26 against the powder XRD pattern recorded for a commercial sample of GaN and indicates that the hexagonal phase has mainly formed. This suggests that at lower temperatures cubic GaN is formed and at higher temperatures the hexagonal phase is dominant. Compound **32** was also annealed at temperatures above 850 °C and the powder XRD was obtained. However, similar patterns to that recorded for the sample decomposed at 850 °C were obtained. Decomposition under an NH_3 atmosphere did not lead to any difference in the powder XRD recorded or to the amount of impurities found in the samples prepared. A study carried out by Gladfelter *et al* in which samples of cubic GaN were heated to 900 °C for various lengths of time, showed that a phase transition from cubic to hexagonal occurs.[58] However, after 7 hours partial transition had occurred and a powder XRD showing both cubic and hexagonal phases was recorded. These results suggest that cubic GaN may be formed during the decomposition, however, at higher temperatures a phase transition takes place leading to the formation of some hexagonal GaN.

Pyrolysis experiments were also carried out on $[Cl_3Ga\{NH(SiMe_3)_2\}]$ (**39**) and $[Cl_2Ga\{NH(SiMe_2Ph)\}]_2$ (**83**). It was found that **39** could be used to prepare cubic GaN and mixed cubic/hexagonal GaN in a similar manner to **32**. However, the decomposition of **83** led to the formation of amorphous material at all decomposition temperatures and higher levels of impurities were detected. This supports the TGA data which suggested that a complex decomposition pathway may occur.

2.3.8 Bulk decomposition of $[Cl_2Ga\{As(SiMe_2Ph)_2\}]_n$ (102)

The bulk decomposition of $[Cl_2Ga\{As(SiMe_2Ph)_2\}]_n$ (**102**) was carried out in a similar manner to that described in 2.3.7. A decomposition temperature of 750 °C was used and a black powder was formed. Energy dispersive X-ray analysis (EDXA) was carried out on the powder and an approximately 1:1 ratio of Ga:As was found. Chlorine (1.7%) and silicon (11.2%) impurities were also observed in the powder, although it may be possible to reduce the impurity levels by annealing the powder or carrying the decomposition out at a higher temperature. Powder XRD was carried out and the results are shown in Figure 2.27 along with the calculated pattern for GaAs. The results show that crystalline GaAs has been formed and a good match between the experimental and calculated data is observed.

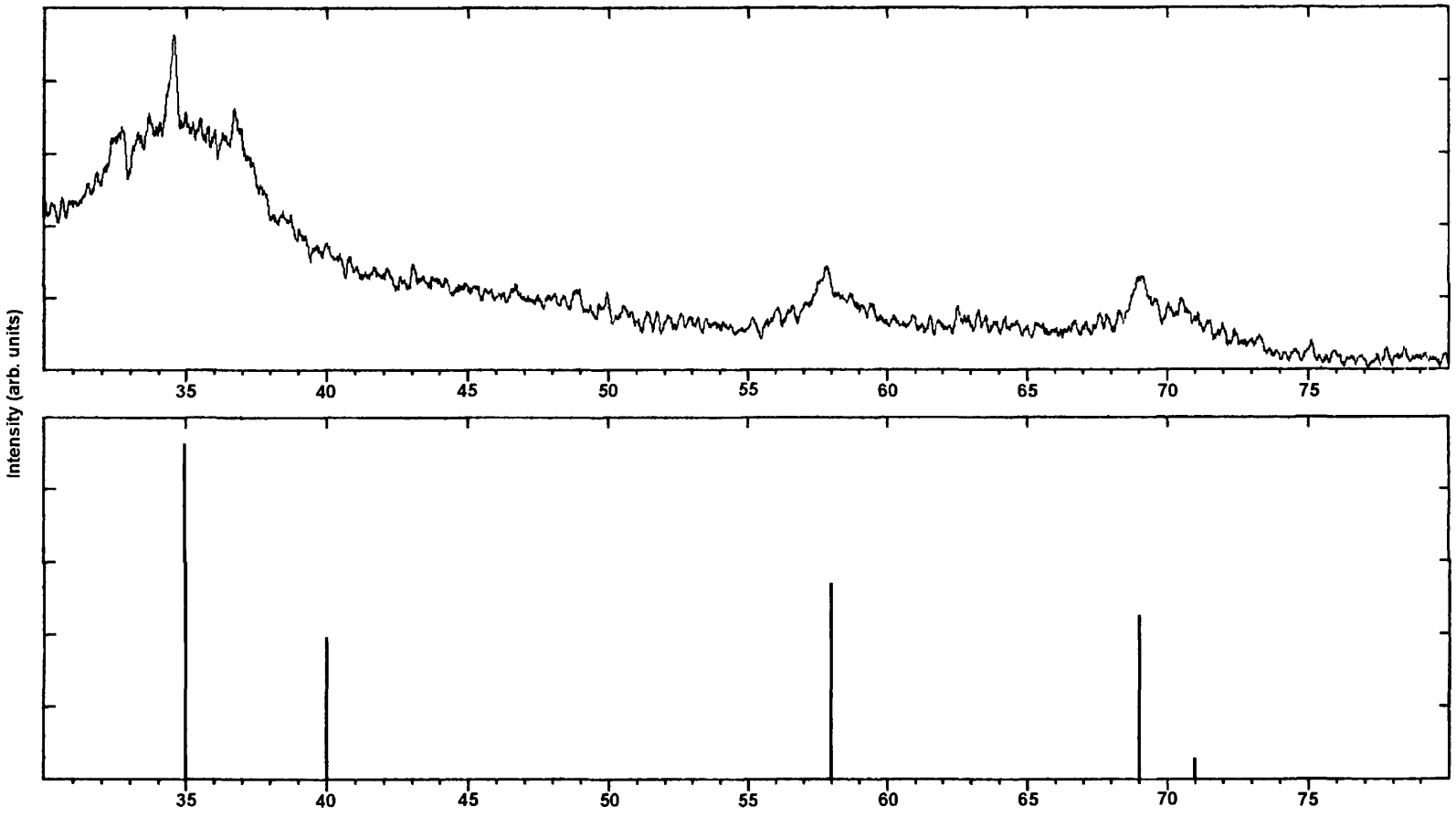

Figure 2.25 XRD pattern for sample of GaN prepared at 750 °C (upper) and the calculated pattern for cubic GaN (lower)

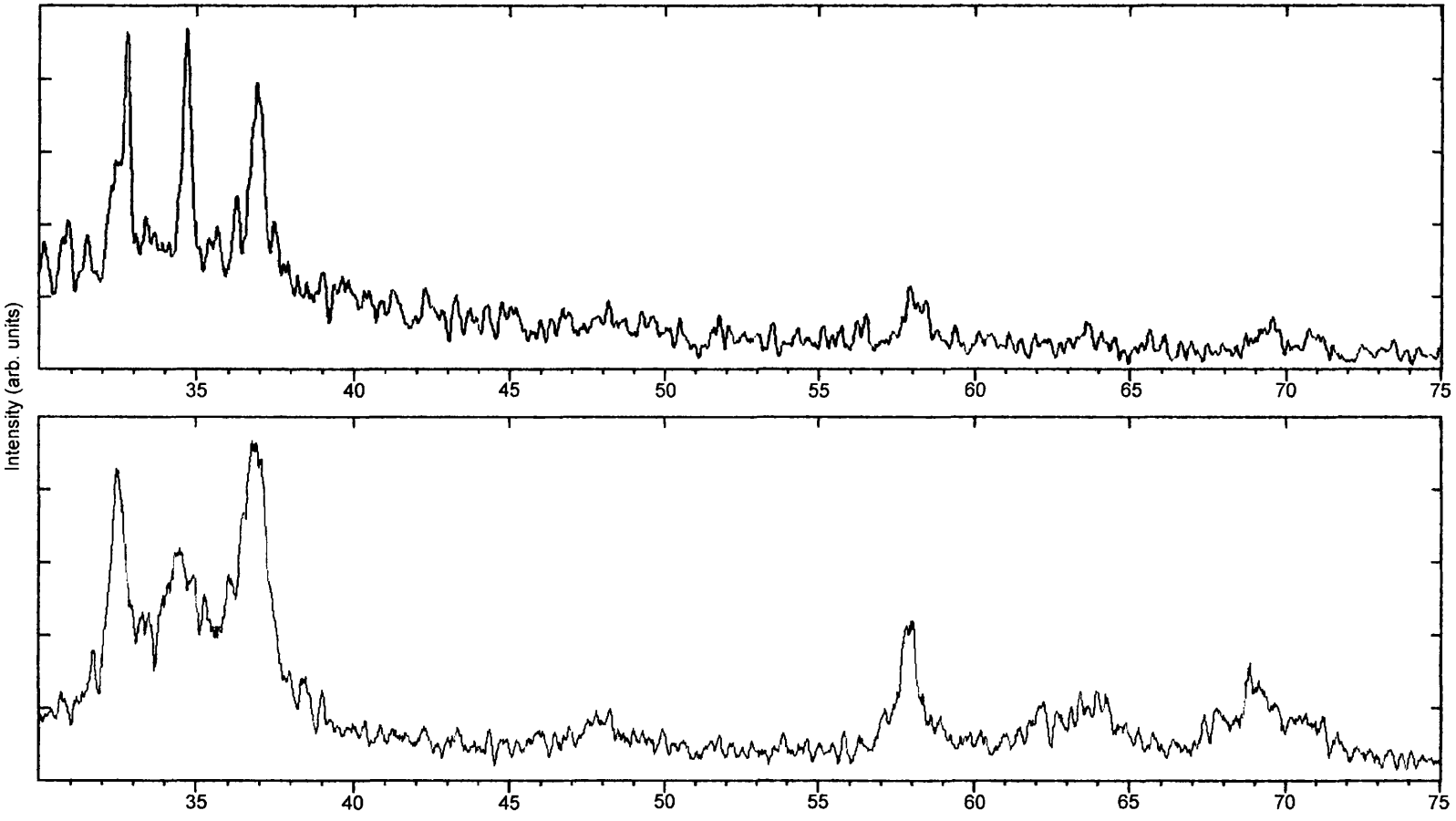

Figure 2.26 Powder XRD for the sample of GaN prepared at 850 °C (upper) and a commercial sample of GaN (lower)

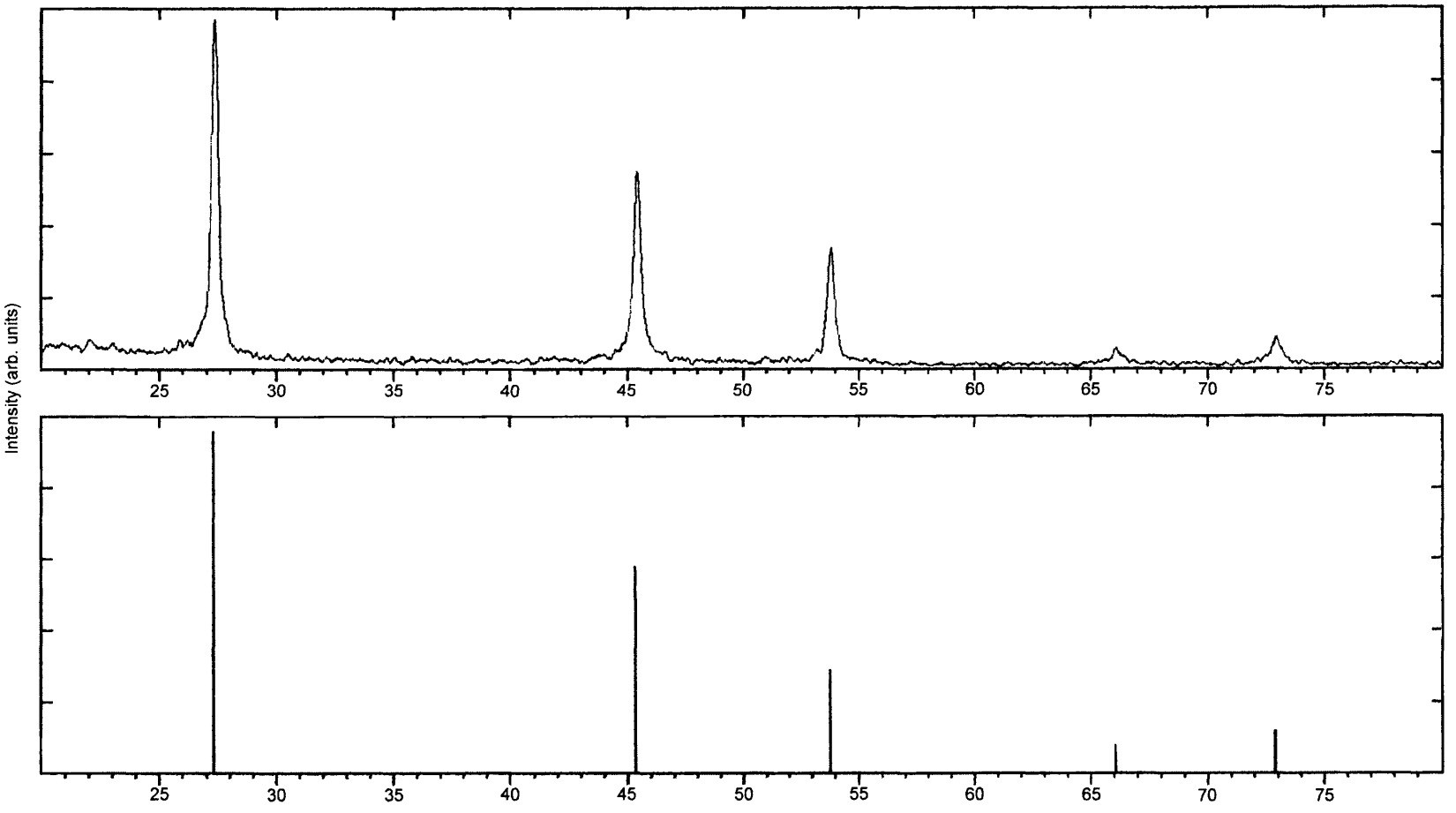

Figure 2.27 Powder XRD of the GaAs prepared (upper) and the calculated diffraction pattern for GaAs (lower)

2.3.9 Vapour-phase thin film studies

Given the results obtained from TGA and bulk pyrolysis, tube furnace reactions were carried out on $[Et_2Al\{N(SiMe_2H)_2\}]_n$ (**89**), $[Cl_3Ga\{NH(SiMe_3)_2\}]$ (**39**) and $[Cl_2Ga\{As(SiMe_2Ph)_2\}]_n$ (**102**) in order to assess whether thin films of group 13 pnictides could be obtained at low pressure. The apparatus used is shown in Figure 2.28 and the experimental procedure is described at the end of the chapter.

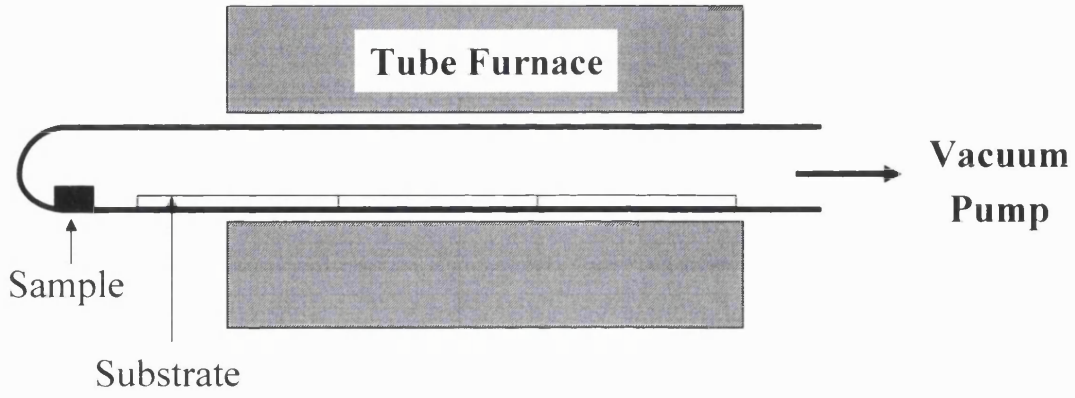

Figure 2.28 Tube furnace apparatus for vapour-phase deposition studies

In the case of **89** a thick highly reflective gold coloured film was deposited on the substrate (glass slides) and the inside of the glass tube. When the film was moved an interference pattern, which is due to the thickness of the film varying, was observed. The EDXA data for the film deposited showed the presence of both aluminium and nitrogen in the film but an accurate ratio could not be obtained due to the presence of peaks from the underlying glass. The presence of high levels of carbon were also found in the film due to incomplete decomposition of the precursor. However, this process is unoptimised and the use of a low pressure CVD reactor which offers more precise control over the flow rate of the precursor and the temperature of the substrate may lead to lower levels of impurities. One decomposition temperature (550 °C) was also tried and impurity levels are known to have a high dependency on the temperature used. Powder XRD showed the film to be amorphous. The Raman spectrum was recorded but no peaks were observed. A UV-vis spectrum was obtained and showed that the film has a direct band gap of 5

eV. This is lower than the literature value of 6.2 eV.[5] The more conducting nature of the film is thought to be due to the presence of high levels of carbon contamination.

The use of $[Cl_3Ga\{NH(SiMe_3)_2\}]$ (**39**) as the precursor led to the formation of a thick gold film mostly on the glass slides. When the film was moved an interference pattern, which is due to the thickness of the film varying, was observed. The EDXA data showed the presence of gallium and nitrogen in the film, however, as the film was very thin, most of the elements observed were due to the glass substrate. Chlorine contamination was observed in the film but it was not possible to determine the precise amount. The Powder XRD showed the film to be amorphous. The Raman spectrum was recorded but no peaks were observed. A UV-vis spectrum was recorded and showed that the film has a direct band gap of 3.6 eV. This compares well with the literature value of 3.4 eV.[16]

A vapour-phase reaction was attempted with $[Cl_2Ga\{As(SiMe_2Ph)_2\}]_n$ (**102**), however, the precursor proved to have a low volatility under vacuum and no appreciable vapour transport was observed. This suggests that this compound may not be a suitable LPCVD precursor although a better vacuum may lead to some vapour transport.

2.4 Experimental

General Procedures. All manipulations were performed under a dry, oxygen-free dinitrogen atmosphere using standard Schlenk techniques or in a MBraun Unilab glove box. All solvents were distilled from appropriate drying agents prior to use (sodium/benzophenone for toluene, hexanes, ether and thf; CaH_2 for CH_2Cl_2). $[LiN(SiMe_2Ph)_2]$, $As(SiMe_2Ph)_3$[161] and $As(SiMe_2{}^tBu)_3$[162] were prepared according to literature procedures. All other reagents were procured commercially from Aldrich, Fluka or Strem and used without further purification. Microanalytical data was obtained at University College London.

Physical Measurements. NMR spectra were recorded on a Brüker AMX 400 spectrometer at UCL. The NMR spectra are referenced to CD_2Cl_2, $CDCl_3$ or C_6D_6 which were degassed and dried over molecular sieves prior to use; ^1H and ^{13}C

chemical shifts are reported relative to $SiMe_4$ (0.00 ppm). Mass spectra (CI) were run on a micromass ZABSE instrument. IR spectra were collected as either KBr discs, between KBr plates (liquid samples) or as nujol mulls on a Shimadzu FTIR-8200 instrument. Paraffin oil (nujol) was degassed and dried over molecular sieves prior to use. Melting points were obtained in sealed glass capillaries under nitrogen and are uncorrected.

2.4.1 Preparation of $[Cl_2Ga\{NH(SiMe_3)\}]_2$ (32)

A solution of $HN(SiMe_3)_2$ (0.42 cm^3, 2.0 mmol) in CH_2Cl_2 (10 cm^3) was added dropwise with stirring to a cooled solution (-78 °C) of $[GaCl_3]$ (0.35 g, 1.99 mmol). During the addition the solution turned from colourless to slightly pink. After stirring for about 5 min a white precipitate formed in the cooled solution. The solution was allowed to warm slowly to room temperature during which time the precipitate redissolved. The mixture was stirred for 1 h at room temperature and the solvent was removed under reduced pressure. The resulting white crystalline solid was dissolved in a minimum amount of CH_2Cl_2 giving a clear solution, which was cooled to -20 °C for 24 h. Colourless plate-like crystals of **32** were obtained (0.174 g, 36.33% yield), mp 153 °C. Anal. Calc. for $C_3H_{10}Cl_2NSiGa(CH_2Cl_2)_{0.3}$: C, 15.67; H, 4.31; N, 5.85; Cl, 33.31. Found: C, 14.91; H, 4.30; N, 5.69; Cl, 32.95. ^1H NMR δ/ppm ($CDCl_3$): δ 0.40 (s, $SiCH_3$), 0.56 (s, $SiCH_3$), 2.07 (s, br, NH), 2.80 (s, br, NH), 5.28 (s, CH_2Cl_2). ^{13}C NMR ($CDCl_3$): δ 1.3 (s, $SiCH_3$), 2.8 (s, $SiCH_3$). IR (KBr disc, cm^{-1}): 3205 s, 2950 m, 1410 m, 1260 s, 1130 m, 1060 w br, 925 m, 850 vs, 770 w, 740 m, 705 w, 640 w, 535 m, 500 m, 405 m.

2.4.2 Preparation of $[Cl_2Ga\{NH(SiMe_2Ph)\}]_2$ (83)

A solution of $HN(SiMe_2Ph)_2$ (1.64 cm^3, 5.68 mmol) in CH_2Cl_2 (10 cm^3) was added to a stirred solution of $[GaCl_3]$ (1.00 g, 5.68 mmol) in CH_2Cl_2 (15 cm^3) at -78 °C with stirring. A white precipitate formed immediately and the reaction mixture was allowed to warm to room temperature. The resulting colourless solution was reduced *in vacuo* to ~5 cm^3. Cooling of this solution to -20 °C afforded colourless crystals after a few days. These crystals were redissolved in diethyl ether (5 cm^3) and

cooled to -20 °C. X-ray quality crystals of **83** were obtained after a few weeks (1.04 g, 63% yield), mp 104 - 107 °C. ^{1}H NMR δ/ppm (CD_2Cl_2): δ 0.78 (s, SiCH_3), 0.82 (s, SiCH_3), 2.41 (s, NH), 7.00 - 7.39 (m, SiC$_6H_5$). ^{13}C{^{1}H} NMR (CD_2Cl_2): δ 1.16 (s, SiCH$_3$), 3.10 (s, SiCH$_3$), 127.9, 128.4 (s, *m*-SiC_6H$_5$), 129.3, 131.0 (s, *p*-SiC_6H$_5$), 133.7, 133.9 (s, *o*- SiC_6H$_5$), 134.4 (s, *ipso*-SiC_6H$_5$). IR (KBr disc, cm^{-1}): 3213 s br, 2957 m, 1428 s, 1258 s, 1180 m, 1116 vs, 1051 m, 998 w, 933 s, 831 vs, 800 vs, 748 m, 699 vs, 687 w, 594 w, 471 w.

2.4.3 Attempted Preparation of [Cl$_2$Ga{NH(SiMe$_2$H)}]$_2$

A solution of HN(SiMe$_2$H)$_2$ (1.0 cm^3, 5.68 mmol) in CH_2Cl_2 (10 cm^3) was added to a red coloured solution of [$GaCl_3$] (1.0 g, 5.68 mmol) in CH_2Cl_2 (15 cm^3) at room temperature with stirring. On addition of the silylamine the solution turned colourless. The resulting solution was reduced *in vacuo* yielding a white oil (0.99g). After *ca.* 1 week at room temperature colourless crystals and a grey solid formed. Anal. Calc. for $C_2H_8NSiCl_2Ga$: C, 11.18; H, 3.75; N, 6.52. Found: C, 14.10; H, 4.31; N, 4.27.

2.4.4 Preparation of [Cl$_2$Ga{NH^{t}Bu}]$_2$ (84)

HN^{t}Bu(SiMe$_3$) (1 cm^3, 5.68 mmol) was added dropwise to a solution of [$GaCl_3$] (1.0 g, 5.68 mmol) in CH_2Cl_2 (15 cm^3) at room temperature with stirring. The reaction mixture was refluxed for 24 hours. The resulting solution was reduced to *ca.* 5 cm^3. Colourless X-ray quality crystals of **84** were obtained by cooling the solution to -20 °C for 24 hours, (0.757 g, 63 % yield). Anal. Calc. for $C_4H_{10}NCl_2Ga$ C, 22.58; H, 4.74; N, 6.58. Found C, 22.58; H, 4.80; N, 5.62. ^{1}H NMR δ/ppm ($CDCl_3$): δ 1.36 (s, C(CH_3)$_3$), 1.44 (s, C(CH_3)$_3$), 1.46 (s, C(CH_3)$_3$), 1.50 (s, C(CH_3)$_3$), 2.56 (s, br, NH), 2.68 (s, br, NH), 3.57 (s br, NH). ^{13}C{^{1}H} NMR ($CDCl_3$): δ 30.1 (s, NC(CH_3)$_3$), 31.3 (s, NC(CH_3)$_3$), 31.6 (s, NC(CH_3)$_3$), 56.8 (s, NC(CH$_3$)$_3$), 57.0 (s, NC(CH$_3$)$_3$).

2.4.5 Preparation of $[Br_2Ga\{NH(SiMe_3)\}]_2$ (33)

$HN(SiMe_3)_2$ (0.27 cm^3, 1.29 mmol) was added dropwise to a stirred solution of $[GaBr_3]$ (0.4 g, 1.29 mmol) in CH_2Cl_2 (15 cm^3) at room temperature. On addition of the amine the yellow solution turned red/pink. On stirring at room temperature for approximately 1 minute the mixture changed colour to pale straw. The reaction mixture was stirred for a further hour at room temperature. The solution was reduced to *ca.* 5 cm^3 and cooled to -20 °C overnight. After this time a white solid had formed (0.13 g, 32% yield). Anal. Calc. for $C_3H_{10}NBr_2SiGa$: C, 11.34; H, 3.17; N, 4.41. Found C, 12.35; H, 3.35; N, 2.25. ^1H NMR δ/ppm (CD_2Cl_2): δ 0.43 (s, $Si(CH_3)_3$), 0.54 (s, $Si(CH_3)_3$), 0.63 (s, $Si(CH_3)_3$), 0.73 (s, $Si(CH_3)_3$), 3.08 (s, br, NH). $^{13}C\{^1H\}$ NMR (CD_2Cl_2): δ 0.7 (s, $Si(CH_3)_3$), 1.7 (s, $Si(CH_3)_3$), 3.8 (s, $Si(CH_3)_3$), 4.2 (s, $Si(CH_3)_3$). IR (nujol, cm^{-1}): 3193 m, 1515 m, 1260 vs br, 1172 m, 1129 m, 1096 m, 991 w, 848 vs br, 519 m, 490 m.

2.4.6 Preparation of $[Cl_2In\{NH(SiMe_3)\}]_n$ (85)

$HN(SiMe_3)_2$ (0.5 cm^3, 2.37 mmol) was added to a stirred suspension of $[InCl_3]$ (0.5 g, 2.37 mmol) in diethyl ether (25 cm^5). The resulting cloudy white mixture was stirred at room temperature for 5 days. The mixture was filtered giving a colourless solution which was reduced under vacuum to *ca.* 5 cm^3. Cooling to -20 °C for 1 week resulted in the formation of a white solid (0.22 g, 34% yield), mp 159 - 161 °C. Anal. Calc for $C_3H_{10}NCl_2SiIn(CH_2Cl_2)_{0.25}$: C, 16.43; H, 4.31; N, 4.80. Found C, 16.21; H, 4.32; N, 2.71. ^1H NMR δ/ppm (CD_2Cl_2): δ 0.34 (s, $Si(CH_3)_3$), 0.40 (s, $Si(CH_3)_3$), 1.12 (t, $O(CH_2CH_3)_2$), 2.47 (s br, NH), 3.60 (q, $O(CH_2CH_3)_2$).

2.4.7 Preparation of $[MeGaCl_2]_2$ (86)

A solution of $N(SiMe_3)_3$ (0.66 g, 2.84 mmol) in CH_2Cl_2 (10 cm^3) was added dropwise to a cooled (-78 °C) solution of $[GaCl_3]$ (0.50 g, 2.84 mmol) in CH_2Cl_2 (10 cm^3) with stirring. The reaction temperature was maintained at -78 °C for 1 hour, after which the mixture was allowed to warm slowly to room temperature. After being stirred for an additional 1 hour, during which a colour change occurred from

colourless to light straw, the mixture was stirred at 40 °C for 30 minutes. The solvent was then removed *in vacuo* and the resulting light brown coloured oil was dissolved in CH_2Cl_2 (2 cm^3). Cooling of this solution to -20 °C overnight afforded colourless crystals of **86**. Anal. (carried out on oil) Calc. for CH_3Cl_2Ga: C, 7.72; H, 1.94; Cl, 45.55. Found C, 9.39; H, 2.40; Cl, 41.32. ^1H NMR ($CDCl_3$): δ 0.42 - 0.62 (m, CH_3). $^{13}C\{^1H\}$ NMR ($CDCl_3$) 3.2, 2.9, 2.1, 1.8, 1.6.

2.4.8 Reaction of $GaCl_3$ with $N(SiMe_3)_3$ in hexane

A solution of $N(SiMe_3)_3$ (1.56 g, 6.60 mmol) in hexane (10 cm^3) was added to a solution of [$GaCl_3$] (1.2 g, 6.60 mmol) in hexane (15 cm^3) with stirring. A white precipitate formed immediately. The mixture was stirred for 5 mins and the solvent removed. The resulting white powder was dried *in vacuo*. After standing for 24 hours at room temperature the white powder had transformed into a colourless oil. On standing for a further 24 hours colourless crystals suitable for X-ray crystallography formed (0.41g). Anal. Calc. for $C_3H_9Cl_3Ga_2$: C, 12.39; H, 3.12. Found C, 11.36; H, 2.58.

2.4.9 Reaction of [$GaCl_3$], $HN(SiMe_3)_2$ and 3,5-$Me_2C_5H_3N$

3,5-$Me_2C_5H_3N$ (1.37 cm^3, 12 mmol) was added dropwise to a solution of [$GaCl_3$] (1.05 g, 6 mmol) in CH_2Cl_2 (15 cm^3) which was cooled to -78 °C. A solution of $HN(SiMe_3)_2$ (1.26 cm^3, 6 mmol) in CH_2Cl_2 (10 cm^3) was then added dropwise. A white precipitate formed after *ca.* 2 minutes. The mixture was allowed to warm slowly to room temperature during which time the precipitate redissolved. After stirring overnight at room temperature the mixture was a dark straw colour. The mixture was reduced under vacuum to *ca.* 5 cm^3 and cooled to -20 °C for 24 hours. This afforded large colourless crystals of **87**. Anal. Calc. for $C_{14}H_{18}N_2Cl_3Ga$: C, 43.07; H, 4.65; N, 7.18. Found C, 42.84; H, 4.73; N, 7.02. ^1H NMR δ/ppm (CD_2Cl_2): δ 2.38 (s, 6H, $NC_5H_3(CH_3)_2$), 7.55 (s, 1H, *p*-$NC_5H_3(CH_3)_2$), 8.34 (s, 2H, *o*-$NC_5H_3(CH_3)_2$). $^{13}C\{^1H\}$ NMR (CD_2Cl_2): δ 18.5 (s, $NC_5H_3(CH_3)_2$), 135.4 (s, $NC_5H_3(CH_3)_2$), 141.7 (s, $NC_5H_3(CH_3)_2$), 145.6 (s, $NC_5H_3(CH_3)_2$).

2.4.10 Reaction of $[Cl_2Ga\{NH(SiMe_3)\}]_2$ and 3,5-$Me_2C_5H_3N$

3,5-$Me_2C_5H_3N$ (0.5 cm^3, 4.37 mmol) was added to a solution of compound **32** (0.5 g, 1.09 mmol) in CH_2Cl_2 (15 cm^3) in a dropwise manner. The resulting solution was stirred at room temperature for 5 hours. The mixture was reduced to *ca.* 5 cm^3 under vacuum. Cooling to -20 °C afforded large colourless crystals of **87** (0.19 g). Anal. Calc. for $C_{14}H_{18}N_2Cl_3Ga$: C, 43.07; H, 4.65; N, 7.18. Found C, 42.85; H, 4.37; N, 6.67.

2.4.11 Preparation of $[Cl(Me)Al\{NH(SiMe_2H)\}]_n$ (88)

A solution of $HN(SiMe_2H)_2$ (1.77 cm^3, 10 mmol) in CH_2Cl_2 (10 cm^3) was added dropwise to a solution of $[Me_2AlCl]$ (10 cm^3, 1.0M in hexanes) in CH_2Cl_2 (15 cm^3) at -78 °C with stirring. The mixture was stirred and allowed to warm to room temperature. The solvent was removed *in vacuo* resulting in a colourless oil. After standing at room temperature over several weeks colourless crystals of **88** suitable for X-ray diffraction were afforded (0.56 g, 37% yield). ^1H NMR δ/ppm ($CDCl_3$): δ -0.73 (s, $AlCH_3$), -0.70 (s, $AlCH_3$), -0.51 (s, $AlCH_3$), -0.47 (s, $AlCH_3$), 0.31 - 0.44 (m, $Si(CH_3)_2H$), 1.01 (s, br), 1.27 (s, br), 4.33-4.64 (m, $Si(CH_3)_2H$). $^{13}C\{^1H\}$ NMR ($CDCl_3$); δ -9.5 (s, br, $AlCH_3$), -0.2 (t, $Si(CH_3)_2H$).

2.4.12 Reaction of $[AlEt_3]$ and $N(SiMe_3)_3$

A solution of $N(SiMe_3)_3$ (2.04 g, 8.75 mmol) in CH_2Cl_2 (10 cm^3) was added to a solution of $[Et_3Al]$ (1.2 cm^3, 8.75 mmol) in CH_2Cl_2 (15 cm^3) in a dropwise manner. The mixture was stirred for 30 minutes at room temperature. The mixture warmed slightly and a white vapour was observed. The solvent was removed under vacuum yielding a colourless liquid. ^1H NMR δ/ppm ($CDCl_3$): δ 0.20 (s, 9H, $Si(CH_3)_3$), 0.33 (q, J = 23 Hz, 2H, $AlCH_2CH_3$), 1.10 (t, J = 14 Hz, 3H, $AlCH_2CH_3$). $^{13}C\{^1H\}$ NMR ($CDCl_3$): δ 0.3 (s, $Si(CH_3)_3$), 5.5 (s, $AlCH_2CH_3$), 8.6 (s, $AlCH_2CH_3$). IR (nujol, cm^{-1}): 2944 s, 2902 s, 2865 s, 1460 w, 1409 w, 1253 s, 1261 s, 983 w, 918 vs, 846 s, 822 m, 765 m, 668 m, 620 m, 545 w, 473 w, 401 m.

2.4.13 Preparation of $[Et_2Al\{N(SiMe_2H)_2\}]_n$ (89)

A solution of $HN(SiMe_2H)_2$ (3.1 cm^3, 17.5 mmol) in CH_2Cl_2 (10 cm^3) was added dropwise to a solution of $[Et_3Al]$ (2.4 cm^3, 17.5 mmol) in CH_2Cl_2 (20 cm^3) at -78 °C with stirring. The evolution of a colourless gas was observed on addition of the amine. The mixture was stirred and allowed to warm to room temperature. The solvent was removed *in vacuo* resulting in a white crystalline solid. This solid was dissolved in a minimum amount of CH_2Cl_2 (~5 cm^3) and cooled to -20 °C affording colourless plates (3.24 g, 85 %), mp 106 - 107 °C. Anal Calc for $C_8H_{24}NSi_2Al$: C, 44.19; H, 11.13; N, 6.44. Found: C, 45.17; H, 11.81; N, 6.09. ^1H NMR δ/ppm ($CDCl_3$): δ 0.25 (q, J = 24 Hz, 4H, $AlCH_2CH_3$), 0.38 (s, 12H, $Si(CH_3)_2H$), 1.08 (t, J = 17 Hz, 6H, $AlCH_2CH_3$), 4.68 (s, 2H, $Si(CH_3)_2H$). IR (KBr, cm^{-1}): 2750 w, 2180 vs, 1411 m, 1258 vs, 1235 w, 1197 m, 1100 w, 913 s br, 847 s br, 785 m, 682 m, 629 s, 552 s, 500 w, 415 m.

2.4.14 Preparation of $[Et_2Al\{N(SiMe_3)_2\}]_n$ (90)

$HN(SiMe_3)_2$ (3.69 cm^3, 17.5 mmol) was added to a solution of $[Et_3Al]$ (2.4 cm^3, 17.5 mmol) in CH_2Cl_2 (20 cm^3) in a dropwise manner at room temperature. The mixture was stirred for 2 hours during which time a slight warming and the formation of a white vapour were observed. The solvent was removed under vacuum to give a colourless liquid, (4.17 g). ^1H NMR δ/ppm ($CDCl_3$): δ 0.13 (s, 18H, $Si(CH_3)_3$), 0.31 - 0.34 (m, 4H $AlCH_2CH_3$), 1.07 (t, J = 17 Hz, 6H, $AlCH_2CH_3$). $^{13}C\{^1H\}$ NMR ($CDCl_3$): δ 3.5 (s, $Si(CH_3)_3$), 5.0 (s, $AlCH_2CH_3$), 5.8 (s, $AlCH_2CH_3$), 8.3 - 9.3 (m, $AlCH_2CH_3$). IR (KBr, cm^{-1}): 2949 s, 2902 s, 2867 s, 1464 w, 1404 w, 1260 s, 1250 ws, 989 s, 893 s, 835 s, 755 w, 675 m, 645 m, 621 m, 552 m, 475 w.

2.4.15 Reaction $[Et_3Ga]$ and $N(SiMe_3)_3$

A solution of $N(SiMe_3)_3$ (0.79 g, 3.37 mmol) in ether (15 cm^3) was added to a solution of $[Et_3Ga]$ (0.5 cm^3, 3.37 mmol) in ether (15 cm^3) at room temperature in a dropwise manner. The resulting mixture was refluxed for 4 hours. The solvent was removed under vacuum affording a colourless liquid (0.87g). ^1H NMR δ/ppm

($CDCl_3$): δ 0.19 (s, 9H, $Si(CH_3)_3$), 0.38-0.43 (m, 4H, $GaCH_2CH_3$), 1.08 - 1.19 (m, 6H, $GaCH_2CH_3$). $^{13}C\{^1H\}$ NMR ($CDCl_3$): δ 1.0 (s, $Si(CH_3)_3$), 3.8 (s, $Si(CH_3)_3$), 5.4 (s, $GaCH_2CH_3$), 6.2 (s, $GaCH_2CH_3$), 9.4 (s, $GaCH_2CH_3$), 10.1 (s, $GaCH_2CH_3$). IR (KBr, cm^{-1}): 2946 vs, 2900 vs, 2866 vs, 2812 m, 1466 w, 1449 w, 1418 m, 1386 s, 1253 vs, 1190 m, 1152 m, 1098 s, 1057 s, 1001 w, 919 vs br, 846 s, 882 m, 766 w, 675 m, 650 w, 620 m, 562 m, 537 m, 401 m.

2.4.16 Preparation of $[Cl_2Ga\{N(SiMe_3)_2\}]_n$ (42)

A solution of $[LiN(SiMe_3)_2]$ (1.91 g, 11.4 mmol) in hexane (15 cm^3) was added to a stirred solution of $[GaCl_3]$ (2.00 g, 11.4 mmol) in hexane (15 cm^3) in a dropwise manner. A white precipitate formed immediately. The reaction mixture was refluxed for 24 hours. The resulting mixture was filtered through Celite and the solvent removed under vacuum affording a white coloured oil. This oil was dissolved in a minimum amount of CH_2Cl_2 (5 cm^3) and the solution cooled to -20 °C. Small orange crystals of **42** formed after several weeks (0.21 g, 6% yield). Anal. Calc. for $C_6H_{18}NCl_2Si_2Ga$: C, 23.94; H, 6.03; N, 4.63. Found: C, 24.43; H, 5.99; N, 3.55.

2.4.17 Preparation of $[Cl(Ph)Ga\{N(SiMe_2Ph)_2\}]_2$ (92)

[^{n}BuLi] (1.78cm^3, 2.84 mmol, 1.6M in hexanes) was added dropwise to a solution of $HN(SiMe_2Ph)_2$ (0.82 cm^3, 2.84 mmol) in hexane (10 cm^3) at -78 °C with stirring. A white precipitate formed after a few minutes and the mixture was stirred at -78 °C for 2 hours. The resulting slurry was then added dropwise to a solution of $[GaCl_3]$ (0.5 g, 2.84 mmol) in hexane (10 cm^3) at -78 °C with stirring. The reaction mixture was allowed to warm slowly to room temperature with stirring. The mixture was filtered through Celite giving a pale yellow solution. Cooling of this solution to -20 °C for 2 weeks afforded single colourless crystals suitable for crystallography (0.29 g, 22% yield), mp 126-128 °C. ^1H NMR δ/ppm (CD_2Cl_2): δ 0.17 (s, $SiCH_3$), 0.25 (s, $SiCH_3$), 7.20 - 7.63 (m, SiC_6H_5 and GaC_6H_5). $^{13}C\{^1H\}$ NMR (CD_2Cl_2): δ 1.6, 2.7 (s, $SiCH_3$), 126.1, 126.5 (s, *m*-SiC_6H_5), 131.9, 132.3 (s, *p*-SiC_6H_5), 140.8, 142.0 (s, *o*-SiC_6H_5), 128.3, 128.5 (s, *m*-GaC_6H_5), 131.4, 131.6 (s, *p*-GaC_6H_5), 140.2, (s, *o*-GaC_6H_5), *ipso*-carbon not detected. IR (KBr disk, cm^{-1}): 2957 m, 2899 w, 1483

w, 1427 s, 1406 w, 1302 w, 1258 vs, 1180 w, 1112 s, 1022 s, 999 w, 947 s, 868 vs, 798 vs, 729 s, 700 s, 648 w, 522 w, 472 w, 449 w, 407 w.

2.4.18 Preparation of $[Cl_3Ga\{NH(SiMe_3)_2\}]$ (39)

$HN(SiMe_3)_2$ (2.52 cm^3, 12 mmol) was added dropwise to a solution of $[GaCl_3]$ (2.1 g, 12 mmol) in hexane (20 cm^3) at room temperature. A white precipitate formed immediately. The mixture was stirred for 1 h at room temperature. The white solid was separated and dried under vacuum. Compound **39** was obtained as a white powder (3.62 g, 90% yield), mp 126-128 °C. Anal. Calc. for $C_6H_{19}NCl_3Si_2Ga$ C, 21.35; H, 5.67; N, 4.15. Found C, 21.43; H, 5.73; N, 3.41.

2.4.19 Preparation of $[Cl_3Ga\{NH(SiMe_2Ph)_2\}]$ (93)

A solution of $HN(SiMe_2Ph)_2$ (1.45 cm^3, 5.0 mmol) in hexane (10 cm^3) was added dropwise to a solution of $[GaCl_3]$ (0.88 g, 5.0 mmol) in hexane (15 cm^3) at room temperature with stirring. A white precipitate formed immediately. The reaction mixture was stirred for 30 mins. The liquid was removed and the resulting solid dried *in vacuo*. Compound **93** was isolated as a white powder (2.14 g 93% yield). Anal. Calc for $C_{16}H_{23}NCl_3SiGa$: C, 41.64; H, 5.02; N, 3.03. Found C, 41.28; H, 5.23; N, 2.04. IR (KBr, cm^{-1}): 3115w, 2959w, 1427m, 1259vs, 1180br, 1117s, 1024w, 934m, 860w, 800m, 740w, 731w, 700m, 594w, 460w.

2.4.20 Attempted Preparation of $[Cl_3Ga\{NH(SiMe_2H)_2\}]$

A solution of $HN(SiMe_2H)_2$ (1.0 cm^3 5.68 mmol) in hexane (10 cm^3) was added dropwise to a solution of $[GaCl_3]$ (1.0 g 5.68 mmol) in hexane (15 cm^3) at room temperature with stirring. A white precipitate formed immediately. The mixture was stirred for 30 mins. The liquid was removed and the resulting solid dried *in vacuo* to give in a white powder (1.05 g). This white powder decomposed to give colourless crystals and a sticky grey material.

2.4.21 Preparation of $[Cl_3Ga\{NH(^tBu)(SiMe_3)\}]$ (95)

$HN^tBu(SiMe_3)$ (1 cm^3, 5.68 mmol) was added dropwise to a solution of $[GaCl_3]$ (1.0 g, 5.68 mmol) in hexane (15 cm^3) at room temperature. A white precipitate formed immediately. The mixture was stirred for 5 mins at room temperature. The liquid was removed and the precipitate was dried *in vacuo* giving a white powder. (1.44 g, 79 % yield), mp 126 °C. Anal. Calc. for $C_7H_{19}NCl_3SiGa$ C, 26.16; H, 5.96; N, 4.36. Found C, 25.17; H, 5.79; N, 4.58. IR (nujol, cm^{-1}): 3152 vs, 1564 m, 1408 m, 1337 m, 1261 vs, 1240 w, 1177 s, 1079 s, 1027 m, 932 w, 845 vs br, 772 m, 735 s, 664 m, 627 m, 568 m, 416 w.

2.4.22 Preparation of $[Br_3Ga\{NH(SiMe_3)_2\}]$ (96)

$HN(SiMe_3)_2$ (0.34 cm^3 1.61 mmol) was added dropwise to a solution of $[GaBr_3]$ (0.50 g, 1.16 mmol) in hexane (25 cm^3) at room temperature with stirring. A white precipitate formed immediately on addition of the amine. The white solid was separated and dried *in vacuo*. Compound **96** was obtained as a white powder (0.47 g, 56% yield), mp 113 - 115 °C. Anal. Calc. for $C_6H_{19}NBr_3Si_2Ga$ C,15.31; H 4.07; N, 2.98. Found C, 15.30; H, 3.85; N, 1.56. IR (KBr Disc) 3410 m, 3141 m, 2960 m, 2361 w, 1399 m, 1260 vs, 1062 s, 848 s, 757 w, 677 w, 580 w.

2.4.23 Preparation of $[Br_3Ga\{NH(SiMe_2Ph)_2\}]$ (97)

$NH(SiMe_2Ph)_2$ (0.37 cm^3, 1.29 mmol) was added to a stirred solution of $[GaBr_3]$ (0.40g, 1.29 mmol) in hexane (25 cm^3) in a dropwise manner at room temperature. A white precipitate formed immediately on addition of the amine. The precipitate was isolated and dried under vacuum yielding a white powder (0.59 g, 76.9% yield), mp 108 - 109 °C. Anal. Calc. for $C_{16}H_{23}NBr_3Si_2Ga$: C, 32.30; H, 3.90; N, 2.35. Found: C, 32.08; H, 3.93; N, 0.57. IR (nujol, cm^{-1}): 3155 m, 3070 w, 1590 m, 1428 s, 1258 s, 1178 w, 1161 w, 1116 vs, 1015 s, 998 m, 931 m, 884 s, 830 s, 801 s, 740 m, 672 m, 635 m, 585 s, 507 s, 465 s, 457 s.

2.4.24 Preparation of $[Br_3Ga\{NH(^tBu)(SiMe_3)\}]$ (98)

$HN(^tBu)SiMe_3$ (0.25 cm^3, 1.29 mmol) was added dropwise to a stirred solution of $[GaBr_3]$ (0.4 g, 1.29 mmol) in hexane (25 cm^3) at room temperature. A white precipitate was observed to form on addition of the amine. The precipitate was separated and dried under vacuum yielding a white powder (0.38 g, 65% yield), sample decomposed without melting below 230 °C. Anal. Calc. for $C_7H_{19}NBr_3SiGa$: C, 18.49; H, 4.21. Found C, 17.65; H, 4.00. IR (nujol, cm^{-1}): 3145 s, 1261 s, 1173 s, 1071 s, 1025 w, 851 s br, 772 m, 656 w, 623 w, 561 w, 418 w.

2.4.25 Preparation of $[Cl_2(Me)Al\{NH(SiMe_2Ph)_2\}]$ (99)

$HN(SiMe_2Ph)_2$ (1.5 cm^3, 5 mmol) was added dropwise to a solution of $[Me_2AlCl]$ (5 cm^3, 1.0M in hexane, 5 mmol) in CH_2Cl_2 (15 cm^3) at -78 °C. A white precipitate formed and the mixture was allowed to warm slowly to room temperature during which time the precipitate redissolved. The mixture was reduced in volume to 5 cm^3 and cooled to -20 °C. Colourless crystals suitable for X-ray crystallography were formed (0.15 g, 8% yield). ^1H NMR δ/ppm (CD_2Cl_2): δ -0.46 (s, $AlCH_3$), -0.39 (s, $AlCH_3$), 0.30 (s, $Si(CH_3)_2$), 0.68 (s, $Si(CH_3)_2$), 0.77 (s, $Si(CH_3)_2$), 2.21 (s br, NH), 7.26 - 7.67 (m, SiC_6H_5). ^{13}C NMR (CD_2Cl_2): δ -0.7 (s, $AlCH_3$), 0.0 (s, $AlCH_3$), 1.3 (s, $Si(CH_3)_2$), 2.2 (s, $Si(CH_3)_2$), 3.1 (s, $Si(CH_3)_2$), 128.1 (s, *m*-SiC_6H_5), 128.5 (s, *m*-SiC_6H_5), 128.7 (s, *m*-SiC_6H_5), 129.4 (s, *p*-SiC_6H_5), 130.9 (s, *p*-SiC_6H_5), 133.7 (s, *o*-SiC_6H_5), 135.7 (s, *ipso*-SiC_6H_5).

2.4.26 Preparation of $As(SiMe_2Ph)_3$

Sodium (1.01g, 44 mmol) was used to make a sodium mirror on the inside of a round bottom Schlenk flask. Arsenic powder (1.1g, 14.6 mmol), a few crystals of napthalene and thf (30 cm^3) were added at room temperature with stirring. The mixture was refluxed overnight. After cooling to room temperature, $PhMe_2SiCl$ (7.4 cm^3, 44 mmol) was added dropwise to the reaction mixture. Immediately the mixture turned black in colour. The reaction mixture was refluxed for 24 hours resulting in the formation of a grey slurry. The solvent was removed *in vacuo* and toluene (30

cm^3) was added. The mixture was filtered and a pale yellow solution was obtained. Cooling in a freezer resulted in the formation of pale yellow crystals.

2.4.27 Preparation of $As(SiMe_2{}^tBu)_3$

Sodium (1.06g, 46 mmol) was used to make a sodium mirror on the inside of a flask. Arsenic powder (1.0g, 13.3 mmol), a few crystals of napthalene and thf (30 cm^3) were added at room temperature with stirring. The mixture was refluxed overnight. After cooling to room temperature $^tBuMe_2SiCl$ (6.0 g, 39.8 mmol) was added dropwise. Immediately the reaction mixture turned black in colour. The reaction mixture was refluxed for 24 hours resulting in the formation of a grey slurry. The solvent was removed *in vacuo* and toluene was (30 cm^3) was added. The mixture was filtered and a pale yellow solution was obtained. Cooling to -20 °C resulted in the formation of pale yellow crystals after 24 hours (1.26 g, 65% yield). Anal. Calc. for $C_{18}H_{45}Si_3As$: C, 51.39; H, 10.78. Found C, 51.22; H, 11.00.

2.4.28 Preparation of $[Cl_2Ga\{As(SiMe_2Ph)_2\}]$ (102)

A solution of $As(SiMe_2Ph)_3$ (0.75 g, 1.56 mmol) in CH_2Cl_2 (25 cm^3) was added dropwise to a cooled (-78 °C) solution of $[GaCl_3]$ (0.27 g, 1.56 mmol) in CH_2Cl_2 (20 cm^3) with stirring. On addition of the arsine a cream precipitate formed and the solution was orange. The mixture was allowed to warm slowly to room temperature with stirring and the orange of the solution intensified. The mixture was filtered through Celite giving an orange solution which was cooled to -20 °C. An orange powder formed after 1 week. This was separated and dried under vacuum resulting in an orange powder (0.25 g, 33%), decomposed with out melting below 230 °C. Anal. Calc. for $C_{16}H_{22}AsCl_2Si_2Ga$: C, 39.54; H, 4.56. Found C, 38.92; H, 4.64. ^1H NMR δ/ppm (CD_2Cl_2): δ 0.33 (s, $SiCH_3$), 0.51 (s, $SiCH_3$), 0.69 (s, $SiCH_3$), 0.81 (s, $SiCH_3$), 0.84 (s, $SiCH_3$), 7.21-7.70 (m, SiC_6H_5). $^{13}C\{^1H\}$ NMR (CD_2Cl_2): δ 1.0 (s, $SiCH_3$), 2.1 (s, $SiCH_3$), 128.0 (s, *m*-SiC_6H_5), 128.3 (s, *m*-SiC_6H_5), 129.0 (s, *p*-SiC_6H_5), 129.5 (s, *o*-SiC_6H_5), 133.3 (s, *ipso*-SiC_6H_5).

2.4.29 Attempted preparation of $[Cl_2Ga\{As(SiMe_2{}^tBu)_2\}]_n$

A solution of $As(SiMe_2{}^tBu)_3$ (0.39 g, 0.93 mmol) in CH_2Cl_2 (15 cm^3) was added to a solution of $[GaCl_3]$ (0.16 g, 0.93 mmol) in CH_2Cl_2 (10 cm^3) at -78 °C. A cream coloured precipitate formed which was removed by filtration through Celite. The resulting yellow solution was reduced to 5 cm^3 and cooled to -20 °C. After 12 hours a dark brown precipitate formed.

2.4.30 Pyrolysis studies

Typically, a sample of precursor (0.30 g) was loaded into a glass or quartz ampoule (30 cm length x 9 mm diameter) in the glove box. The ampoule was then placed in a furnace, which had been pre-heated to the decomposition temperature, such that the sample was in the centre of the furnace. The ampoule was heated for 5 minutes under a N_2 atmosphere and for a further 4 hours under a dynamic vacuum. The furnace was then allowed to cool to room temperature. The powder produced was analysed by powder XRD, EDXA (in the case of GaAs) and elemental analysis (in the case of GaN).

2.4.31 Vapour-phase studies

Typically, a sample of the precursor (0.30 g) was loaded into a glass ampoule (40 cm length x 1.5 cm diameter) in the glove box. Pieces of microscope slide, which had been cut into thin strips (*ca.* 1cm width), were placed along the centre of the ampoule. The ampoule was then placed in a furnace such that 30 cm was inside the furnace and the end containing the precursor protruded by 5 cm. The ampoule was heated to 550 °C under dynamic vacuum. The ampoule was slowly drawn into the furnace over the period of a few minutes until the sample started to melt. The ampoule was then drawn into the furnace over 4 hours until all the sample had vaporised or decomposed. The furnace was allowed to cool to room temperature. Films were deposited on the glass microscope slides and the inside wall of the ampoule where the tube was in the furnace. The films were analysed by EDXA/SEM, Raman spectroscopy and UV/Vis.

2.5 References

1. A. N. Gleizes, *Chem. Vap. Deposition,* 2000, **6**, 155.
2. N. N. Greenwood & A. Earnshaw, Chemistry of the Elements, 1995.
3. D. A. Neumayer & J. G. Ekerdt, *Chem. Mater.,* 1996, **8**, 9.
4. R. Juza & H. Hahn, *Z. Anorg. Allg. Chem.,* 1938, **239**, 282.
5. S. Strite & H. Morkoc, *J. Vac. Sci. Technol. B,* 1992, **10**, 1237.
6. R. Juza & H. Hahn, *Z. Anorg. Allg. Chem.,* 1940, **244**, 133.
7. R. Niewa & F. J. DiSalv, *Chem. Mater.*, 1998, **10**, 2733.
8. T. D. Getman & G. W. Franklin, *Comments Inorg. Chem.,* 1995, **17**, 79.
9. T. L. Chu & R. W. Kelm, Jr., *J. Electrochem. Soc.*, 1975, **122**, 995.
10. L. V. Linterrante, W. Lee, M. McConnel, N. Lewis & E. Hall, *J. Electrochem. Soc.,* 1989, **136**, 472.
11. R. Riedel, G. Petzow & U. Klingebeil, *J. Mater. Sci. Lett.,* 1990, **9**, 222.
12. H. Okano, N. Tanaka, Y. Takahashi, T. Tanaka, K. Shibata & S. Nakano, *Appl. Phys. Lett.,* 1994, **64**, 166.
13. Y. Takahashi, K. Yamashita, S. Motojima & K. Sugiyama, *Surf. Sci.,* 1979, **86**, 238.
14. T. Schleid, *Eur. J. Solid State Inorg. Chem.,* 1996, **33**, 227.
15. A. Simon, *Coord. Chem. Rev.,* 1997, **163**, 253.
16. S. W. Choi, K. J. Bachmann & G. Lucovsky, *J. Mater. Res.,* 1993, **8** 847.
17. R. C. Powell, N. E. Lee, Y. W. KIm & J. E. Greene, *J. Appl. Phys.,* 1993, **73**, 189.
18. C. R. Eddy, Jr., T. D. Moustakas & J. Scanlon, *J. Appl. Phys.,* 1993, **73**, 448.
19. M. A. Khan, Q. Chen, R. A. Skogman & J. N. Kuznia, *Appl. Phys. Lett.,* 1995, **66**, 2046.
20. B. Goldenberg, J. D. Zook & R. J. Ulmer, *App. Phys. Lett.*, 1993, **62**, 381.
21. M. A. Khan, J. N. Kuznia, D. T. Olson, J. M Van Hove & M. Blasingame, *Appl. Phys. Lett.*, 1992, **60**, 2917.
22. K. S. Stevens, M. Kinniburgh & R. Beresford, *Appl. Phys. Lett.,* 1995, **66**, 3518.
23. M. A. Khan, J. N. Kuznia, A. R. Bhattarai & D. T. Olson, *Appl. Phys. Lett.*, 1993, **62**, 1786.

24. A. Wakahara, T. Tsuchiya & A. Yoshida, *Vacuum,* 1990, **41**, 1071.
25. F. Ren, C. R. Abernathy, S. N. G. Chu, J. R. Lothian & S. J. Pearton, *Appl. Phys. Lett.,* 1995, **66**, 1503.
26. S. Nakamura, M. Senoh & T. Mukai, *Appl. Phys. Lett.,* 1993, **62** 2390.
27. S. Nakamura, M. Senoh, N. Iwasa & S. Nagahama, *Appl. Phys. Lett.,* 1995, **67**, 1868.
28. H. Morkoc & S. N. Mohammad, *Science*, 1995, **267**, 51.
29. S. Nakamura, T. Mukai & M. Senoh, *Appl. Phys. Lett.,* 1994, **64**, 1687.
30. M. A. Khan, A. Bhattarai, J. N. Kuznia & D. T. Olson, *Appl. Phys. Lett.,* 1993, **63**, 1214.
31. M. A. Khan, J. N. Kuznia, D. T. Olson, W. J. Schaff, J. W. Burm & M. S. Shur, *Appl. Phys. Lett.,* 1994, **65**, 1121.
32. A. J. Downs, *Chemistry of Aluminium, Gallium, Indium and Thallium,* Chapman & Hall, London, 1993.
33. W. S. Rees Jr. Ed, *CVD of Nonmetals,* VCH Publishers, New York, 1996.
34. Fichter & Spengel, *Z. Anorg. Allg. Chem.*, 1913, **82**, 192.
35. E. Tiede, M. Thimann & K. Sensse, *Chem. Ber.,* 1928, **61**, 1568.
36. W. C. Johnson, J. B. Parsons & M. C. Crew, *J. Phys. Chem.,* 1932, **36**, 2561.
37. R. C. Schoonmaker & C. E. Burton, *Inorg. Synth.,* 1963, **7**, 16.
38. R. Juza & H. Hahn, *Z. Anorg. Allg. Chem.,* 1940, **244**, 111.
39. C. M. Balkas & R. F. Davis, *J. Am. Ceram. Soc.,* 1996, **79**, 2309.
40. S.T. Barry, S. A. Ruoff & A. L. Ruoff, *Chem. Mater.*, 1998, **10**, 2571.
41. G. L. Wood, E. A. Pruss & R. T. Paine, *Chem. Mater.,* 2001, **13**, 12.
42. A. P. Purdy, *Chem. Mater.,* 1999, **11**, 1648.
43. Fischer & Schroter, *Ber.*, 1910, **43**, 1465.
44. R. Juza & H. Hahn, *Z. Anorg. Allg. Chem.,* 1938, **239**, 282.
45. R. L. Wells, C. G. Pitt, A. T. McPhail, A. P. Purdy, S. Shafieezad & R. B. Hallock, *Chem. Mater.,* 1989, **1**, 4.
46. R. L. Wells, C*oord. Chem. Rev.,* 1992, **112**, 273.
47. R. L. Wells, S. R. Aubuchon, S. S. Kher & M. S. Lube, *Chem. Mater.,* 1995, 793.
48. M. A. Olshavsky, A. N. Goldstein & A. P. Alivisatos, *J. Am. Chem. Soc.*, 1990, **112**, 9438.

49. L. Butler, G. Redmond & D. Fitzmaurice, *J. Phys. Chem.*, 1993, **97**, 10750.

50. H. Uchida, C. J. Curtis, P. V. Kamat, K. M. Jones & A. J. Nozik, *J. Phys. Chem.*, 1992, **96**, 1156.

51. T. Trindade, P. O'Brien & N. L. Pickett, *Chem. Mater.*, 2001, **13**, 3843.

52. J. A. Jegier, S. McKernan, A. P. Purdy & W. L. Gladfelter, *Chem. Mater.*, 2000, **12**, 1003.

53. L. Maya, *Adv. Ceram. Mater.*, 1986, **1**, 150.

54. W. Rockensüss & H. W. Roesky, *Adv. Mater.*, 1993, **5**, 443.

55. R. Riedel, S. Schaible, U. Klingebiel, M. Noltemeyer & E. Werner, *Z. Anorg. Allg. Chem.*, 1991, **603**, 119.

56. S. T. Barry & D. S. Richeson, *Chem. Mater.*, 1994, **6**, 2220.

57. J. Hwang, S. A. Hanson, D. Britton, J. F. Evans, K. F. Jensen & W. L. Gladfelter, *Chem. Mater.*, 1990, **2**, 342.

58. J. Hwang, J. P. Capbell, J. Kozubowski, S. A. Hanson, J. F. Evans & W. L. Gladfelter, *Chem. Mater.*, 1995, **7**, 517.

59. J. A. Jegier, S. McKernan, A. P. Purdy & W. L. Gladfelter, *Chem. Mater.*, 2000, **12**, 1003.

60. J. F. Janik & R. L. Wells, *Chem. Mater.*, 1996, **8**, 2708.

61. J. L. Coffer, T. W. Zerda, R. Appel, R. L. Wells & J. F. Janik, *Chem. Mater.*, 1999, **11**, 20.

62. O. I. Mićić, S. P. Ahrenkiel, D. Bertram & A. J. Nozik, *Appl. Phys. Lett.*, 1999, **75**, 478.

63. J. L. Coffer, M. A. Johnson, L. Zhang, R. L. Wells & J. F. Janik, *Chem. Mater.*, 1997, **9**, 2671.

64. S. D. Dingman, N. P. Rath, P. D. Markowitz, P. C. Gibbons & W. E. Buhro, *Angew. Chem. Int. Ed.*, 2000, **39**, 1470.

65. E. K. Byrne, L. Parkanyi & K. H. Theopold, *Science*, 1988, **241**, 332.

66. R. L. Wells, R. B. Hallock, A. T. McPhail, C. G. Pitt & J. D. Johansen, *Chem. Mater.*, 1991, **3**, 381.

67. J. F. Janik, R. L. Wells, V. G. Young Jr, A. L. Rheingold & I. A. Guzei, *J. Am. Chem. Soc.*, 1998, **120**, 532.

68. W. M. Yin, E. J. Stofko, P. J. Zanzucchi, J. I. PAnkove, M. Ettenberg & S. L. Gilbert, *J. Appl. Phys.*, 1973, **44**, 292.

69. Y. Someno, M. Sasaki & T. Hirai, *Jpn. J. Appl. Phys.,* 1991, **30**, 1792.

70. M. Morita, S. Isogai, N. Shimizu, K. Tsubouchi & N. Mikoshiba, *Jpn. J. Appl. Phys.,* 1981, **19**, L173.

71. M. Morita, M. Useugi, S. Isogai, , K. Tsubouchi & N. Mikoshiba, *Jpn. J. Appl. Phys.,* 1981, **20**, 17.

72. A. C. Jones, C. R. Whitehouse & J. S. Roberts, *Chem. Vap. Deposition,* 1995, **1**, 65.

73. J. J. Alwan & J. G. Eden, *Chem. Vap. Deposition,* 1997, **3**, 209.

74. M. A. Khan, J. N. Kuznia, R. A. Skogman, D. T. Olson, M. M. Millan & W. J. Choyke, *J. Appl. Phys. Lett.,* 1992, **61**, 2539.

75. W. Zhang, Y. Someno, M. Sasaki & T. Hirai, *J. Cryst. Growth,* 1993, **130**, 308.

76. A.C. Jones, J. Auld, S. A. Rushworth, E. W. Williams, P. W. Haycock, C. C. Tang & G. W. Critchlow, *Adv. Mater.,* 1994, **6**, 229

77. A. C. Jones, J. Auld, S. A. Rushworth, D. J. Houlton & G. W. Critchlow, *J. Mater. Chem.,* 1994, **4**, 1591.

78. J. Auld, D. J. Houlton, A. C. Jones, S. A. Rushworth G. W. Critchlow, *J. Mater. Chem.,* 1994, **4**, 1245.

79. H. Morkoc, *J. Mater. Sci.,* 2001, **12**, 677.

80. H. P. Maruska & J. J. Tietjen, *Appl. Phys. Lett.,* 1969, **15**, 327.

81. L. Baixia, L. Yinkui & L. Yi, *J. Mater. Chem.,*1993, **3**, 117.

82. M. Matloubian & M. Gershenzon, *J. Electron. Mater.,* 1985, **14**, 633.

83. P. J. Born & D. S. Robertson, *J. Mater. Sci.,* 1980, **15**, 3003.

84. C. I. Park, J. H. Kang, K. C. Kim, K. S. Nahm, E. K. Suh & K. Y. Lim, *Thin Solid Films,* 2001, **401**, 60.

85. W. T. Young, S. R. P. Silva, J. V. Anguita, J. M. Shannon, K. P. Homewood & B. J. Sealy, *Diamond and Related Materials,* 2000, **9**, 456.

86. D. M. Hoffman, *Polyhedron,* 1994, **13**, 1169.

87. E. D. Bourret-Corchesne, Q. Ye, K. M. Yu & J. W. Ager, *J. Cryst. Growth,* 2001, **231**, 89.

88. H. J. Hovel & J. J. Cuomo, *Appl. Phys. Lett.,* 1972, **20**, 71.

89. A. Wakahara & A. Yosida, *Appl. Phys. Lett.,* 1989, **54**, 709.

90. Y. Bu, L. Ma & M. C. Lin, *J. Vac. Sci. Technol.,* 1993, **A11**, 2931.

91. W. E. Hoke, P. J. Lemonias & D. G. Weir, *J. Cryst. Growth,* 1990, **111**, 1024.

92. L. A. Marasina, I. G. Pichugin & M. Tlaczala, *Krist. Tech.*, 1977, **12**, 541.

93. B. C. Harrison & E. H. Tompkins, *Inorg. Chem.,* 1962, **1**, 951.

94. H. M. Manasevit, *Appl. Phys. Lett.,* 1968, **12**, 156.

95. A. H. Cowley & R. A. Jones, *Angew. Chem. Int. Ed. Engl.,* 1989, **28**, 1208.

96. R. L. Wells, *Coord. Chem. Rev.,* 1992, **112**, 273 and references therein.

97. H. M. Manasevit & W. I. Simpson, *J. Electrochem. Soc.,* 1969, **116**, 1725.

98. T, Nakanisi, *J. Cryst. Growth,* 1984, **68**, 282.

99. G. B. Stringfellow, *J. Electon. Mater.,* 1988, **17**, 327.

100. T. L. Chu & R. W. Kelm Jnr, *J. Electrochem. Soc.,* 1975, **122**, 995.

101. Y. Takahashi, K. Yamashita, S. Motojima & K. Sugiyama, *Surf. Sci.,* 1979, **86**, 238.

102. L. V. Interrante, W. Lee, A. McConnell, N. Lewis & E. Hall, *J. Electrochem. Soc.,* 1989, **136**, 472.

103. A. C. Jones, S. A. Rushworth, D. J. Houlton, J. S. Roberts, V. Roberts & C. R. Whitehouse, *Chem. Vap. Deposition,* 1996, **2**, 5.

104. T. L. Chu, *J. Electrochem. Soc.,* 1971, **118**, 1200.

105. H. S. Park, S. D. Waezsada, A. H. Cowley & H. W. Roesky, *Chem. Mater.,* 1998, **10**, 2251.

106. J. Kouvetakis & D. B. Beach, *Chem. Mater.,* 1989, **1** 476.

107. M. M. Sung, C. Kim, S. H. Yoo, C. G. Kim & Y. Kim, *Chem. Vap. Deposition,* 2002, **8**, 50.

108. A. Devi, W. Rogge, A. Wohlfart, F. Hipler, H. W. Becker & R. A. Fischer, *Chem. Vap. Deposition,* 2000, **6**, 245.

109. H. Winker, A. Devi, A. Manz, A. Wohlfart, W. Rogge & R. A. Fischer, *Phys. Stat. Sol.,* 2000, **177**, 27.

110. R. A. Fischer, A. Miehr, T. Metzger, E. Born, O. Ambacher, H. Angerer & R. Dimitrov, *Chem. Mater.,* 1996, **8**, 1356.

111. H. Parala, A. Devi, F. Hipler, E. Maile, A. Birkner, H. W. Becker & R. A. Fischer, *J. Cryst. Growth,* 2001, **231**, 68.

112. B. J. Bae, J. E. Park, B. Kim & J. T. Park, *J. Organomet. Chem.,* 2000, **616**, 128.

113. A. Zaouk, E. Salvetat, J. Sakaya, F. Maury & G. Constant, *J. Cryst. Growth,* 1981, **55**, 135.

114. A. Zaouk & G. Constant, *J. Phys.,* 1982, **C5**, 43.

115. A. Zaouk, A. Lebugle & G. Constant, *J. Cryst. Growth,* 1979, **46**, 415.

116. F. Maury, A. E. Hammadi & G. Constant, *J. Cryst. Growth,* 1984, **68**, 88.

117. F. Maury, G. Constant, P. Fontaine & J. P. Biberian, *J. Cryst. Growth,* 1986, **78**, 185.

118. A. H. Cowley, B. L. Benac, J. G. Ekerdt, R. A. Jones, K. B. Kidd, J. Y. Lee & J. E. Miller, *J. Am. Chem. Soc.,* 1988, **110**, 6248.

119. A. H. Cowley & R. A. Jones, *Polyhedron,* 1994, **13**, 1149.

120. J. G. Ekerdt, Y. M. Sun, M. S. Jackson, V. Lakhotia, K. A. Pacheco, S. U. Koschmieder, A. H. Cowley & R. A. Jones, *J. Cryst. Growth,* 1992, **124**, 158.

121. C. J. Carmalt, *Coord. Chem. Rev.,* 2001, **223**, 217.

122. W. R. Nutt, J. A. Anderson, J. D. Odom, M. W. Williamson & B. H. Rubin, *Inorg. Chem.,* 1985, **24**, 159.

123. W. R. Nutt, J. S. Blanton, F. O. Kroh & J. D. Odom, *Inorg. Chem.,* 1989, **28**, 2224.

124. N.L. Pickett, O. Just, D.G. VanDerveer & W.S. Rees Jr, *Acta Cryst.,* 2000, C**56**, 560.

125. S. Kühner, R. Kuhnle, H. D. Hausen & J. Weidlein, *Z. Anorg. Allg. Chem.,* 1997, **623**, 25.

126. W. Uhl, J. Molter & R. Koch, *Eur. J. Inorg. Chem.,* 1999, 2021.

127. R. J. Wehmschulte & P. P. Power, *Inorg. Chem.,* 1998, **37**, 6906.

128. N. Wiberg & K. H. Schmid, *Z. Anorg. Allg. Chem.,* 1966, **345**, 93.

129. M. Jansen & T. Jäschke, *Z. Naturforsch.,* 2000, **55b**, 763.

130. S. Kühner, H. D. Hausen & J Weidlein, *Z. Anorg. Allg. Chem.,* 1998, **624**, 13.

131. S. T. Barry & D. S. Richeson, *Chem. Mater.,* 1994, **6**, 2220.

132. M. Veith, S. Hill & V. Huch, *Eur. J. Inorg. Chem.,* 1999, 1343.

133. P. J. Brothers, R. J. Wehmschulte, M. M. Olmstead, K. Ruhlandt-Senge, S. R. Parkin & P. P. Power, *Organometallics,* 1994, **13**, 2792.

134. H. Bürger, J. Cichon, U. Goetze, U. Wannagat & H. J. Wismar, *J.*

Organomet. Chem., 1971, **33**, 1.

135. M. A. Petrie, K. Ruhlandt-Senge, H. Hope & P. P. Power, *Bull. Soc. Chim. Fr.,* 1993, **130**, 851.

136. D. A. Atwood, V. O. Atwood, A. H. Cowley, R. A. Jones, J. L. Atwood & S. G. Bott, *Inorg. Chem.,* 1994, **33**, 3251.

137. J. Kim, S. G. Bott & D. M. Hoffman, *Inorg. Chem.,* 1998, **37**, 3835.

138. D. M. Choquette, M. J. Timm, J. L. Hobbs, M. M. Rahim, Z. J. Ahmed & R. P. Planalp, *Organometallics,* 1992, **11**, 529.

139. B. J. Bae, J. E. Park, Y. Kim, J. T. Park & I. H. Suh, *Organometallics,* 1999, **18**, 2513.

140. E. K. Styron, S. J. Schauer, C. H. Lake, C. L. Watkins & L. K. Krannich, *J. Orgnaomet. Chem.,* 1999, **585**, 266.

141. K. A. Aitchison, J. D. J. Backer-Dirks, D. C. Bradley, M. M. Faktor, D. M. Frigo, M. B. Hursthouse, B. Hussain & R. L. Short, *J. Organomet. Chem.,* 1989, **366**, 11.

142. M. Porchia, F. Benetollo, N. Brianese, G. Rossetto, P. Zanella & G. Bombieri, *J. Organomet. Chem.,* 1992, **424**, 1.

143. J. J. Byers, W. T. Pennington, G. H. Robinson & D. C. Hrncir, *Polyhedron,* 1990, **9**, 2205.

144. S. Kühner, K. W. Klinkhammer, W. Schwarz & J. Weidlein, *Z. Anorg. Allg. Chem.,* 1998, **624**, 1051.

145. R. L. Wells, A.T. McPhail & T. M. Speer, *Eur. J. Solid State Inorg. Chem.,* 1992, **29**, 63.

146. R. L. Wells, A. T. McPhail & T. M. Speer, *Organometallics,* 1992, **11**, 690.

147. F. Thomas, S. Schulz & M. Nieger, *Eur. J. Inorg. Chem.,* 2001, 161.

148. R. L. Wells, A. T. McPhail & A. Alvanipour, *Polyhedron,* 1992, **11**, 839.

149. M. A. Olshavsky, A. N. Goldstein & A. P. Alivisatos, *J. Am. Chem. Soc.,* 1990, **112**, 9438.

150. R. L. Wells, A. T. McPhail, J. W. Paterczyk & A. Alvanipour, *Organometallics,* 1992, **11**, 226.

151. R. L. Wells, J. W. Pasterczyk, A. T. McPhail, J. D. Johansen & A. Alvanipour, *J. Orgnaomet. Chem.,* 1991, **407**, 17.

152. R. L. Wells, A. T. McPhail, L. J. Jones & M. F. Self, *Polyhedron,* 1993, **12**,

141.

153. L. J. Jones, A. T. McPhail, & R. L. Wells, *Organometallics,* 1994, **13**, 3643.

154. R. L. Wells, L. J. Jones, A. T. McPhail & A. Alvanipour, *Organometallics,* 1991, **10**, 2345.

155. W. K. Holley, R. L. Wells, S. Shafieezad, A. T. McPhail & C. G. Pitt, *J. Organomet. Chem.,* 1990, **381**, 15.

156. J. B. Hill, T. A. Talley, W. T. Pennington & G. H. Robinson, *J. Chem. Cryst.*, 1994, **24**, 61.

157. H. Schimidaur & W. Findeiss, *Chem. Ber.,* 1966, **141**, 2187.

158. J. Weidlein, *J. Organomet. Chem.*, 1969, **17**, 213.

159. G. Allegra, G. Perego & A. Immirzi, *Makromol. Chem.*, 1963, **63**, 69.

160. D. A. Atwood, A. H. Cowley, R. A. Jones, M. A. Mardones & J. L. Atwood, *J. Coord. Chem.,* 1992, **25**, 233.

161. C. J. Carmalt & J. W. Steed, *Polyhedron,* 2000, **19**, 1639.

162. R. A. Baldwin, H. Rahbarnoohi, L. J. Jones III, A. T. McPhail & R. L. Wells, *Heteroatom Chem.*, 1996, **7**, 409.

163. A. Y. Timoshkin, H. F. Bettinger & H. F. Schaefer III, *Inorg. Chem.,* 2002, **41**, 738.

3. Group 13 chalcogenides

3.1 Introduction

Group 13 chalcogenides have a wide range of potential applications including as wear resistant coatings (Al_2O_3),[1,2] dielectrics (Al_2O_3),[3] photovoltaics (In_2S_3),[4,5] switching devices,[5] non-linear optics[6] and displays. In this study, the preparation of aluminium alkoxides and thiolates, which could act as single-source precursors to aluminium oxide and sulfide respectively, was investigated.

Aluminium oxide (alumina) only exists in the stoichiometric form Al_2O_3 although there are various crystalline forms. The most stable of these forms is α-Al_2O_3, which occurs naturally as the mineral corundum. It has a rhombohedral crystal structure in which the oxygen atoms adopt a hexagonal close packed array with aluminium atoms ordered on two-thirds of the octahedral interstices. The second common phase is γ-Al_2O_3 which has a less compact defect spinel structure. The oxygen atoms form a 32-atom face centred cubic arrangement and a random occupation of 21⅓ of the 24 available octahedral and tetrahedral sites. Aluminium sulfide also exists only in the stoichiometric form Al_2S_3 although there are several crystalline forms. Two common forms are based on the hexagonal zinc sulfide (wurtzite) structure in which there are two interpenetrating hexagonal close packed lattices, one fully occupied with sulfur atoms and the other two thirds occupied with aluminium atoms. In α-Al_2S_3 the aluminium atoms fill the lattice in an ordered manner and in β-Al_2S_3 the aluminium atoms fill the lattice in a random fashion. A third common phase of Al_2S_3 is γ-Al_2S_3 which has a defect spinel structure similar to γ-Al_2O_3.[7]

3.1.1 Aluminium chalcogenides

Aluminium oxide has many useful properties including a high melting point (2045 °C), low volatility, chemical inertness, good electrical insulating properties and great hardness. These properties make Al_2O_3 a versatile material with a wide range of engineering applications.[8] Uses of bulk Al_2O_3 powders includes in

abrasives, refractory materials and ceramics. Thin films of Al_2O_3 have also been investigated as high temperature wear resistant coatings,[1,9] corrosion resistant coatings,[10] mechanical barriers against air or moisture penetration[11,12] and high temperature diffusion barriers.[13] The dielectric constant of Al_2O_3 is a factor of two higher than that of SiO_2,[14] making thin films of Al_2O_3 useful as dielectrics in electronic devices[15] such as capacitors.[3] The less stable γ-Al_2O_3 has a far higher surface area than α-Al_2O_3 and is important in the preparation of catalyst supports.

3.1.2 Synthesis of bulk materials

Industrially, α-Al_2O_3 is prepared by igniting [$Al(OH)_3$] or [AlO(OH)] at high temperatures (1200 °C). Bulk samples of α-Al_2O_3 may be prepared by combustion of aluminium metal. The less stable γ-Al_2O_3 is formed by dehydration of [γ-$Al(OH)_3$] or [γ-AlO(OH)] at low temperatures (<450 °C). Aluminium sulfide is formed by the reaction of aluminium and sulfur at high temperatures (>1000 °C).[7] Al_2S_3 is moisture sensitive, reacting with water to form [$Al(OH)_3$] and H_2S.

3.1.3 Preparation of thin films by dual-source routes

Traditionally, Al_2O_3 films are prepared by a dual-source CVD reaction involving a trialkyl aluminium complex (typically [Me_3Al]) and an oxygen source (e.g. O_2, N_2O).[8] One of the first oxygen sources used was N_2O which reacts with [Me_3Al] at a substrate temperature of 650 °C to form either amorphous or γ-Al_2O_3.[16] More recently, thin films of Al_2O_3 have been grown using the same precursors at both higher (1000 °C)[17,18] and lower (360 °C)[19] substrate temperatures. Deposition of Al_2O_3 films has been carried out at lower temperatures (around 350 °C)[20] by the CVD reaction of [Me_3Al] and O_2.[21,22] It has also been reported that using O_2 as opposed to N_2O leads to the formation of higher quality films.[8] Other oxygen sources which have been used with [Me_3Al] to form Al_2O_3 include H_2O[23] and H_2O_2.[19]

Amorphous Al_2O_3 thin films have been grown in a low-pressure MOCVD experiment using [$Al(acac)_3$] and H_2O at a substrate temperature of 330 °C.[15] It was found that when H_2O was not used, Al_2O_3 films were produced but these contained

high levels of carbon contamination (~25% by XPS). When H_2O was used as a co-reactant near stoichiometric carbon free films (by XPS, AES and RBS) were formed. The dialkylaluminium acetylacetonate precursors, [$R_2Al(acac)$] (where R = Me, Et, ^tBu) have been used to prepare Al_2O_3 thin films when reacted with either O_2 or H_2O at substrate temperatures between 400 and 520 °C.[24]

Other techniques which use the precursor systems described above, have also been used to form Al_2O_3. Atomic layer deposition has been used to form thin films of Al_2O_3 at low substrate temperatures (300 °C).[25] In this process, [Me_3Al] and H_2O were used to form carbon free (> 0.1%) films. Sequential reactions of [Me_3Al] and either H_2O[26,27] or H_2O_2[28] have been used extensively to form Al_2O_3 at substrate temperatures as low as 100 °C. Molecular beam epitaxy (MBE) was used to prepare γ-Al_2O_3 films at substrate temperatures between 720 and 800 °C by the use of N_2O.[29]

3.1.4 Preparation of thin films by single-source routes

Metal alkoxides are well established precursors to metal oxides[30] and aluminium alkoxides are no exception. The aluminium alkoxides [$Al(OR)_3$] (where R = ^iPr (**1**),[31,32] ^tBu (**2**)[9,10]) have been used as single-source precursors in CVD reactions to form Al_2O_3 thin films. Typically, substrate temperatures below 450 °C were used in the depositions. The effect of the atmosphere in the CVD reactor during the deposition of Al_2O_3 from **1** has been investigated.[14] It was found that although **1** may act as a single-source precursor, the rate of deposition decreases as the substrate temperature decreases, if however H_2O is used in the reaction, the deposition rate increases at lower temperatures.

Volatile dialkylaluminium alkoxides, [$R_2Al(OR')$] (where R = Me, R' = ^iPr (**3**), ^tBu (**4**); R = Et, R' = ^iPr (**5**)) have been prepared and used as single-source precursors to Al_2O_3.[33] The precursors were found to be volatile at room temperature under reduced pressure. The resulting films were found to contain no carbon contamination (by Auger depth profiling).

Although [$Al(acac)_3$] (**6**) has been used in a dual-source reaction to form Al_2O_3, **6** may be used as a single-source precursor at substrate temperatures as low as

250 °C.[34] The fluorinated analogue of **6**, $[Al(C_5F_7O_2)_3]$ (**7**) has been prepared.[35] It was found that **7** has a significantly higher vapour pressure than **6** at temperatures below the decomposition temperature. This makes handling the precursor in the vapour phase easier as lower temperatures may be used. The single-source precursor $[Al(C_8H_{15}O_2)_3]$ (**8**) has also been prepared.[36] The composition[37] and optical properties[38] of films of Al_2O_3 deposited from **8** were found to contain high levels of carbon. Another precursor which is of interest is $[H_2Al(O^tBu)]_2$ (**9**), which has been used to prepare a Al/Al_2O_3 composite material with low levels of carbon contamination.[39]

The preparation of thin films of Al_2S_3 has not been reported as having been attempted. However, the CVD of other group 13 sulfides, in particular gallium sulfide and indium sulfide are well known and have been comprehensively reviewed.[40,41]

3.1.5 Group 13 alkoxides

Aluminium alkoxides of the type $[Al(OR)_3]_n$ (where R = Me (**10**), Et (**11**), ^{i}Pr (**12**), ^{n}Bu (**13**), ^{t}Bu (**14**)) were first prepared by Nöth *et al* by the reaction of $[AlH_3]$ and 3 equivalents of ROH, as shown in Eq. 3.1.[42]

$$AlH_3 + 3\,ROH \longrightarrow Al(OR)_3 + 3H_2 \quad \textbf{(3.1)}$$

The structure of **12** has been determined by X-ray crystallography. It was found that in the solid state a tetrameric structure is formed (Figure 3.1).[43,44] The structure of **12** consists of a central aluminium surrounded by six bridging ^{i}PrO groups to three other aluminium atoms. This central core has been likened to the emblem of the Mitsubishi company.[44,45] Each of the outer aluminium atoms has two terminal ^{i}PrO groups attached.

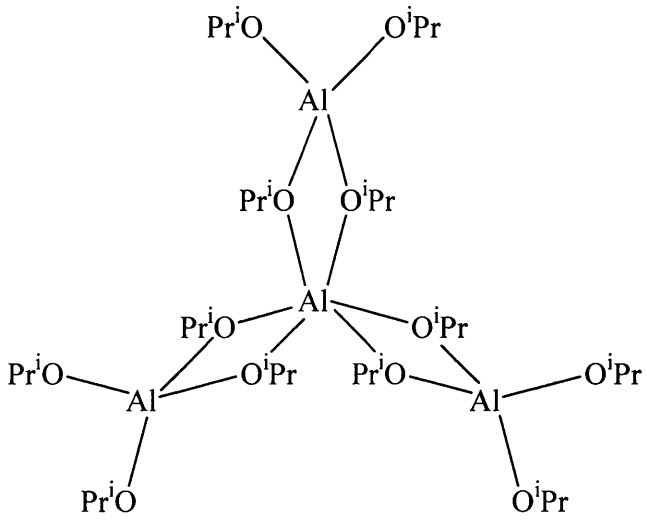

Figure 3.1 Structure of $[Al(O^iPr)_3]_4$ (12)

Dimeric metal alkoxides, $[M(OR)_3]_2$, may adopt one of two possible structural types I and II. Type I (shown in Figure 3.2) involves the alkoxide groups bridging the two aluminium centres whereas type II (shown in Figure 3.3) involves a direct M-M bond. The aluminium alkoxides $[M(OR)_3]_2$ can only adopt type I structures as the M-M bond in the type II structures involves π bonding between the d orbitals. The structure of **14** has been determined and was found to be alkoxide bridged.[46]

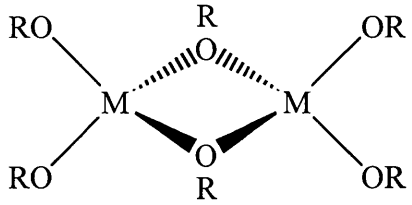

Figure 3.2 Structural type I metal alkoxides

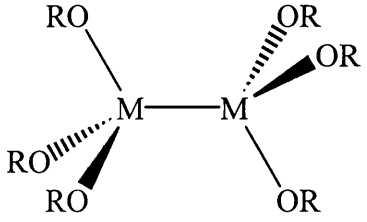

Figure 3.3 Structural type II metal alkoxides

The monomeric *tris* aluminium alkoxide, $[Al(OR)_3]$ (where R = 2,6-$^tBu_2$-4-MeC_6H_2 (**15**)[47]) has been prepared by a two step synthesis via $[HAl(OR)_2(OEt_2)]$. The structure of **15** was found to be monomeric with the aluminium centre adopting a trigonal planar geometry, as shown in Figure 3.4.

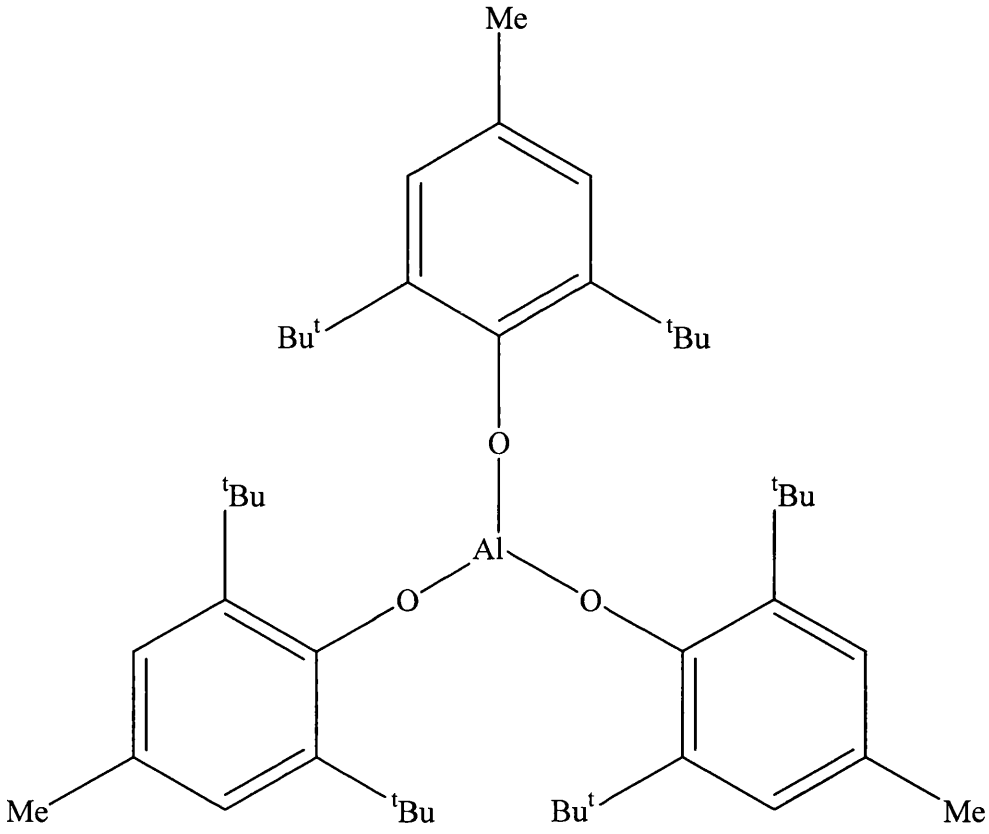

Figure 3.4 Structure of $[Al(OC_6H_2{}^tBu_2Me)_3]$ (15)

The *tris* aluminium alkoxide, $[Al(OCy)_3]_3$ (**16**)[48] has been prepared by the reaction of CyOH and aluminium metal in refluxing xylene. Compound **16** adopts a structure, similar to the structure of **12** (Figure 3.1) but with only four OR bridges, as shown in Figure 3.5.

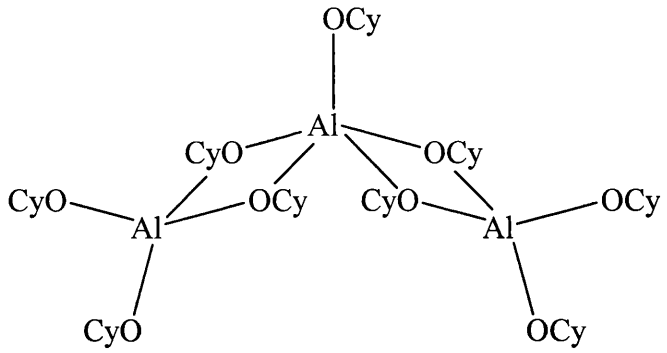

Figure 3.5 Structure of $[Al(OCy)_3]_3$ (16)

The hydride containing alkoxides, $[HAl(OR)_2]$ (where R = Me (**17**), Et (**18**), ^{i}Pr (**19**), ^{n}Bu (**20**), ^{t}Bu (**21**)) were prepared by the reaction of $[AlH_3]_n$ and two equivalents of ROH.[42] The structure of **21** was found to be dimeric, with two ^{t}BuO groups bridging the two aluminium atoms.[49] One terminal ^{t}BuO group and one hydride are also attached to each of the aluminium atoms, as shown in Figure 3.6. The two terminal ^{t}BuO groups were found to be arranged in a *trans* fashion.

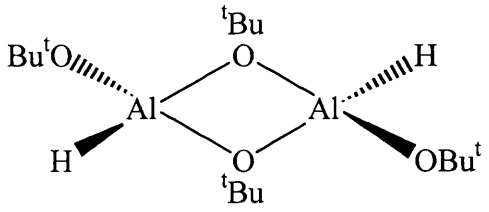

Figure 3.6 Structure of $[HAl(O^{t}Bu)_2]$ (21)

The reaction of $[AlH_3(NR'_3)]$ and two equivalents of ROH lead to the formation of monomeric species if the R group has sufficient steric bulk. The reaction of $[AlH_3(NMe_2Et)]$ and two equivalents of either 2,6-$^{i}Pr_2C_6H_3OH$ or Ph_3COH resulted in the formation of $[HAl(OC_6H_3{}^{i}Pr_2\text{-}2,6)_2(thf)_2]$ (**22**) and $[HAl(OCPh_3)_2(thf)]$ (**23**), respectively.[50] The monomeric species $[HAl(OR)_2(NMe_3)]$ (where R = 2,6-$^{t}Bu_2$-4MeC_6H_2 (**24**)) was formed by a ligand redistribution reaction involving $[H_2Al(OR)(NMe_3)]$ (where R = 2,6-$^{t}Bu_2$-4MeC_6H_2 (**25**)) and $NH_2{}^{t}Bu$.[51] It was found that **24** is monomeric with the aluminium atom adopting a distorted tetrahedral geometry, as shown in Figure 3.7. The reaction of $[AlH_3(NMe_3)]$ and two

equivalents of an amino alcohol (R'OH) has been used to form $[HAl(OR')_2]$ (where R' = $CH_2CH_2CH_2NMe_2$ (**26**)).[52]

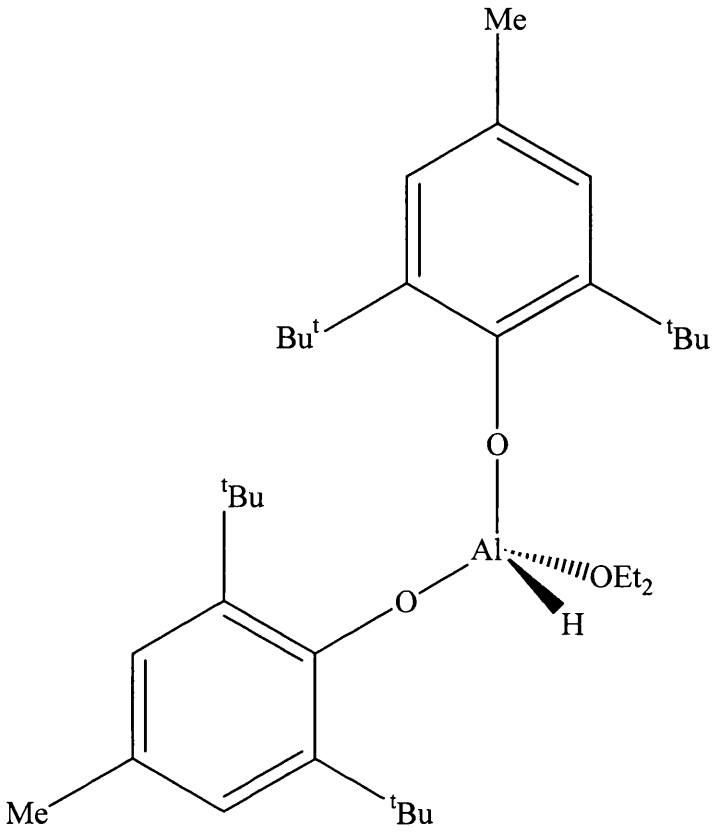

Figure 3.7 Structure of $[HAl(OC_6H_2{}^tBu_2Me)_2(NMe_3)]$ (24)

The *bis* hydrides $[H_2Al(OR)]_n$ (where R = Me (**27**), Et (**28**), ^{i}Pr (**29**), ^{n}Bu (**30**), ^{t}Bu (**31**)) have been formed by the reaction of $[AlH_3]_n$ with one equivalent of ROH.[42] The structure of **31** has been determined and was found to be dimeric (Figure 3.8).[49]

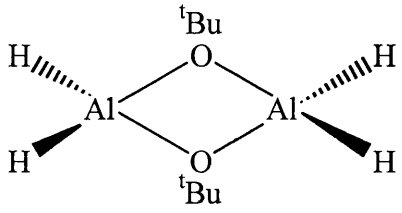

Figure 3.8 Structure of $[H_2Al(O^tBu)]_2$ (31)

Recently, $[H_2Al(OSiMe_3)]_n$ (**32**) was prepared by the reaction of $[AlH_3]_n$ and Me_3SiOH.[53] Compound **32** is tetrameric in solution and polymeric in the solid state. The compounds $[H_2Al(OR')]$ (where R' = $CH_2CH_2NMe_2$ (**33**), $CH(Ph)CH(Me)NMe_2$ (**34**), $CH_2CH_2CH_2NMe_2$ (**35**)) have also been formed from the reaction of $[AlH_3(NMe_3)]$ and the corresponding amino alcohol.[52]

3.1.6 Group 13 thiolates

The homoleptic aluminium thiolate complex $[Al(S^tBu)_3]_2$ (**36**) was isolated from the reaction of $[AlBr_3]$ and three equivalents of NaS^tBu.[54] The analogous complex $[Al(S^iPr)_3]_2$ (**37**) was prepared by the reaction of $[AlH_3(OEt_2)]$ and an excess of ^{i}PrSH. Both of these complexes were found to be dimeric in the solid state, similar to that shown in Figure 3.2. The monomeric thf adduct $[Al(S^tBu)_3(thf)]$ (**38**) resulted from the reaction of $[Al(N^iPr_2)_3]_2$ and a large excess of ^{t}BuSH in thf, as shown in Eq. 3.2.[54]

$$[Al(N^iPr_2)_3] + \text{xs } {}^t\text{BuSH} \longrightarrow [Al(S^tBu)_3(thf)] + 3\ HN^iPr_2 \quad \textbf{(3.2)}$$

The amine adducts $[Al(SR)_3(NHMe_2)]$ (where R = ^{i}Pr (**39**), ^{t}Bu (**40**)) have been prepared by the reaction of $[Al(NMe_2)_3]_2$ and a large excess of RSH, as shown in Eq. 3.3.[54]

$$[Al(NMe_2)_3]_2 + \text{xs RSH} \longrightarrow 2\ [Al(SR)_3(NHMe_2)] + 4\ NHR_2 \quad \textbf{(3.3)}$$

Similar amine adducts, $[Al(SR)_3(NMe_2Et)]$ (where R = ^{i}Pr (**41**), ^{t}Bu (**42**)), were prepared by the reaction of $[AlH_3(NMe_2Et)]$ and an excess of RSH, as shown in Eq. 3.4.[54]

$$[AlH_3(NMe_2Et)] + \text{xs RSH} \longrightarrow [Al(SR)_3(NMe_2Et)] + 3\ H_2 \quad \textbf{(3.4)}$$

The structures of **38** and **40** were determined and found to be monomeric with a distorted trigonal pyramidal geometry.[54]

The hydride containing species $[HAl(S^tBu)_2(NMe_3)]$ (**43**) was isolated from the reaction of $[AlH_3(NMe_3)]$ and two equivalents of ^tBuSH.[55] The *bis* hydrides $[H_2Al(SR)(NMe_3)]$ (where R = Et (**44**), ^{i}Pr (**45**), ^{t}Bu (**46**)) were prepared by the reaction of $[AlH_3(NMe_3)]$ and one equivalent of ^tBuSH.[55] The structure of **43** was determined and found to be monomeric in the solid state with a distorted tetrahedral geometry around the aluminium, similar to that shown in Figure 3.7.[55]

3.2 Results and discussion

3.2.1 Synthetic strategies for aluminium chalcogenides

Two main synthetic approaches were employed in the preparation of aluminium chalcogenides.

Method A $[AlH_3(OEt_2)]$, was prepared *in situ* by the reaction of $[AlCl_3]$ and $[LiAlH_4]$ as shown in Eq. 3.5.

$$[AlCl_3] + 3\,[LiAlH_4] \longrightarrow 4\,[AlH_3(OEt_2)] + 3\,LiCl \quad \textbf{(3.5)}$$

This was then reacted with either one or two equivalents of an alcohol or thiol in an attempt to form $[H_2Al(ER)]_n$ or $[HAl(ER)_2]_n$ (where E = O or S, R = alkyl or aryl, n = 2, 3).

Method B In this method, $[AlH_3(NMe_2Et)]$, was reacted directly with the appropriate alcohol or thiol. This reaction could result in species which contain the amine attached to the aluminium, such as $[H_2Al(ER)(NMe_2Et)]$ (where E = O or S, R = alkyl or aryl), which may be monomeric. Alternatively, the amine could be lost to give similar products to those formed by method A.

In both of the above methods it is important that a stoichiometeric amount of alcohol or thiol is used otherwise mixtures may result.

3.2.2 Reaction of $[AlH_3(OEt_2)]$ and ^iPrOH

The reaction of $[AlH_3(OEt_2)]$ (generated *in situ* from $[LiAlH_4]$ and $[AlCl_3]$ as described in section 3.2.1) and 1 equivalent of ^iPrOH was carried out at room temperature in diethyl ether. After work-up and cooling to -20 °C, colourless crystals suitable for X-ray crystallography were obtained in 43% yield. Analytical and spectroscopic data showed that $[Al_5(\mu_4\text{-}O)(\mu\text{-}O^iPr)_7H_6]$ (**47**) had been formed, as shown in Eq 3.6.

$$[AlH_3(OEt_2)] + {}^iPrOH \longrightarrow [Al_5(\mu_4\text{-}O)(\mu\text{-}O^iPr)_7H_6] \quad (\mathbf{3.6})$$

The ^1H NMR spectrum of **47** shows a number of overlapping multiplets corresponding to $CH(CH_3)_2$ (1.40 - 1.50 ppm) and $CH(CH_3)_2$ (4.56 - 4.63 and 4.75 ppm). This suggests that the solution behaviour of **47** is complex and the solid state structure may be lost. The infra-red spectrum was recorded and shows the expected peaks for the terminal hydrides (1830, 1822, 784 and 725 cm^{-1}).

3.2.3 X-ray structure of $[Al_5(\mu_4\text{-}O)(\mu\text{-}O^iPr)_7H_6]$ (47)

The structure of compound **47** was determined by X-ray crystallography, the results of which are shown in Figure 3.9; selected bond lengths and angles are given in Table 3.1. The structure of **47** has crystallographic C_s symmetry about a plane containing Al(3), Al(4) and O(4). The geometry at the four coordinate central oxygen atom can be thought of as square pyrimidal, with Al(4) occupying the apical position, but with the basal site opposite to Al(3) vacant. The Al(1) atom which could occupy that site has flipped out of the Al(2)/Al(2A)/Al(3) plane away from Al(4). The oxygen atom lies 0.26 Å out of the Al(2)/Al(2A)/Al(3) plane in the direction of Al(4). The Al-O(^{i}Pr) distances involving Al(2), Al(3) and Al(4) are typical, whereas those to the bridging Al(1) are significantly shorter (by 0.04 Å); conversely, the Al-O bonds to the central oxygen atom are longer (by 0.04 Å), with that to Al(4) being the longest.

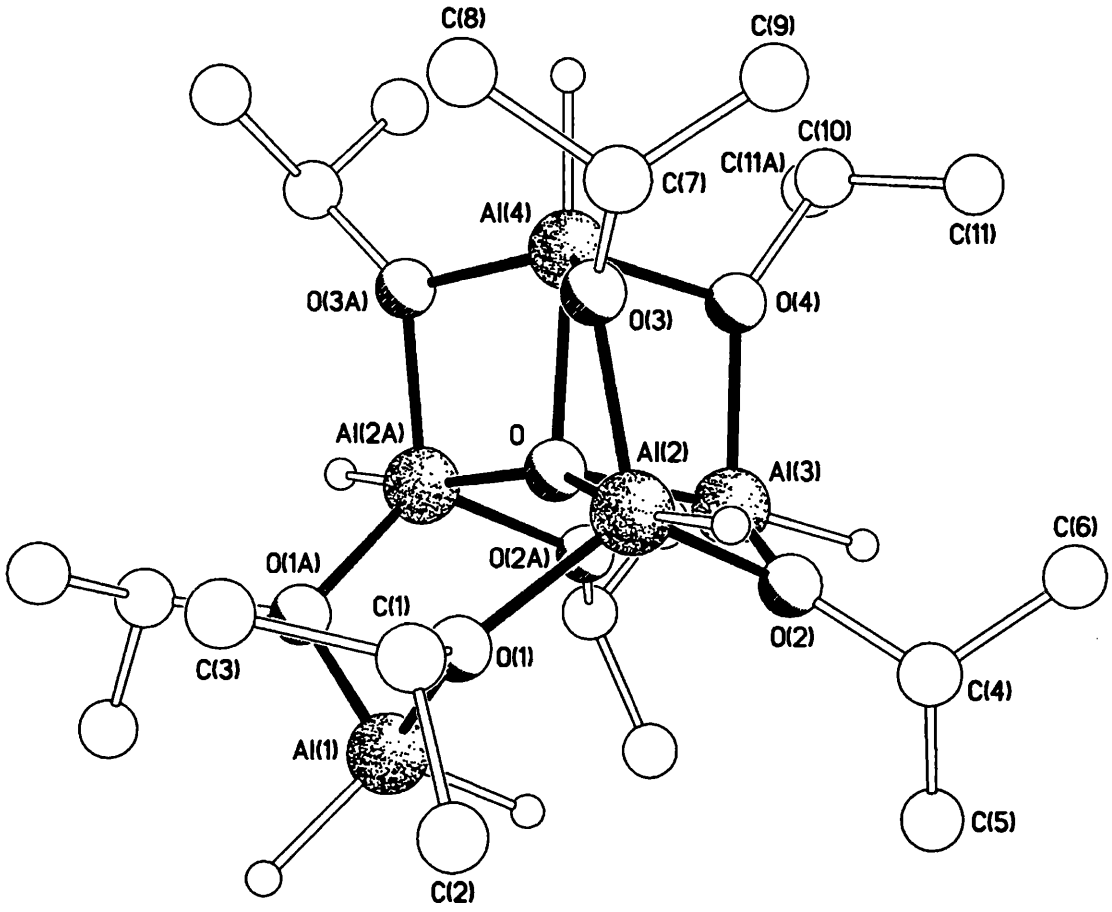

Figure 3.9 X-ray structure of $[Al_5(\mu_4\text{-}O)(\mu\text{-}O^iPr)_7H_6]$ (47)

Table 3.1 Selected bond lengths (°) and angles (Å) for $[Al_5(\mu_4\text{-}O)(\mu\text{-}O^iPr)_7H_6]$ (47)

Al(1)-O(1)	1.815(2)	Al(2)-O(3)	1.850(2)
Al(1)-O(1A)	1.815(2)	Al(2)-O(1)	1.851(2)
Al(2)-O(2)	1.843(2)	Al(2)-O	1.8873(9)
Al(2)-Al(4)	2.8859(12)	Al(3)-O(2A)	1.858(2)
Al(2)-Al(3)	2.8900(12)	Al(3)-O(2)	1.858(2)
Al(3)-O(4)	1.853(4)	Al(3)-O	1.913(3)
Al(3)-Al(2A)	2.8900(12)	Al(4)-O(3)	1.844(2)
Al(3)-Al(4)	2.907(2)	Al(4)-O(4)	1.845(4)
Al(4)-O(3A)	1.844(2)	Al(4)-O	1.940(3)
Al(4)-Al(2)	2.8859(12)	O-Al(2)	1.8873(9)

O(1)-Al(1)-O(1A)	106.62(14)	O(3)-Al(2)-O(1)	116.44(10)
O(2)-Al(2)-O(3)	119.97(11)	O(2)-Al(2)-O	78.48(10)
O(2)-Al(2)-O(1)	118.67(10)	O(3)-Al(2)-O	78.68(10)
O(1)-Al(2)-O	90.97(10)	O(1)-Al(2)-Al(4)	116.15(8)
O(2)-Al(2)-Al(4)	94.80(8)	O-Al(2)-Al(4)	41.75(8)
O(3)-Al(2)-Al(4)	38.55(6)	O(2)-Al(2)-Al(3)	38.84(7)
O(3)-Al(2)-Al(3)	95.64(7)	Al(4)-Al(2)-Al(3)	60.45(4)
O(1)-Al(2)-Al(3)	115.96(8)	O(4)-Al(3)-O(2A)	107.47(8)
O-Al(2)-Al(3)	40.82(8)	O(4)-Al(3)-O(2)	107.47(8)
O(2A)-Al(3)-O(2)	131.81(15)	O(2A)-Al(3)-O	77.47(7)
O(4)-Al(3)-O	79.44(13)	O(2)-Al(3)-O	77.47(7)
O(4)-Al(3)-Al(2A)	87.88(9)	O-Al(3)-Al(2A)	40.16(3)
O(2A)-Al(3)-Al(2A)	38.46(7)	O(4)-Al(3)-Al(2)	87.88(9)
O(2)-Al(3)-Al(2A)	112.27(8)	O(2A)-Al(3)-Al(2)	112.27(8)
O(2)-Al(3)-Al(2)	38.46(7)	O(4)-Al(3)-Al(4)	38.08(10)
O-Al(3)-Al(2)	40.16(3)	O(2A)-Al(3)-Al(4)	93.76(8)
Al(2A)-Al(3)-Al(2)	79.05(4)	O(2)-Al(3)-Al(4)	93.76(8)
O-Al(3)-Al(4)	41.36(8)	O(3A)-Al(4)-O(3)	126.83(15)
Al(2A)-Al(3)-Al(4)	59.71(3)	O(3A)-Al(4)-O(4)	110.04(8)
Al(2)-Al(3)-Al(4)	59.71(3)	O(3)-Al(4)-O(4)	110.04(8)
O(3A)-Al(4)-O	77.48(7)	O(3A)-Al(4)-Al(2A)	38.69(7)
O(3)-Al(4)-O	77.48(7)	O(3)-Al(4)-Al(2A)	111.06(8)
O(4)-Al(4)-O	78.93(13)	O(4)-Al(4)-Al(2A)	88.15(9)
O-Al(4)-Al(2A)	40.38(3)	O(4)-Al(4)-Al(2)	88.15(9)
O(3A)-Al(4)-Al(2)	111.06(8)	O-Al(4)-Al(2)	40.38(3)
O(3)-Al(4)-Al(2)	38.69(7)	Al(2A)-Al(4)-Al(2)	79.18(4)
O(3A)-Al(4)-Al(3)	95.20(8)	O-Al(4)-Al(3)	40.66(8)
O(3)-Al(4)-Al(3)	95.20(8)	Al(2A)-Al(4)-Al(3)	59.85(3)
O(4)-Al(4)-Al(3)	38.27(11)	Al(2)-Al(4)-Al(3)	59.85(3)
Al(2A)-O-Al(2)	154.09(15)	Al(2A)-O-Al(4)	97.88(8)
Al(2A)-O-Al(3)	99.02(8)	Al(2)-O-Al(4)	97.88(8)
Al(2)-O-Al(3)	99.02(8)	Al(3)-O-Al(4)	97.99(12)
C(1')-O(1)-Al(1)	105.0(5)	C(1)-O(1)-Al(2)	110.2(3)

C(1)-O(1)-Al(1)	131.5(3)	Al(1)-O(1)-Al(2)	117.98(11)
C(1')-O(1)-Al(2)	137.0(5)	C(4)-O(2)-Al(2)	125.0(2)
C(4)-O(2)-Al(3)	132.1(2)	C(7)-O(3)-Al(2)	125.7(2)
Al(2)-O(2)-Al(3)	102.70(10)	Al(4)-O(3)-Al(2)	102.76(10)
C(7)-O(3)-Al(4)	130.1(2)	C(10)-O(4)-Al(4)	115.6(4)
C(10')-O(4)-Al(4)	148.8(7)	Al(4)-O(4)-Al(3)	103.64(15)
C(10)-O(4)-Al(3)	140.7(4)		

3.2.4 Preparation of $[Al_5(\mu_5\text{-}O)(\mu\text{-}O^iPr)_8(Cl)H_4]$ (48)

The reaction described in 3.2.2 was repeated, however incomplete reaction occurred between $[AlCl_3]$ and $[LiAlH_4]$. After work-up and cooling to -20 °C colourless crystals resulted. Analytical and spectroscopic data showed that $[Al_5(\mu_5\text{-}O)(\mu\text{-}O^iPr)_8(Cl)H_4]$ (**48**) had been formed in 39% yield, as shown in Eq. 3.7.

$$[AlCl_3] + 3\,[LiAlH_4] + 4\,{}^iPrOH \longrightarrow [Al_5(\mu_5\text{-}O)(\mu\text{-}O^iPr)_8(Cl)H_4] \quad (\mathbf{3.7})$$

Compound **48** may be formed if an incomplete reaction between $[AlCl_3]$ and $[LiAlH_4]$ takes place and $[AlH_3(OEt_2)]$ is not the exclusive product. This accounts for the incorporation of a chlorine atom into **48**. Both the ^1H and ^{13}C NMR show that four O^iPr environments exist in solution; this indicates that two species are present as each species would give rise to two environments. This suggests that the solid state structure may not be fully retained in solution. The infra-red spectra of **48** was recorded and most notably shows the characteristic absorption bands for the Al-H bond at 1820 and 797 cm^{-1}.

3.2.5 X-ray structure of $[Al_5(\mu_5\text{-}O)(\mu\text{-}O^iPr)_8(Cl)H_4]$ (48)

The X-ray structure determination showed the crystals of **48** to contain two crystallographically independent C_2 symmetric penta-aluminium cages, one of which is shown in Figure 3.10; selected bond lengths and angles are given in Table 3.2. The structure of **48** shows similarity with $[Al_5(\mu_5\text{-}O)(O^iBu)_8H_5]$ (**49**), the only major difference between the two structures being the occupation of the apical site by a

chloride in **48** as opposed to a hydride in **49**. The cage structure adopted by **48** and **49** is essentially identical, with the bonds between O(1), O(2), O(1A) and O(2A) to the apical aluminium Al(1) being about 0.15 Å longer than the bonds with Al(2) and Al(3). Similarly, bond lengths between the central O and the basal aluminium atoms are 0.15 Å longer than the bond with the apical aluminium. The only significant difference between the structures of **48** and **49** is the Al(1)-O bond length (1.843(3) and 1.852(4) Å) which is shorter than in **49** (1.900(4) Å). The displacement of the apical aluminium from the O(1)/O(1A)/O(2)/O(2A) plane (0.32 Å) is also less than in **49** (0.36 Å). There are no significant interactions beyond the molecule.

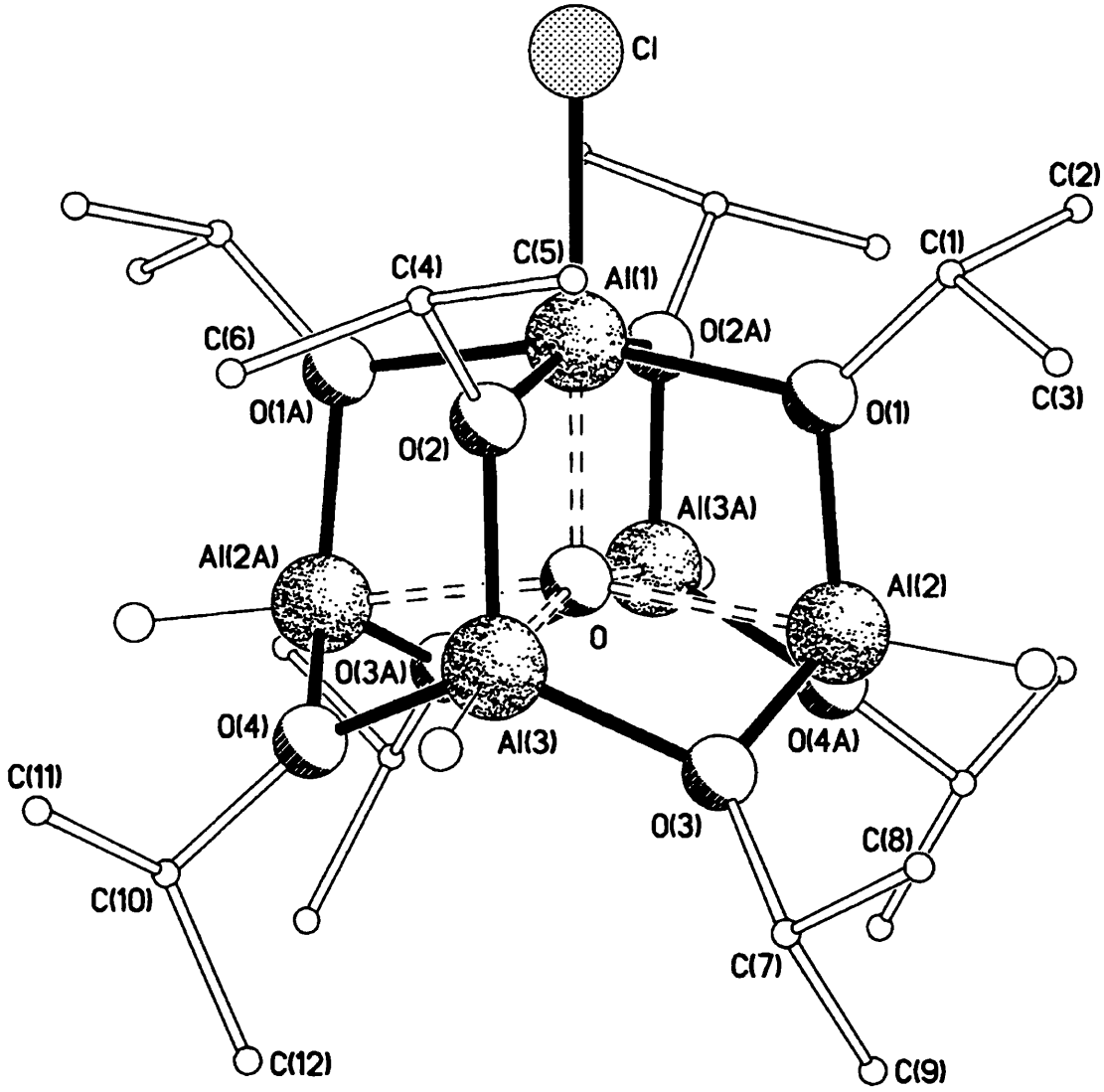

Figure 3.10 X-ray structure of $[Al_5(\mu_5\text{-}O)(\mu\text{-}O^iPr)_8(Cl)H_4]$ (48)

Table 3.2 Selected bond lengths (°) and angles (Å) for $[Al_5(\mu_5\text{-}O)(\mu\text{-}O^iPr)_8(Cl)H_4]$ (48)

	A	B
Al(1)-Cl	2.188(2)	2.184(3)
Al(1)-O(1)	1.950(3)	1.963(3)
Al(2)-O	2.062(1)	2.177(2)
Al(2)-O(3)	1.826(3)	1.817(3)
Al(3)-O	2.126(1)	2.006(1)
Al(3)-O(3)	1.828(3)	1.833(3)
Al(1)-O	1.843(4)	1.852(4)
Al(1)-O(2)	1.964(3)	1.937(3)
Al(2)-O(1)	1.813(3)	1.810(3)
Al(2)-O(4A)	1.830(3)	1.814(3)
Al(3)-O(2)	1.816(3)	1.817(3)
Al(3)-O(4)	1.817(3)	1.839(3)
Cl-Al(1)-O	180.0	180.0
Cl-Al(1)-O(1)	99.63(9)	98.78(10)
Cl-Al(1)-O(2)	99.10(9)	100.08(10)
O-Al(1)-O(1)	80.37(9)	81.22(10)
O-Al(1)-O(2)	80.90(9)	79.92(10)
O(1)-Al(1)-O(1A)	160.7(2)	162.4(2)
O(1)-Al(1)-O(2)	88.17(12)	88.43(12)
O(1)-Al(1)-O(2A)	88.80(12)	88.51(12)
O(2)-Al(1)-O(2A)	161.8(2)	159.8(2)
O-Al(2)-O(1)	78.10(14)	76.5(2)
O-Al(2)-O(3)	78.49(11)	75.88(12)
O-Al(2)-O(4A)	78.88(10)	75.94(12)
O(1)-Al(2)-O(3)	110.80(14)	116.0(2)
O(1)-Al(2)-O(4A)	115.34(14)	109.8(2)
O(3)-Al(2)-O(4A)	122.18(14)	117.4(2)
O(2)-Al(3)-O	77.23(14)	78.9(2)

O(3)-Al(3)-O	76.79(10)	80.04(12)
O(4)-Al(3)-O	77.48(10)	79.90(12)
O(2)-Al(3)-O(3)	116.48(14)	109.3(2)
O(2)-Al(3)-O(4)	109.64(14)	115.5(2)
O(3)-Al(3)-O(4)	119.42(14)	125.6(2)
Al(1)-O-Al(2)	98.05(11)	96.32(11)
Al(1)-O-Al(3)	97.36(10)	98.59(12)
Al(2)-O-Al(2A)	163.9(2)	167.4(2)
Al(2)-O-Al(3)	88.94(5)	88.99(6)
Al(2)-O-Al(3A)	89.00(5)	89.12(6)
Al(3)-O-Al(3A)	165.3(2)	162.8(2)
Al(1)-O(1)-Al(2)	103.29(14)	105.8(2)
Al(1)-O(2)-Al(3)	104.35(14)	102.4(2)
Al(2)-O(3)-Al(3)	106.83(14)	107.0(2)
Al(3)-O(4)-Al(2A)	107.20(14)	107.0(2)

3.2.6 Reaction of $[AlH_3(NMe_2Et)]$ and ^iPrOH

In an attempt to prepare $[H_2Al(O^iPr)(NMe_2Et)]$ (**50**), the reaction of $[AlH_3(NMe_2Et)]$ and 1 equivalent of ^iPrOH was carried out in diethyl ether at room temperature. After work-up and cooling to -20 °C colourless crystals were obatined. Analytical and spectroscopic data showed $[Al(O^iPr)_3]_4$ (**12**) had been formed. Compound **50** may have formed but rearranged (during the reaction) to give **12** and another species such as $[AlH_3(NMe_2Et)]$, which was not isolated. The infra-red spectrum does not show any peaks due to the presence of terminal hydrides attached to the aluminium, suggesting that **12** was the major product in the reaction.

3.2.7 X-ray structure of $[Al(O^iPr)_3]_4$

The structure of compound **12** was confirmed by X-ray crystallography, the results of which are shown in Figure 3.11; selected bond lengths and angles are shown in Table 3.3. Compound **12** adopts a tetrameric Mitsubishi structure, which has been reported previously and is discussed in section 3.15.[43,44]

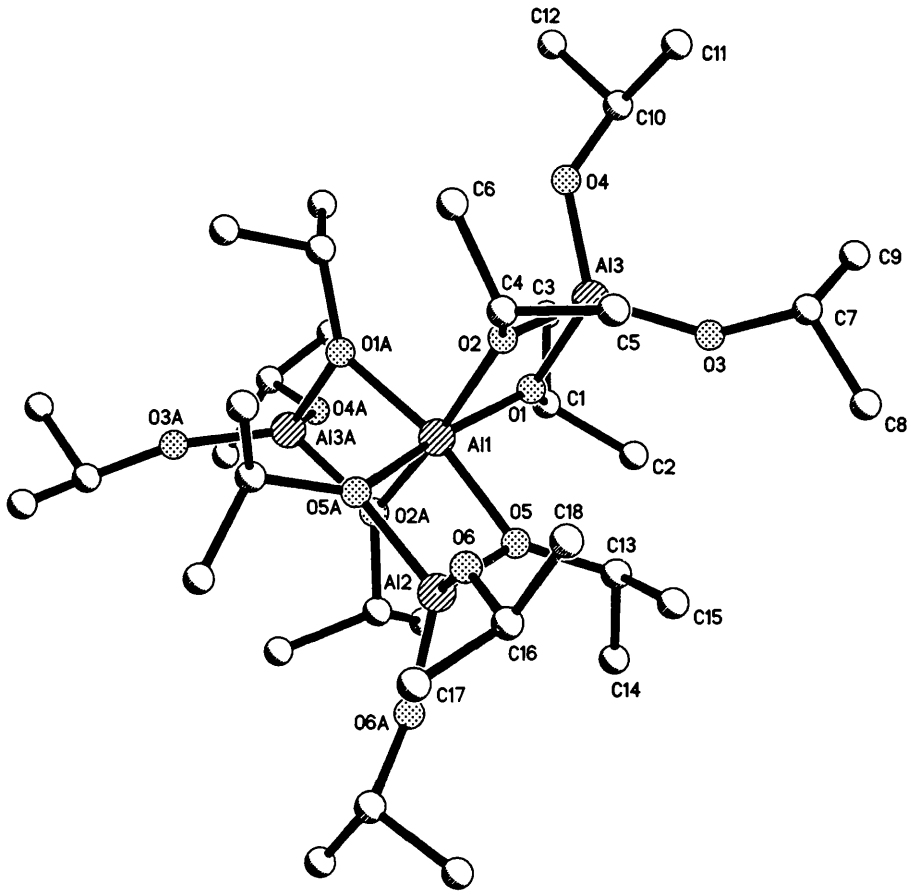

Figure 3.11 X-ray structure of $[Al(O^iPr)_3]_4$ (12)

Table 3.3 Selected bond lengths (Å) and angles (°) for $[Al(O^iPr)_3]_4$ (12)

Al(1)–O(2A)	1.9121(8)	Al(1)–O(2)	1.9121(8)
Al(1)–O(1A)	1.9194(9)	Al(1)–O(1)	1.9194(9)
Al(1)–O(5)	1.9215(9)	Al(1)–O(5A)	1.9215(9)
Al(1)–Al(3A)	2.8565(4)	Al(1)–Al(3)	2.8565(4)
Al(1)–Al(2)	2.8706(7)	Al(2)–O(6A)	1.7022(10)
Al(2)–O(6)	1.7022(10)	Al(2)–O(5A)	1.7965(9)
Al(2)–O(5)	1.7965(9)	Al(3)–O(3)	1.6920(10)
Al(3)–O(4)	1.7051(11)	Al(3)–O(1)	1.7982(9)
Al(3)–O(2)	1.8002(9)	O(1)–C(1)	1.4535(14)

O(2)–C(4)	1.4526(14)	O(3)–C(7)	1.3943(16)
O(4)–C(10)	1.3965(17)	O(5)–C(13)	1.4507(14)
O(6)–C(16)	1.4039(16)	C(1)–C(2)	1.499(2)
C(1)–C(3)	1.501(2)		
O(2A)–Al(1)–O(2)	168.76(6)	O(2A)–Al(1)–O(1A)	76.54(4)
O(2)–Al(1)–O(1A)	95.62(4)	O(2A)–Al(1)–O(1)	95.62(4)
O(2)–Al(1)–O(1)	76.54(4)	O(1A)–Al(1)–O(1)	92.98(6)
O(2A)–Al(1)–O(5)	96.43(4)	O(2)–Al(1)–O(5)	92.44(4)
O(1A)–Al(1)–O(5)	169.12(4)	O(1)–Al(1)–O(5)	96.00(4)
O(2A)–Al(1)–O(5A)	92.44(4)	O(2)–Al(1)–O(5A)	96.43(4)
O(1A)–Al(1)–O(5A)	96.00(4)	O(1)–Al(1)–O(5A)	169.12(4)
O(5)–Al(1)–O(5A)	75.79(5)	O(2)–Al(1)–Al(3A)	133.45(3)
O(1)–Al(1)–Al(3A)	95.81(3)	O(5)–Al(1)–Al(3A)	134.11(3)
O(5A)–Al(1)–Al(3A)	95.05(3)	O(2A)–Al(1)–Al(3)	133.45(3)
O(2)–Al(1)–Al(3)	38.28(3)	O(1A)–Al(1)–Al(3)	95.81(3)
O(1)–Al(1)–Al(3)	38.26(3)	O(5)–Al(1)–Al(3)	95.05(3)
O(5A)–Al(1)–Al(3)	134.11(3)	Al(3A)–Al(1)–Al(3)	120.43(2)
O(2A)–Al(1)–Al(2)	95.62(3)	O(2)–Al(1)–Al(2)	95.62(3)
O(1A)–Al(1)–Al(2)	133.51(3)	O(1)–Al(1)–Al(2)	133.51(3)
Al(3A)–Al(1)–Al(2)	119.786(11)	Al(3)–Al(1)–Al(2)	119.786(11)
O(6A)–Al(2)–O(6)	119.37(7)	O(6A)–Al(2)–O(5A)	118.77(5)
O(6)–Al(2)–O(5A)	106.25(5)	O(6A)–Al(2)–O(5)	106.25(5)
O(6)–Al(2)–O(5)	118.77(5)	O(5A)–Al(2)–O(5)	82.14(5)
O(6A)–Al(2)–Al(1)	120.32(4)	O(6)–Al(2)–Al(1)	120.32(4)
O(5A)–Al(2)–Al(1)	41.07(3)	O(5)–Al(2)–Al(1)	41.07(3)
O(3)–Al(3)–O(4)	119.17(6)	O(3)–Al(3)–O(1)	106.64(5)
O(4)–Al(3)–O(1)	117.70(5)	O(3)–Al(3)–O(2)	118.72(5)
O(4)–Al(3)–O(2)	106.88(5)	O(1)–Al(3)–O(2)	82.52(4)
O(3)–Al(3)–Al(1)	120.33(4)	O(4)–Al(3)–Al(1)	120.50(4)
O(1)–Al(3)–Al(1)	41.37(3)	O(2)–Al(3)–Al(1)	41.15(3)
C(1)–O(1)–Al(3)	125.97(8)	C(1)–O(1)–Al(1)	133.13(8)
Al(3)–O(1)–Al(1)	100.37(4)	C(4)–O(2)–Al(3)	126.03(7)

C(4)–O(2)–Al(1)	131.98(7)	Al(3)–O(2)–Al(1)	100.57(4)
C(7)–O(3)–Al(3)	146.45(11)	C(10)–O(4)–Al(3)	134.96(10)
C(13)–O(5)–Al(2)	125.03(8)	C(13)–O(5)–Al(1)	133.36(8)
Al(2)–O(5)–Al(1)	101.03(4)	C(16)–O(6)–Al(2)	138.68(10)
O(1)–C(1)–C(2)	111.09(11)	O(1)–C(1)–C(3)	110.79(11)
C(2)–C(1)–C(3)	110.76(13)	O(2)–C(4)–C(5)	109.93(10)
O(2)–C(4)–C(6)	109.76(11)	C(5)–C(4)–C(6)	110.16(11)

3.2.8 Reaction of $[AlH_3(NMe_2Et)]$ and ^tBuOH

The synthesis of $[HAl(O^tBu)_2(NMe_2Et)]$ (**51**) was attempted by the reaction of $[AlH_3(NMe_2Et)]$ and two equivalents of ^tBuOH in diethyl ether. After work-up, colourless crystals were obtained in 93% yield. Analytical and spectroscopic data showed that $[HAl(O^tBu)_2]_2$ (**21**) had formed, as shown in Eq. 3.8.

$$[AlH_3(NMe_2Et)] + 2\,{}^tBuOH \longrightarrow 1/n\,[HAl(O^tBu)_2)] + 2\,H_2 + NMe_2Et \quad \textbf{(3.8)}$$

The percentage of nitrogen found (0.00%) confirmed that no amine was present. Compound **21** would be expected to adopt a dimeric structure in the solid state (Figure 3.6). The infra-red spectrum was recorded and shows the expected peaks due to the Al-H bond at 1872 and 776 cm^{-1}.

3.2.9 Reaction of $[AlH_3(NMe_2Et)]$ and 3-HF_4C_6OH

The reaction of $[AlH_3(NMe_2Et)]$ and 3-HF_4C_6OH was carried out, as described in section 3.2.1. After work-up and cooling to -20 °C a white powder was obtained in 79% yield. Spectroscopic data indicated that $[H_2Al(OC_6F_4H)(NMe_2Et)]$ (**52**) had been formed, as shown in Eq. 3.9.

$$[AlH_3(NMe_2Et)] + HF_4C_6OH \longrightarrow [H_2Al(OC_6F_4H\text{-}3)_2)(NMe_2Et)] + H_2 \quad \textbf{(3.9)}$$

The melting point (42 °C) is low, suggesting that **52** is volatile. The use of fluorinated alcohols or thiols in single-source precursors is of particular interest as it

may lead to a significant increase in volatility. The ^{1}H NMR spectrum (Figure 3.12) of **52** shows clearly only one species is present in solution suggesting that **52** is formed cleanly. The integrals show a 1:1 ratio of amine to OC_6F_4H, as would be expected for **52**. The ^{13}C NMR confirms that only one species is present in solution. The infra-red spectrum was also recorded and shows peaks due to Al-H at 1897 and 772 cm^{-1}.

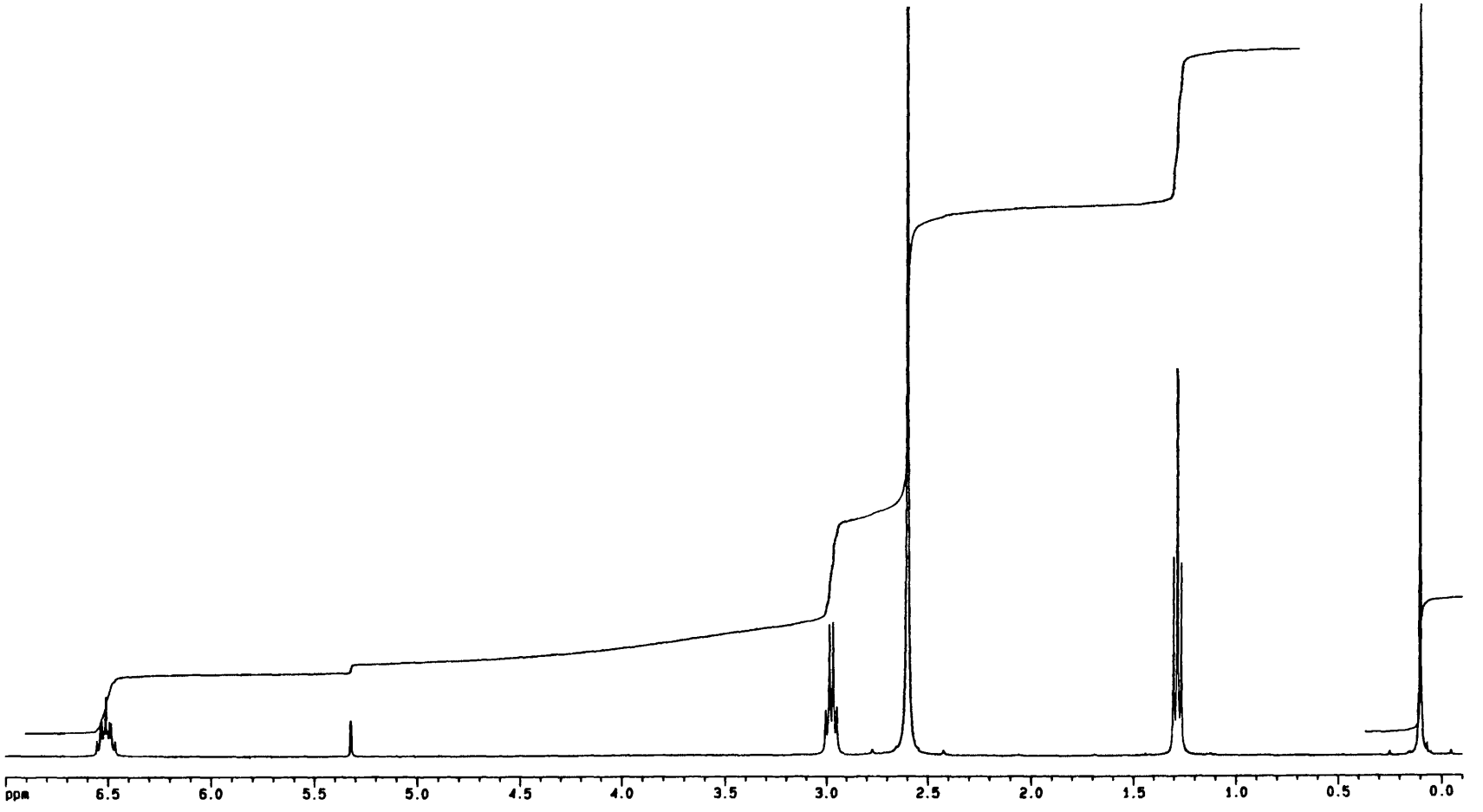

Figure 3.12. ^{1}H NMR spectrum of [$H_2Al(OC_6F_4H\text{-}3)(NMe_2Et)$] (52)

3.2.10 Reaction of $[AlH_3(NMe_2Et)]$ and two equivalents of 3-HF_4C_6OH

The reaction of $[AlH_3(NMe_2Et)]$ and two equivalents of 3-HF_4C_6OH was carried out, as described in section 3.2.1. After work-up and cooling to -20 °C a white powder was obtained in 75% yield. Analytical and spectroscopic data shows that $[HAl(OC_6F_4H\text{-}3)_2(NMe_2Et)]$ (**53**) had formed, as shown in Eq. 3.10.

$$[AlH_3(NMe_2Et)] + 2\ 3\text{-}HF_4C_6OH \longrightarrow [HAl(OC_6F_4H\text{-}3)_2)_2(NMe_2Et)] + 2\ H_2 \quad \textbf{(3.10)}$$

Like compound **52**, the melting point of **53** (46 - 48 °C) is low indicating that the compound may be volatile. The ^1H NMR spectrum of **53** shows the presence only one set of peaks for each proton environment, however, the peaks are broad suggesting that a fluxional process is occuring in solution at room temperature. The integrals show a 1:2 ratio of amine to OC_6F_4H groups, as expected for **53**. The ^{13}C NMR also shows one environment is present in solution with broader peaks than were observed for **52**. The infra-red spectrum was recorded and shows peaks due to Al-H at 1896 and 773 cm^{-1}.

3.2.11 Reaction of $[AlH_3(NMe_2Et)]$ and two equivalents of 2,6-$Me_2C_6H_3OH$

The reaction of $[AlH_3(NMe_2Et)]$ and two equivalents of 2,6-$Me_2C_6H_3OH$ was carried out, as described in section 3.2.1. After work-up and cooling to -20 °C colourless crystals were obtained in 48% yield. Analytical and spectroscopic data shows that $[HAl(OC_6H_3Me_2\text{-}2,6)_2(NMe_2Et)]$ (**54**) had been formed. The melting point of **54** (58 - 60 °C) is higher than was observed for the fluorinated compounds **52** and **53**. The ^1H NMR spectrum of **54** shows one set of peaks indicating that one species is present in solution. The ratio of integrals of the amine and $OC_6H_3Me_2$ groups also indicates that **54** was formed. The ^{13}C NMR spectrum confirms that only one species is present in solution. Peaks at 1843 and 760 cm^{-1} in the infra-red spectrum show the presence of an Al-H bond in the product formed although a peak due to the hydride is not observed in the ^1H NMR spectrum.

3.2.12 Reaction of $[AlH_3(OEt_2)]$ and ^tBuSH

The reaction of $[AlH_3(OEt_2)]$ and one equivalent of ^tBuSH was carried out, as described in 3.2.1. After work-up and cooling to -20 °C, colourless crystals were obtained. Analytical and spectroscopic data indicated that the expected product, $[H_2Al(S^tBu)]_2$, had not been formed. X-ray crystallography showed the crystals to be $[HAl(S^tBu)(\mu\text{-}O^tBu)]_2$ (**55**), which is probably the product of hydrolysis of $[HAl(S^tBu)_2]_n$, formed during the reaction. However, the analytical data suggests that a mixture of products has been formed, which is expected if hydrolysis has occurred.

3.2.13 X-ray structure of $[HAl(S^tBu)(\mu\text{-}O^tBu)]_2$ (55)

An X-ray crystallographic study was undertaken to determine the nature of **55**, the results of which are shown in Figure 3.13; selected bond lengths and angles are given in Table 3.4. The structure of **55** consists of a central Al_2O_2 ring, with one S^tBu group and one hyride attached to each aluminium. Unexpectedly the S^tBu groups were found to adopt a *cis* arrangement. The Al-O bond lengths are within statistical significance identical (1.846(12), 1.850(12) and 1.837(13) Å), and comparable with the bridging Al-O bond length observed in $[HAl(O^tBu)_2]_2$ (**21**) (1.817(3) Å).[49] The Al(1)-O(1)-Al(2) and Al(2)-O(2)-Al(1) angles (98.9(6) and 99.1(6) ° respectively) are within statistical significance the same, as are the O(1)-Al(1)-O(2) and O(2)-Al(2)-O(1) angles (80.6(5) and 81.0(5)° respectively) and comparable to those found in **21** (99.2(2) and 80.8(2)° respectively). The Al-S bond lengths are also within statistical significance identical (2.204(7) and 2.209(8) Å) and are comparable with the terminal Al-S bond lengths in the related compound $[Al(S^tBu)_3]_2$ (**36**) (2.2096(18) and 2.2085(18)°).[54] The hydrogen atoms in the structure of **55** were not located.

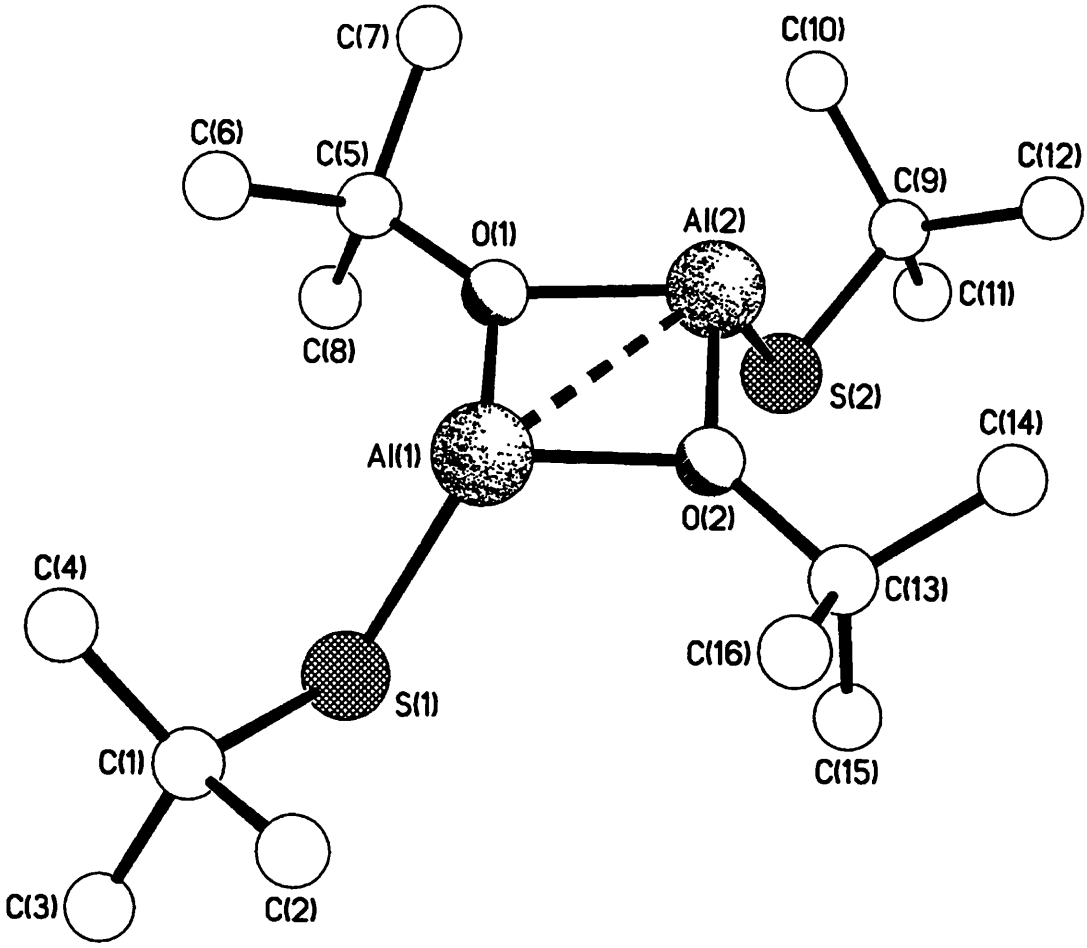

Figure 3.13 X-ray structure of $[HAl(S^tBu)(\mu\text{-}O^tBu)]_2$ (55) with the terminal hydrides omitted

Table 3.4. Selected bond lengths (Å) and angles (°) for $[HAl(S^tBu)(\mu\text{-}O^tBu)]_2$ (55)

Al(1)-O(1)	1.846(12)	Al(1)-Al(2)	2.806(7)
Al(1)-O(2)	1.850(12)	Al(2)-O(2)	1.837(13)
Al(1)-S(1)	2.204(7)	Al(2)-O(1)	1.846(12)
Al(2)-S(2)	2.209(8)	O(1)-C(5)	1.46(2)
S(1)-C(1)	1.89(2)	O(2)-C(13)	1.45(2)
S(2)-C(9)	1.83(2)		
O(1)-Al(1)-O(2)	80.6(5)	S(1)-Al(1)-Al(2)	124.0(3)
O(1)-Al(1)-S(1)	111.9(5)	O(2)-Al(2)-O(1)	81.0(5)
O(2)-Al(1)-S(1)	114.4(5)	O(2)-Al(2)-S(2)	111.6(5)
O(1)-Al(2)-S(2)	115.0(5)	C(9)-S(2)-Al(2)	106.5(9)
S(2)-Al(2)-Al(1)	124.3(3)	C(5)-O(1)-Al(1)	129.9(11)
C(1)-S(1)-Al(1)	107.7(6)	C(5)-O(1)-Al(2)	131.2(11)
Al(1)-O(1)-Al(2)	98.9(6)	C(13)-O(2)-Al(1)	128.8(10)
C(13)-O(2)-Al(2)	132.1(10)	Al(2)-O(2)-Al(1)	99.1(6)

3.2.14 Reaction of $[AlH_3(NMe_2Et)]$ and one equivalent of ^{t}BuSH

The reaction of $[AlH_3(NMe_2Et)]$ and one equivalent of ^{t}BuSH was carried out as described in 3.2.1. After work-up and cooling to -20 °C colourless crystals were obtained in 41% yield. Analytical and spectroscopic data showed that $[Al(S^tBu)_3(NMe_2Et)]$ (**42**) had been formed. The expected product, $[H_2Al(S^tBu)(NMe_2Et)]$ was not formed as the major product in the reaction. The ^{1}H NMR spectrum of **42** (Figure 3.14) shows two peaks (in approximately a 1:6 ratio) which correspond to the ^{t}BuS protons, this indicates that either two species exist in solution, for example a monomer and dimer, or **42** was not formed cleanly in the reaction. The ^{1}H NMR results reported by Hoffman *et al* for **42** indicate that only one species is expected in solution, however, a different NMR solvent was used (C_6D_6) and this could lead to different solution behaviour. Since compound **42** is not the

expected product of the reaction, the formation of other products in the reaction is a distinct possibility. Previous reports show that the reaction of $[AlH_3(NMe_3)]$ and one or two equivalents of ^tBuSH resulted in the formation of $[H_2Al(S^tBu)(NMe_3)]$ (**46**) and $[HAl(S^tBu)_2(NMe_3)]$ (**43**).[55] Only one peak was reported for the ^tBuS groups in each compound which suggests that **43** and **46** were formed cleanly. However, the analytical data reported for **46** was significantly different with the expected results which does suggest that **46** may not have been the exclusive product. The reaction of $[GaH_3(NMe_3)]$ and either one or two equivalents of ^tBuSH is reported to yield mixtures of products, one of which was $[Ga(S^tBu)_3(NMe_3)]$ (**56**).[56] This suggests that $[M(S^tBu)_3(NR_3)]$ may be a stable species which is formed in varying amounts dependent on the reaction conditions, particularly the solvent used.

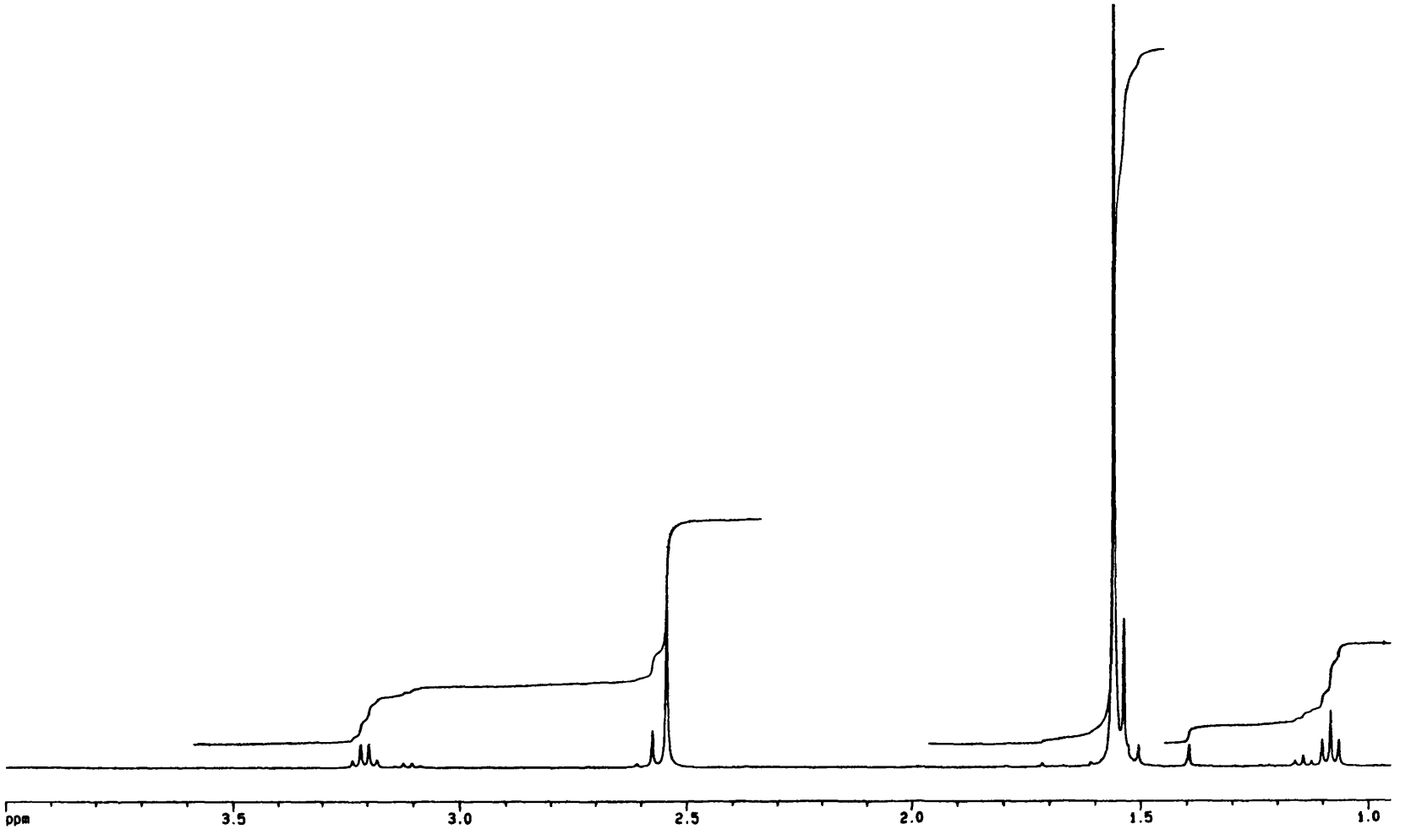

Figure 3.14 ^{1}H NMR spectrum of [Al(S^{t}Bu)$_3${NMe$_2$Et}] (42)

3.2.15 X-ray structure of $[Al(S^tBu)_3(NMe_2Et)]$ (42)

The structure of compound **42** was confirmed by X-ray crystallography, the results of which are shown in Figure 3.15; selected bond lengths and angles are given in Table 3.5. The structure of **42** resembles closely the structures of $[Al(S^tBu)_3(thf)]$ (**38**) and $[Al(S^iPr)_3(HNMe_2)]$ (**39**).[54] The structure of **42** is monomeric, with the geometry around the central Al being distorted trigonal pyramidal in which the NMe_2Et occupies the apical site. The Al-S bond lengths are significantly longer than those found in **38** (Al-S 2.2207(12) - 2.2236(12) Å) and **39** (Al-S 2.2150(14) - 2.2298(14) Å). The aluminium and three sulfur atoms approach planarity, as observed in both **38** and **39**.

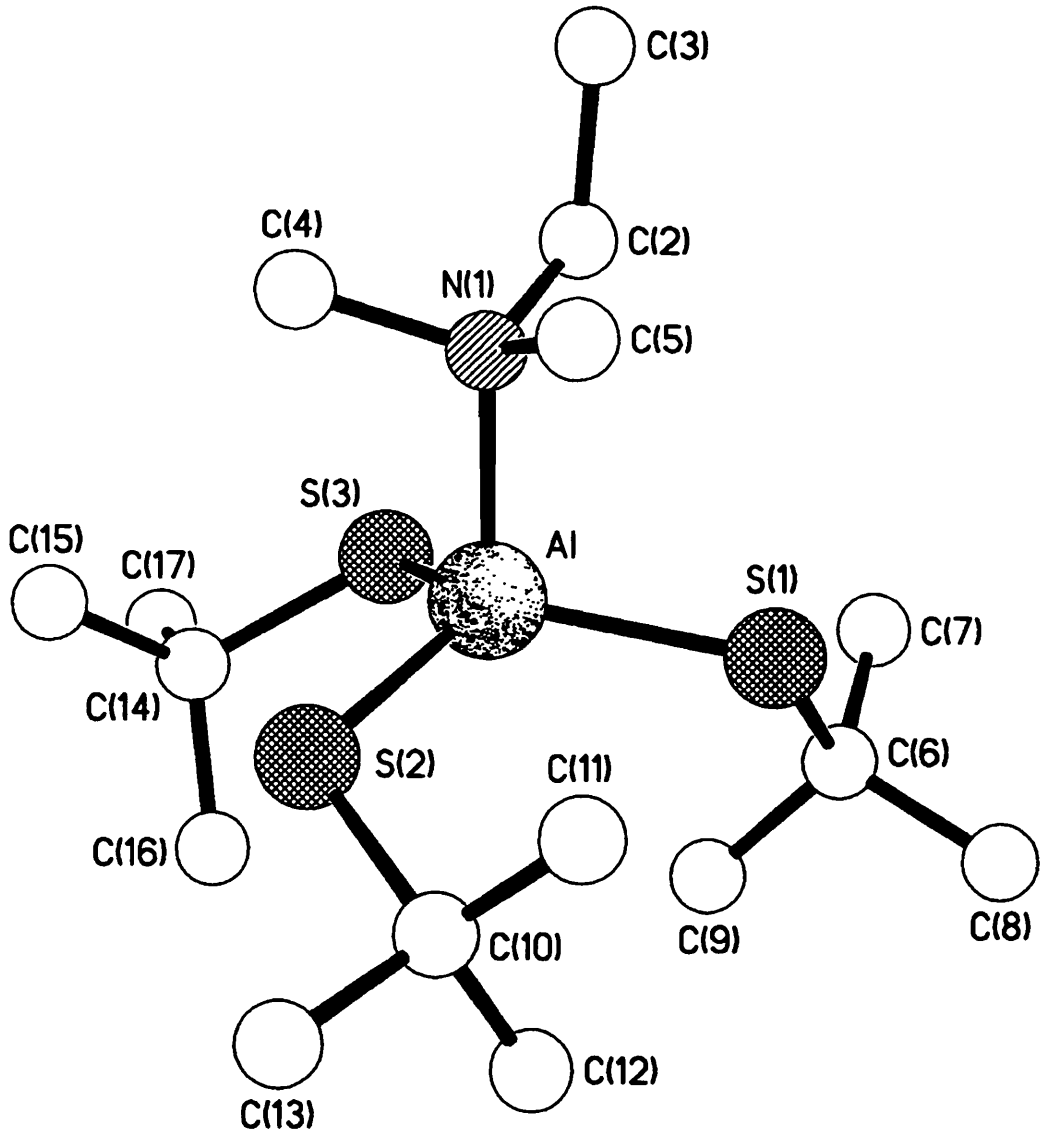

Figure 3.15 X-ray structure of $[Al(S^tBu)_3(NMe_2Et)]$ (42)

Table 3.5 Selected bond lengths (Å) and angles (°) for [Al(S^{t}Bu)$_3$(NMe$_2$Et)] (42)

Al-N(1)	2.038(2)	Al-S(2)	2.2356(8)
Al-S(3)	2.2337(8)	Al-S(1)	2.2366(8)
S(1)-C(6)	1.852(2)	S(3)-C(14)	1.858(2)
S(2)-C(10)	1.862(2)		
N(1)-Al-S(3)	101.16(6)	S(3)-Al-S(2)	115.68(3)
N(1)-Al-S(2)	104.00(6)	N(1)-Al-S(1)	99.83(6)
S(3)-Al-S(1)	116.21(3)	C(6)-S(1)-Al	112.65(7)
S(2)-Al-S(1)	116.17(4)	C(10)-S(2)-Al	112.91(7)
C(14)-S(3)-Al	112.46(8)		

3.2.16 Reaction of [AlH$_3$(OEt$_2$)] and 2,6-Me$_2$C$_6$H$_3$SH

The reaction of [AlH$_3$(OEt$_2$)] (formed *in situ* from [AlCl$_3$] and [LiAlH$_4$]) and one equivalent of 2,6-Me$_2$C$_6$H$_3$SH was carried out at room temperature. After work-up and cooling to -20 °C, colourless crystals were obtained in a 28% yield. Analytical and spectroscopic data showed [Al(SC$_6$H$_3$Me$_2$-2,6)$_3$(OEt$_2$)] (**57**) had been formed, as shown in Eq. 3.11.

$$[AlH_3(OEt_2)] + 2,6\text{-}Me_2C_6H_3SH \longrightarrow [Al(SC_6H_3Me_2\text{-}2,6)_3(OEt_2)] + H_2 \quad (\mathbf{3.11})$$

The anticipated product, [H$_2$Al(SC$_6$H$_3$Me$_2$-2,6)]$_n$ (**58**) was not formed during the reaction and the ^{1}H NMR data (Figure 3.16) shows clearly that one product was cleanly isolated (**57**). This is similar to the results of the reaction between [AlH$_3$(NMe$_2$Et)] and one equivalent of ^{t}BuSH, (see section 3.2.14) where [Al(S^{t}Bu)$_3$(NMe$_2$Et)] was the major product of the reaction.

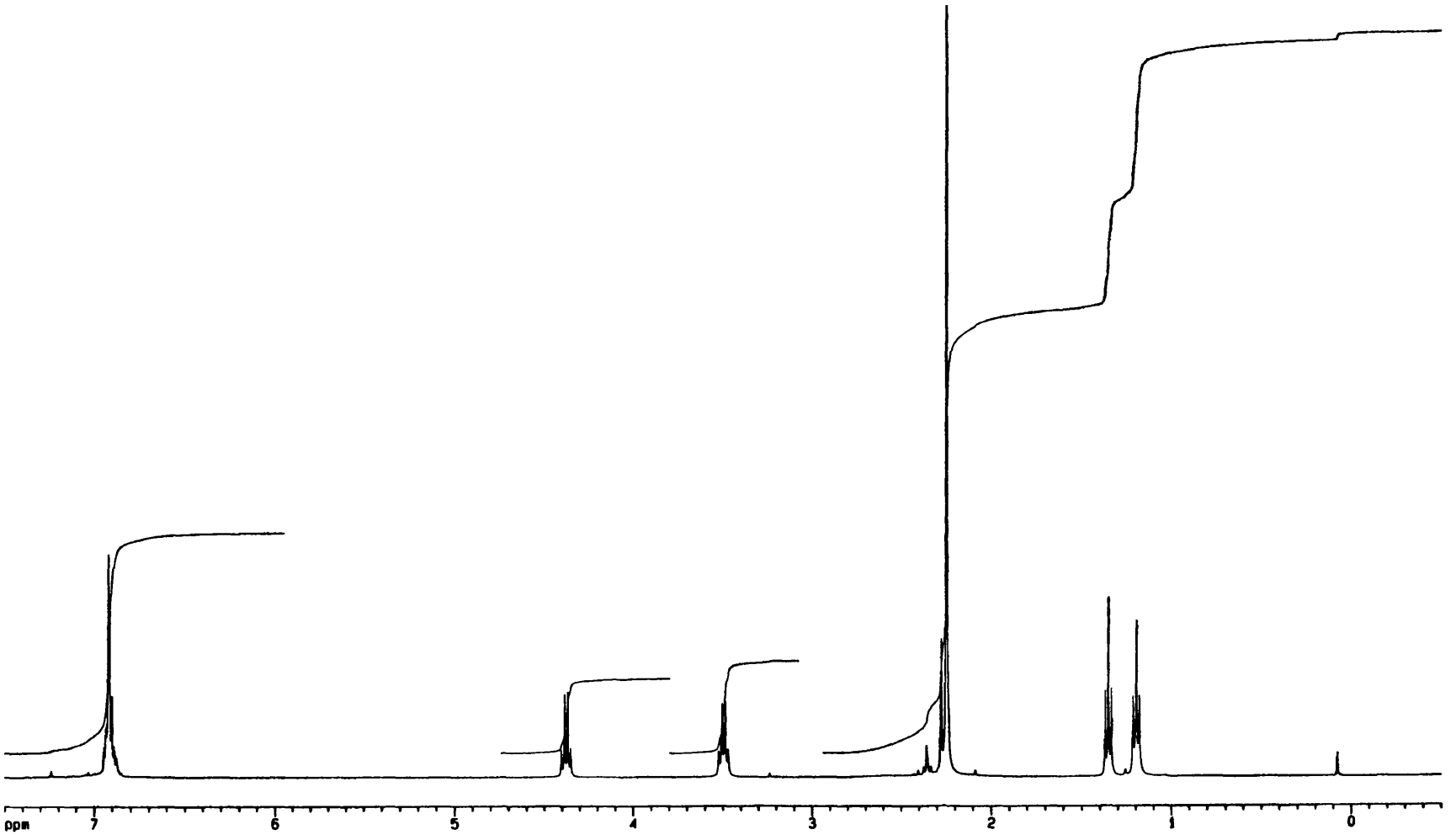

Figure 3.16 ^{1}H NMR spectrum of $[Al(SC_6H_3Me_2\text{-}2,6)_3(OEt_2)]$ (57)

3.2.17 X-ray structure of $[Al(SC_6H_3Me_2)_3(OEt_2)]$

The structure of compound **57** was confirmed by X-ray crystallography, the results of which are shown in Figure 3.17; selected bond lengths and angles are given in Table 3.6. The structure of **57** is similar to that of **42** (described in 3.2.15). The geometry of the central Al in **57** is trigonal pyrimidal with the OEt_2 occupying the apical site. The structure (ignoring the two ethyl groups) has pseudo C_3 symmetry about the O-Al bond creating a propeller-like geometry. This leads to the existence of two isomers, however, the crystal is racemic and so both isomers must be present in equal numbers. The propeller-like geometry results in one of the methyl groups of each 2,6-dimethylphenyl ring system being directed into the face of its nearest neighbour aryl ring, the shortest H···π distance being 2.78 Å. The Al-S bond lengths (2.2266(11) - 2.2384(11) Å) are comparable to those observed in **42** (Al-S 2.2337(8) - 2.2356(8) Å). The aluminium and three sulfur atoms approach planarity, as observed in **42**, with the aluminium lying 0.43 Å out of the basal S_3 face in the direction of the oxygen atom. There are no intermolecular interactions of note.

Table 3.6 Selected bond lengths (Å) and angles (°) for $[Al(SC_6H_3Me_2)_3(OEt_2)]$ (57)

Al-O	1.907(2)	Al-S(3)	2.2336(11)
Al-S(1)	2.2266(11)	Al-S(2)	2.2384(11)
S(1)-C(11)	1.794(3)	S(3)-C(31)	1.796(3)
S(2)-C(21)	1.797(3)	O-C(3)	1.476(4)
O-C(1)	1.479(3)		
O-Al-S(1)	104.03(7)	S(1)-Al-S(3)	112.73(4)
O-Al-S(3)	102.01(7)	O-Al-S(2)	97.34(7)
S(1)-Al-S(2)	120.81(5)	C(11)-S(1)-Al	106.12(9)
S(3)-Al-S(2)	115.61(4)	C(21)-S(2)-Al	107.03(9)
C(31)-S(3)-Al	107.98(9)	C(3)-O-Al	117.8(2)
C(1)-O-Al	126.1(2)		

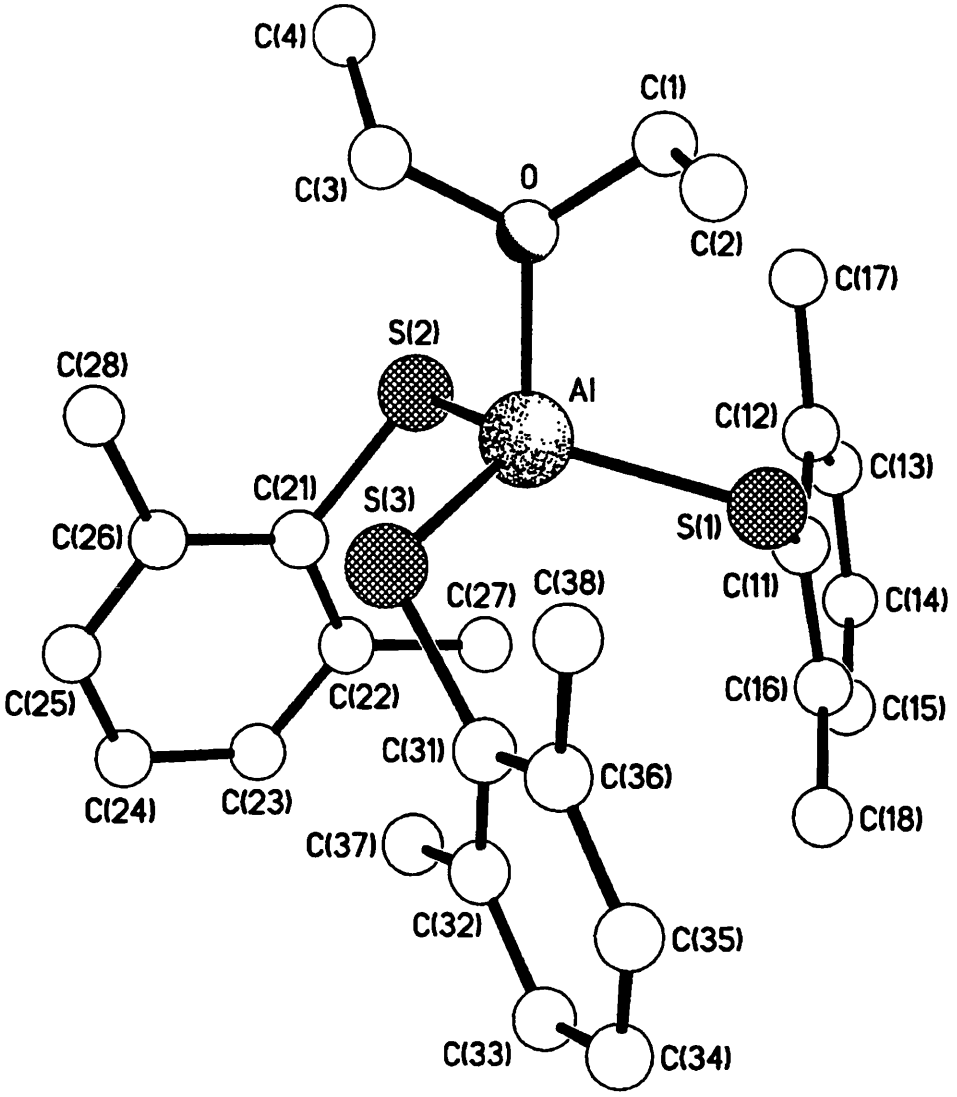

Figure 3.17 X-ray structure of $[Al(SC_6H_3Me_2\text{-}2,6)_3(OEt_2)]$ (57)

3.2.18 Reaction of $[AlH_3(OEt_2)]$ and 2,6-$Me_2C_6H_3SH$

The reaction of $[AlH_3(OEt_2)]$ (formed *in situ* from $[AlCl_3]$ and $[LiAlH_4]$) and one equivalent of 2,6-$Me_2C_6H_3SH$ (described in section 3.2.16) was repeated, however, incomplete reaction of $[AlCl_3]$ and $[LiAlH_4]$ had occurred. After work-up and cooling to -20 °, colourless crystals in 25% yield were obtained. Analytical and spectroscopic data shows that $[Li(OEt_2)_3][Al(SC_6H_3Me_2\text{-}2,6)_4]$ (**59**) had been formed. The ^1H NMR of **59** shows that only one species is present in solution which suggests that **59** is formed cleanly in the reaction (Figure 3.18).

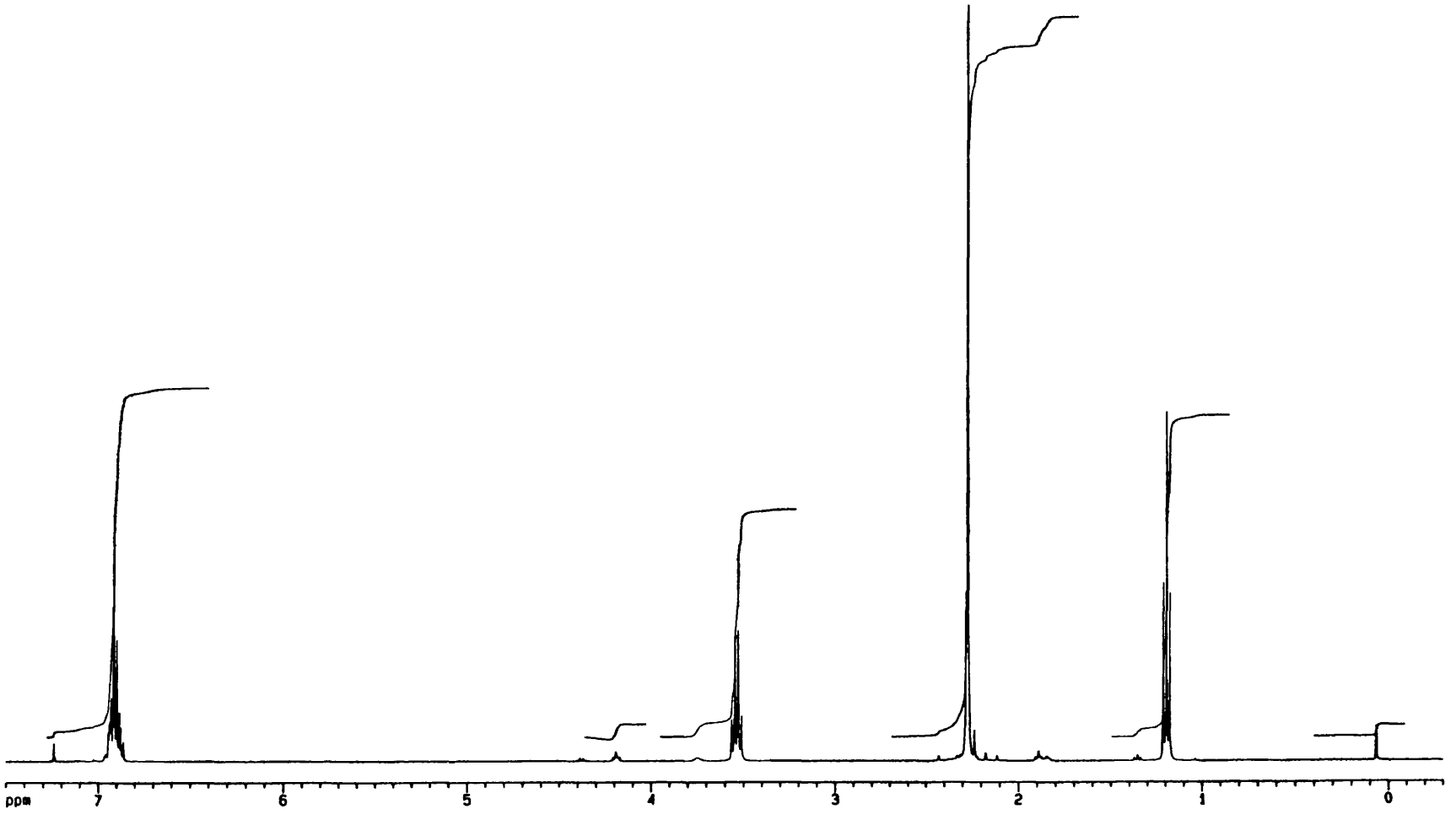

Figure 3.18 ^{1}H NMR spectrum of $[Li(OEt_2)_3]$ $[Al(SC_6H_3Me_2\text{-}2,6)_4]$ (59)

3.2.19 X-ray structure of $[Li(OEt_2)_3][Al(SC_6H_3Me_2)_4]$

The structure of compound **59** was confirmed by X-ray crystallography, the $[Al(SC_6H_3Me_2\text{-}2,6)_4]^-$ anion is shown in Figure 3.19; selected bond lengths and angles are given in Table 3.7. The anion has S_4 symmetry about an axis which bisects the S-Al-S(0A) angle. The geometry at aluminium is distorted tetrahedral with unique angles 104.85(3) and 119.16(6)°, reflecting a slight flattening of the tetrahedron about the S_4 axis. The $[Li(OEt_2)_3]^+$ cation is disordered.

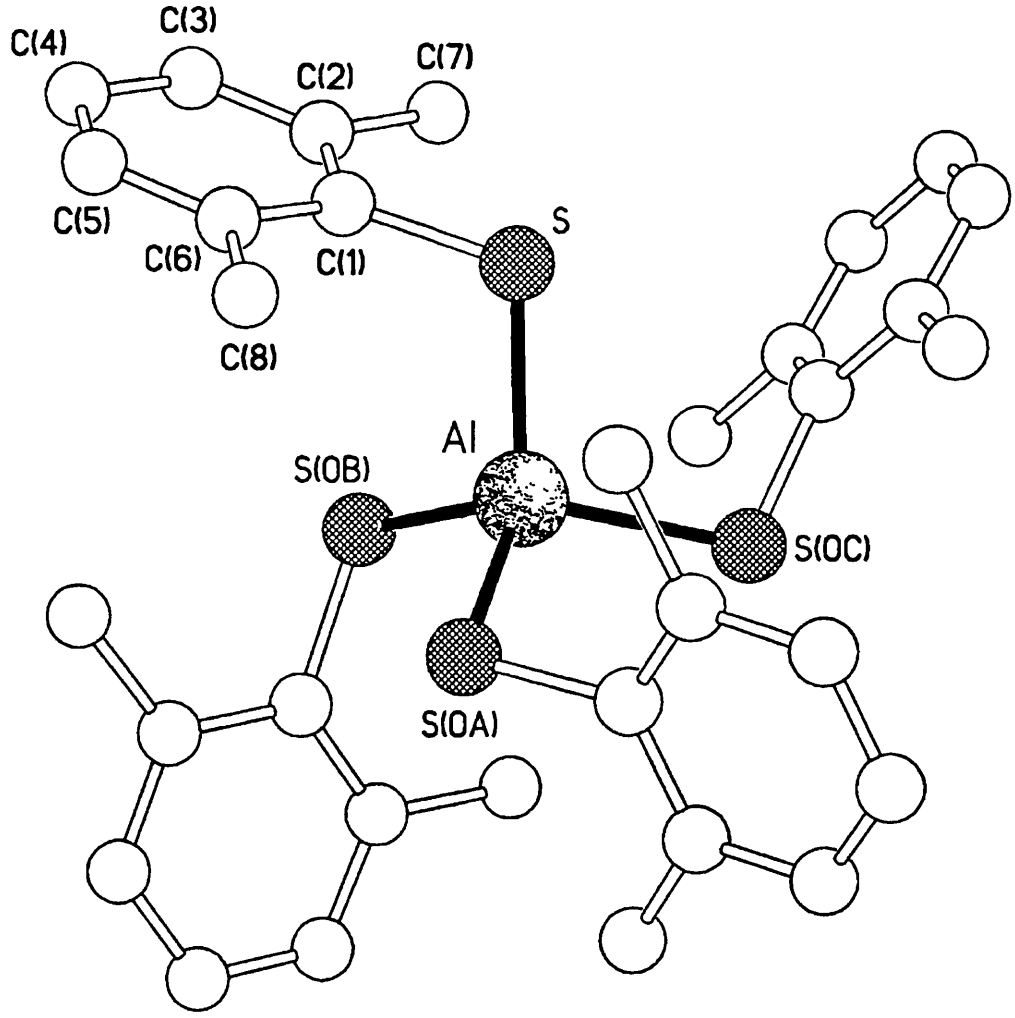

Figure 3.19. X-ray structure of the anion in $[Li(OEt_2)_3][Al(SC_6H_3Me_2\text{-}2,6)_4]$ (59)

Table 3.7 Selected bond lengths (Å) and angles (°) for the anion in $[Li(OEt_2)_3][Al(SC_6H_3Me_2\text{-}2,6)_4]$ (59)

Al-S	2.2534(9)	Al-S(0B)	2.2534(9)
Al-S(0A)	2.2534(9)	Al-S(0C)	2.2534(9)
S-C(1)	1.784(4)		
S-Al-S(0A)	119.16(6)	S-Al-S(0B)	104.85(3)
S(0A)-Al-S(0B)	104.85(3)	S(0A)-Al-S(0C)	104.85(3)
S-Al-S(0C)	104.85(3)	C(1)-S-Al	107.42(12)
S(0B)-Al-S(0C)	119.16(6)		

3.2.20 Reaction of $[AlH_3(NMe_2Et)]$ and 2,6-$Me_2C_6H_3SH$

The reaction of $[AlH_3(NMe_2Et)]$ and one equivalent of 2,6-$Me_2C_6H_3SH$ was carried out, as described in 3.2.1. After work-up and cooling to -20 °C colourless crystals were obtained in 97% yield. Analytical and spectroscopic data showed that $[Al(SC_6H_3Me_2\text{-}2,6)_3(HSC_6H_3Me_2\text{-}2,6)]$ (**60**) had been formed. The ^1H NMR spectrum of **60** shows two sets of peaks due to the methyl groups attached to the aryl ring and three small peaks in the same region suggesting that the solution behaviour of **60** is complex. Two sets of peaks due to the NMe_2Et ligand (present in the crystal structure) are observed which suggests that an exchange of the coordinated thiol and the free amine may exist in solution. The ^{13}C NMR of **60** confirms the complex solution behaviour. The NMR spectra could also indicate that **60** had not been formed cleanly, which is confirmed by the discrepancy between the observed and calculated values inn the analytical data.

3.2.21 X-ray structure of $[Al(SC_6H_3Me_2\text{-}2,6)_3(HSC_6H_3Me_2\text{-}2,6)]$ (60)

The structure of compound **60** was confirmed by X-ray crystallography, the results of which are shown in Figure 3.20; selected bond lengths and angles are given in Table 3.8. The X-ray structure determination showed that compound **60** co-crystallised with NMe_2Et. The structure of **60** is similar that of the anion in **59** (see section 3.2.18). However, **60** is a neutral species as S(2) is protonated, shown by

the significantly longer Al-S(2) bond length (2.275(2) Å) compared with the three other Al-S bond lengths (2.250(2) - 2.254(3) Å). Although NMe_2Et is present in the crystal structure, no evidence was found for the presence of a $[HNMe_2Et]^+$ cation.

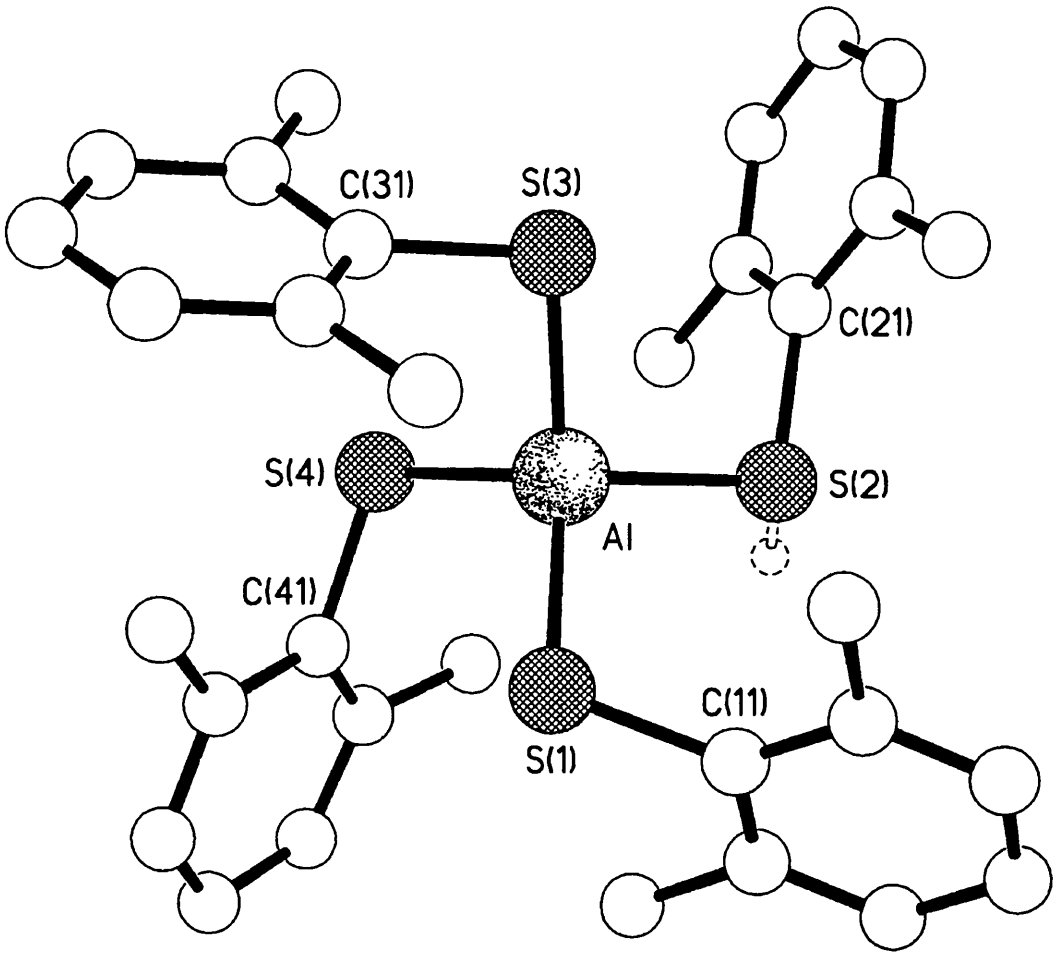

Figure 3.20 X-ray structure of $[Al(SC_6H_3Me_2\text{-}2,6)_3(HSC_6H_3Me_2\text{-}2,6)]$ (60)

Table 3.7 Selected bond lengths (Å) and angles (°) for $[Al(SC_6H_3Me_2\text{-}2,6)_3(HSC_6H_3Me_2\text{-}2,6)]$ (60)

Al-S(4)	2.250(2)	Al-S(3)	2.254(3)
Al-S(1)	2.250(2)	Al-S(2)	2.275(2)
S(1)-C(11)	1.771(6)	S(3)-C(31)	1.792(6)
S(2)-C(21)	1.790(6)	S(4)-C(41)	1.794(7)
S(4)-Al-S(1)	108.28(9)	S(1)-Al-S(3)	119.45(10)
S(4)-Al-S(3)	103.79(9)	S(4)-Al-S(2)	116.49(9)
S(1)-Al-S(2)	104.65(8)	C(11)-S(1)-Al	102.5(2)
S(3)-Al-S(2)	104.78(9)	C(21)-S(2)-Al	103.7(2)
C(31)-S(3)-Al	101.9(2)	C(41)-S(4)-Al	107.0(2)

3.3 Decomposition studies

In this section the potential of the aluminium alkoxides and thiolates as precursors to thin films and bulk materials is explored. The decomposition pathways of some of the precursors, whose preparation was described in section 3.2, were explored by Thermal Gravimetric Analysis (TGA), as described in section 2.3.1. Vapour-phase deposition studies of $[HAl(O^tBu)_2]_2$ (**21**) and $[Al(S^tBu)_3(NMe_2Et)]$ (**42**) were carried out in order to assess the ability of these compounds to produce thin films.

3.3.1 Decomposition properties of $[Al_5(\mu_5\text{-}O)(\mu\text{-}O^iPr)_8(Cl)H_4]$ (48)

The decomposition properties of $[Al_5(\mu_5\text{-}O)(\mu\text{-}O^iPr)_8(Cl)H_4]$ (**48**) were determined by TGA and the results are shown in Figure 3.21. The decomposition of **48** shows a total weight loss of 50% below 500 °C which is lower than the expected weight loss of 62% if Al_2O_3 was formed. The difference in the observed and expected weight losses be due to high levels of contamination in the material formed. The observation of a steep weight loss followed by a more gradual loss of weight

(200 - 500 °C) suggests that most of the decomposition occurs below 200 °C. Further investigations would need to be carried out to establish the nature of the decomposition pathway followed by **48**, which may be complex. As **48** is a cluster, it would not be expected to have a high volatility and would not be suitable for use as a single-source precursor in CVD.

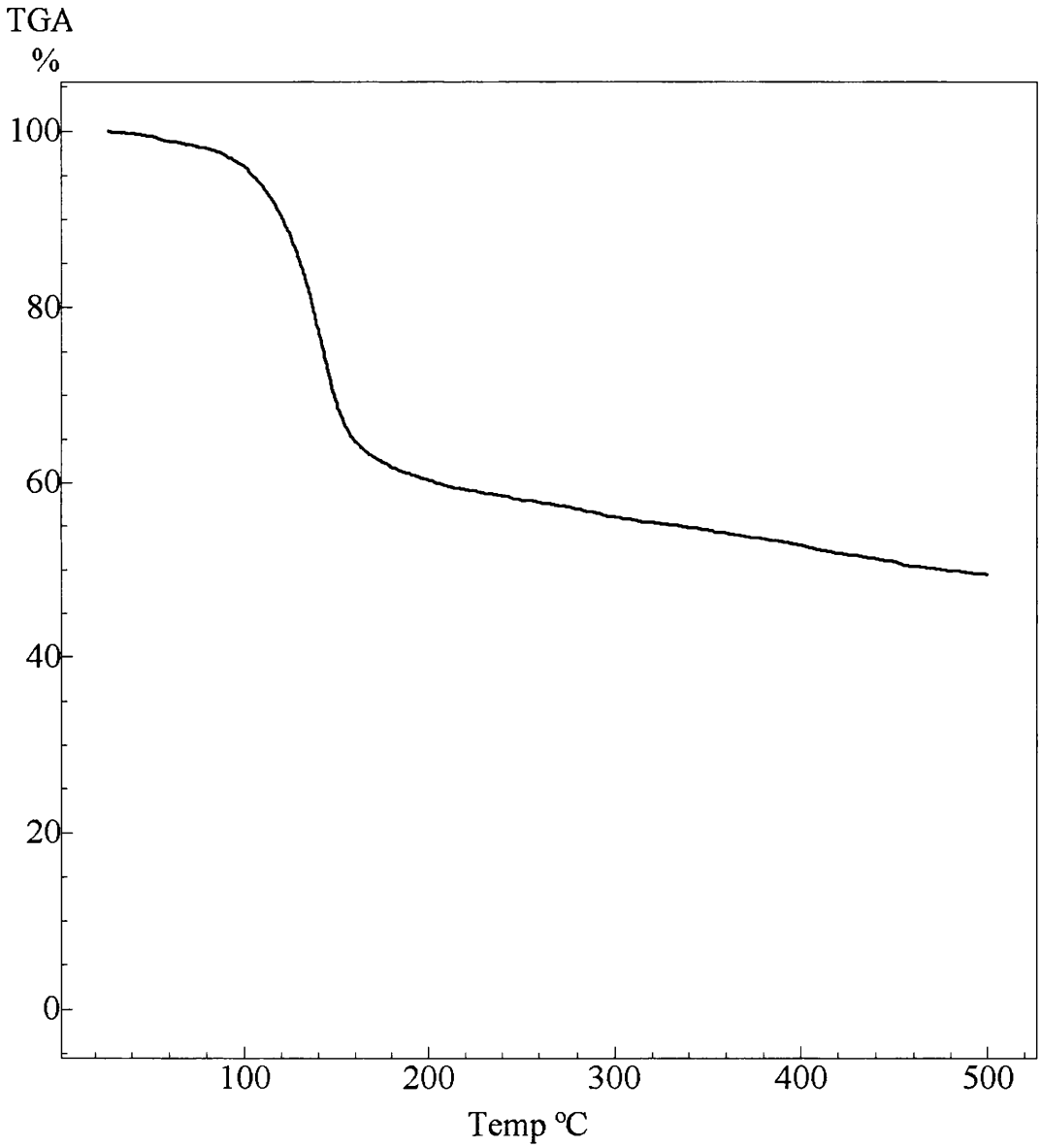

Figure 3.21 TGA of $[Al_5(\mu_5\text{-}O)(\mu\text{-}O^iPr)_8(Cl)H_4]$ (48)

3.3.2 Decomposition properties of $[HAl(OR)_2(NMe_2Et)]$

The synthesis of the alkoxides $[HAl(OR)_2(NMe_2Et)]$ (where R = C_6F_4H-3 (**53**) or $C_6H_3Me_2$-2,6 (**54**)) is described in section 3.2. The TGA of **53** (Figure 2.32) shows a total weight loss of 78% which is less than the 88% weight loss expected if decomposition to Al_2O_3 has occurred. The TGA of **54** also shows that incomplete weight loss has occurred as the total weight loss (77%) is less than that expected (85%). The difference in the observed and expected weight losses may also be due to high levels of contamination in the material formed. Both TGA show three weight losses, the first of which (19% and 23% respectively) corresponds to the loss of NMe_2Et (calculated as 17% and 21% respectively). The decomposition pathways of **53** and **54** are complex and further investigations would need to be carried out to determine them.

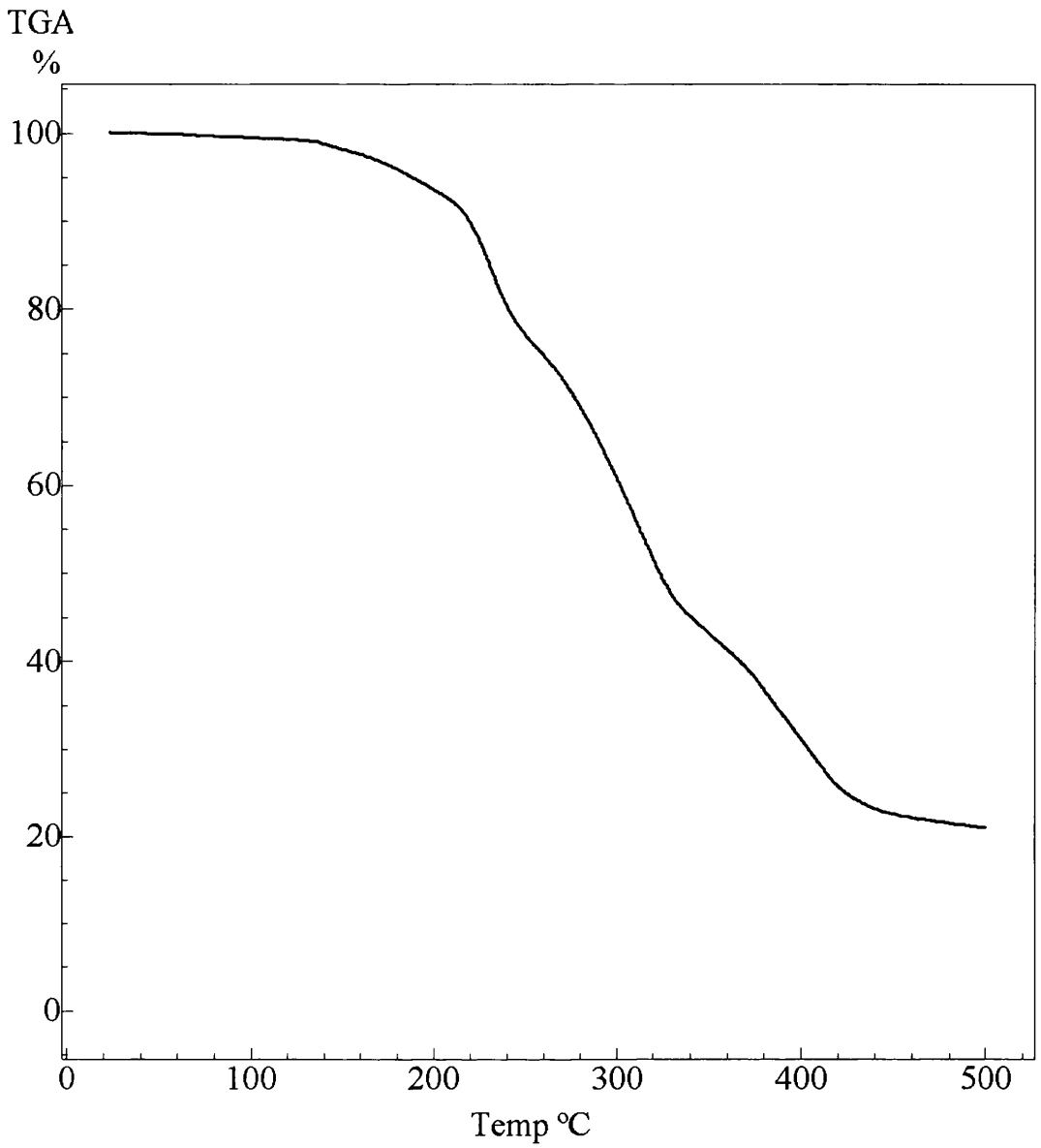

Figure 3.22. TGA of [HAl(OC$_6$F$_4$H-3)$_2$(NMe$_2$Et)] (53)

3.3.3 Decomposition properties of [Al(SC$_6$H$_3$Me$_2$-2,6)$_3$(OEt$_2$)]

The decomposition properties of [Al(SC$_6$H$_3$Me$_2$-2,6)$_3$(OEt$_2$)] (**58**) were investigated by TGA and the results are shown in Figure 3.23. The decomposition of **58** is clean and shows a total weight loss of 73%. This is in good agreement with the calculated value for complete decomposition of **58** to Al_2S_3 (71%). Two distinct weight losses are observed, the first (19%) corresponds to the loss of solvent from **58** (20%). The second (54%) corresponds to the formation of Al_2S_3 from [Al(SC$_6$H$_3$Me$_2$-2,6)$_3$] (52%). One possible decomposition mechanism involves the

formation of R_2S and Al_2S_3. This agrees with the TGA data, however, further studies would need to be carried out in order to establish the exact mechanism.

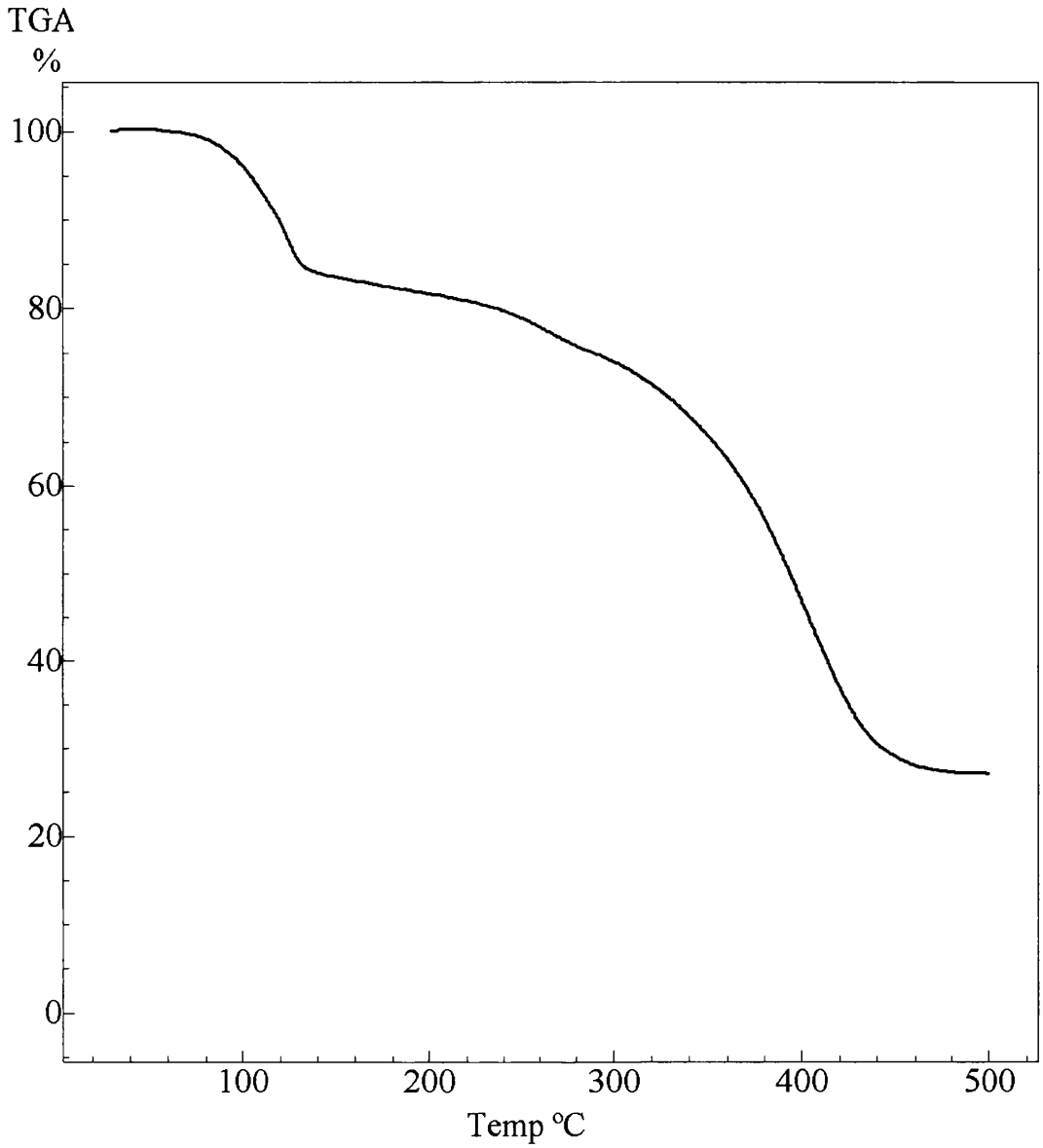

Figure 3.23 TGA of $[Al(SC_6H_3Me_2\text{-}2,6)_3(OEt_2)]$ (58)

2.3.4 Vapour-phase thin film studies

Tube furnace reactions were carried out on $[HAl(O^tBu)_2]_2$ (**21**) and $[Al(S^tBu)_3(NMe_2Et)]$ (**42**) in order to assess whether thin films of aluminium chalcogenides could be obtained at low pressure. The apparatus used in these reactions is shown in section 2.3.9 and the experimental procedure described in

section 2.4.41. In the case of **21**, a thick white film formed on the glass, which had been in the hot zone of the furnace and a thinner colourless film formed on the glass which had been in the cooler part of the furnace. The thinner film was observed to exhibit an interference pattern, when it was moved, which is due to the thickness of the film varying across the surface of the glass.

The thick film was easily removed when it was rubbed with a piece of tissue, the thinner film however, could not be removed by tissue but was scratched by stainless steel. The thicker film was found to be particulate by SEM; EDXA showed that aluminium and oxygen were present in the correct stoichiometeric ratio for Al_2O_3. A small amount of silicon was observed from the underlying glass and no peaks due to carbon were observed. The thinner film was also analysed by EDXA, however, most of the elements observed were due to the glass substrate. Glancing angle XRD showed the thicker film to be amorphous. X-ray photoelectron spectroscopy (XPS) was carried out on the thicker film and shows that Al_2O_3 was formed (Figure 3.24 shows the 1s peak). XPS showed the presence of aluminium, oxygen, carbon and silicon (from the glass substrate). Both Al_{2p} and O_{1s} XPS binding energies of 74.8 and 531.3 eV matched previous measurements for Al_2O_3. However, oxygen was also present as an oxide probably from the glass substrate and in a third environment, probably oxygen attached to the surface of the film (shown in Figure 3.24), therefore, an accurate Al:O ratio could not be obtained.

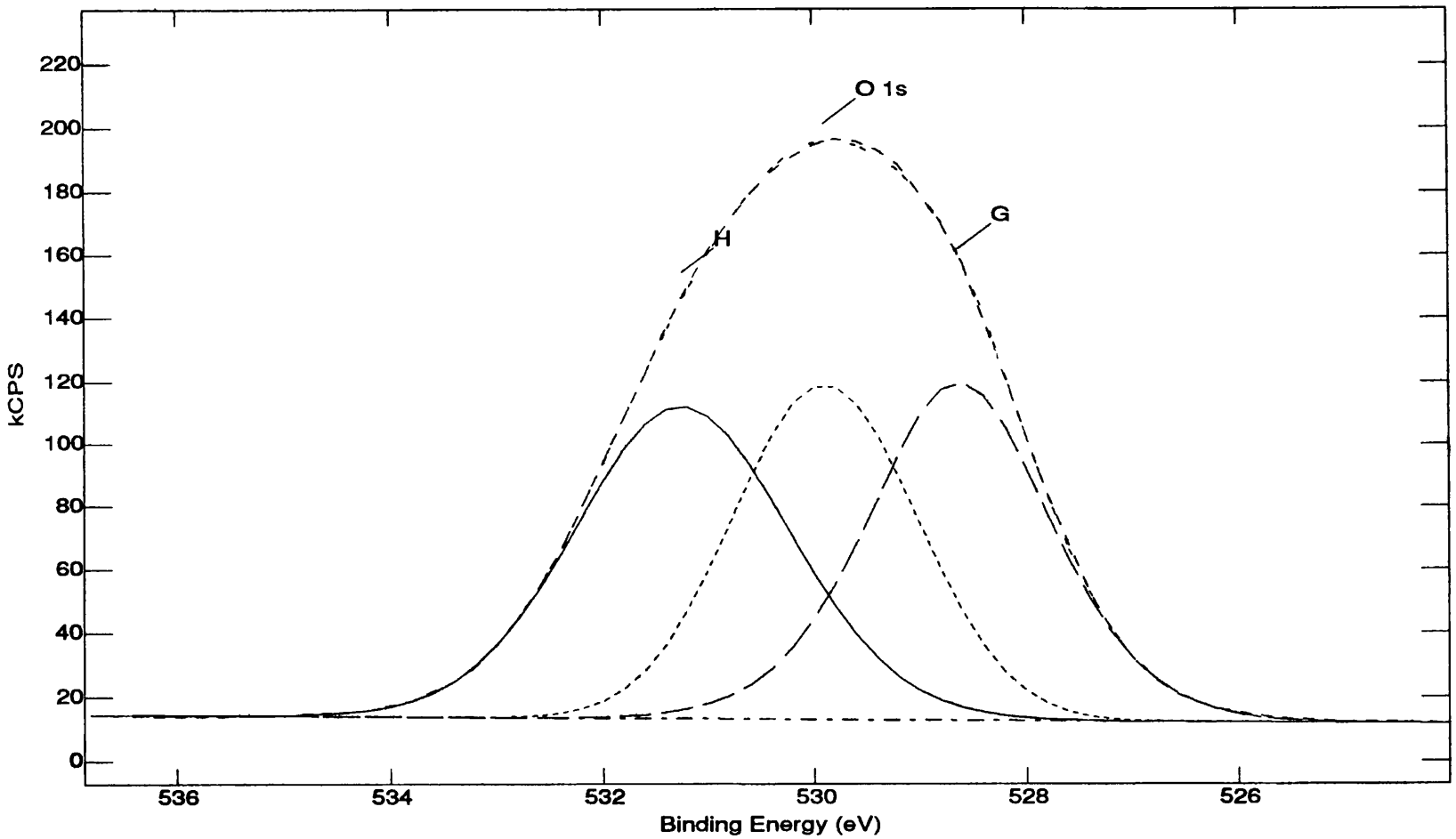

Figure 3.24 XPS of Al_2O_3 film

3.4 Experimental

3.4.1 Preparation of $[Al_5(\mu_4\text{-}O)(\mu\text{-}O^iPr)_7H_6]$ (47)

Following literature routes,[42] a solution of $[AlCl_3]$ (0.59 g, 4.39 mmol) in diethyl ether (15 cm^3) was added dropwise to a stirred slurry of $[LiAlH_4]$ (0.50 g, 13.2 mmol) also in diethyl ether (15 cm^3). After stirring at room temperature for 30 min, ^iPrOH (1.34 cm^3, 17.6 mmol) was added and evolution of hydrogen was observed. The resulting grey slurry was stirred at room temperature for 4 hours. After filtering through Celite, the solvent was reduced under vacuum to ~5 cm^3. Cooling to -20 °C for a few weeks resulted in the formation of colourless crystals of **47** were obtained (0.54 g, 43% yield), mp 190-193 °C. Anal. Calc. for $C_{21}H_{55}O_8Al_5$: C, 44.21; H, 9.72. Found C, 43.51; H, 9.03. ^1H NMR δ/ppm (C_6D_6): δ 1.40-1.50 (m, $OCH(CH_3)_2$, 4.46-4.63 (m, $OCH(CH_3)_2$), 4.75 (spt, J = 29 Hz, $OCH(CH_3)_2$), Al*H* not detected. $^{13}C\{^1H\}$ NMR (C_6D_6): δ 23.7 (s $OCH(CH_3)_2$), 24.6 (s $OCH(CH_3)_2$), 25.0 (s $OCH(CH_3)_2$), 25.3 (s $OCH(CH_3)_2$), 66.3 (s $OCH(CH_3)_2$), 66.9 (s $OCH(CH_3)_2$). IR (KBr disc cm^{-1}): 2975 s, 2930 m, 2874 w, 1830 w, 1822 m br, 1719 w, 1454 w, 1376 m, 1262 w, 1175 m, 1130 s, 1132 s, 977 s, 946 m, 840 s, 784 s, 725 s, 647 s, 566 w, 532 m.

3.4.2 Preparation of $[Al_5(\mu_5\text{-}O)(\mu\text{-}O^iPr)_8(Cl)H_4]$ (48)

Following literature routes,[42] a solution of $[AlCl_3]$ (0.59 g, 4.39 mmol) in diethyl ether (15 cm^3) was added dropwise to a stirred slurry of $[LiAlH_4]$ (0.50 g, 13.2 mmol) also in diethyl ether (15 cm^3). ^iPrOH (1.34 cm^3, 17.6 mmol) was added and effervescence was observed immediately. The mixture was stirred at room temperature for 24 hours. After filtering through Celite the solvent was reduced *in vacuo* to approximately 5 cm^3 and cooled to -20 °C. Colourless crystals formed over several weeks (0.51 g, 39% yield), mp 82 -84 °C. Anal. calc. for $C_{24}H_{60}ClO_9Al_5$: C, 43.47; H, 9.12. Found C, 44.27, 9.40. ^1H NMR δ/ppm (C_6D_6): δ 1.32 - 1.48 (m, 24H, $OCH(CH_3)_2$), 4.20 (spt, J = 32 Hz), 4.35 (spt, J = 32 Hz), 4.58 (spt, J = 32 Hz), 4.76 (spt, J = 32 Hz), (ratio 1:1:2:2, $OCH(CH_3)_2$), Al*H* not detected. $^{13}C\{^1H\}$ NMR (C_6D_6): δ 25.2, 25.4, 28.1, 28.2 (s, $OCH(CH_3)_2$), 63.7, 66.9, 67.5, 67.9 (s,

O*C*H(CH$_3$)$_2$). IR (KBr disc, cm^{-1}): 2971 s, 2931 m, 2875 w, 1820 br m, 1384 m, 1375 m, 1270 w, 1175 m, 1128 s, 1010 w, 965 s, 844 m, 824 s, 769 m, 669 s.

3.4.3 Preparation of [Al(O^{i}Pr)$_3$]$_4$ (12)

^{i}PrOH (0.17 cm^3, 2.26 mol) was added to a solution of [AlH$_3$(NMe$_2$Et)] (0.3 cm^3, 2.26 mmol) in diethyl ether (25 cm^3). Evolution of hydrogen was observed and the mixture was allowed to stir for 5 minutes. The solvent was removed under vacuum yielding a colourless oil. Standing at room temperature for 1 week yielded colourless crystals of **12** (0.14 g, 91% yield). Anal. Calc. for $C_9H_{21}O_3Al$: C, 52.93; H, 10.36. Found C, 51.74; H, 9.82. IR (nujol, cm^{-1}): 1261 w, 1171 s, 1120 s, 1034 s, 948 s, 834 s, 703 m, 613 m, 580 m, 485 m.

3.4.4 Preparation of [HAl(O^{t}Bu)$_2$]$_n$ (21)

^{t}BuOH (1.44 cm^3, 15.1 mmol) was added dropwise to a solution of [AlH$_3$(NMe$_2$Et)] (1.0 cm^3, 7.54 mmol) in diethyl ether (20 cm^3) at room temperature. Evolution of hydrogen was observed on addition of the alcohol and the mixture was stirred for 1 hour. The mixture was reduced in volume under vacuum to *ca.* 5 cm^3. Cooling to -20 °C for 24 hours resulted in the formation of colourless crystals of **21** (1.22 g, 93% yield). Anal. Calc. for $C_8H_{19}O_2Al$: C, 55.40; H, 10.99. Found: C, 54.27; H, 9.93. IR (nujol, cm^{-1}): 1872 w, 1358 vs, 1211 vs, 1182 s, 1080 s, 1056 s, 1023 m, 908 s, 810 m, 793 m, 776 s, 706 s, 664 s, 547 s, 481 m, 469 m, 424 w, 411 w.

3.4.5 Preparation of [H$_2$Al(OC$_6$F$_4$H-3)(NMe$_2$Et)]$_n$ (52)

A solution of C$_6$F$_4$H-3OH (0.63 g, 3.77 mmol) in diethyl ether (10 cm^3) was added dropwise to a solution of [AlH$_3$(NMe$_2$Et)] (0.5 cm^3, 3.77 mmol) also in diethyl ether (10 cm^3) at room temperature. The evolution of hydrogen was observed and the mixture was allowed to stir for one hour. The volume of the solution was reduced under vacuum to *ca.* 5 cm^3. Cooling to -20 °C afforded a white powder of **52** (0.58 g, 79%), mp 42 °C. ^{1}H NMR δ/ppm (CD$_2$Cl$_2$): δ 1.26 (t, *J* = 14 Hz, 3H, NCH$_2$C*H*$_3$), 2.60 (s, 6H, N(C*H*$_3$)$_2$), 2.97 (q, *J* = 25 Hz, 2H, NC*H*$_2$CH$_3$), 6.53 (spt, *J* = 21 Hz, 1H, C$_6$F$_4$*H*), Al*H* not detected. ^{13}C{^{1}H} NMR (CD$_2$Cl$_2$): δ 8.8 (s, NCH$_2$*C*H$_3$), 43.6 (s,

$N(CH_3)_2$), 94.5 (s, NCH_2CH_3), 139.3 (s, *p*-OC_6F_4H), 141.7 (s, *m*-OC_6F_4H), 145.6 (s, *o*-OC_6F_4H), 148.0 (s, *OC*). IR (nujol, cm^{-1}): 3079 w, 1897 s, 1650 s, 1515 s, 1261 s, 1169 s, 1108 s br, 1038 w, 1020 w, 944 s, 925 w, 820 w, 805 m, 772 m, 738 m, 722 m, 687 w, 668 w, 644 w, 570 w, 480 w, 457 w, 428w.

3.4.6 Preparation of $[HAl(OC_6F_4H\text{-}3)_2(NMe_2Et)]_n$ (53)

A solution of C_6F_4H-3OH (1.25 g, 7.54 mmol) in diethyl ether (15 cm^3) was added dropwise to a solution of $[AlH_3(NMe_2Et)]$ (0.5 cm^3, 3.77 mmol) in diethyl ether (10 cm^3) at room temperature. The evolution of hydrogen was observed and the mixture was allowed to stir for one hour. The volume of the solution was reduced under vacuum to *ca.* 5 cm^3. Cooling to -20 °C afforded a white powder of **53** (1.01 g, 75%), mp 46-48 °C. ^1H NMR δ/ppm (CD_2Cl_2): δ 1.34 (t, *J* = 14 Hz, 3H, NCH_2CH_3), 2.72 (s, 6H, $N(CH_3)_2$), 3.07 (d br, *J* = 11 Hz, 2H, NCH_2CH_3), 6.53 (s br, 2H, C_6F_4H), Al*H* not detected. $^{13}C\{^1H\}$ NMR (CD_2Cl_2): δ 8.8 (s, NCH_2CH_3), 43.0 (s, $N(CH_3)_2$), 94.7 (s, NCH_2CH_3), 95.4 (s, NCH_2CH_3), 139.4 (s, *p*-OC_6F_4H), 141.7 (s, *m*-OC_6F_4H), 145.6 (s, *o*-OC_6F_4H), 148.0 (s, *ipso*-OC_6F_4H). IR (nujol, cm^{-1}): 3075 w, 1896 s, 1651 s, 1505 s br, 1280 w, 1261 m, 1168 s, 1109 s br, 1037 m, 993 w, 940 vs, 821 w, 806 w, 773 w, 727 w, 702 w, 686 m, 644 m, 568 m, 538 m, 531 m, 517 w, 481 s, 458 w, 425 w.

3.4.7 Preparation of $[HAl(OC_6H_3Me_2\text{-}2,6)_2(NMe_2Et)]$ (54)

A solution of 2,6-$Me_2C_6H_3OH$ (1.84 g, 15.1 mmol) in diethyl ether (15 cm^3) was added to a solution of $[AlH_3(NMe_2Et)]$ (1.0 cm^3, 7.54 mmol) in diethyl ether (10 cm^3) at room temperature. Formation of hydrogen was observed and the mixture was stirred at room temperature for 1 hour. The mixture was reduced in volume to *ca.* 5 cm^3. Cooling to -20 °C afforded colourless crystals of **54** (1.24 g, 48% yield), mp 58-60 °C. Anal. Calc. for $C_{20}H_{30}NO_2Al$: C, 69.94; H, 8.81; N, 4.08. Found: C, 68.72; H, 8.24; N, 4.15. ^1H NMR δ/ppm (CD_2Cl_2): δ 1.39 (t, *J* = 10 Hz, 3H, NCH_2CH_3), 2.28 (s, 12H, $OC_6H_3(CH_3)_2$), 2.75 (s, 6H, $N(CH_3)_2$), 3.15 (q, *J* = 20 Hz, 2H, NCH_2CH_3), 6.75 (t, *J* = 17 Hz, 2H, *p*- $OC_6H_3(CH_3)_2$), 7.01 (d, *J* = 8 Hz, 4H, *m*- $OC_6H_3(CH_3)_2$). $^{13}C\{^1H\}$ NMR (CD_2Cl_2): δ 8.4 (s, NCH_2CH_3), 18.1 (s, $OC_6H_3(CH_3)_2$), 18.3 (s,

$N(CH_3)_2$), 43.3 (s, NCH_2CH_3), 118.4 (s, *p*-$OC_6H_3(CH_3)_2$), 127.0 (s, *p*-$OC_6H_3(CH_3)_2$), 128.6 (s, *o*-$OC_6H_3(CH_3)_2$), 155.9 (s, *ipso*-$OC_6H_3(CH_3)_2$). IR (nujol, cm^{-1}): 1843 s, 1594 s, 1429 w, 1281 s, 1237 s, 1182 m, 1093, 1036 m, 997 m, 919 s, 897 s, 760 s, 749 s, 679 s br, 532 m, 402 w.

3.4.8 Preparation of $[HAl(S^tBu)(\mu\text{-}O^tBu)]_2$ (55)

A solution of [$AlCl_3$] (0.44 g, 3.33 mmol) in diethyl ether (15 cm^3) was added to a stirred slurry of [$LiAlH_4$] (0.38 g, 10.0 mmol) in diethyl ether (10 cm^3). ^tBuSH (1.5 cm^3, 13.3 mmol) was added dropwise and the immediate evolution of hydrogen was observed. The resulting grey coloured mixture was stirred at room temperature for 24 hours. After filtering through Celite the solvent was reduced under vacuum to *ca.* 10 cm^3. Cooling to -20 °C for 24 hours resulted in the formation of colourless crystals of **55**, decomposed without melting below 230 °C. Anal. Calc. for $C_8H_{19}OSAl$: C, 50.50; H, 10.06. Found: C, 32.40; H, 6.56. IR (KBr disc, cm^{-1}): 2963 s, 2897 m, 2862 w, 1458 s, 1391 m, 1364 s, 1261 s, 1155 s br, 1096 m br, 1028 m br, 887 w br, 799 w br, 648 m br, 513 m br, 457 w br.

3.4.9 Preparation of $[Al(S^tBu)_3(NMe_2Et)]$ (42)

^tBuSH (0.43 cm^3, 3.77 mmol) was added dropwise to a solution of [$AlH_3(NMe_2Et)$] (0.5 cm^3, 3.77 mmol) in diethyl ether (20 cm^3) at room temperature. The evolution of hydrogen was observed and the mixture was stirred at room temperature for 1.5 hours. The solution was reduced in volume to *ca.* 5 cm^3 under vacuum. Cooling to -20 °C for 24 hours resulted in the formation of colourless crystals of **42** (0.19 g, 41% yield), mp 84-86 °C. Anal. Calc. for $C_{16}H_{38}NS_3Al$: C, 52.27; H, 10.48; N, 3.81. Found: C, 51.38; H, 9.92; N, 3.46. ^1H NMR δ/ppm (CD_2Cl_2): δ 1.12 (t, J = 10 Hz, 3H, NCH_2CH_3), 1.41 (s, $SC(SH_3)_3$), 1.57 (s, 27H, $SC(SH_3)_3$), 2.56 (s, 6H, $N(CH_3)_2$), 3.22 (q, 2H, NCH_2CH_3). $^{13}C\{^1H\}$NMR (CD_2Cl_2): δ 5.9 (s, NCH_2CH_3), 35.1 (s, $SC(CH_3)_3$), 36.7 (s, $SC(CH_3)_3$), 41.8 (s, $N(CH_3)_2$), 45.2 (s, $SC(CH_3)_3$), 50.7 (s, NCH_2CH_3).

3.4.10 Preparation of $[Al(SC_6H_3Me_2\text{-}2,6)_3(OEt_2)]$ (58)

Following literature routes,[42] a solution of $[AlCl_3]$ (0.22 g, 1.60 mmol) in diethyl ether (10 cm^3) was added dropwise to a stirred slurry of $[LiAlH_4]$ (0.19 g, 5.0 mmol) in diethyl ether (15 cm^3). 2,6-$Me_2C_6H_3SH$ (0.88 cm^3, 6.65 mmol) was added dropwise was added dropwise with stirring and immediate evolution of hydrogen was observed. The resulting grey slurry was stirred at room temperature for 24 hours. After filtering through Celite the solvent was reduced under vacuum to approximately 5 cm^3. Cooling to -20 °C afforded colourless crystals of **58** (1.09 g, 28% yield), mp 103-104 °C. Anal. Calc. for $C_{28}H_{37}OS_3Al$: C, 65.59; H, 7.27. Found: C, 63.51; H, 7.41. ^1H NMR δ/ppm ($CDCl_3$): δ 1.12 (t, J = 11 Hz, 6H, $O(CH_2CH_3)_2$), 1.35 (t, J = 11 Hz, 4.5H, $O(CH_2CH_3)_2$), 2.25 (s, 18H, $SC_6H_3(CH_3)_2$), 3.42 (q, J = 21 Hz, 4H, $O(CH_2CH_3)_2$), 4.37 (q, J = 21 Hz, 2H, $O(CH_2CH_3)_2$), 6.77-6.95 (m, 9H, $SC_6H_3(CH_3)_2$). $^{13}C\{^1H\}$ NMR ($CDCl_3$): δ 13.4 (s, $O(CH_2CH_3)_2$), 15.1 (s, $O(CH_2CH_3)_2$), 23.6 (s, $SC_6H_3(CH_3)_2$), 65.8 (s, $O(CH_2CH_3)_2$), 68.8 (s, $O(CH_2CH_3)_2$), 125.5 (s, *m*-$SC_6H_3(CH_3)_2$), 127.5 (s, *ipso*-$SC_6H_3(CH_3)_2$), 132.4 (s, *p*-$SC_6H_3(CH_3)_2$), 142.0 (s, *o*-$SC_6H_3(CH_3)_2$). IR (KBr disc, cm^{-1}): 3057 m, 2977 m, 2922 w, 1460 s, 1436 m, 1371 m, 1323 w br, 1262 w, 1188 m, 1162 m, 1149 m, 1088 m, 1051 s, 1009 s, 989 m, 878 s, 831 w, 760 vs, 718 s, 588 m, 528 s, 496 s, 480 s, 413 m.

3.4.11 Preparation of $[Li(OEt_2)_3][Al(SC_6H_3Me_2\text{-}2,6)_4]$ (59)

Following literature routes,[42] a solution of $[AlCl_3]$ (0.22 g, 1.60 mmol) in diethyl ether (10 cm^3) was added dropwise to a stirred slurry of $[LiAlH_4]$ (0.19 g, 5.0 mmol) in diethyl ether (15 cm^3). 2,6-$Me_2C_6H_3SH$ (0.88 cm^3, 6.65 mmol) was added dropwise with stirring and immediate evolution of hydrogen was observed. The resulting grey slurry was stirred at room temperature for 24 hours. After filtering through Celite the solvent was reduced under vacuum to approximately 5 cm^3. Cooling to -20 °C afforded colourless crystals of **59** (0.24 g, 25% yield), decomposed without melting below 230 °C. Anal. Calc. for $C_{44}H_{66}O_3S_4LiAl$: C, 65.63; H, 8.26. Found: C, 63.71; H, 7.51. ^1H NMR δ/ppm ($CDCl_3$): δ 2.00 (t, J = 14 Hz, $O(CH_2CH_3)_2$), 2.27 (s, 24H, $SC_6H_3(CH_3)_2$), 3.53 (q, J = 21 Hz, $O(CH_2CH_3)_2$), 6.86-6.97 (m, 9H, $SC_6H_3(CH_3)_2$). $^{13}C\{^1H\}$ NMR ($CDCl_3$): δ 14.8 (s, $O(CH_2CH_3)_2$), 23.8

(s, $SC_6H_3(CH_3)_2$), 66.0 (s, $O(CH_2CH_3)_2$), 125.0 (s, *m*-$SC_6H_3(CH_3)_2$), 127.1 (s, *ipso*-$SC_6H_3(CH_3)_2$), 134.8 (s, *p*-$SC_6H_3(CH_3)_2$), 142.3 (s, *o*-$SC_6H_3(CH_3)_2$). IR (KBr disc, cm^{-1}): 1583 w, 1303 w, 1257 w, 1161 wm 1092 m, 1051 s, 1022 m, 912 m, 838 w, 798 m, 771 s, 759 m, 587 m, 521 m, 492 m, 468 m, 436 m, 408 m.

3.4.12 Preparation of $[Al(SC_6H_3Me_2\text{-}2,6)_3(HSC_6H_3Me_2\text{-}2,6)]$ (60)

2,6-$Me_2C_6H_3SH$ (0.3 cm^3, 2.26 mmol) was added dropwise to a solution of $[AlH_3(NMe_2Et)]$ (0.3 cm^3, 2.26 mmol) in diethyl ether (15 cm^3) with stirring at room temperature. Evolution of hydrogen was observed and a white precipitate formed. The solvent was removed under vacuum yielding a white powder (0.39 g, 97% yield). Recrystalisation from a minimum of CH_2Cl_2 yielded colourless crystals of **60** suitable for X-ray crystallography. Anal. Calc. for $C_{36}H_{48}NS_4Al$: C, 67.13; H, 7.30; N, 1.78. Found: C, 64.20; H, 6.72; N, 1.35. ^1H NMR δ/ppm (CD_2Cl_2): δ 1.10 (t, J = 11 Hz, NCH_2CH_3), 1.17 (t, J = 11 Hz, NCH_2CH_3), 2.14 (s, $SC_6H_3(CH_3)_2$), 2.29 (s, $SC_6H_3(CH_3)_2$), 2.34 (s, $SC_6H_3(CH_3)_2$), 2.36 (s, $SC_6H_3(CH_3)_2$), 2.38 (s, $SC_6H_3(CH_3)_2$), 2.45 (s, $(CH_3)_2$), 2.73 (s, $N(CH_3)_2$), 2.77 (q, J = 19 Hz, NCH_2CH_3), 3.31 (q, J = 19 Hz, NCH_2CH_3), 6.86-7.01 (m, 9H, $SC_6H_3(CH_3)_2$). $^{13}C\{^1H\}$ NMR ($CDCl_3$): δ 6.0 (s, NCH_2CH_3), 9.9 (s, NCH_2CH_3), 23.8 (s, $SC_6H_3(CH_3)_2$), 24.1 (s, $SC_6H_3(CH_3)_2$), 42.7 (s, NCH_2CH_3), 43.2 (s, NCH_2CH_3), 51.8 (s, $N(CH_3)_2$), 125.2 (s, *m*-$SC_6H_3(CH_3)_2$), 126.0 (s, *m*-$SC_6H_3(CH_3)_2$), 127.3 (s, *ipso*-$SC_6H_3(CH_3)_2$), 127.9 (s, *ipso*-$SC_6H_3(CH_3)_2$), 133.1 (s, *p*-$SC_6H_3(CH_3)_2$), 136.2 (s, *p*-$SC_6H_3(CH_3)_2$), 142.8 (s, *o*-$SC_6H_3(CH_3)_2$). IR (nujol, cm^{-1}): 3143 m, 1581 m, 1375 s, 1161 m, 1115 m, 1082 w, 1062 s, 1021 m, 988 s, 914 s, 812 m, 764 vs, 720 s, 586 s, 544 s, 469 s, 458 m, 442 w.

3.5 References

1. U. Leushake, T. Krell, U. Schulz, M. Peters, W. A. Kaysser & B. H. Rabin, *Surf. Coat. Technol.*, 1997, **94/95**, 131.
2. H. Holleck, *Surf. Eng.*, 1991, **7**, 137.
3. D. Temple & A. Reisman, *J. Electron. Mater.*, 1990, **19**, 995.
4. W. T. Kim & C. D. Kim, *J. Appl. Phys.*, 1986, **60**, 2631.

5. R. S. Becker, T. Zheng, J. Elton & M. Saeki, *Sol. Eng. Mater.,* 1986, **13**, 97.
6. A. M. Mancini, G. Mcocci & A. Rizzo, *Mater. Chem. Phys.,* 1983, **9**, 29.
7. N. N. Greenwood & A. Earnshaw, *Chemistry of The Elements,* 1995.
8. K. M. Gustin & R. G. Gordon, *J. Electron. Mater.,* 1988, **17**, 509.
9. H. D. Van Corbach, V. A. C. Haanappel, T. Fransen & P. J. Gellings, *Thin Solid Films,* 1994, **239**, 31.
10. V. A. C. Haanappel, H. D. Van Corbach, T. Fransen & P. J. Gellings, *Thin Solid Films,* 1993, **230**, 138.
11. W. A. Pliskin, *J. Vac. Sci. Technol.,* 1977, **14**, 1064.
12. P. C. Munro & H. W. Thompson Jr., *J. Electrochem. Soc.,* 1975, **122,** 127.
13. T. Tsujide, S. Nakanuma & Y. Ikushima, *J. Electrochem. Soc.,* 1970, **117**, 703.
14. J. Saraie, K. Ono & S. Takeuchi, *J. Electrochem. Soc.,* 1989, **136**, 3139.
15. J. S. Kim, H. A. Marzouk, P. J. Reucroft, J. D. Robertson & C. E. Hamrin Jr., *Appl. Phys. Lett.,* 1993, **62**, 681.
16. L. H. Hall & W. C. Robinette, *J. Electrochem Soc.,* 1971, **118**, 1624.
17. M. Ishida, I. Katakabe, T. Nakamura & N. Ohtake, *Appl. Phys. Lett.,* 1988, **52**, 1326.
18. M. Ishida, Y. T. Lee, T. Higashino, H. Seo & T. Nakamura, *Jpn. J. Appl. Phys.*, 1995, **34**, 831.
19. H. Kumagai, K. Toyoda, M. Matsumoto & M. Obara, *Jpn. J. Appl. Phys.,* 1993, **32**, 6137.
20. R. S. Ehle, B. J. Baliga & W. Katz, *J. Electron. Mater.,* 1983, **12**, 587.
21. T. H. Hua & M. Armgarth, *J. Electron. Mater.,* 1987, **16**, 27.
22. L. G. Meiners, *Thin Solid Films,* 1984, **113**, 85.
23. C. Soto & W. T. Tysoe, *J. Vac. Sci. Technol.,* 1991, **A9**, 2686.
24. G.A. Battiston, G. Carta, G. Cavinato, R. Gerbasi, M. Porchia & G. Rossetto, *Chem. Vap. Deposition,* 2001, **7**, 69.
25. M. Ritala, M. Leskelä, J. P. Dekker, C. Mutsaers, P. J. Soininen & J. Skarp, *Chem. Vap. Deposition*, 1999, **5**, 7.
26. G. S. Higashi & C. G. Fleming, *Appl. Phys. Lett.,* 1989, **55**, 1963.
27. A. C. Dillion, A. W. Ott, J. D. Way & S. M. George, *Surf. Sci.*, 1995, **322**,

230.

28. J. F. Fan & K. Toyoda, *Jpn. J. Appl. Phys.*, 1993, **32**, L1349.
29. K. Sawada, M. Ishida, T. Nakamura & N. Ohtake, *Appl. Phys. Lett.*, 1988, **52**, 1672.
30. D. C. Bradley, *Chem. Rev.*, 1989, **89**, 1317.
31. J. A. Aboaf, *J. Electrochem. Soc.*, 1967, **114**, 948.
32. J. Saraie, J. Kwon & Y. Yodogawa, *J. Electrochem. Soc.*, 1985, **132**, 890.
33. W. Koh, S. J. Ku & Y. Kim, *Thin Solid Films*, 1997, **304**, 222.
34. T. Marauyama & S. Arai, *Appl. Phys. Lett.*, 1992, **60**, 322.
35. D. Temple & A. Reisman, *J. Electron. Mater.*, 1990, **19**, 995.
36. T. Maruyama & T. Nakai, *Appl. Phys. Lett.*, 1991, **58**, 2079.
37. O. B. Ajayi, M. S. Akanni, J. N. Lambi, C. Jeynes & J. F. Watts, *Thin Solid Films*, 1990, **185**, 123.
38. O. B. Ajayi, M. S. Akanni, J. N. Lambi, H. D. Burrows, O. Osasona & B. Podor, *Thin Solid Films*, 1986, **138**, 91.
39. M. Veith, S. Faber, R. Hempelmann, S. Janssen, J. Prewo & H. Eckerlebe, *J. Mater. Sci.*, 1996, **31**, 2009.
40. A. R. Barron, *Adv. Mater. Opt. Electron.*, 1995, **5**, 245.
41. M. Lazell, P. O'Brien, D. J. Otway & J. H. Park, *J. Chem. Soc., Dalton Trans.*, 2000, 4479.
42. H. Nöth & H. Suchy, *Z. Anorg. Allg. Chem.*, 1968, **358**, 44.
43. N. Y. Turova, V. A. Fozunov, A. I. Yanovskii, N. G. Bokii, Y. T. Struchkov & B. L. Tarnoploskii, *J. Inorg. Nucl. Chem.*, 1979, **41**, 5.
44. K. Folting, W. E. Streib, K. G. Caulton, O. Poncelet & L. G. Hubert-Pfalzgraf, *Polyhedron*, 1991, **10**, 1639.
45. D. A. Atwood, J. A. Jegier, S. Liu, D. Rutherford, P. Wei & R. C. Tucker, *Organometallics*, 1999, **18**, 976.
46. R. H. Cayton, M. H. Chisholm, E. R. Davidson, V. F. DiStasi, P. Du & J. C. Huffman, *Inorg. Chem.*, 1991, **30**, 1020.
47. M. D. Healy & A. R. Barron, *Angew. Chem. Int. Ed. Engl.*, 1992, **31**, 921.
48. J. Pauls & B. Neumüller, *Z. Anorg. Allg. Chem.*, 2000, **626**, 270.
49. M. Veith, S. Faber, H. Wolfanger & V. Huch, *Chem. Ber.*, 1996, **129**, 381.
50. J. P. Campbell & W. L. Gladfelter, *Inorg. Chem.*, 1997, **36**, 4094.

51. M. D. Healy, M. R. Mason, P. W. Gravelle, S. G. Bott & A. R. Barron, *J. Chem. Soc., Dalton Trans.,* 1993, 441.

52. H. Nöth, A. Schlegel, B. Singaram, J. Knizek, P. Mayer & T. Seifert, *Eur. J. Inorg. Chem.,* 2001, 173.

53. M. Veith, O. Schutt, J. Blin, S. Becker, J. Freres & V. Huch, *Z. Anorg. Allg. Chem.,* 2002, **628**, 138.

54. S. Daniel & D. M. Hoffman, *Inorg. Chem.,* 2002, **41**, 3843.

55. J. Knizek, H. Nöth & A. Schlegel, *Eur. J. Inorg. Chem.,* 2001, 181.

56. L. A. Mîinea & D. M. Hoffman, *Polyhedron,* 2001, **20**, 2425.

4. Mixed-metal chalcogenides

4.1 Introduction

Mixed-metal chalcogenides are used widely in integrated optic applications (e.g. $LiNbO_3$, $LiTaO_3$, $BaTiO_3$) and as ferroelectrics in memory devices (e.g. $BaTiO_3$, $SrBi_2Ta_2O_9$).[1] Of particular interest are mixed-metal chalcogenides of the general form AB_2E_4 (often called spinels as they adopt a spinel structure), which are important technological materials. The best known of this type of material is magnesium aluminium oxide (spinel), $MgAl_2O_4$, which has a number of important properties. Oxide spinels are used as magnetic materials,[2] pigments (e.g. $CoAl_2O_4$),[3] catalysts (e.g. $ZnAl_2O_4$),[4] refractory materials (e.g. $CaAl_2O_4$)[5] and sensors (e.g. $MgAl_2O_4$).[6]

Materials of the type AB_2E_4 may adopt either a normal or inverse spinel structure. The structure is based on chalcogenide atoms (E) in a face centred cubic arrangement. In the normal spinel structure, atoms of metal A occupy one-eighth of the tetrahedral holes and atoms of metal B occupy one-half of the octahedral holes. The structure may be symbolised by $A[B_2]E_4$, where brackets enclose the ions which are in octahedral sites. The structure, shown in Figure 4.1, can be built up from 8 units of alternating AE_4 tetrahedra (A) and B_4E_4 cubes (B - shaded), as shown in Figure 4.1(a). This is located within a face centred array of A ions as shown in Figure 4.1(b) (for clarity only two B units are shown).[7]

The structure described above is termed the normal spinel structure. An inverse structure contains half of the B atoms in tetrahedral holes and the A atoms along with the rest of the B atoms in octahedral holes.[7] This structure may be symbolised by $B[AB]E_4$, and often occurs when the A atoms have a stronger preference for octahedral co-ordination than the B atoms.[8]

In this project the synthesis of new single-source precursors to mixed-metal oxides, $MgAl_2O_4$, $CaAl_2O_4$, $NiAl_2O_4$, $ZnAl_2O_4$ and mixed-metal sulfide, $MgAl_2S_4$ has been attempted.

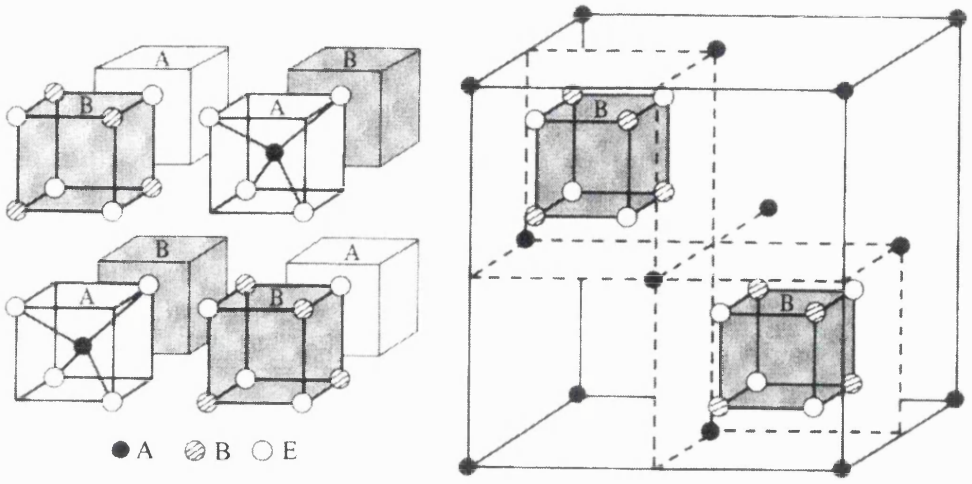

(a) (b)

Figure 4.1 The spinel structure[7]

4.1.1 Mixed-metal oxides

Mixed-metal oxides with a spinel type structure are widely used as heterogeneous catalysts and catalyst supports, some of which are currently used industrially.[9] The catalytic properties of $ZnAl_2O_4$ have been recently reported,[4] in particular, its use as a catalyst for the decomposition of nitrogen oxides[10] and the formation of thymol by the alkylation of *m*-cresol,[11] have been described in detail. $ZnAl_2O_4$ is also an active component of catalysts for the synthesis of methanol.[12] $NiAl_2O_4$ has been investigated as an electrode material for use in fuel cells.[13] The spinel oxides $NiAl_2O_4$,[2,14] $ZnAl_2O_4$[15] and $CaAl_2O_4$[16] are also important catalyst supports due to the ability to prepare these materials with high surface areas and their chemical and thermal stability.

There is considerable interest in $MgAl_2O_4$ due to the combination of its electronic properties, in particular low dielectric constant and close match of the oxygen ion lattice with silicon.[17] Thin films of the technologically important material GaN have been grown on $MgAl_2O_4$ substrates.[18,19] Moreover, $MgAl_2O_4$ films have been used as a buffer layer to grow GaN (on Si) and ferroelectric oxide films.[20] Films of $MgAl_2O_4$ are also of interest as the active material in humidity sensors, due to the ease of miniaturisation of ceramic microelectrodes.[6]

Another use of $MgAl_2O_4$ is in the fabrication of ultrafiltration membranes.[21] It is thought that ultrafiltration membranes made of $MgAl_2O_4$ will offer better high temperature stability, higher resistance to chemical attack and smaller pore sizes than the polymer and ceramic membranes currently available. $CaAl_2O_4$ is the main component of calcium aluminate cements, which have a wide range of uses particularly in refractory applications.[22]

Recently, there has been interest in the luminescence properties of doped spinel oxides. The material $CaAl_2O_4:Eu^{2+}$ shows 440 nm blue emission and is thought to be suitable for use in plasma display panels.[23,24] Blue violet phosphorescence lasting more than 10 hours has been observed with the material $CaAl_2O_4:Ce^{3+}$, whereas when $CaAl_2O_4:Tb^{3+},Ce^{3+}$ was excited green emission occurred.[25] Luminescence was observed from $ZnAl_2O_4$:Mn when it was subjected to a external source of mechanical stress such as friction, compression or tension (stress-stimulated luminescence).[26]

4.1.2 Preparation of bulk materials

In this section an overview of some of the techniques used to prepare bulk mixed-metal chalcogenides is given. Traditionally, oxide spinels have been prepared by a ceramic route, which involves a solid state reaction between metal compounds (typically oxides) at temperatures above 1000 °C over several days.[27] Before the reaction can take place numerous grinding steps must be used to mechanically mix the materials. Such reactions are still commonly used to prepare bulk spinel oxides.[13] The mechanism for the formation of $CaAl_2O_4$ from calcium carbonate and α-Al_2O_3 has been investigated and was found to proceed via the intermediate phases $Ca_3Al_2O_6$ and $Ca_{12}Al_{14}O_{33}$.[5] One major disadvantage of the ceramic route is that the temperatures involved lead to a small surface area which is unsuitable for catalysis applications.

A number of solution based routes have been used to prepare high surface area spinel oxides for use as catalysts and catalyst supports. Sol-gel, coprecipitation and wet mixing have been used to prepare $ZnAl_2O_4$ from aluminium alkoxide and

zinc nitrate.[28] A sol-gel route using mixtures of aluminium and aluminium alkoxides in the presence of acetic acid[29] or isopropanol[30] has been used to prepare $MgAl_2O_4$. A mixture of nickel nitrate and aluminium nitrate in the presence of NH_4OH is reported to yield $NiAl_2O_4$ after calcining at 300 °C.[14] A hydrothermal route was used to prepare nanocrystalline $ZnAl_2O_4$ from aluminium hydroxide, basic aluminium nitrate and zinc acetate.[4,11,15] Sonochemical methods have also been employed to produce nanosized $NiAl_2O_4$ particles using nickel nitrate, aluminium nitrate and urea as precursors.[2] Nanoparticulate $MgAl_2O_4$ was prepared, however a microemulsion technique was used.[31]

The single-source precursor routes, which have been used in the preparation of spinel oxides, typically use lower temperatures than dual-source routes. Lower temperatures may lead to the formation of nanocrystalline and nanoparticulate materials in addition to materials with a high surface area. Most single-source precursor routes use a mixed-metal alkoxide of the type $[M\{Al(OR)_4\}_2]$ (where M = Ca, Mg, Ni, Zn R = various) often in a sol-gel or modified sol-gel reaction. Mixed-metal alkoxides may act as precursors in sol-gel reactions used to prepare $MgAl_2O_4$,[21,32] $NiAl_2O_4$[27] and $ZnAl_2O_4$.[9] A microemulsion mediated sol-gel route has been used to prepare nanoparticulate $CoAl_2O_4$.[33] An alternative route used to prepare $MgAl_2O_4$ is the decomposition of $[Mg\{Al(OBu)_4\}_2]$ in supercritical ethanol.[34]

4.1.3 Preparation of thin films by dual-source routes

Thin films of $MgAl_2O_4$ have been prepared by conventional CVD techniques using $MgCl_2$, Al, HCl, H_2 and CO_2.[35] However, high temperatures were required for volatilisation of the precursors and a substrate temperature of 900 °C. Controlling the stoichiometry of the films was found to be a serious problem with this system. A similar system using $MgCl_2$, $AlCl_3$, CO_2, H_2, transported in dinitrogen carrier gas, has also been used to deposit films of $MgAl_2O_4$ using a substrate temperature of 980 °C. This process is shown in Eq. 4.1.[20]

$$MgCl_2 + 2AlCl_3 + 4CO_2 + 4H_2 \longrightarrow MgAl_2O_4 + 4CO + 8HCl \quad \textbf{(4.1)}$$

Thin films of $MgAl_2O_4$ have been prepared by dual-source CVD using $[Mg\{Al(O^iPr)_4\}_2]$ (**1**) with a 3:1 oxygen/argon carrier gas and deposition temperatures between 500 and 1000 °C.[36] Combustion CVD was used to prepare thin films of $MgAl_2O_4$ and $NiAl_2O_4$ from $[Al(acac)_2]$ with either magnesium napthenate or $[Ni(acac)_2]$.[37,38] Other vapour phase techniques including electron-beam PVD have been employed to prepare thin films of spinel oxides.[39]

Thin films of $ZnAl_2O_4$ can be prepared by a sol-gel technique in which a solution is spin coated onto the substrate.[40] Using this route, crack free, dense films were produced when an annealing temperature of 700 °C was used.

Mixed-metal alkoxides have also been used in CVD as dual-source precursors for complex mixed-metal oxide systems. For example, $Mg[Nb(OEt)_6]_2$ (**2**) has been reacted with $[Pb(thd)_2]$ (thd = 2,26,6-tetramethylheptane-3,5,-dionate) to prepare films of $Pb(Mg_{0.33}Nb_{0.66})O_3$.[41]

4.1.4 Preparation of thin films by single-source routes

Thin films of $MgAl_2O_4$ have been grown from the single-source precursor $[Mg\{Al(O^iPr)_4\}_2]$ (**1**) at substrate temperatures as low as 300 °C, which is significantly lower than the temperatures used in conventional dual-source CVD (typically 1000 °C), as discussed in section 4.1.3.[17,42] Deposition of $MgAl_2O_4$ using **1** was, however, not straightforward due to oligomerization into less volatile forms such as $[Mg\{Al(O^iPr)_4\}_2]_2$ (**3**) and $[Mg_3Al_3(^iOPr)_{13}]$ (**4**).[43] This was overcome either by dissolving the precursor in a solvent[17] or ensuring the distance between the precursor and the substrate was at a minimum.[42] The precursor $[Mg\{Al(O^tBu)_4\}_2]$ (**5**) was more stable with respect to oligomerization but had a vapour pressure which was too low for practical applications.[44] In an attempt to produce carbon free $MgAl_2O_4$ thin films at low temperatures, the precursors $[Mg\{(\mu\text{-}O^iPr)_2AlMe_2\}_2]$ (**6**) and $[Mg\{(\mu\text{-}O^tBu)_2AlMe_2\}_2]$ (**7**) were prepared.[44,45] Both **6** and **7** have been used to deposit carbon free films at substrate temperatures between 270 and 600 °C. The absence of carbon contamination, despite the alkyl groups directly bonded to the aluminium, occurs because of the β-hydrogen elimination decomposition pathway.

The presence of an equal number of acidic -OR (where R = ^{i}Pr, ^{t}Bu) and basic -Me substituents leads to clean decomposition of **6** and **7**, as shown in Equations 4.2 and 4.3 respectively.

$$[Mg\{(\mu\text{-}O^{i}Pr)_2AlMe_2\}_2] \longrightarrow MgAl_2O_4 + 4CH_4 + 4H_2C{=}CH(CH_3) \quad \textbf{(4.2)}$$

$$[Mg\{(\mu\text{-}O^{t}Bu)_2AlMe_2\}_2] \longrightarrow MgAl_2O_4 + 4CH_4 + 4H_2C{=}C(CH_3)_2 \quad \textbf{(4.3)}$$

High purity carbon free films have also been obtained from $[Mg\{(\mu\text{-}O^{t}Bu)_2AlH_2\}_2]$ (**8**) at a substrate temperature of 450 °C.[46,47] The *in situ* mass spectroscopic analysis of the exhaust gases from the CVD experiment, using the deuterated compound $[Mg\{(\mu\text{-}O^{t}Bu)_2AlD_2\}_2]$ (**9**), was used to investigate the decomposition route. The mechanism was proposed to occur via β-hydrogen elimination, as shown in Eq. 4.4.

$$[Mg\{(\mu\text{-}O^{t}Bu)_2AlD_2\}_2] \longrightarrow MgAl_2O_4 + 4HD + 4H_2C{=}C(CH_3)_2 \quad \textbf{(4.4)}$$

The use of compound **9** gave an insight into the mechanism of the decomposition of **8**. It was noted that when **9** decomposes HD rather than H_2 is formed almost exclusively, which can only be explained if one of the hydrogen atoms comes from a *tert*-butyl group. Based on this, the reaction mechanism shown in Figure 4.2, was suggested as the major decomposition route. However, it was noted that other decomposition pathways, for example involving radicals, could not be ruled out.

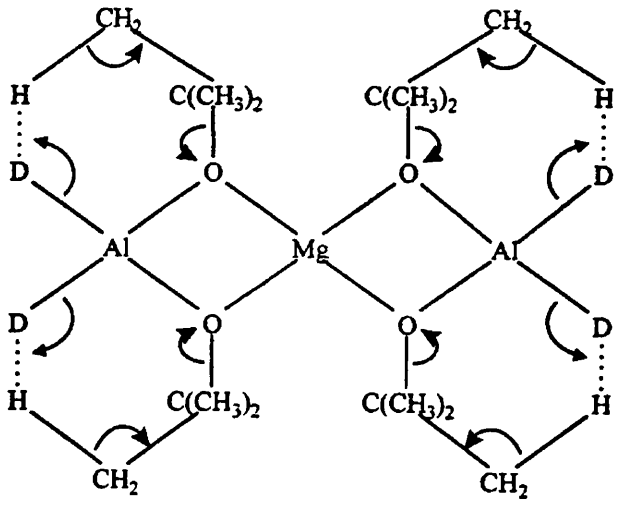

Figure 4.2 The proposed decomposition mechanism of $[Mg\{(\mu\text{-}O^tBu)_2AlH_2\}_2]$ (9)[46]

4.1.5 Mixed-metal alkoxides

In this project, the preparation of mixed-metal alkoxides and thiolates as single-source precursors to spinel oxides and sulfides have been investigated. In this section, the synthesis of mixed-metal alkoxides, reported in the literature, is discussed. There have been two comprehensive reviews on the subject which were published in 1994[48] and 1998.[49]

The magnesium aluminium alkoxide, $[Mg\{Al(O^iPr)_4\}_2]$ (**1**), has been prepared by refluxing a 1:2 molar ratio of Mg and $[Al(O^iPr)_3]$ in ^iPrOH as shown in Eq. 4.5.[50]

$$2\ Mg + 4\ [Al(O^iPr)_3] \xrightarrow[reflux]{^iPrOH} 2\ [Mg\{Al(O^iPr)_4\}_2] \quad (\mathbf{4.5})$$

Mass spectroscopy studies[43] have indicated that **1** is in equilibrium with the dimer $[Mg\{Al(O^iPr)_4\}_2]_2$ (**3**), as shown in Eq. 4.6.

$$2[Mg\{Al(O^iPr)_4\}_2] \rightleftharpoons [Mg\{Al(O^iPr)_4\}_2]_2 \quad (\mathbf{4.6})$$

The structure of **1**, in the form of an adduct with 2 ^{i}PrOH molecules, has been determined and is shown in Figure 4.3.[51] The structure was found to consist of a central magnesium connected to each of the aluminium atoms by two bridging O^{i}Pr groups with two further terminal O^{i}Pr groups attached.

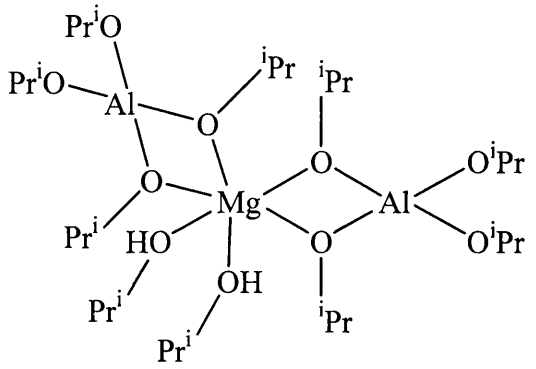

Figure 4.3 Structure of [Mg{Al(O^{i}Pr)$_4$}$_2$].2^{i}PrOH (1)[51]

The reaction of **1** with higher alcohols, e.g. ^{t}BuOH or Me$_2$EtCOH, results in the isolation of [Mg{Al(O^{i}Pr)$_3$(O^{t}Bu)}$_2$] (**10**) and [Mg{Al(O^{i}Pr)$_3$(OCMe$_2$Et)}$_2$] (**11**) respectively.[50] The mixed-metal alkoxides [Mg{Al(OR)$_4$}$_2$] (where R = Me (**12**),[52] Et (**13**),[53] ^{n}Bu (**14**),[53] ^{sec}Bu (**15**),[54] ^{t}Bu (**16**),[44,45] Ph (**17**)[54]) have also been prepared by similar synthetic routes to those employed for **1**. The complexes, which have been structurally characterised, have been found to have similar structures to **1**.

Complexes of the type [Mg{(μ-OR)$_2$AlMe$_2$}$_2$] are well known organoaluminium complexes.[55] The precursors discussed in section 4.1.4, [Mg{(μ-OR)$_2$AlMe$_2$}$_2$] (where R = ^{i}Pr (**6**), ^{t}Bu (**7**)), were prepared by the reaction of [Me$_2$AlOR], [MOR] (M = Li, Na, K) and [MgCl$_2$] according to Eq. 4.7.[44,45]

$$2\,[Me_2AlOR] + 2\,[MOR] + [MgCl_2] \longrightarrow [Mg\{(\mu\text{-}OR)_2AlMe_2\}_2] + MCl \quad (\mathbf{4.7})$$

The structure of **6** has been determined (see Figure 4.4) and was found to be similar to the structure of **1** but with Me groups in place of the terminal O^{i}Pr groups and no coordinated alcohols.

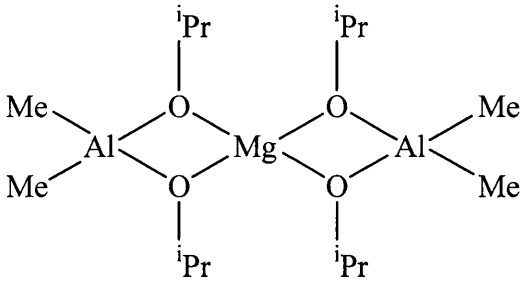

Figure 4.4 Structure of $[Mg\{(\mu\text{-}O^iPr)_2AlMe_2\}_2]$ (6)[55]

More recently, $[Mg\{(\mu\text{-}O^tBu)_2AlH_2\}_2]$ (**8**), which was successfully used as a precursor to $MgAl_2O_4$ (see section 4.1.4), has been prepared from the reaction of ^tBuOH, $[LiAlH_4]$ and $[MgCl_2]$ in a two step synthesis, according to Equations 4.8 and 4.9.[46]

$$4\ [LiAlH_4] + 8\ ^tBuOH \longrightarrow [Li(O^tBu)_2AlH_2]_4 + 8\ H_2 \quad \textbf{(4.8)}$$

$$[Li(O^tBu)_2AlH_2]_4 + 2\ [MgCl_2] \xrightarrow[\text{reflux}]{\text{ether}} 2\ [Mg\{(\mu\text{-}O^tBu)_2AlH_2\}_2] + 4\ LiCl \quad \textbf{(4.9)}$$

The structure of **8** has also been determined and was found to be similar to that of **6**, except that the terminal Me groups are replaced by H atoms (Figure 4.5).

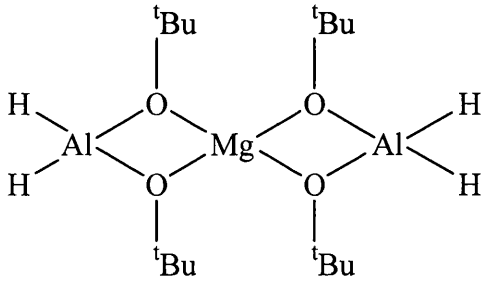

Figure 4.5 Structure of $[Mg\{(\mu\text{-}O^tBu)_2AlH_2\}_2]$ (8)[46]

The complex $[Ni\{Al(O^iPr)_4\}_2]$ (**18**) was prepared from the reaction of $[NiCl_2]$ with $[KAl(O^iPr)_4]$, as shown in Eq. 4.10.[56]

$$[NiCl_2] + 2\ [KAl(O^iPr)_4] \longrightarrow [Ni\{Al(O^iPr)_4\}_2] + 2\ KCl \quad \textbf{(4.10)}$$

Compound **18** undergoes alcoholysis reactions with various alcohols.[57] The complexes $[Ni\{Al(OR)_4\}_2]$ (where R = Me (**19**), Et (**20**), CH_2CF_3 (**21**), CH_2CCl_3 (**22**), Bu (**23**), $C(CH_2Cl)_2$ (**24**)) were formed when **18** is reacted with an excess of the appropriate alcohol. When **18** was reacted with an excess of ^tBuOH the mixed alkoxide $[Ni\{Al(O^iPr)(O^tBu)_3\}_2]$ (**25**) was formed. Spectroscopic investigations suggested that the Ni atom is in an octahedral geometry. As the R group increases in bulk an increasing proportion of tetrahedral nickel species are in equilibrium with the octahedral forms. It was suggested that the $[Al(OR)_4]^-$ anion may act as a tridentate ligand forming octahedral as well as tetrahedral Ni geometries, as shown in Figure 4.6.

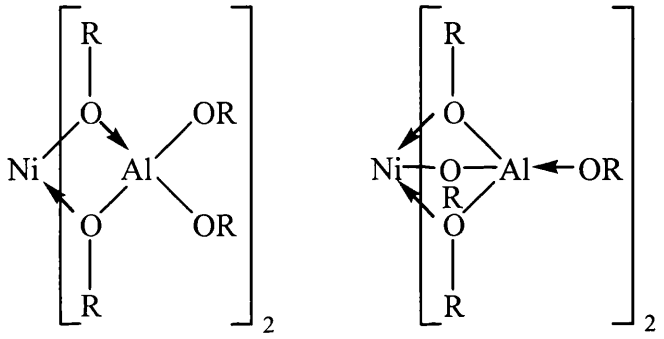

Figure 4.6 Tetrahedral and octahedral co-ordination of the Ni[57]

Recently, the structure of **18** has been determined and it was found that the Ni was octahedral with two ^iPrOH molecules co-ordinated to the Ni, as shown in Figure 4.7.[33]

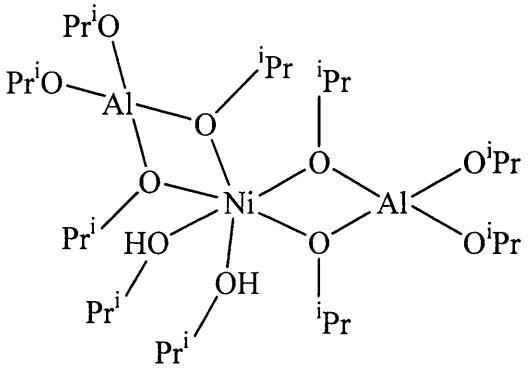

Figure 4.7 Structure of $[Ni\{Al(O^iPr)_4\}_2]$ (18)

The zinc containing complex $[Zn\{Al(O^iPr)_4\}_2]$ (**26**) has been prepared from $[ZnCl_2]$ using a similar synthetic route to that employed for **18**, which is described above.[48,49]

4.2 Results and discussion

One of the most successful low temperature single-source precursors described previously was $[Mg\{(\mu\text{-}O^tBu)_2AlH_2\}_2]$ (**8**) (see section 2.1).[46] For the purpose of synthesising novel mixed-metal alkoxides and thiolates, it was decided to prepare hydrido-heterobimetallic chalcogenides of the type $[M\{(ER)_2AlH_2\}_2]$ (where E = O, M = Mg, Ca, Ni, Zn; E = S, M = Mg).

4.2.1 Synthesis of mixed-metal alkoxides

Hydrido-heterobimetallic alkoxides of the type $[M\{(OR)_2AlH_2\}_2]$ were prepared in a similar manner to the synthesis of **8** reported in the literature.[46] This involves a two step synthesis, in the first step $[LiAlH_4]$ is reacted with 2 equivalents of an alcohol as shown in Eq. 4.11.

$$4\,[LiAlH_4] + 8\,ROH \longrightarrow [Li(\mu\text{-}OR)_2AlH_2]_4 + 8\,H_2 \quad \textbf{(4.11)}$$

In the preparation of **8**, a tetrameric species of the type $[Li(\mu\text{-}OR)_2AlH_2]_4$ was thought to have been formed although it was not isolated. The other product is H_2, which is evolved on addition of the alcohol to $[LiAlH_4]$. In the second step $[Li(\mu\text{-}OR)_2AlH_2]_n$ reacts with the appropriate metal chloride with the formation of lithium chloride, which is the driving force for this reaction, as shown in Eq. 4.12.

$$2\,[Li(OR)_2AlH_2]_n + MCl_2 \longrightarrow n\,[M\{(OR)_2AlH_2\}_2] + LiCl \quad \textbf{(4.12)}$$

4.2.2 Synthesis of magnesium aluminium alkoxides

In an attempt to prepare novel hydrido-magnesium aluminium alkoxides the synthetic pathway described in section 4.2.1 was employed. A range of alcohols (e.g. $Me_2NCH_2CH_2OH$ and 3,5-$Me_2C_6H_3OH$) were used.

4.2.3 Synthesis of $[Mg\{(\mu\text{-}O^tBu)_2AlH_2\}_2]$ (8)

The complex $[Mg\{(\mu\text{-}O^tBu)_2AlH_2\}_2]$ (**8**) was prepared by a route similar to that reported in the literature by Veith *et al,* as described in 4.2.1.[46] The product was purified by recrystallisation from diethyl ether and colourless crystals were grown at -20 °C. As expected analytical and spectroscopic data showed the major product of the reaction to be compound **8**. However, small amounts of impurities also appear to have been formed, probably by side reactions and have not been effectively separated by recrystallisation. This is suggested by the spectroscopic data and is reinforced by the difference between the observed and calculated analytical data for **8**.

4.2.4 Spectroscopic data for $[Mg\{(\mu\text{-}O^tBu)_2AlH_2\}_2]$ (8)

The ^1H NMR of **8** shows three singlets in the region 1.33 - 1.41 ppm, which correspond to the O^tBu protons. The largest of these peaks at 1.33 ppm corresponds well with the literature value of 1.34 ppm given for the O^tBu protons in **8**.[46] The other two peaks are probably due to side products from the reaction. These peaks were not reported in the synthesis of **8** reported by Veith, but in that synthesis the product was purified by sublimation which possibly led to greater purification. These three peaks integrated in a ratio 12:2:5 which suggests that although **8** is the major product of the reaction there are significant levels of other compounds present. The AlH_2 protons were not observed in the ^1H NMR spectrum.

An infrared spectrum of **8** was taken and compared with the results published by Veith *et al.*[46] The peak at 1831 cm^{-1}, which is due to the hydride groups attached to the aluminium, corresponds well to the value published of 1809 cm^{-1}. The small difference is probably due to the different methods used in recording the infrared

spectrum. Mass spectroscopy proved useful and a peak at 373 corresponding to **8** confirms its formation. It also confirms the stability of **8** in the vapour phase, which is an important requirement for CVD precursors in order to avoid decomposition prior to the reactor chamber. The mass spectrum also gives an insight into the possible formulation of the other compounds formed in the reaction. There is a peak at 517 which corresponds to the formula $[Mg\{Al_2(O^tBu)_6H_2\}]$ and a peak at 315 corresponding to $[Mg\{Al(O^tBu)_4\}]$.

4.2.5 Reaction of $[MgCl_2]$, $[LiAlH_4]$ and 3,5-$Me_2C_6H_3OH$

The reaction between $[LiAlH_4]$ and 3,5-$Me_2C_6H_3OH$ was carried out in diethyl ether at room temperature. On addition of the alcohol, effervescence was observed immediately. The reaction was refluxed for 24 hours during which time the mixture lost its grey colour and a thick white precipitate formed. After work-up and cooling to -20 °C overnight a white powder resulted in a 15% yield. Analytical and spectroscopic data showed the powder to be $[Mg\{(OC_6H_3Me_2\text{-}3,5)_2AlH_2\}_2]$ (**27**), as shown in Eq. 4.13.

$$[MgCl_2] + 2\,[LiAlH_4] + 4\,3,5\text{-}Me_2C_6H_3OH \longrightarrow [Mg\{(OC_6H_3Me_2\text{-}3,5)_2AlH_2\}_2] \quad \textbf{(4.13)}$$

The expected product, compound **27**, was therefore isolated, although the low yield suggests that this is not the only product of the reaction. It is possible that an insoluble product was also formed which was removed by filtration along with LiCl. The decomposition of **27** without melting at a relatively low temperature (50 - 52 °C) suggests that this complex may not be stable in the vapour phase.

4.2.6 Spectroscopic data for $[Mg\{(OC_6H_3Me_2\text{-}3,5)_2AlH_2\}_2]$

The ^1H NMR spectrum of **27** shows two peaks due to the protons of the methyl groups and a multiplet of broad peaks due to the SC_6H_3 protons. This indicates that either the solution behaviour of **27** is complex or that more than one product was formed in the reaction. Two very broad singlets due to diethyl ether suggest that a dynamic process involving exchange of ether is taking place.

Crystals suitable for X-ray analysis could not be grown and so the structure of **27** is unknown. However, it is expected that the structure would be similar to **8** with the alcohol groups bridging the Mg and Al atoms with two terminal hydrides attached to each of the Al atoms.

4.2.7 Reaction of $[MgCl_2]$, $[LiAlH_4]$ and $Me_2NCH_2CH_2OH$

The reaction between $[LiAlH_4]$ and $Me_2NCH_2CH_2OH$ was carried out using the general method described in 4.2.1. After work-up, a white powder was obtained in a 81% yield. Analytical and spectroscopic data suggested that $[Mg\{Al(OCH_2CH_2NMe)_2\}_2]$ (**28**), has formed, as shown in equation 4.14.

$$[MgCl_2] + 2\,[LiAlH_4] + 4\,Me_2NCH_2CH_2OH \rightarrow [Mg\{(OCH_2CH_2NMe)_2Al\}_2] \quad \textbf{(4.14)}$$

The other species produced during this reaction would presumably include H_2 and CH_4, however these are volatile and easily removed during work up. Any [LiCl] formed during the reaction was removed by filtration. The anticipated product, $[Mg\{(OCH_2CH_2NMe_2)_2AlH_2\}_2]$ (**29**), does not appear to have been formed. It was expected that the nitrogen atom would co-ordinate to the aluminium centre. This has been observed in the related compound $[H_2M(OCH_2CH_2NMe_2)]_2$, which was isolated from the reaction of $[MH_3(NMe_3)]$ (M = Al, Ga) and $HOCH_2CH_2NMe_2$.[58,59] The formation of the Al-N bond in **28** is unusual and has not been observed previously. To ensure that **28** is indeed formed, the experiment would need to be repeated and further analysis such as low temperature ^1H NMR and X-ray crystallography carried out.

The decomposition of **28** before it melted suggests that it may not be volatile enough for use in CVD experiments. The absence of hydrogen atoms attached to the aluminium and the presence of a direct Al-N bond means that there may not be a straightforward decomposition route for **28**. This would lead to the possibility of nitrogen contamination and higher levels of carbon contamination.

4.2.8 Spectroscopic data for $[Mg\{Al(OCH_2CH_2NMe)_2\}_2]$ (28)

The ^1H NMR of **28** shows both peaks due to the OCH_2CH_2NMe group and to residual solvent molecules (ether). A broad singlet at 2.07 ppm corresponds to the protons of the CH_3 group, which is attached to the nitrogen atom. The broadness of this singlet is due to the fact that it overlaps with two peaks at 2.15 and 2.24 ppm ($OCH_2C\mathit{H}_2N$). A triplet would be expect to arise from these protons, this is not observed as one of peaks is masked by the broad singlet. A broad complex multiplet is observed between 3.33 and 3.70 ppm, which is due to the $OC\mathit{H}_2CH_2N$ protons. The chemical shifts of these peaks corresponds closely to those observed for the related complex $[H_2Al(OCH_2CH_2NMe_2)]_2$.[58] Peaks due to the presence of solvent (ether) were also observed in the ^1H NMR spectra at 0.92 and 3.28 ppm which is shifted from the expected values for free ether in $CDCl_3$ of 1.20 and 3.48 ppm. This suggests that the solvent is co-ordinated to the Mg and the sharpness of the peaks and the observance of only one set of peaks suggest that the ether molecules are co-ordinated in only one environment.

The infra-red spectrum of the compound showed the expected peaks when compared to the reported values for $[H_2Al(OCH_2CH_2NMe_2)]_2$.[58] The spectrum also showed the absence of any peaks due to Al-H which would be present if the expected complex had been prepared. These are usually found to be between 1700 - 1800 cm^{-1} and no peaks were observed in this region of the spectra. This gives further evidence that the expected product was not formed.

4.2.9 Synthesis of other mixed-metal alkoxides

In an attempt to prepare novel hydrido-metal aluminium alkoxides, $[M\{(OR)_2AlH_2\}_2]$ (where M = Ca, Zn, Ni) the synthetic pathway described in section 4.2.1 was employed.

2.2.10 Reaction of $[CaCl_2]$, $[LiAlH_4]$ and ^tBuOH

The reaction of $[LiAlH_4]$ and ^tBuOH was carried out in the same manner as that used in the preparation of **8**. The mixture was then refluxed with $[CaCl_2]$ for 24

hours. After work-up and cooling to -20 °C colourless crystals were obtained in a 9% yield. Analytical and spectroscopic data suggested that these crystals were $[Ca\{(O^tBu)_2AlH_2\}_2]$ (**30**), as shown in 4.15.

$$[CaCl_2] + 2\,[LiAlH_4] + 4\,{}^tBuOH \longrightarrow [Ca\{(O^tBu)_2AlH_2\}_2] \quad \textbf{(4.15)}$$

The anticipated product, **30**, appears to have been formed. However, as the crystals proved unsuitable for X-ray crystallography, the structure was not determined, but it would be expected that **30** would have a similar structure to **8**. The expected structure of **30** is shown in Figure 4.8.

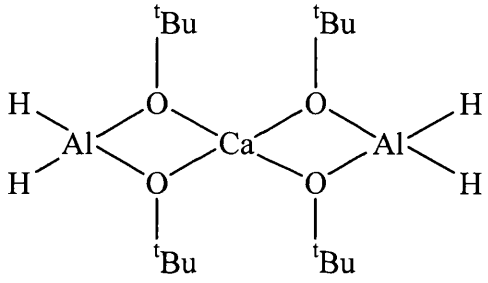

Figure 4.8 Predicted structure of $[Ca\{(O^tBu)_2AlH_2\}_2]$ (30)

The analytical data suggests that **30** is the major product from the reaction and there is reasonable agreement between the calculated and observed results. The ^1H NMR of **30** contains several peaks in the region 1.26 - 1.38 ppm. This indicates that the solution behaviour of **30** may be complex with a number of isomers present and so several ^{t}BuO environments. This does not correspond with the solution behaviour of **8** which would be expected to be similar to that of **30**. In the ^1H NMR of **8** published by Veith *et al*, only one ^{t}BuO environment was observed. Another explanation is that more than one product may be formed as observed in the synthesis of **8** (see section 4.2.4). This may also explain the small discrepancy in the analytical data.

4.2.11 Reaction of [$ZnCl_2$], [$LiAlH_4$] and ^tBuOH

This reaction was carried out in a similar manner to the method used to prepare **30** which is described in section 4.2.9. Colourless crystals were obtained in poor yield. The analytical data suggests that impure [$Zn\{Al(O^tBu)_4\}_2$] may have been formed although the infra-red spectrum shows a peak (1867 cm^{-1}) which may be due to Al-H bonds. Therefore the product could not be identified due to the low yield. The reaction would need to be repeated and attempts made to isolate a pure product in order to understand what is formed during the reaction.

4.2.12 Reaction of [$NiCl_2$], [$LiAlH_4$] and ^tBuOH

The addition of diethyl ether to a mixture of [$NiCl_2$] and [$LiAlH_4$] resulted in the formation of a black precipitate and evolution of a colourless gas. Similar decomposition also occurred if a solution of [$NiCl_2$] was added once the [$LiAlH_4$] had reacted with the alcohol. It has been suggested that in solution [$LiAlH_4$] reacts with halides of metals whose electronegativity is higher than aluminium. The order in which the reaction was carried out did not appear to have an effect on is decomposition. The ^1H NMR of the product obtained by the second method showed only the presence of free ^tBuOH.

4.2.13 Synthesis of magnesium aluminium thiolates

In an attempt to prepare novel hydrido-magnesium aluminium thiolates the synthetic pathway described in section 4.2.1 was employed.

4.2.14 Reaction of [$MgCl_2$], [$LiAlH_4$] and ^tBuSH

The reaction between [$LiAlH_4$] and ^tBuSH was carried out in diethyl ether at room temperature and the product reacted *in situ* with [$MgCl_2$]. A colourless gas was evolved during the first step of the reaction. Colourless crystals resulted after work-up and cooling to -20 °C. Analytical and spectroscopic data indicated that [$Mg\{(S^tBu)_2AlH_2\}_2$] (**31**) had formed, as shown in equation 4.16.

$$[MgCl_2] + 2\,[LiAlH_4] + 4\,{}^tBuSH \longrightarrow [Mg\{(S^tBu)_2AlH_2\}_2] \quad \textbf{(4.16)}$$

The ^1H NMR spectrum of **31** showed the presence of ^tBuS groups in only one environment. The ^1H NMR also shows the presence of diethyl ether, the chemical shifts showing that it is uncoordinated and is probably solvent of crystallisation which was not completely removed under vacuum.

Although the structure of **31** could not be determined by X-ray crystallography, it would be expected to be similar to that of **8**. The structure of **31** can be predicted as having two bridging thiolate groups between each of the aluminium atoms and the magnesium with the remaining four hydrides attached in a terminal fashion to the aluminium. The predicated structure of **31** is shown in Figure 4.9.

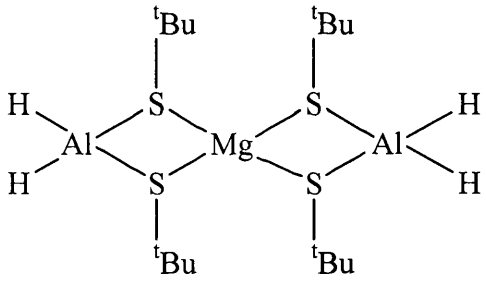

Figure 4.9 Predicted structure of $[Mg\{(S^tBu)_2AlH_2\}_2]$ (31)

4.2.15 Reaction of $[MgCl_2]$, $[LiAlH_4]$ and 2,6-$Me_2C_6H_3SH$

The reaction of $[MgCl_2]$, $[LiAlH_4]$ and 2,6-$Me_2C_6H_3SH$ was carried out using the method described in 4.2.1. After work-up and standing at room temperature for several days a white solid was obtained in 72% yield. Analytical and spectroscopic data showed that $[Mg\{(SC_6H_3Me_2\text{-}2,6)_2AlH_2\}_2]$ (**32**) had been formed cleanly. The ^1H NMR spectrum of **32** shows two sets of peaks due to the methyl groups and a multiplet arising from the aryl protons. This suggests that the 2 $Me_2C_6H_3S$ groups are inequivalent or that the methyl groups are inequivalent. This suggests that the structure of **32** may be different to **8**. Alternativly, the two sets of peaks may be due

to complex solution behaviour. The close match of the expected and observed analytical data suggests however that **32** was found cleanly.

4.3 Decomposition studies

4.3.1 Thermal gravimetric analysis

Initial investigations into the suitability of compounds **8**, **27**, **28**, **30** and **31** as single-source precursors to mixed-metal oxides or thiolates involved the TGA of some of the compounds described above.

4.3.2 Decomposition properties of $[Mg\{(O^tBu)_2AlH_2\}_2]$ (8)

The TGA of **8** was recorded and shows two weight losses, the first between 100 - 200 °C (16%) and a second from 200 - 400 °C (61%). The second weight loss corresponds well with the calculated total weight loss (62%) for decomposition to $MgAl_2O_4$. The first weight loss may be due to loss of solvent from the sample or vaporisation of a small amount of the sample. This one clean decomposition step corresponds with the concerted mechanism suggested by Veith in which both H_2 and butene are lost in one step.[46] However, if the loss of H_2 occurred in a different temperature range it may not be observed in the TGA as the percentage weight loss would be small (*ca.* 2% which is about the same as the error in this technique).

4.3.3 Decomposition properties of $[Mg\{(OC_6H_3Me_2\text{-}3,5)_2AlH_2\}_2]$ (27)

The decomposition properties of **27** were determined by carrying out a TGA, the results of which are shown in Figure 4.10.

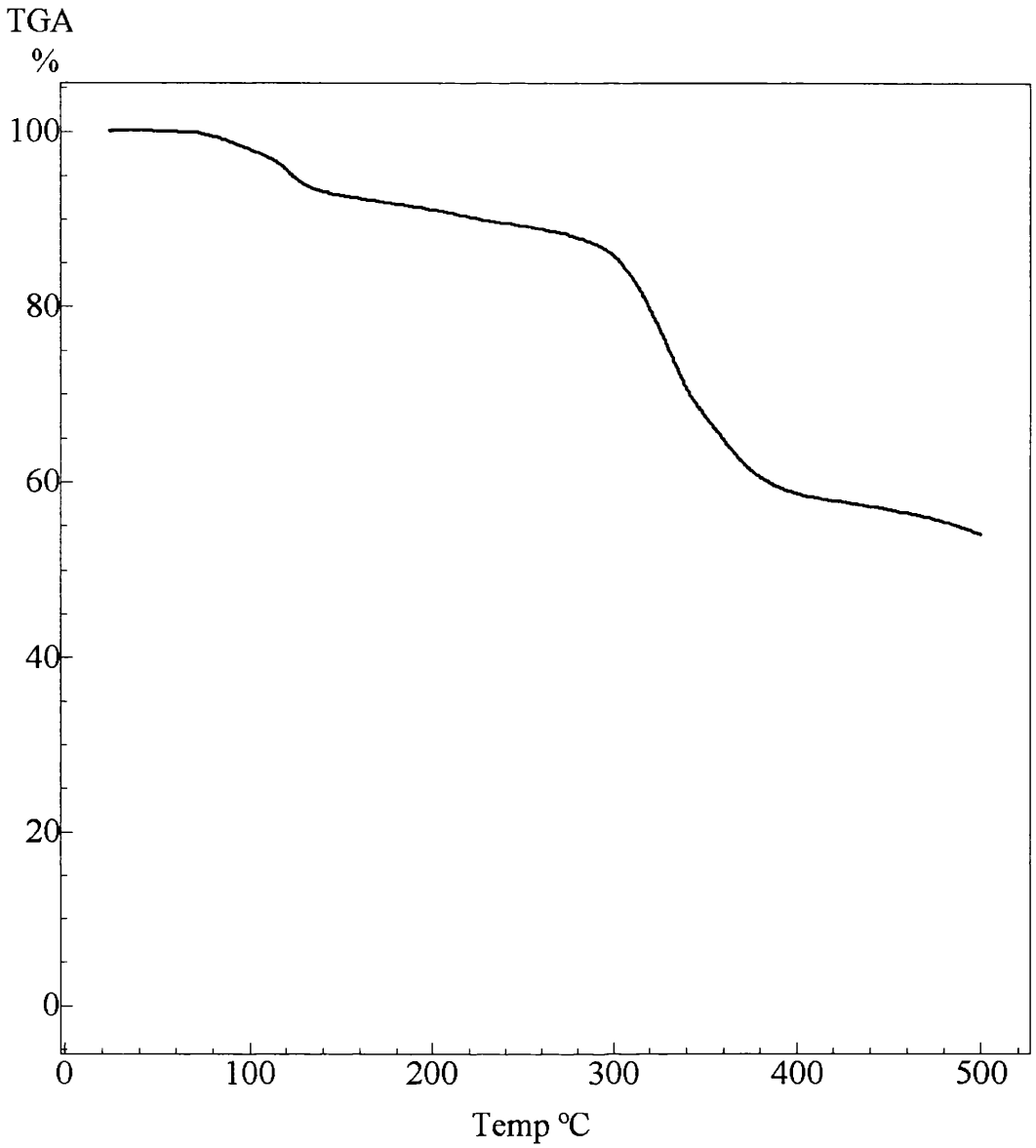

Figure 4.10 TGA of $[Mg\{(OC_6H_3Me_2\text{-}3,5)_2AlH_2\}_2]$ (27)

The TGA of **27** shows a total weight loss of 44% which indicates that complete decomposition to $MgAl_2O_4$ has not occurred (calculated 75%). This may be due to the inability of the $OC_6H_3Me_2$ group to undergo β-hydrogen elimination. Vieth proposed that the O^tBu group is eliminated via β-hydrogen elimination during the decomposition of $[Mg\{(O^tBu)_2AlH_2\}_2]$. Decomposition may occur at higher temperatures, however, the TGA experiment was limited to 500 °C. This suggests that groups which cannot undergo β-hydrogen elimination may make poor leaving groups in heterobimetallic alkoxides and thiolates.

4.3.4 Decomposition properties of $[Mg\{Al(OCH_2CH_2NMe)_2]$ (28)

A TGA of **28** was carried out in order to determine its decomposition properties. A small weight loss of 6% was observed between 120 and 260 °C which is probably due to loss of solvent. A second weight loss of 63% was observed between 260 and 420 °C which suggests complete decomposition to $MgAl_2O_4$ (calculated 62%).

4.3.5 Decomposition properties of $[Ca\{(O^tBu)_2AlH_2\}_2]$ (30)

The decomposition properties of **30** were determined by TGA, the results of which are shown in Figure 4.11. The TGA of **30** shows two weight losses, the first between 80 and 140 °C is 7% and is probably due to loss of solvent. The second weight loss of 58% occurs between 200 and 400 °C. This indicates that complete decomposition to form $CaAl_2O_4$ may have occurred. The mechanism for this decomposition is probably similar to compound **8** involving β-hydrogen elimination from the O^tBu groups.

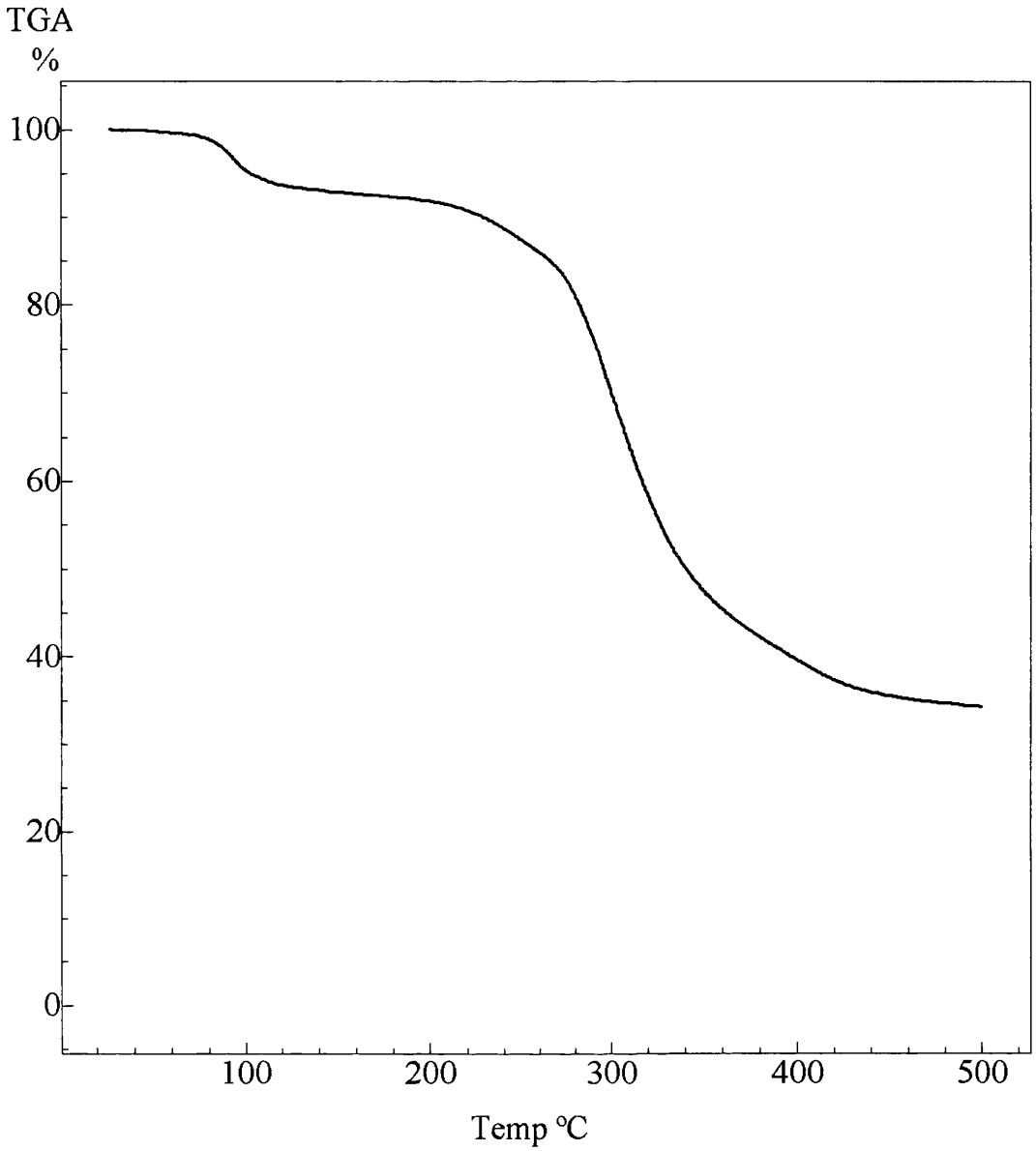

Figure 4.11 TGA of [Ca{(O^{t}Bu)$_2$AlH$_2$}$_2$] (30)

4.3.6 Decomposition properties of [Mg{(S^{t}Bu)$_2$AlH$_2$}$_2$] (31)

The decomposition properties of **31** were determined by TGA. The first weight loss (11%), which occurs between 30 and 140 °C is probably due to loss of solvent from the material. The total of the remaining weight losses, are 55% occurring in the temperature range 150 - 500 °C. This indicates complete decomposition to $MgAl_2S_4$ has occurred, which is calculated to involve a weight loss of 53%. Three weight losses are observed in this temperature region, which suggest,

that the decomposition mechanism may not be as straight forward as that proposed for **8**.

4.3.7 Vapour-phase thin-film studies using $[Mg\{(OC_6H_3Me_2\text{-}3,5)_2AlH_2\}_2]$ (27)

To study the effectiveness of hydride containing hetero-bimetallic alkoxides, other than $[Mg\{(O^tBu)_2AlH_2\}_2]$, as single-source precursors to thin films of $MgAl_2O_4$ a tube furnace reaction was carried out using $[Mg\{(OC_6H_3Me_2)_2AlH_2\}_2]$ (**27**). This compound was chosen to assess whether its decomposition properties would be different when used in a vapour phase reaction as opposed to those suggested by TGA. A very thin white film was deposited on the glass slides and the walls of the tube at the entrance to the furnace, however most of the precursor decomposed without being transported. EDAX did not detect the film and showed only peaks which were due to the underlying glass substrate. By SEM the film was found to be very particulate and rubbing with a piece of tissue easily removed the film. This indicates that although a very thin $MgAl_2O_4$ film may have been prepared, **27** is not an effective single-source precursor to thin films of $MgAl_2O_4$ by vapour-phase routes. This is probably because of its thermal instability and lack of clean decomposition routes. However, more detail studies in which the substrate temperature and precursor flow rates were varied would need to be carried out. Due to the instability of the film prepared from an aluminium thiolate and the difficulties this caused with analysis, the formation of thin films using $[Mg\{(S^tBu)_2AlH_2\}_2]$ was not attempted.

4.4 Experimental

4.4.1 Preparation of $[Mg\{(\mu\text{-}O^tBu)_2AlH_2\}_2]$ (8)

A solution of ^{t}BuOH (1.48 g, 20 mmol) in diethyl ether (5 cm^3) was added dropwise to a slurry of $[MgCl_2]$ (0.47 g, 5 mmol) and $[LiAlH_4]$ (0.38 g, 10 mmol) also in diethylether (15 cm^3). Vigorous effervescence was observed immediately on addition of ^{t}BuOH. The resulting grey coloured slurry was refluxed for 8 hours during which time the mixture lost some of its grey colour and a white precipitate formed. The mixture was filtered through Celite. The solvent was removed *in vacuo*

giving a white solid. Recrystallisation from diethyl ether (5 cm^3) afforded colourless crystals of **8**. Anal. Calc. for $C_{16}H_{40}O_4Al_2Mg$: C, 51.28; H, 10.76. Found C, 48.00; H, 10.68. Mass Spec. *m/z* 517 ([Mg{(μ-O^{t}Bu)$_2$Al(O^{t}Bu)H}$_2$]), 445 ([Mg{(μ-O^{t}Bu)$_2$AlH$_2$}{(μ-O^{t}Bu)$_2$Al(O^{t}Bu)H}]), 373 ([Mg{(μ-O^{t}Bu)$_2$AlH$_2$}$_2$]), 347 ([Mg{Al(O^{t}Bu)$_4$}]), 315 ([Mg(O^{t}Bu)$_4$]), 275 ([Mg{AlH(O^{t}Bu)$_3$}]), 203 ([Mg{AlH$_2$(O^{t}Bu)$_2$}]), 113, 73 (^{t}BuO), 53. ^{1}H NMR δ/ppm (C_6D_6): δ 1.33 (s, 36H, OC(C*H*$_3$)$_3$), 1.37 (s, 6H, OC(C*H*$_3$)$_3$), 1.41 (s, 15H, OC(C*H*$_3$)$_3$). IR (KBr disc, cm^{-1}): 2969 vs, 2932 m, 2906 m, 2871 m, 1831 vs, 1485 s, 1391 m, 1366 vs, 1262 vs, 1227 s, 1202 s, 1099 vs, 1051 vs, 1021 vs, 937 vs, 865 w, 799 vs, 775 w, 702 s, 664 s, 621 w, 597 w, 502 w, 492 w.

4.4.2 Preparation of [Mg{Al(OC$_6$H$_3$Me$_2$-3,5)$_2$H$_2$}$_2$] (27)

A solution of 3,5-Me$_2$C$_6$H$_3$OH (2.44 g, 20 mmol) in diethyl ether (15 cm^3) was added to a slurry of [LiAlH$_4$] (0.38 g, 10 mmol) and [MgCl$_2$] (0.47 g, 5 mmol) in diethyl ether (15 cm^3). Effervescence occurred immediately on addition of the alcohol. The mixture was refluxed for 24 hours resulting in loss of the grey colour and formation of a thick white precipitate. The mixture was filtered through Celite and reduced in volume to approximately 10 cm^3 under vacuum. Cooling to -20 °C overnight resulted in the formation of a white solid **27** (0.42 g, 15% yield), decomposed without melting 50-52 °C. ^{1}H NMR δ/ppm (CD_2Cl_2): δ 1.1 (s br, O(CH$_2$C*H*$_3$)$_2$), 2.05 (s, 3H, OC$_6$H$_3$(C*H*$_3$)$_2$), 2.13 (s, 3H, OC$_6$H$_3$(C*H*$_3$)$_2$), 3.50 (s br, O(C*H*$_2$CH$_3$)$_2$), 6.29 - 6.61 (m, 3H, OC$_6$*H*$_3$(CH$_3$)$_2$).

4.4.3 Preparation of [Mg{Al(O(CH$_2$CH$_2$)NMe)$_2$}$_2$] (28)

A grey coloured slurry was formed by mixing [LiAlH$_4$] (0.38 g, 10 mmol) and [MgCl$_2$] (0.47 g, 5 mmol) in diethyl ether (30 cm^3). Me$_2$NCH$_2$CH$_2$OH (2.0 cm^3, 20 mmol) was added dropwise and effervescence was observed immediately. The reaction mixture was refluxed for 24 hours resulting in loss the grey colour and formation of a white precipitate. After filtering through Celite the mixture was pumped down to dryness under vacuum resulting in a white powder (1.73 g, 81% yield), decomposed without melting below 230 °C. Anal. Calc. for

$C_{12}H_{28}N_4O_4Al_2Mg(OEt_2)_{0.75}$: C, 42.27; H, 8.39; N, 13.14. Found C, 42.16; H, 8.57; N, 12.56. ^{1}H NMR δ/ppm ($CDCl_3$): δ 0.92 (t, $O(CH_2CH_3)_2$), 2.07 (s, 12H, $OCH_2CH_2NCH_3$), 2.15 (s, 4H, $OCH_2CH_2OCH_3$), 2.24 (s, 4H, $OCH_2CH_2OCH_3$), 3.28 (q, $O(CH_2CH_3)_2$), 3.33 - 3.70 (m, 8H, $OCH_2CH_2NCH_3$). $^{13}C\{^1H\}$ NMR ($CDCl_3$) 14.5 ($O(CH_2CH_3)_2$), 44.7 ($OCH_2CH_2NCH_3$), 58.2 ($OCH_2CH_2NCH_3$), 61.3 ($OCH_2CH_2NCH_3$), 65.2 ($O(CH_2CH_3)_2$). IR (nujol, cm^{-1}): 2792 s, 1365 s, 1275 m, 1261 m, 1109 vs, 1032 s, 951 s, 903 m br, 804 w, 782 w, 528 w.

4.4.4 Preparation of $[Ca\{(O^tBu)_2AlH_2\}_2]$ (30)

Diethyl ether (30 cm^3) was added to a mixture of $[LiAlH_4]$ (0.38 g, 10 mmol) and $[CaCl_2]$ (0.55 g, 5 mmol) to give a pale grey slurry. ^{t}BuOH (1.48 g, 20 mmol) was then added dropwise resulting in immediate effervescence. The resulting mixture was refluxed for 24 hours and the solution lost some of its grey colour. Diethyl ether (10 cm^3) was added and the mixture was filtered through Celite and reduced under vacuum to *ca.* 5 cm^3. Cooling to -20 °C for 48 hours afforded colourless crystals of **30** (0.18 g, 9% yield). Anal. Calc. for $C_{16}H_{40}O_4Al_2Ca$: C, 49.21; H, 10.32. Found C, 48.73; H, 9.51. ^{1}H NMR δ/ppm (CD_2Cl_2): 1.15 (t, $O(CH_2CH_3)_2$), 1.26 - 1.38 (m, 36H, $OC(CH_3)_3$), 3.44 (q, $O(CH_2CH_3)_2$). $^{13}C\{^1H\}$ NMR (CD_2Cl_2): δ 33.5 ($C(CH_3)_3$). IR (nujol, cm^{-1}) 2923 vs, 2853 vs, 1627 vs br, 1261 m, 1230 m, 1206 m, 1089 m br, 1024 w br, 996 w br, 809 s, 404 w.

2.4.5 Attempted preparation of $[Zn\{(O^tBu)_2AlH_2\}_2]$

Diethyl ether (30 cm^3) was added to a mixture of $[LiAlH_4]$ (0.38 g, 10 mmol) and $[ZnCl_2]$ (0.68 g, 5 mmol). ^{t}BuOH (1.48 g, 20 mmol) was added dropwise resulting in immediate effervescence. The reaction mixture was refluxed for 24 hours. After filtering through Celite the solution was pumped down to dryness under vacuum resulting in a white oil. This oil was dissolved in hexane giving a colourless solution and a white suspension. The mixture was filtered through Celite and the solution reduced to *ca.* 5 cm^3 under vacuum. Cooling to -20 °C for several days afforded colourless crystals (0.127 g). Found: C, 54.25; H, 9.71. IR (KBr disc, cm^{-1}):

2970 s, 1867 w br, 1655 m, 1358 s, 1261 m, 1211 s, 1182 w, 1082 s br, 1060 w, 1024 w, 907 s, 812 m, 795 w, 777 s, 704 s, 664 s, 599 m, 548 s, 488 m br.

2.4.6 Attempted preparation of $[Ni\{(O^tBu)_2AlH_2\}_2]$

Method A: $[LiAlH_4]$ (0.38 g, 10 mmol) and $[NiCl_2]$ (0.65 g, 5 mmol) were placed in a Schlenk flask together and diethyl ether (15 cm^3) was added. Immediately on addition of ether effervescence was observed and the reaction mixture turned from pale grey to black. A solution of ^tBuOH (1.48 g, 20 mmol) in diethyl ether (10 cm^3) was added dropwise and further effervescence was observed. The reaction mixture was refluxed for 8 hours and stirred at room temperature for a further 72 hours. The mixture was filtered through Celite and reduced to *ca.* 10 cm^3, cooling at -20 °C for 24 hours resulted in the formation of a grey precipitate.

Method B: A solution of ^tBuOH (1.48 g, 20 mmol) in diethyl ether (10 cm^3) was added to a slurry of $[LiAlH_4]$ (0.38 g, 10 mmol) in diethyl ether (10 cm^3). Vigorous effervescence was observed on addition of ^tBuOH and the colour of the mixture lightened. A slurry of $[NiCl_2]$ (0.65 g, 5 mmol) was added slowly to the reaction mixture and further effervescence was observed. On addition, the mixture turned dark brown in colour. The mixture was stirred at room temperature overnight and then refluxed for 5 hours. After filtering through Celite, the solvent was removed *in vacuo* affording a small amount of a white solid.

4.4.7 Preparation of $[Mg\{Al(S^tBu)_2H_2\}_2]$ (31)

A solution of ^tBuSH (2.25 cm^3, 20 mmol) in diethyl ether (10 cm^3) was added to a grey coloured slurry of $[LiAlH_4]$ (0.38 g, 10 mmol) and $[MgCl_2]$ (0.47 g, 5 mmol) in diethyl ether (15 cm^3). Vigorous effervescence was observed on addition of the thiol solution. The mixture was refluxed for 8 hours followed by stirring at room temperature for 24 hours. During this time the mixture lost some of its grey colour. After filtering through Celite the solvent was removed under vacuum giving a white solid. This was dissolved in a minimum amount of diethyl ether. Cooling to -20 °C afforded colourless crystals of **31**. Anal. Calc. $C_{16}H_{40}S_4Al_2Mg$: C, 43.77; H, 9.18.

Found C, 41.52; H, 8.74. ^{1}H NMR δ/ppm (C_6D_6): δ 1.10 (t, $O(CH_2CH_3)_2$), 1.69 (s, 36H, $C(CH_3)_3$), 3.30 (q, $O(CH_2CH_3)_2$), 4.45 (s, 4H, AlH_2). $^{13}C\{^1H\}$ NMR (C_6D_6): δ 15.4 ($O(CH_2CH_3)_2$), 36.3 ($C(CH_3)_3$), 45.6 ($O(CH_2CH_3)_2$), 65.8 ($C(CH_3)_3$.

4.3.8 Preparation of [Mg{Al($SC_6H_3Me_2$-2,6)$_2H_2$}$_2$]

2,6-$Me_2C_6H_3SH$ (2.76 g, 20 mmol) was added dropwise to a grey coloured slurry of [$LiAlH_4$] (0.38 g, 10 mmol) and [$MgCl_2$] (0.47 g, 5 mmol) in diethyl ether (15 cm^3) resulting in vigorous effervescence. The mixture was refluxed for 24 hours resulting in the formation of a white precipitate. The mixture was filtered through Celite resulting in a white emulsion. On standing overnight a colourless liquid had separated and was found in the bottom of the flask below the solvent. On mixing a white emulsion formed again. The solvent was pumped off under vacuum leaving a viscous white coloured oil which solidified over several days (2.28 g, 72% yield). Anal. Calc. For $C_{36}H_{40}S_4Al_2Mg(OEt)_{1.5}$: C, 61.48; H, 7.47. Found C, 61.07; H, 7.38. ^{1}H NMR δ/ppm (CD_2Cl_2): δ 1.14 (s br, 9H, $O(CH_2CH_3)_2$), 2.30 (s, 15 H, $SC_6H_3(CH_3)_2$), 2.35 (s, 9 H, $SC_6H_3(CH_3)_2$), 3.54 (s br, 6H, $O(CH_2CH_3)_2$), 6.90 - 6.99 (m, 12 H, $SC_6H_3(CH_3)_2$). $^{13}C\{^1H\}$ NMR (CD_2Cl_2): δ 14.7 (s, $O(CH_2CH_3)_2$), 24.0 (s, $SC_6H_3(CH_3)_2$), 66.3 (s, $O(CH_2CH_3)_2$), 125.2 (s, *m*-$C_6H_3(CH_3)_2$), 127.4 *ipso*-(s, $C_6H_3(CH_3)_2$), 135.7 (s, *p*-$C_6H_3(CH_3)_2$), 142.8 (s, o-$C_6H_3(CH_3)_2$).

4.5 References

1. Gleizes A., *Chem. Vap. Deposition,* 2000, **6**, 155.
2. P. Jeevanandam, Y. Koltypin & A. Gedanken, *Mater. Sci. Eng.,* 2002, **B90**, 125.
3. J. Merikhi, H. O. Jungk & C. Feldmann, *J. Mater. Chem.,* 2000, **10**, 1311.
4. J. Wrzyszcz, M. Zawadzki, J. Trawczyński, H. Grabowska & W. Miśta, *Appl. Catal. A: Gen.,* 2001, **210**, 263.
5. B. M. Mohamed & J. H. Sharp, *J. Mater. Chem.,* 1997, **7**, 1595.
6. G. Mattogno, G. Righini, G. Montesperelli & E. Traversa, *J. Mater. Res.,* 1994, **9**, 1426.
7. N. N. Greenwood & A. Earnshaw, Chemistry of the Elements, 1995.

8. F. A. Cotton & G. Wilkinson, Advanced Inorganic Chemistry, 1988.
9. C. O. Areán, B. S. Sintes, G. T. Palomino, C. M. Carbonell, E. E. Platero & J. B. P. Soto, *Microporous Materials,* 1997, **8**, 187.
10. R. Revel, D. Bazin, E. Elkaim, Y. Kihn & H. Dexpert, *J. Phys. Chem. B,* 2000, **104**, 9828.
11. H. Grabowska, W. Miśta, J. Trawczyński, J. Wrzyszcz & M. Zawadzki, *Appl. Catal. A: Gen.,* 2001, **220**, 207.
12. C. Chauvin, J. Jaussey, J. C. Lavalley, H. Idriss, J. P. Hidermann, A. Kiennemann, P. Chaumette & P. Coutry, *J. Catal.,* 1990, **121**, 56.
13. L. Kou & J. R. Selman, *J. Appl. Electrochem.,* 2000, **30**, 1433.
14. Y. Cesteros, P. Salagre, F. Medina & J. E. Sueiras, *Chem. Mater.,* 2000, **12**, 331.
15. M. Zawadzki, W. Miśta & L. Kepiński, *Vacuum,* 2001, **63**, 291.
16. Y. Lu, Y. Liu & S. Shen, *J. Catal.*, 1998, **177**, 386.
17. J. Zhang, G. T. Stauf, R. Gardiner, P. Van Buskirk & J. Steinbeck, *J. Mater. Res.,* 1994, **9**, 1333.
18. A. Kuramata, K. Horino, K. Domen K. Shinohara & T. Tanahashi, *Appl. Phys. Lett.,* 1995, **67**, 2521.
19. T. George, E. Jacobsohn, W. T. Pike, P. C. Chein, M. A. Khan, J. W. Yang & S. Mahajan, *Appl. Phys. Lett.,*1996, **68**, 337.
20. S. Matsubara, S. Miura, Y. Miyasaka & N. Shohata, *J. Appl. Phys.,* 1989, **66**, 5826.
21. K. B. Pflanz, R. Riedel & H. Chmiel, *Adv. Mater.,* 1992, **4**, 662.
22. B. M. Mohamed & J. H. Sharp, *J. Mater. Chem.,* 1997, **7**, 1595.
23. S. Tanaka, I. Ozaki, T. Kunimoto, K. Ohmi & H. Kobayashi, *J. Lumin.,* 2000, **87-89**, 1250.
24. J. Hölsa, H. Jungner, M. Lastusaari & J. Niittykoski, *J. Alloys Compd.*, 2001, **323-324**, 326.
25. D. Jia, R. S. Meltzer, W. M. Yen, W. Jia & X. Wang, *Appl. Phys. Lett.,* 2002, **80**, 1535.
26. H. Matsui, C. N. Xu & H. Tateyama, *Appl. Phys. Lett.,* 2001, **78**, 1068.
27. C. O. Areán, M. P. Mentruit, A. J. L. López & J. B. Parra, *Colloids & Surfaces A,* 2001, **180**, 253.

28. M. A. Valenzula, P. Bosch, G. Aguliar-Rios, A. Montoya & I. Schifter, *J. Sol. Gel. Sci. Technol.,* 1997, **8**, 107.

29. S. Rezgui & B. C. Gates, *J. Non Crys. Sol.*, 1997, **210**, 287.

30. R. Vacassy, C. Guizard, A. Larbot & L. Cot, *J. Mater. Sci. Lett.,* 1996, **15**, 2109.

31. R. Winter, M. Quinten, A. Dierstein, R. Hempelmann, A. Altherr & M. Veith, *J. Appl. Cryst.,* 2000, **33**, 507.

32. M. Sugiura & O. Kamigaito, *Yogyo. Kyokaishi,* 1984, **92**, 605.

33. F. Meyer, R. Hempelmann, S. Mathur & M. Veith, *J. Mater. Chem.,* 1999, **9**, 1755.

34. M. Barj, J. F. Bocquet, K. Chhor & C. Pommier, *J. Mater. Sci.,* 1992, **27**, 2187.

35. M. Ihara, Y. Arimoto, M. Jifuku, T. Kimura& S. Kodama, *J. Electrochem. Soc.,* 1982, **129**, 2569.

36. G. Stauf, P. Van Buskirk, P. Kirlin & W. Kosar , *MRS Symp. Proc.,* 1993, **299**, 291.

37. D. W. Stollberg, W. B. Carter & J. M. Hampikian, *Surf. Coat. Technol.,* 1997, **94-95**, 137.

38. J. M. Hampikian & W. B. Carter, *Mater. Sci. Eng,* 1999, **A267**, 7.

39. U. Leushake, T. Krell, U. Schulz, M. Peters, W. A. Kaysser & B. H. Rabin, *Surf. Coat. Technol.,* 1997, **94-95**, 131.

40. A. R. Phani, M. Passacantando & S. Santucci, *Mater. Chem. Phys.,* 2001, **68**, 66.

41. A. Jones, H. Davies, T. Leedham, P. Wright, M. Crosbie, A. Steiner, J. Bickley, P. O'Brien, A. White, D. Williams, *J. Mater. Chem.,* 2001, **11**, 544.

42. R. E. Rocheleau, Z. Zhang, J. W. Gilje & J. A. Meese-Marktscheffel, *Chem. Mater.,* 1994, **6**, 1615.

43. J. Meese-Marktscheffel, R. Fukuchi, M. Kido, G. Tachibana, C. Jensen & J. Gilje, *Chem. Mater.,* 1993, **5**, 755.

44. W. Koh, S. -J. Ku & Y. Kim, *Chem. Vap. Deposition,* 1998, **4**, 192.

45. J. H. Boo, S. -B. Lee, S. -J. Ku, W. Koh, C. Kim, K. -S. Yu & Y. Kim, *Appl. Surf. Sci.,* 2001, **169-170**, 581.

46. M. Veith, A. Altherr & H. Wolfanger, *Chem. Vap. Deposition,* 1999, **5**, 87.

47. M. Veith, A. Altherr, N. Lecerf, S. MAthur, K. Valtchev & E. Fritscher, *NanoStructured Materials,* 1999, **12**, 191.

48. R. C. Mehrotra, A. Singh & S. Sogani, *Chem. Rev.,* 1994, **94**, 1643.

49. M. Veith, S. Mathur & C. Mathur, *Polyhedron,* 1998, **17**, 1005.

50. R. Mehrotra, S. Goel, A. Goel, R. King & K. Nainan, *Inorg. Chim. Acta,* 1978, **29**, 131.

51. J. Saβmannshausen, R. Riedel, K. B. Pflanz & H. Chmiel, *Z. Naturforsch.,* 1993, **48b**, 7.

52. R. Scholder & H. Protzer, *Z. Anorg. Allg. Chem.,* 1965, **340**, 23.

53. S. Govil & R. C. Mehrotra, *Synth. React. Inorg. Metal-Org. Chem.,* 1975, **5**, 267.

54. J. A. Meese-Marktscheffel, R. E. Camer & J. W. Gilje, *Polyherdron,* 1994, **13**, 1045.

55. C. -C. Chang, W. -H. Lee, T. -Y. Her, G. -H. Lee, S. -M. peng & Y. Wang, *J. Chem. Soc., Dalton Trans.,* 1994, 315.

56. J. V. Singh, N. C. Jain & R. C. Mehrotra, *Synth. React. Inorg. Metal-Org. Chem.* 1979, **9**, 79.

57. R. C. Mehrotra & J. Singh, *Can. J. Chem.,* 1984, **62**, 1003.

58. H. Nöth, A. Schlegel, B. Singaram, J. Knizek, P. Mayer & T. Seifert, *Eur. J. Inorg. Chem.,* 2001, 173.

59. S. J. Rettig, A. Storr & J. Trotter, *Can. J. Chem.,* 1975, **53**, 58.

Conclusion

The use of compounds containing a trimethyl silyl ($SiMe_3$) as single-source precursors to AlN, GaP and GaAs has been reported previously. Compounds which contain a halide and a silyl group are of interest as single-source precursors as they have the potential to decompose via the loss of a labile silyl halide. Similarly, compounds which contain and alkyl group and a silyl group have the potential to decompose via loss of a silane, however, if the alkyl group contains a β-hydrogen then decomposition involving β-hydride elimination can occur.

Previously, the single-source precursor $[Cl_2Al\{NH(SiMe_3)\}]_2$ has been used to prepare AlN at temperatures below 500 °C. The potential precursors $[Cl(Me)Al\{NH(SiMe_2H)\}]_2$ and $[Et_2Al\{N(SiMe_2H)_2\}]_n$ were prepared and the decomposition properties of the latter were investigated by TGA and vapour phase studies. The TGA suggested that $[Et_2Al\{N(SiMe_2H)_2\}]_n$ decomposed below 300 °C which is lower than the temperature required to decompose $[Cl_2Al\{NH(SiMe_3)\}]_2$. Vapour-phase experiments lead to the formation of a thick highly reflective gold coloured coating at a substrate temperature of 550 °C.

The use of silyl amides as single-source precursors to GaN has not been reported previously. The decomposition of $[X_2Ga\{NH(SiMe_2R)\}]_n$ (X = Cl, Br; R = Me, Ph), was investigated by TGA (up to 500 °C), it was found that where R = Me decomposition to $[XGaNH]_n$ occurred, as was the case for $[Cl_2Al\{NH(SiMe_3)\}]_2$, however, for R = Ph a more complex decomposition pathway appeared to be followed. Bulk pyrolysis of $[Cl_2Ga\{NH(SiMe_3)\}]_2$ was carried out at 750 °C and GaN with a mixed cubic/hexagonal structure was formed. At higher temperatures, the material formed had predominantly hexagonal character. The decomposition of $[X_3Ga\{NH(SiMe_2R)_2\}]$ (X = Cl, Br; R = Me, Ph) was investigated by TGA and bulk pyrolysis and was found to be similar. Vapour-phase thin film studies resulted in the formation of a thin film of GaN from $[Cl_3Ga\{NH(SiMe_3)_2]$ at a substrate temperature of 550 °C.

The preparation of the novel gallium silylarsenide precursor, $[Cl_2Ga\{As(SiMe_2Ph)_2\}]_n$, was carried out by the reaction of $GaCl_3$ and $As(SiMe_2Ph)_3$. The isolation of a molecular compound was of interest as in the corresponding reaction of GaX_3 and $As(SiMe_3)_3$ it is not possible to isolate a molecular species so the best of our knowledge $[Cl_2Ga\{As(SiMe_2Ph)_2\}]_n$ is the only halide containing gallium silylarsenide. This is of interest as it could be used in a single-source precursor approach to GaAs. TGA suggested that $[Cl_2Ga\{As(SiMe_2Ph)_2\}]_n$ decomposed to form GaAs below 200 °C. However, $[Cl_2Ga\{As(SiMe_2Ph)_2\}]_n$ proved to be insufficiently volatile for use in vapour-phase reactions.

The synthesis of hydrio-aluminium alkoxides and thiolates was investigated in an attempt to prepare single-source precursors to aluminium oxide or sulfide. The decomposition properties of some of the compounds produced was investigated by TGA. Vapour-phase deposition studies are carried out in order to test the potential of the aluminium alkoxides and thiolates as single-source precursors to aluminium oxide and sulfide respectively.

The reaction of $[AlH_3]$ and $^{i}PrOH$ lead to the isolation of two different aluminium alkoxide clusters both of which contained a central oxo species. The reaction of $[AlH_3\{NMe_2Et\}]$ and $^{i}PrOH$ lead to the formation of $[Al(O^{i}Pr)_3]_4$. The bulky nature of these species means that they would not be expected to be volatile enough for use in CVD. $[HAl(O^{t}Bu)_2]_2$ was formed by the reaction of $[AlH_3\{NMe_2Et\}]$ and two equivalents of $^{t}BuOH$. Vapour phase studies were carried out using $[HAl(O^{t}Bu)_2]_2$ and a thin film of Al_2O_3 was formed, whereas, the use of $[H_2Al(O^{t}Bu)]_2$ had been reported as yielding the composite material Al/Al_2O_3. The fluorinated species $[H_2Al(OC_6F_4H)(NMe_2Et)]$ was formed by the reaction of $[AlH_3\{NMe_2Et\}]$ and one equivalent of $3\text{-}HF_4C_6OH$. Fluorinated species are of particular interest as single-source precursor because of the enhanced volatility brought about by the use of a fluorinated ligand. TGA of $[H_2Al(OC_6F_4H)(NMe_2Et)]$ did not show full decomposition to Al_2O_3.

The reaction of $[AlH_3]$ and one equivalent of $^{t}BuSH$ lead to the isolation of $[HAl(S^{t}Bu)(\mu\text{-}O^{t}Bu)]_2$ which was formed as a result of hydrolysis. The reaction of

$[AlH_3\{NMe_2Et\}]$ and one equivalent of ^tBuSH resulted in the formation of $[Al(S^tBu)_3\{NMe_2Et\}]$. Vapour-phase studies using $[Al(S^tBu)_3\{NMe_2Et\}]$ were carried out, however, the thin films prepared decomposed before they could be analysed. The corresponding reactions of $[AlH_3\{NMe_2Et\}]$ and 2,6-$Me_2C_6H_3SH$ resulted in the formation of numerous products including $[Al(SC_6H_3Me_2\text{-}2,6)_3(OEt_2)]$, $[Li(OEt_2)_3][Al(SC_6H_3Me_2)_4]$ and $[Al(SC_6H_3Me_2\text{-}2,6)_3(HSC_6H_3Me_2\text{-}2,6)]$. TGA was carried out on $[Al(SC_6H_3Me_2\text{-}2,6)_3(OEt_2)]$ and suggests that Al_2S_3 has been cleanly formed.

The synthesis of precursors to mixed-metal chalcogenides, in particular $MgAl_2O_4$, $MgAl_2S_4$, $CaAl_2O_4$ and $ZnAl_2O_4$, was also investigated. This involved the synthesis of a number of mixed-metal alkoxide and thiolates of the form $[M\{H_2Al(ER)_2\}_2]$ (where M = Mg, Ca, Zn, E = O, R = various; M = Mg, E = S, R = ^tBu. The decomposition properties of $[Mg\{(O^tBu)_2AlH_2\}_2]$, which was used by Vieth as a single-source CVD precursor to $MgAl_2O_4$, were determined by TGA. This showed that decomposition occurred in one step below 400 °C, which confirms the β-hydride elimination pathway suggested by Vieth may be correct. The related compound $[Ca\{(O^tBu)_2AlH_2\}_2]$ was prepared and TGA was also carried out. This showed that weight loss to form $CaAl_2O_4$ had occurred, which may have been via a similar β-hydride elimination pathway. TGA carried out on $[Mg\{(OC_6H_3Me_2\text{-}3,5)_2AlH_2\}_2]$ shows that complete decomposition to $MgAl_2O_4$ does not occur, which may be due to the absence of a β-hydride elimination pathway by which decomposition may occur. TGA carried out on $[Mg\{(S^tBu)_2AlH_2\}_2]$ suggests that $MgAl_2S_4$ is formed below 500 °C, however, it would be expected that this material would unstable like Al_2S_3 so vapour-phase studies were not carried out.

List of Publications

Synthesis and Characterisation of a Bridging Nitrido Complex of Titanium, C.J. Carmalt, J.D. Mileham, A.J.P. White & D.J. Williams, *New J. Chem.*, 2000, **24**, 929.

Synthesis and Characterisation of Gallium Silylamides, C. J. Carmalt, J. D. Mileham, A. J. P. White, D. J. Williams & J. W. Steed, *Inorg. Chem.* 2001, **40**, 6035.

Pentanuclear alkoxyaluminium hydrides, C. J. Carmalt, J. D. Mileham, A. J. P. White & D. J. Williams, *New. J. Chem.,* 2002, **26**, 902.

Appendix

Crystal data for $[Cl_2Ga\{NH(SiMe_2Ph)]_2$

Empirical formula	$C_{16}H_{24}N_2Si_2Cl_2Ga_2$
Formula weight	581.8
Crystal colour/morphology	Clear blocks
Crystal size (mm)	0.47 x 0.42 0.20
a (Å)	12.530(1)
b (Å)	14.472(2)
c (Å)	13.457(1)
α (°)	90
β (°)	93.85(1)
γ (°)	90
V ($Å^3$)	2434.8(4)
Z	4
Crystal system	monoclinic
Space group	*C2/c*(no. 15)
Wavelength (Å)	0.71073
Density (calculated) (Mg/m^3)	1.587
Absorption coefficient (mm^{-1})	2.76
Reflections collected	2252
Independent reflections (R_{int})	2150 (0.0529)
Observed reflections [$I>4\sigma(I)$]	1722
R indices (all data)	R1 = 0.0578, wR2 = 0.0986
Final R indices [$I>4\sigma(I)$]	R1 = 0.0404, wR2 = 0.0862
Goodness-of-fit on F^2	1.029
Largest diff. peak and hole ($eÅ^{-3}$)	0.470 and -0.381

Bond lengths (Å) and angles (°) for $[Cl_2Ga\{NH(SiMe_2Ph)]_2$

Ga–N'	1.968(3)	Ga–N	1.988(4)
Ga–Cl(1)	2.1380(13)	Ga–Cl(2)	2.1540(14)
Ga–Ga'	2.8033(9)	Si–N	1.801(4)
Si–C(2)	1.852(5)	Si–C(1)	1.852(5)
Si–C(8)	1.897(3)	N–Ga'	1.968(3)
C(3)–C(4)	1.39	C(3)–C(8)	1.39
C(4)–C(5)	1.39	C(5)–C(6)	1.39
C(6)–C(7)	1.39	C(7)–C(8)	1.39
N'–Ga–N	89.74(14)	N'–Ga–Cl(1)	115.86(11)
N–Ga–Cl(1)	110.55(11)	N'–Ga–Cl(2)	110.73(11)
N–Ga–Cl(2)	114.88(11)	Cl(1)–Ga–Cl(2)	113.12(6)
N–Si–C(2)	109.5(2)	N–Si–C(1)	106.2(2)
C(2)–Si–C(1)	111.5(3)	N–Si–C(8)	108.1(2)
C(2)–Si–C(8)	109.6(2)	C(1)–Si–C(8)	111.9(2)
Si–N–Ga'	127.2(2)	Si–N–Ga	120.1(2)
Ga'–N–Ga	90.26(14)	C(4)–C(3)–C(8)	120.0
C(5)–C(4)–C(3)	120.0	C(4)–C(5)–C(6)	120.0
C(5)–C(6)–C(7)	120.0	C(6)–C(7)–C(8)	120.0
C(7)–C(8)–C(3)	120.0	C(7)–C(8)–Si	123.4(2)
C(3)–C(8)–Si	116.5(2)		

Crystal data for $[Cl_2Ga\{NH(^tBu)\}]_2$

Empirical formula	$C_8 H_{20} N_2 Cl_4 Ga_2$
Formula weight	425.50
Crystal colour/morphology	Colourless prisms
Crystal size (mm)	30 x 30 x 30
a (Å)	6.4619(10)
b (Å)	11.8491(15)
c (Å)	10.730(2)
α (°)	90.00
β (°)	96.286(13)
γ (°)	90.00
V ($Å^3$)	816.7(2)
Z	2
Crystal system	Monoclinic
Space group	P2(1)/n
Wavelength (Å)	1.54178
Density (calculated) (Mg/m^3)	1.730
Absorption coefficient (mm^{-1})	9.898
Reflections collected	1490
Independent reflections (R_{int})	1361 (0.0555)
Observed reflections [I>2sigma(I)]	1343
R indices (all data)	R1 = 0.0406, wR1 = 0.1070
Final R indices [I>2sigma(I)]	R2 = 0.0345, wR2 = 0.0928
Goodness-of-fit on F^2	1.206
Largest diff. peak and hole ($eÅ^{-3}$)	0.653 and -0.749

Bond lengths (Å) and angles (°) for $[Cl_2Ga\{NH(^tBu)]_2$

Ga-N(0A)	1.973(2)	N-C(1)	1.516(4)
Ga-N	1.977(2)	Ga(A)-N	1.973(2)
Ga-Cl(2)	2.1408(9)	C(1)-C(4)	1.518(4)
Ga-Cl(1)	2.1579(9)	C(1)-C(3)	1.524(5)
Ga-Ga	2.8695(8)	C(1)-C(2)	1.526(5)
N-Ga-N(0A)	86.82(10)	Cl(2)-Ga-Cl(1)	110.26(4)
N(0A)-Ga-Cl(2)	110.33(8)	C(1)-N-Ga(A)	125.4(2)
N-Ga-Cl(2)	118.81(8)	C(1)-N-Ga	124.3(2)
N(0A)-Ga-Cl(1)	119.44(8)	Ga(A)-N-Ga	93.18(10)
N-Ga-Cl(1)	109.89(8)	C(4)-C(1)-C(3)	110.8(3)
N(0A)-Ga-Ga(A)	43.46(7)	N-Ga-Ga(A)	43.36(7)
Cl(2)-Ga-Ga(A)	124.82(3)	Cl(1)-Ga-Ga(A)	124.91(3)
N-C(1)-C(4)	109.6(2)	N-C(1)-C(3)	107.9(3)
N-C(1)-C(2)	107.2(3)	C(4)-C(1)-C(3)	110.8(3)
C(4)-C(1)-C(2)	110.8(3)	C(3)-C(1)-C(2)	110.5(3)

Crystal data for $[MeGaCl_2]_2$

Empirical formula	$C_2H_6Cl_4Ga_2$
Formula weight	311.31
Crystal size (mm)	0.40 × 0.15 × 0.15
a (Å)	11.9989(16)
b (Å)	6.7370(11)
c (Å)	7.2181(9)
α (°)	90.00
β (°)	126.201(7)
γ (°)	90.00
V ($Å^3$)	470.8(1)
Z	2
Crystal system	Monoclinic
Space group	C2/m
Wavelength (Å)	0.71073
Density (calculated) (Mg/m^3)	2.196
Absorption coefficient (mm^{-1})	6.770
Reflections collected	2898
Independent reflections (R_{int})	585 (R_{int} = 0.045)
Observed reflections [I>2sigma(I)]	585
R indices (all data)	R1 = 0.0541; wR1 = 0.1522
Final R indices [I>2sigma(I)]	R2 = 0.0563; wR2 = 0.1540
Goodness-of-fit on F^2	1.171
Largest diff. peak and hole ($eÅ^{-3}$)	1.934 and -1.310

Bond lengths (Å) and angles (°) for $[MeGaCl_2]_2$

Ga(1)-C(1)	1.928(7)	Ga(1)-Cl(2)	2.3324(12)
Ga(1)-Cl(1)	2.1547(19)	Ga(1)-Cl(2')	2.3324(12)
C(1)-Ga(1)-Cl(1)	127.0(3)	Cl(1)-Ga(1)-Cl(2)	103.83(4)
C(1)-Ga(1)-Cl(2)	113.17(17)	Cl(1)-Ga(1)-Cl(2')	103.83(4)
C(1)-Ga(1)-Cl(2)	113.17(17)	Cl(2')-Ga(1)-Cl(2)	88.89(6)
Ga(1')-Cl(2)-Ga(1)	91.11(6)		

Crystal data for $[Cl(Me)Al\{NH(SiMe_2H)\}]_2$

Empirical formula	$C_6H_{22}N_2Si_2Cl_2Al_2$
Formula weight	303.30
Crystal colour/morphology	Colourless blocks
Crystal size (mm)	0.80 x 0.37 x 0.25
a (Å)	6.1308(7)
b (Å)	9.0541(15)
c (Å)	16.073(2)
α (°)	91.843(11)
β (°)	98.604(9)
γ (°)	99.142(11)
V ($Å^3$)	869.5(2)
Z	2
Crystal system	Triclinic
Space group	P-1
Wavelength (Å)	1.54178
Density (calculated) (Mg/m^3)	1.158
Absorption coefficient (mm^{-1})	5.465
Reflections collected	2854
Independent reflections (R_{int})	2578 (0.0163)
Observed reflections [I>2sigma(I)]	2216
R indices (all data)	R1 = 0.0553, wR1 = 0.1271
Final R indices [I>2sigma(I)]	R2 = 0.0466, wR2 = 0.1184
Goodness-of-fit on F^2	1.052
Largest diff. peak and hole ($eÅ^{-3}$)	0.411 and -0.440

Bond lengths (Å) and angles (°) for $[Cl(Me)Al\{NH(SiMe_2H)\}]_2$

	A	B
Al-N(0A)	1.920(3)	1.922(3)
Al-N	1.924(3)	1.923(3)
Al-C(1)	1.971(3)	1.932(5)
Al-Cl	2.1357(14)	2.151(2)
AlA-Al	2.737(2)	2.737(2)
N-Si	1.773(3)	1.770(3)
N-AlA	1.920(3)	1.923(3)
Si-C(3)	1.832(5)	1.848(5)
Si-C(2)	1.855(4)	1.851(5)
N-Al-N(0A)	89.22(13)	89.24(13)
N-Al-C(1A)	113.58(15)	117.6(2)
N-Al-C(1)	115.48(14)	115.9(2)
N-Al-Cl(A)	110.70(10)	106.32(11)
N-Al-Cl	107.35(11)	108.16(11)
C(1)-Al-Cl	117.08(12)	116.2(2)
N(0A)-Al-Al(A)	44.67(10)	44.63(10)
N-Al-Al(A)	44.54(9)	44.62(9)
C(1)-Al-Al(A)	125.67(12)	129.2(2)
Cl-Al-Al(A)	117.24(7)	114.60(8)
Si(A)-N(0A)-Al	126.3(2)	121.4(2)
Si-N-Al	119.1(2)	124.5(2)
Al(A)-N-Al	90.78(13)	90.76(13)
N-Si-C(3)	111.1(2)	109.0(2)
N-Si-C(2)	107.2(2)	108.4(2)
C(3)-Si-C(2)	111.6(2)	111.9(3)

Crystal data for $[(EtO)EtAl\{N(SiMe_3)_2\}]_2$

Empirical formula	$C_{20}H_{56}N_2O_2Si_4Al_2$
Formula weight	522.99
Crystal colour/morphology	Colourless plates
Crystal size (mm)	0.57 x 0.23 x 0.10
a (Å)	8.949(2)
b (Å)	9.635(4)
c (Å)	10.077(3)
α (°)	86.11(3)
β (°)	69.72(2)
γ (°)	80.38(2)
V ($Å^3$)	803.5(4)
Z	1
Crystal system	Triclinic
Space group	P-1
Wavelength (Å)	1.54178
Density (calculated) (Mg/m^3)	1.081
Absorption coefficient (mm^{-1})	2.378
Reflections collected	2520
Independent reflections (R_{int})	2348 (0.0432)
Observed reflections [I>2sigma(I)]	1846
R indices (all data)	R1 = 0.1068, wR1 = 0.2675
Final R indices [I>2sigma(I)]	R2 = 0.0852, wR2 = 0.2228
Goodness-of-fit on F^2	1.084
Largest diff. peak and hole ($eÅ^{-3}$)	0.133 and -0.729

Bond lengths (Å) and angles (°) for $[(EtO)EtAl\{N(SiMe_3)_2\}]_2$

Al-O(0A)	1.836(3)	Al-AlA	2.835(3)
Al-N	1.840(4)	Si(1)-N	1.726(5)
Al-O	1.852(3)	Si(1)-C(5)	1.861(6)
Al-C(3)	1.970(6)	Si(1)-C(6)	1.864(6)
Si(1)-C(7)	1.869(6)	Si(2)-C(8)	1.879(6)
Si(2)-N	1.749(4)	O-C(1)	1.458(6)
Si(2)-C(10)	1.857(6)	O-AlA	1.836(3)
Si(2)-C(9)	1.876(6)	C(1)-C(2)	1.503(7)
C(3)-C(4)	1.539(7)		
O-Al-N(0A)	117.5(2)	N-Al-C(3)	121.7(2)
O-Al-O(0A)	79.5(2)	O-Al-C(3)	110.3(2)
N-Al-O	111.1(2)	O(0A)-AlA-Al	39.97(10)
O(0A)-Al-C(3)	108.8(2)	N-AlA-Al	122.3(2)
O-AlA-Al	39.57(10)	C(5)-Si(1)-C(6)	105.6(3)
C(3)-Al-AlA	115.8(2)	N-Si(1)-C(7)	111.9(3)
N-Si(1)-C(5)	114.2(2)	C(5)-Si(1)-C(7)	104.7(3)
N-Si(1)-C(6)	111.0(3)	C(6)-Si(1)-C(7)	109.1(3)
N-Si(2)-C(10)	112.8(2)	C(10)-Si(2)-C(8)	104.1(3)
N-Si(2)-C(9)	111.9(2)	C(9)-Si(2)-C(8)	106.8(3)
C(10)-Si(2)-C(9)	107.9(3)	C(1)-O-AlA	131.8(3)
N-Si(2)-C(8)	112.8(2)	C(1)-O-Al	125.2(3)
AlA-O-Al	100.5(2)	Si(2)-N-Al	117.2(3)
Si(1)-N-Si(2)	117.5(2)	O-C(1)-C(2)	111.7(4)
Si(1)-N-Al	125.1(2)	C(4)-C(3)-Al	121.3(4)

Crystal data for $[Cl(Ph)Ga\{N(SiMe_2Ph)_2\}]_2$

Empirical formula	$C_{44}H_{54}N_2Si_4Cl_2Ga_2$
Formula weight	933.59
Crystal colour/morphology	Colourless needles
Crystal size (mm)	0.63 x 0.13 x 0.10
a (Å)	10.2961(10)
b (Å)	13.9703(10)
c (Å)	17.7560(12)
α (°)	73.503(5)
β (°)	83.418(7)
γ (°)	75.594(7)
V ($Å^3$)	2369.2(3)
Z	2
Crystal system	Triclinic
Space group	P-1
Wavelength (Å)	1.54178
Density (calculated) (Mg/m^3)	1.309
Absorption coefficient (mm^{-1})	3.636
Reflections collected	7431
Independent reflections (R_{int})	6981 (0.0244)
Observed reflections [I>2sigma(I)]	5903
R indices (all data)	R1 = 0.0475, wR1 = 0.0936
Final R indices [I>2sigma(I)]	R2 = 0.0366, wR2 = 0.0867
Goodness-of-fit on F^2	1.023
Largest diff. peak and hole ($eÅ^{-3}$)	0.490 and -0.355

Bond lengths (Å) for $[Cl(Ph)Ga\{N(SiMe_2Ph)_2\}]_2$

Ga(1)-N(1)	1.850(3)	Ga(2)-N(2)	1.846(2)
Ga(1)-C(6)	1.952(2)	Ga(2)-C(28)	1.957(2)
Ga(1)-Cl(1)	2.3587(9)	Ga(2)-Cl(2)	2.3651(9)
Ga(1)-Cl(2)	2.3813(8)	Ga(2)-Cl(1)	2.4025(8)
Si(1)-N(1)	1.739(3)	Si(2)-N(1)	1.738(3)
Si(1)-C(8)	1.863(4)	Si(2)-C(15)	1.861(4)
Si(1)-C(7)	1.866(4)	Si(2)-C(16)	.876(4)
Si(1)-C(14)	1.904(2)	Si(2)-C(22)	1.904(2)
Si(3)-N(2)	1.738(3)	Si(4)-N(2)	1.740(3)
Si(3)-C(37)	1.864(4)	Si(4)-C(30)	1.866(4)
Si(3)-C(38)	1.865(4)	Si(4)-C(29)	1.867(4)
Si(3)-C(44)	1.900(2)	Si(4)-C(36)	1.904(2)
C(1)-C(2)	1.39	C(4)-C(5)	1.39
C(1)-C(6)	1.39	C(5)-C(6)	1.39
C(2)-C(3)	1.39	C(9)-C(10)	1.39
C(3)-C(4)	1.39	C(9)-C(14)	1.39
C(10)-C(11)	1.39	C(17)-C(18)	1.39
C(11)-C(12)	1.39	C(17)-C(22)	1.39
C(12)-C(13)	1.39	C(18)-C(19)	1.39
C(13)-C(14)	1.39	C(19)-C(20)	1.39
C(20)-C(21)	1.39	C(24)-C(25)	1.39
C(21)-C(22)	1.39	C(25)-C(26)	1.39
C(23)-C(24)	1.39	C(26)-C(27)	1.39
C(23)-C(28)	1.39	C(27)-C(28)	1.39
C(31)-C(32)	1.39	C(34)-C(35)	1.39
C(31)-C(36)	1.39	C(35)-C(36)	1.39
C(32) C(33)	1.39	C(39)-C(40)	1.39
C(33)-C(34)	1.39	C(39)-C(44)	1.39
C(40)-C(41)	1.39	C(42)-C(43)	1.39
C(41)-C(42)	1.39	C(43)-C(44)	1.39

Bond angles (°) for $[Cl(Ph)Ga\{N(SiMe_2Ph)_2\}]_2$

N(1)-Ga(1)-C(6)	130.04(11)	N(1)-Ga(1)-Cl(2)	106.62(8)
N(1)-Ga(1)-Cl(1)	111.27(9)	C(6)-Ga(1)-Cl(2)	107.12(7)
C(6)-Ga(1)-Cl(1)	105.73(9)	Cl(1)-Ga(1)-Cl(2)	87.89(3)
N(2)-Ga(2)-C(28)	132.93(11)	N(2)-Ga(2)-Cl(1)	106.68(8)
N(2)-Ga(2)-Cl(2)	109.80(9)	C(28)-Ga(2)-Cl(1)	106.76(7)
C(28)-Ga(2)-Cl(2)	103.97(7)	Cl(2)-Ga(2)-Cl(1)	87.25(3)
Ga(1)-Cl(1)-Ga(2)	91.50(3)	N(1)-Si(1)-C(7)	112.1(2)
Ga(2)-Cl(2)-Ga(1)	91.87(3)	C(8)-Si(1)-C(7)	105.7(2)
N(1)-Si(1)-C(8)	112.8(2)	N(1)-Si(1)-C(14)	107.51(12)
C(8)-Si(1)-C(14)	110.5(2)	N(1)-Si(2)-C(16)	111.3(2)
C(7)-Si(1)-C(14)	108.12(14)	C(15)-Si(2)-C(16)	108.0(2)
N(1)-Si(2)-C(15)	110.3(2)	N(1)-Si(2)-C(22)	110.64(12)
C(15)-Si(2)-C(22)	106.97(15)	N(2)-Si(3)-C(38)	111.4(2)
C(16)-Si(2)-C(22)	109.47(15)	C(37)-Si(3)-C(38)	108.5(2)
N(2)-Si(3)-C(37)	110.67(15)	N(2)-Si(3)-C(44)	110.91(12)
C(37)-Si(3)-C(44)	106.4(2)	N(2)-Si(4)-C(29)	112.5(2)
C(38)-Si(3)-C(44)	108.7(2)	C(30)-Si(4)-C(29)	106.3(2)
N(2)-Si(4)-C(30)	112.9(2)	N(2)-Si(4)-C(36)	107.23(11)
C(30)-Si(4)-C(36)	110.2(2)	Si(2)-N(1)-Ga(1)	115.92(14)
C(29)-Si(4)-C(36)	107.54(15)	Si(1)-N(1)-Ga(1)	119.5(2)
Si(2)-N(1)-Si(1)	124.5(2)	Si(3)-N(2)-Si(4)	123.81(15)
Si(3)-N(2)-Ga(2)	118.46(14)	C(3)-C(2)-C(1)	120.0
Si(4)-N(2)-Ga(2)	117.7(2)	C(4)-C(3)-C(2)	120.0
C(2)-C(1)-C(6)	120.0	C(5)-C(4)-C(3)	120.0
C(4)-C(5)-C(6)	120.0	C(1)-C(6)-Ga(1)	119.40(12)
C(5)-C(6)-C(1)	120.0	C(10)-C(9)-C(14)	120.0
C(5)-C(6)-Ga(1)	120.59(12)	C(9)-C(10)-C(11)	120.0
C(10)-C(11)-C(12)	120.0	C(13)-C(14)-C(9)	120.0
C(13)-C(12)-C(11)	120.0	C(13)-C(14)-Si(1)	117.25(13)
C(12)-C(13)-C(14)	120.0	C(9)-C(14)-Si(1)	122.74(13)
C(18)-C(17)-C(22)	120.0	C(19)-C(20)-C(21)	120.0

Bond angles (°) for $[Cl(Ph)Ga\{N(SiMe_2Ph)_2\}]_2$ continued

C(17)-C(18)-C(19)	120.0	C(22)-C(21)-C(20)	120.0
C(20)-C(19)-C(18)	120.0	C(21)-C(22)-C(17)	120.0
C(21)-C(22)-Si(2)	118.48(12)	C(23)-C(24)-C(25)	120.0
C(17)-C(22)-Si(2)	121.49(12)	C(26)-C(25)-C(24)	120.0
C(24)-C(23)-C(28)	120.0	C(27)-C(26)-C(25)	120.0
C(28)-C(27)-C(26)	120.0	C(23)-C(28)-Ga(2)	118.81(12)
C(27)-C(28)-C(23)	120.0	C(32)-C(31)-C(36)	120.0
C(27)-C(28)-Ga(2)	121.19(12)	C(33)-C(32)-C(31)	120.0
C(32)-C(33)-C(34)	120.0	C(35)-C(36)-C(31)	120.0
C(35)-C(34)-C(33)	120.0	C(35)-C(36)-Si(4)	118.56(13)
C(34)-C(35)-C(36)	120.0	C(31)-C(36)-Si(4)	121.39(13)
C(40)-C(39)-C(44)	120.0	C(41)-C(42)-C(43)	120.0
C(39)-C(40)-C(41)	120.0	C(44)-C(43)-C(42)	120.0
C(42)-C(41)-C(40)	120.0	C(43)-C(44)-C(39)	120.0
C(43)-C(44)-Si(3)	118.47(13)	C(39)-C(44)-Si(3)	121.52(13)

Crystal data for $[Cl_3Ga\{NH(SiMe_3)_2\}]$

Empirical formula	$C_6H_{19}NSi_2Cl_3Ga$
Formula weight	337.47
Crystal colour/morphology	Clear platy needles
Crystal size (mm)	0.53 x 0.20 x 0.10
a (Å)	13.1596(7)
b (Å)	11.8563(5)
c (Å)	19.657(2)
α (°)	90.00
β (°)	90.00
γ (°)	90.00
V ($Å^3$)	3066.9(4)
Z	8
Crystal system	Orthorhombic
Space group	Pbca
Wavelength (Å)	1.54178
Density (calculated) (Mg/m^3)	1.462
Absorption coefficient (mm^{-1})	8.497
Reflections collected	2103
Independent reflections (R_{int})	2103 (0.0000)
Observed reflections [I>2sigma(I)]	1663
R indices (all data)	R1 = 0.0776, wR1 = 0.1711
Final R indices [I>2sigma(I)]	R2 = 0.0564, wR2 = 0.1435
Goodness-of-fit on F^2	1.057
Largest diff. peak and hole ($eÅ^{-3}$)	0.387 and -0.610

Bond lengths (Å) and angles (°) for $[Cl_3Ga\{NH(SiMe_3)_2\}]$

	A	B
N-Si(1)	1.841(5)	1.776(14)
N-Si(2)	1.842(4)	1.87(2)
N-Ga	2.007(4)	2.059(11)
Ga-Cl(3)	2.099(3)	2.12
Ga-Cl(1)	2.170(2)	2.12
Ga-Cl(2)	2.187(2)	2.16
Si(1)-C(1)	1.849(8)	1.88
Si(1)-C(2)	1.849(7)	1.88
Si(1)-C(3)	1.851(7)	1.88
Si(2)-C(4)	1.849(8)	1.87
Si(2)-C(5)	1.853(8)	1.87
Si(2)-C(6)	1.884(9)	1.88
Si(1)-N-Si(2)	118.0(2)	120.8(7)
Si(1)-N-Ga	114.9(2)	114.3(7)
Si(2)-N-Ga	112.1(2)	109.4(7)
N-Ga-Cl(3)	115.1(2)	108.0(4)
N-Ga-Cl(1)	106.63(13)	108.9(5)
Cl(3)-Ga-Cl(1)	112.2(2)	111.8
N-Ga-Cl(2)	107.52(14)	108.5(4)
Cl(3)-Ga-Cl(2)	106.02(14)	109.7
Cl(1)-Ga-Cl(2)	109.24(14)	110.0
N-Si(1)-C(1)	109.0(3)	108.7(5)
Si(1)-N-Si(2)	118.0(2)	120.8(7)
Si(1)-N-Ga	114.9(2)	114.3(7)
Si(2)-N-Ga	112.1(2)	109.4(7)
N-Ga-Cl(3)	115.1(2)	108.0(4)
N-Ga-Cl(1)	106.63(13)	108.9(5)
Cl(3)-Ga-Cl(1)	112.2(2)	111.8
N-Ga-Cl(2)	107.52(14)	108.5(4)

Bond lengths (Å) and angles (°) for $[Cl_3Ga\{NH(SiMe_3)_2\}]$ continued

Cl(3)-Ga-Cl(2)	106.02(14)	109.7
Cl(1)-Ga-Cl(2)	109.24(14)	110.0
N-Si(1)-C(1)	109.0(3)	108.7(5)
Si(1)-N-Si(2)	118.0(2)	120.8(7)

Crystal data for $[Cl_2(Me)Al\{NH(SiMe_2Ph)_2\}]$

Empirical formula	$C_{17.20}H_{26.60}NSi_2Cl_{1.80}Al$
	$[C_{17}H_{26}NSi_2Cl_2Al]_{0.8} + [C_{18}H_{29}NSi_2ClAl]_{0.2}$
Formula weight	394.36
Crystal colour/morphology	Colourless blocks
Crystal size (mm)	0.67 x 0.47 x 0.43
a (Å)	11.371(2)
b (Å)	15.023(3)
c (Å)	13.275(2)
α (°)	90
β (°)	108.927(11)
γ (°)	90
V ($Å^3$)	2145.0(6)
Z	4
Crystal system	Monoclinic
Space group	$P2_1/n$
Wavelength (Å)	1.54178
Density (calculated) (Mg/m^3)	1.221
Absorption coefficient (mm^{-1})	3.940
Reflections collected	3354
Independent reflections (R_{int})	3177 (0.0227)
Observed reflections [I>2sigma(I)]	2749
R indices (all data)	R1 = 0.0404, wR1 = 0.1017
Final R indices [I>2sigma(I)]	R2 = 0.0486, wR2 = 0.1093
Goodness-of-fit on F^2	1.068
Largest diff. peak and hole ($eÅ^{-3}$)	0.366 and -0.617

Bond lengths (Å) and angles (°) for $[Cl_2(Me)Al\{NH(SiMe_2Ph)_2\}]$

Al-C(1)	1.932(4)	Al-C(1')	1.959(5)
Al-N	2.001(2)	Al-Cl(2)	2.101(2)
Al-Cl(2')	2.118(4)	Al-Cl(1)	2.1708(12)
N-Si(11)	1.835(2)	N-Si(2)	1.836(2)
Si(2)-C(4)	1.848(3)	Si(2)-C(3)	1.850(3)
Si(2)-C(10)	1.883(2)	C(5)-C(6)	1.39
C(5)-C(10)	1.39	C(6)-C(7)	1.39
C(7)-C(8)	1.39	C(8)-C(9)	1.39
C(9)-C(10)	1.39	Si(11)-C(12)	1.847(3)
Si(11)-C(13)	1.851(3)	Si(11)-C(19)	1.889(2)
C(14)-C(15)	1.39	C(14)-C(19)	1.39
C(15)-C(16)	1.39	C(16)-C(17)	1.39
C(17)-C(18)	1.39	C(18)-C(19)	1.39
C(1)-Al-N	117.1(4)	C(1')-Al-N	111.9(6)
C(1)-Al-Cl(2)	110.3(3)	N-Al-Cl(2)	107.21(13)
C(1')-Al-Cl(2')	110.9(6)	N-Al-Cl(2')	111.7(3)
C(1)-Al-Cl(1)	108.2(3)	C(1')-Al-Cl(1)	112.7(7)
N-Al-Cl(1)	103.77(8)	Cl(2)-Al-Cl(1)	109.98(12)
Cl(2')-Al-Cl(1)	105.6(4)	Si(11)-N-Si(2)	117.27(12)
Si(11)-N-Al	112.41(11)	Si(2)-N-Al	114.88(12)
N-Si(2)-C(4)	110.62(14)	N-Si(2)-C(3)	109.07(14)
C(4)-Si(2)-C(3)	110.5(2)	N-Si(2)-C(10)	108.26(10)
C(4)-Si(2)-C(10)	107.07(14)	C(3)-Si(2)-C(10)	111.31(13)
C(6)-C(5)-C(10)	120.0	C(7)-C(6)-C(5)	120.0
C(8)-C(7)-C(6)	120.0	C(7)-C(8)-C(9)	120.0
C(10)-C(9)-C(8)	120.0	C(9)-C(10)-C(5)	120.0
C(9)-C(10)-Si(2)	121.06(10)	C(5)-C(10)-Si(2)	118.94(10)
N-Si(11)-C(12)	107.09(13)	N-Si(11)-C(13)	108.24(13)
C(12)-Si(11)-C(13)	112.9(2)	N-Si(11)-C(19)	111.92(10)
C(12)-Si(11)-C(19)	106.78(13)	C(13)-Si(11)-C(19)	109.90(12)

Bond lengths (Å) and angles (°) for $[Cl_2(Me)Al\{NH(SiMe_2Ph)_2\}]$ continued

C(15)-C(14)-C(19)	120.0	C(16)-C(15)-C(14)	120.0
C(15)-C(16)-C(17)	120.0	C(18)-C(17)-C(16)	120.0
C(17)-C(18)-C(19)	120.0	C(18)-C(19)-C(14)	120.0
C(18)-C(19)-Si(11)	119.42(10)	C(14)-C(19)-Si(11)	120.48(10)

Crystal data for $[Al_5(\mu_4\text{-}O)(\mu\text{-}O^iPr)_7H_6]$

Empirical formula	$C_{21}H_{55}O_8Al_5$
Formula weight	570.55
Crystal colour/morphology	Colourless platy needles
Crystal size (mm)	1.00 x 0.70 x 0.23
a (Å)	11.8198(6)
b (Å)	18.129(2)
c (Å)	15.7450(7)
α (°)	90.00
β (°)	90.00
γ (°)	90.00
Z	4
V ($Å^3$)	3373.8(5)
Crystal system	Orthorhombic
Space group	Pnma
Wavelength (Å)	1.54178
Density (calculated) (Mg/m^3)	1.123
Absorption coefficient (mm^{-1})	1.832
Reflections collected	2553
Independent reflections	2553
Observed reflections [I>2sigma(I)]	1946
R indices (all data)	R1 = 0.0668, wR1 = 0.1477
Final R indices [I>2sigma(I)]	R2 = 0.0490, wR2 = 0.1314
Goodness-of-fit on F^2	1.045
Largest diff. peak and hole ($eÅ^{-3}$)	0.283 and -0.299

Bond lengths (Å) and angles (°) for $[Al_5(\mu_4\text{-}O)(\mu\text{-}O^iPr)_7H_6]$

Al(1)-O(1)	1.815(2)	Al(2)-O(3)	1.850(2)
Al(1)-O(1A)	1.815(2)	Al(2)-O(1)	1.851(2)
Al(2)-O(2)	1.843(2)	Al(2)-O	1.8873(9)
Al(2)-Al(4)	2.8859(12)	Al(3)-O(2A)	1.858(2)
Al(2)-Al(3)	2.8900(12)	Al(3)-O(2)	1.858(2)
Al(3)-O(4)	1.853(4)	Al(3)-O	1.913(3)
Al(3)-Al(2A)	2.8900(12)	Al(4)-O(3)	1.844(2)
Al(3)-Al(4)	2.907(2)	Al(4)-O(4)	1.845(4)
Al(4)-O(3A)	1.844(2)	Al(4)-O	1.940(3)
Al(4)-Al(2)	2.8859(12)	O(1)-C(1)	1.507(5)
O-Al(2)	1.8873(9)	O(2)-C(4)	1.450(4)
O(1)-C(1)'	1.488(10)	O(3)-C(7)	1.447(4)
O(4)-C(10)	1.504(7)	C(1)-C(3)	1.512(7)
O(4)-C(10)'	1.512(14)	C(1)'-C(3)'	1.476(12)
C(1)-C(2)	1.498(11)	C(1)'-C(2)'	1.515(15)
C(4)-C(6)	1.497(5)	C(7)-C(8)	1.504(5)
C(4)-C(5)	1.498(5)	C(10)-C(11A)	1.472(7)
C(7)-C(9)	1.503(5)	C(10)-C(11)	1.472(7)
C(10)'-C(11A)	1.452(9)	C(10)'-C(11)	1.452(9)
O(1)-Al(1)-O(1A)	106.62(14)	O(3)-Al(2)-O(1)	116.44(10)
O(2)-Al(2)-O(3)	119.97(11)	O(2)-Al(2)-O	78.48(10)
O(2)-Al(2)-O(1)	118.67(10)	O(3)-Al(2)-O	78.68(10)
O(1)-Al(2)-O	90.97(10)	O(1)-Al(2)-Al(4)	116.15(8)
O(2)-Al(2)-Al(4)	94.80(8)	O-Al(2)-Al(4)	41.75(8)
O(3)-Al(2)-Al(4)	38.55(6)	O(2)-Al(2)-Al(3)	38.84(7)
O(3)-Al(2)-Al(3)	95.64(7)	Al(4)-Al(2)-Al(3)	60.45(4)
O(1)-Al(2)-Al(3)	115.96(8)	O(4)-Al(3)-O(2A)	107.47(8)
O-Al(2)-Al(3)	40.82(8)	O(4)-Al(3)-O(2)	107.47(8)
O(2A)-Al(3)-O(2)	131.81(15)	O(2A)-Al(3)-O	77.47(7)
O(4)-Al(3)-O	79.44(13)	O(2)-Al(3)-O	77.47(7)

Bond lengths (Å) and angles (°) for $[Al_5(\mu_4\text{-}O)(\mu\text{-}O^iPr)_7H_6]$ continued

O(4)-Al(3)-Al(2A)	87.88(9)	O-Al(3)-Al(2A)	40.16(3)
O(2A)-Al(3)-Al(2A)	38.46(7)	O(4)-Al(3)-Al(2)	87.88(9)
O(2)-Al(3)-Al(2A)	112.27(8)	O(2A)-Al(3)-Al(2)	112.27(8)
O(2)-Al(3)-Al(2)	38.46(7)	O(4)-Al(3)-Al(4)	38.08(10)
O-Al(3)-Al(2)	40.16(3)	O(2A)-Al(3)-Al(4)	93.76(8)
Al(2A)-Al(3)-Al(2)	79.05(4)	O(2)-Al(3)-Al(4)	93.76(8)
O-Al(3)-Al(4)	41.36(8)	O(3A)-Al(4)-O(3)	126.83(15)
Al(2A)-Al(3)-Al(4)	59.71(3)	O(3A)-Al(4)-O(4)	110.04(8)
Al(2)-Al(3)-Al(4)	59.71(3)	O(3)-Al(4)-O(4)	110.04(8)
O(3A)-Al(4)-O	77.48(7)	O(3A)-Al(4)-Al(2A)	38.69(7)
O(3)-Al(4)-O	77.48(7)	O(3)-Al(4)-Al(2A)	111.06(8)
O(4)-Al(4)-O	78.93(13)	O(4)-Al(4)-Al(2A)	88.15(9)
O-Al(4)-Al(2A)	40.38(3)	O(4)-Al(4)-Al(2)	88.15(9)
O(3A)-Al(4)-Al(2)	111.06(8)	O-Al(4)-Al(2)	40.38(3)
O(3)-Al(4)-Al(2)	38.69(7)	Al(2A)-Al(4)-Al(2)	79.18(4)
O(3A)-Al(4)-Al(3)	95.20(8)	O-Al(4)-Al(3)	40.66(8)
O(3)-Al(4)-Al(3)	95.20(8)	Al(2A)-Al(4)-Al(3)	59.85(3)
O(4)-Al(4)-Al(3)	38.27(11)	Al(2)-Al(4)-Al(3)	59.85(3)
Al(2A)-O-Al(2)	154.09(15)	Al(2A)-O-Al(4)	97.88(8)
Al(2A)-O-Al(3)	99.02(8)	Al(2)-O-Al(4)	97.88(8)
Al(2)-O-Al(3)	99.02(8)	Al(3)-O-Al(4)	97.99(12)
C(1')-O(1)-Al(1)	105.0(5)	C(1)-O(1)-Al(2)	110.2(3)
C(1)-O(1)-Al(1)	131.5(3)	Al(1)-O(1)-Al(2)	117.98(11)
C(1')-O(1)-Al(2)	137.0(5)	C(4)-O(2)-Al(2)	125.0(2)
C(4)-O(2)-Al(3)	132.1(2)	C(7)-O(3)-Al(2)	125.7(2)
Al(2)-O(2)-Al(3)	102.70(10)	Al(4)-O(3)-Al(2)	102.76(10)
C(7)-O(3)-Al(4)	130.1(2)	C(10)-O(4)-Al(4)	115.6(4)
C(10')-O(4)-Al(4)	148.8(7)	Al(4)-O(4)-Al(3)	103.64(15)
C(10)-O(4)-Al(3)	140.7(4)	C(2)-C(1)-O(1)	108.9(8)
C(10')-O(4)-Al(3)	107.6(7)	C(2)-C(1)-C(3)	113.9(8)
O(1)-C(1)-C(3)	105.7(4)	O(1)-C(1')-C(2')	107.2(10)

Bond lengths (Å) and angles (°) for $[Al_5(\mu_4\text{-}O)(\mu\text{-}O^iPr)_7H_6]$ continued

C(3')-C(1')-O(1)	107.3(8)	O(2)-C(4)-C(6)	109.9(3)
C(3')-C(1')-C(2')	114.8(11)	O(2)-C(4)-C(5)	109.8(3)
C(6)-C(4)-C(5)	112.9(4)	C(9)-C(7)-C(8)	113.1(3)
O(3)-C(7)-C(9)	110.0(3)	C(11A)-C(10)-C(11)	119.7(7)
O(3)-C(7)-C(8)	110.0(3)	C(11A)-C(10)-O(4)	106.8(4)
C(11)-C(10)-O(4)	106.8(4)	C(11)-C(10')-O(4)	107.3(7)
C(11)-C(10')-C(11A)	122.5(11)	C(11A)-C(10')-O(4)	107.3(7)

Crystal data for $[Al_5(\mu_5\text{-}O)(\mu\text{-}O^iPr)_8(Cl)H_4]$

Empirical formula	$C_{24}H_{60}O_9ClAl_5$
Formula weight	663.07
Crystal colour/morphology	Colourless prisims
Crystal size (mm)	0.67 x 0.30 x 0.23
a (Å)	20.331(2)
b (Å)	9.3818(10)
c (Å)	20.680(2)
α (°)	90.00
β (°)	109.252(6)
γ (°)	90.00
Z	4
V ($Å^3$)	3723.9(6)
Crystal system	Monoclinic
Space group	P2/c
Wavelength	1.54178
Density (calculated) (Mg/m^3)	1.183
Absorption coefficient (mm^{-1})	2.392
Reflections collected	5710
Independent reflections	5530
Observed reflections [I>2sigma(I)]	4496
R indices (all data)	R1 = 0.0817, wR1 = 0.2093
Final R indices [I>2sigma(I)]	R2 = 0.0658, wR2 = 0.1841
Goodness-of-fit on F^2	1.062
Largest diff. peak and hole ($eÅ^{-3}$)	0.498 and -1.512

Bond lengths (Å) and angles (°) for $[Al_5(\mu_5\text{-}O)(\mu\text{-}O^iPr)_8(Cl)H_4]$

	A	B
Al(1)-O	1.843(4)	1.852(4)
Al(1)-O(1A)	1.950(3)	1.963(3)
Al(1)-O(1)	1.950(3)	1.963(3)
Al(1)-O(2A)	1.964(3)	1.937(3)
Al(1)-O(2)	1.964(3)	1.937(3)
Al(1)-C(l)	2.188(2)	2.184(3)
Al(2)-H(2)	1.51(2)	1.51(2)
Al(2)-O(1)	1.813(3)	1.810(3)
Al(2)-O(3)	1.826(3)	1.817(3)
Al(2)-O(4A)	1.830(3)	1.814(3)
Al(2)-O	2.0623(13)	2.1772(15)
Al(3)-H(3)	1.51(2)	1.51(2)
Al(3)-O(2)	1.816(3)	1.817(3)
Al(3)-O(4)	1.817(3)	1.839(3)
Al(3)-O(3)	1.828(3)	1.833(3)
Al(3)-O	2.1262(13)	2.0060(14)
O-Al(2A)	2.0623(13)	2.1772(15)
O-Al(3A)	2.1262(13)	2.0060(15)
O(1)-C(1)	1.451(5)	1.441(6)
O(2)-C(4)	1.446(5)	1.452(5)
O(3)-C(7)	1.461(5)	1.465(6)
O(4)-C(10)	1.460(5)	1.463(6)
O(4)-Al(2A)	1.830(3)	1.814(3)
C(1)-C(2)	1.523(7)	1.488(8)
C(1)-C(3)	1.537(7)	1.496(8)
C(4)-C(5)	1.506(8)	1.525(8)
C(4)-C(6)	1.530(7)	1.504(8)
C(7)-C(9)	1.508(7)	1.492(9)
C(7)-C(8)	1.509(7)	1.511(8)
C(10)-C(12)	1.501(7)	1.515(9)

Bond lengths (Å) and angles (°) for $[Al_5(\mu_5\text{-}O)(\mu\text{-}O^iPr)_8(Cl)H_4]$ continued

C(10)-C(11)	1.513(6)	1.493(9)
O-Al(1)-O(1A)	80.37(9)	81.22(10)
O-Al(1)-O(1)	80.37(9)	81.22(10)
O(1)-Al(1)-O(1A)	160.7(2)	162.4(2)
O-Al(1)-O(2A)	80.90(9)	79.92(10)
O(1A)-Al(1)-O(2A)	88.17(12)	88.51(12)
O(1)-Al(1)-O(2A)	88.80(12)	88.43(12)
O-Al(1)-O(2)	80.90(9)	79.92(10)
O(1A)-Al(1)-O(2)	88.80(12)	88.43(12)
O(1)-Al(1)-O(2)	88.17(12)	88.51(12)
O(2A)-Al(1)-O(2)	161.8(2)	159.8(2)
O-Al(1)-Cl	180.0	180.0
O(1A)-Al(1)-Cl	99.63(9)	98.78(10)
O(1)-Al(1)-Cl	99.63(9)	98.78(10)
O(2A)-Al(1)-Cl	99.10(9)	100.08(10)
O(2)-Al(1)-Cl	99.10(9)	100.08(10)
H(2)-Al(2)-O(1)	102.2(20)	102.5(26)
H(2)-Al(2)-O(3)	105.2(20)	101.8(24)
O(1)-Al(2)-O(3)	110.80(14)	116.0(2)
H(2)-Al(2)-O(4A)	97.3(19)	107.5(23)
O(1)-Al(2)-O(4A)	115.34(14)	109.8(2)
O(3)-Al(2)-O(4A)	122.18(14)	117.4(2)
H(2)-Al(2)-O	175.8(19)	176.5(23)
O(1)-Al(2)-O	78.10(14)	76.49(15)
O(3)-Al(2)-O	78.49(11)	75.88(12)
O(4)-Al(2)-O	78.88(10)	75.94(12)
H(3)-Al(3)-O(2)	107.1(19)	104.8(21)
H(3)-Al(3)-O(4)	102.7(18)	93.4(20)
O(2)-Al(3)-O(4)	109.64(14)	115.5(2)
H(3)-Al(3)-O(3)	99.0(18)	103.6(20)

Bond lengths (Å) and angles (°) for $[Al_5(\mu_5\text{-}O)(\mu\text{-}O^iPr)_8(Cl)H_4]$ continued

O(2)-Al(3)-O(3)	116.48(14)	109.3(2)
O(4)-Al(3)-O(3)	119.42(14)	125.6(2)
H(3)-Al(3)-O	175.1(19)	173.3(20)
O(2)-Al(3)-O	77.23(14)	78.9(2)
O(4)-Al(3)-O	77.48(10)	79.90(12)
O(3)-Al(3)-O	76.79(10)	80.04(12)
Al(1)-O-Al(2)	98.05(11)	96.32(11)
Al(1)-O-Al(2A)	98.05(11)	96.32(11)
Al(2)-O-Al(2A)	163.9(2)	167.4(2)
Al(1)-O-Al(3)	97.36(10)	98.59(12)
Al(2)-O-Al(3)	88.94(5)	89.13(6)
Al(2A)-O-Al(3)	89.00(5)	88.99(6)
Al(1)-O-Al(3A)	97.36(10)	98.59(12)
Al(2)-O-Al(3A)	89.00(5)	89.12(6)
Al(2A)-O-Al(3A)	88.94(5)	88.99(6)
Al(3)-O-Al(3A)	165.3(2)	162.8(2)
C(1)-O(1)-Al(2)	130.1(3)	129.2(3)
C(1)-O(1)-Al(1)	126.5(3)	124.5(3)
Al(2)-O(1)-Al(1)	103.29(14)	105.8(2)
C(4)-O(2)-Al(3)	128.8(3)	130.3(3)
C(4)-O(2)-Al(1)	126.8(3)	126.8(3)
Al(3)-O(2)-Al(1)	104.35(14)	102.4(2)
C(7)-O(3)-Al(2)	130.0(3)	122.6(3)
C(7)-O(3)-Al(3)	122.7(3)	130.2(3)
Al(2)-O(3)-Al(3)	106.83(14)	107.0(2)
C(10)-O(4)-Al(3)	128.7(3)	124.1(3)
C(10)-O(4)-Al(2A)	123.8(3)	128.1(3)
Al(3)-O(4)-Al(2A)	107.20(14)	107.0(2)
O(1)-C(1)-C(2)	109.8(4)	113.0(5)
O(1)-C(1)-C(3)	111.3(4)	110.0(5)
C(2)-C(1)-C(3)	111.9(4)	113.2(5)

Bond lengths (Å) and angles (°) for $[Al_5(\mu_5\text{-}O)(\mu\text{-}O^iPr)_8(Cl)H_4]$ continued

O(2)-C(4)-C(5)	109.8(4)	110.5(4)
O(2)-C(4)-C(6)	111.4(4)	110.2(4)
C(5)-C(4)-C(6)	111.9(4)	112.4(5)
O(3)-C(7)-C9	109.4(4)	110.3(5)
O(3)-C(7)-C(8)	110.2(4)	110.1(5)
C(9)-C(7)-C(8)	113.5(4)	113.7(6)
O(4)-C(10)-C(12)	109.3(4)	113.7(5)
O(4)-C(10)-C(11)	110.7(4)	111.5(5)
C(12)-C(10)-C(11)	112.8(4)	108.6(5)

Crystal data for $[Al(O^iPr)_3]_4$

Empirical formula	$C_{36}H_{84}Al_4O_{12}$
Formula weight	816.95
Crystal colour/morphology	Colourless
Crystal size (mm)	0.48 × 0.44 × 0.32
a (Å)	12.3356(4)
b (Å)	12.3356(4)
c (Å)	31.6678(19)
α (°)	90
β (°)	90
γ (°)	90
V ($Å^3$)	4818.8(4)
Z	4
Crystal system	tetragonal
Space group	$P4_32_12$
Wavelength (Å)	0.71073
Density (calculated) (Mg/m^3)	1.126
Absorption coefficient (mm^{-1})	0.147
Reflections collected	30277
Independent reflections (R_{int})	5814 (0.0209)
Observed reflections [F^2>2sigma]	5544
R indices (all data)	R1 = 0.0327, wR2 = 0.1002
Final R indices [F^2>2sigma]	R1 = 0.0350, wR2 = 0.1031
Goodness-of-fit on F^2	0.912
Largest diff. peak and hole ($eÅ^{-3}$)	0.319 and –0.248

Bond lengths (Å) and angles (°) for $[Al(O^iPr)_3]_4$

Al(1)–O(2A)	1.9121(8)	Al(1)–O(2)	1.9121(8)
Al(1)–O(1A)	1.9194(9)	Al(1)–O(1)	1.9194(9)
Al(1)–O(5)	1.9215(9)	Al(1)–O(5A)	1.9215(9)
Al(1)–Al(3A)	2.8565(4)	Al(1)–Al(3)	2.8565(4)
Al(1)–Al(2)	2.8706(7)	Al(2)–O(6A)	1.7022(10)
Al(2)–O(6)	1.7022(10)	Al(2)–O(5A)	1.7965(9)
Al(2)–O(5)	1.7965(9)	Al(3)–O(3)	1.6920(10)
Al(3)–O(4)	1.7051(11)	Al(3)–O(1)	1.7982(9)
Al(3)–O(2)	1.8002(9)	O(1)–C(1)	1.4535(14)
O(2)–C(4)	1.4526(14)	O(3)–C(7)	1.3943(16)
O(4)–C(10)	1.3965(17)	O(5)–C(13)	1.4507(14)
O(6)–C(16)	1.4039(16)	C(1)–C(2)	1.499(2)
C(1)–C(3)	1.501(2)	C(4)–C(5)	1.5175(18)
C(4)–C(6)	1.5195(18)	C(7)–C(9)	1.506(2)
C(7)–C(8)	1.515(2)	C(10)–C(12)	1.496(3)
C(10)–C(11)	1.523(2)	C(13)–C(15)	1.5161(19)
C(13)–C(14)	1.522(2)	C(16)–C(18)	1.504(3)
C(16)–C(17)	1.526(2)		
O(2A)–Al(1)–O(2)	168.76(6)	O(2A)–Al(1)–O(1A)	76.54(4)
O(2)–Al(1)–O(1A)	95.62(4)	O(2A)–Al(1)–O(1)	95.62(4)
O(2)–Al(1)–O(1)	76.54(4)	O(1A)–Al(1)–O(1)	92.98(6)
O(2A)–Al(1)–O(5)	96.43(4)	O(2)–Al(1)–O(5)	92.44(4)
O(1A)–Al(1)–O(5)	169.12(4)	O(1)–Al(1)–O(5)	96.00(4)
O(2A)–Al(1)–O(5A)	92.44(4)	O(2)–Al(1)–O(5A)	96.43(4)
O(1A)–Al(1)–O(5A)	96.00(4)	O(1)–Al(1)–O(5A)	169.12(4)
O(5)–Al(1)–O(5A)	75.79(5)	O(2)–Al(1)–Al(3A)	133.45(3)
O(1)–Al(1)–Al(3A)	95.81(3)	O(5)–Al(1)–Al(3A)	134.11(3)
O(5A)–Al(1)–Al(3A)	95.05(3)	O(2A)–Al(1)–Al(3)	133.45(3)
O(2)–Al(1)–Al(3)	38.28(3)	O(1A)–Al(1)–Al(3)	95.81(3)
O(1)–Al(1)–Al(3)	38.26(3)	O(5)–Al(1)–Al(3)	95.05(3)

Bond lengths (Å) and angles (°) for $[Al(O^iPr)_3]_4$ continued

O(5A)–Al(1)–Al(3)	134.11(3)	Al(3A)–Al(1)–Al(3)	120.43(2)
O(2A)–Al(1)–Al(2)	95.62(3)	O(2)–Al(1)–Al(2)	95.62(3)
O(1A)–Al(1)–Al(2)	133.51(3)	O(1)–Al(1)–Al(2)	133.51(3)
Al(3A)–Al(1)–Al(2)	119.786(11)	Al(3)–Al(1)–Al(2)	119.786(11)
O(6A)–Al(2)–O(6)	119.37(7)	O(6A)–Al(2)–O(5A)	118.77(5)
O(6)–Al(2)–O(5A)	106.25(5)	O(6A)–Al(2)–O(5)	106.25(5)
O(6)–Al(2)–O(5)	118.77(5)	O(5A)–Al(2)–O(5)	82.14(5)
O(6A)–Al(2)–Al(1)	120.32(4)	O(6)–Al(2)–Al(1)	120.32(4)
O(5A)–Al(2)–Al(1)	41.07(3)	O(5)–Al(2)–Al(1)	41.07(3)
O(3)–Al(3)–O(4)	119.17(6)	O(3)–Al(3)–O(1)	106.64(5)
O(4)–Al(3)–O(1)	117.70(5)	O(3)–Al(3)–O(2)	118.72(5)
O(4)–Al(3)–O(2)	106.88(5)	O(1)–Al(3)–O(2)	82.52(4)
O(3)–Al(3)–Al(1)	120.33(4)	O(4)–Al(3)–Al(1)	120.50(4)
O(1)–Al(3)–Al(1)	41.37(3)	O(2)–Al(3)–Al(1)	41.15(3)
C(1)–O(1)–Al(3)	125.97(8)	C(1)–O(1)–Al(1)	133.13(8)
Al(3)–O(1)–Al(1)	100.37(4)	C(4)–O(2)–Al(3)	126.03(7)
C(4)–O(2)–Al(1)	131.98(7)	Al(3)–O(2)–Al(1)	100.57(4)
C(7)–O(3)–Al(3)	146.45(11)	C(10)–O(4)–Al(3)	134.96(10)
C(13)–O(5)–Al(2)	125.03(8)	C(13)–O(5)–Al(1)	133.36(8)
Al(2)–O(5)–Al(1)	101.03(4)	C(16)–O(6)–Al(2)	138.68(10)
O(1)–C(1)–C(2)	111.09(11)	O(1)–C(1)–C(3)	110.79(11)
C(2)–C(1)–C(3)	110.76(13)	O(2)–C(4)–C(5)	109.93(10)
O(2)–C(4)–C(6)	109.76(11)	C(5)–C(4)–C(6)	110.16(11)

Crystal data for $[HAl(S^tBu)(\mu\text{-}O^tBu)]_2$

Empirical formula	$C_{16}H_{38}O_2S_2Al_2$
Formula weight	380.54
Crystal colour/morphology	Clear plates
Crystal size (mm)	0.67 x 0.67 x 0.10
a (Å)	21.358(5)
b (Å)	9.353(2)
c (Å)	11.825(7)
α (°)	90.00
β (°)	92.46(4)
γ (°)	90.00
V ($Å^3$)	2360.1(15)
Z	4
Crystal system	Monoclinic
Space group	P2(1)/c
Wavelength (Å)	0.71073
Density (calculated) (Mg/m^3)	1.071
Absorption coefficient (mm^{-1})	0.304
Reflections collected	3270
Independent reflections (R_{int})	3085 (0.0426)
Observed reflections [I>2sigma(I)]	1850
R indices (all data)	R1 = 0.2398, wR1 = 0.5640
Final R indices [I>2sigma(I)]	R2 = 0.1572, wR2 = 0.3928
Goodness-of-fit on F^2	1.194
Largest diff. peak and hole ($eÅ^{-3}$)	0.847 and -0.446

Bond lengths (Å) and angles (°) for $[HAl(S^tBu)(\mu\text{-}O^tBu)]_2$

Al(1)-O(1)	1.846(12)	Al(1)-S(1)	2.20(7)
Al(1)-O(2)	1.850(12)	Al(1)-Al(2)	2.80(7)
Al(2)-O(2)	1.837(13)	Al(2)-S(2)	2.20(8)
Al(2)-O(1)	1.846(12)	S(1)-C(1)	1.8(2)
S(2)-C(9)	1.83(2)	O(2)-C(13)	1.45(2)
O(1)-C(5)	1.46(2)	C(1)-C(4)	1.46(3)
C(1)-C(2)	1.50(3)	C(5)-C(8)	1.51(3)
C(1)-C(3)	1.56(2)	C(5)-C(7)	1.54(3)
C(5)-C(6)	1.55(3)	C(9)-C(12)	1.55(3)
C(9)-C(10)	1.53(3)	C(9)-C(11)	1.55(4)
C(13)-C(16)	1.47(3)	C(13)-C(14)	1.53(3)
C(13)-C(15)	1.52(3)		
O(1)-Al(1)-O(2)	80.6(5)	O(1)-Al(1)-Al(2)	40.5(4)
O(1)-Al(1)-S(1)	111.9(5)	O(2)-Al(1)-Al(2)	40.3(4)
O(2)-Al(1)-S(1)	114.4(5)	S(1)-Al(1)-Al(2)	124.0(3)
O(2)-Al(2)-O(1)	81.0(5)	O(2)-Al(2)-Al(1)	40.6(4)
O(2)-Al(2)-S(2)	111.6(5)	O(1)-Al(2)-Al(1)	40.5(4)
O(1)-Al(2)-S(2)	115.0(5)	S(2)-Al(2)-Al(1)	124.3(3)
C(1)-S(1)-Al(1)	107.7(6)	C(5)-O(1)-Al(2)	131.2(11)
C(9)-S(2)-Al(2)	106.5(9)	Al(1)-O(1)-Al(2)	98.9(4)
C(5)-O(1)-Al(1)	129.9(11)	C(13)-O(2)-Al(2)	132.1(10)
C(13)-O(2)-Al(1)	128.8(10)	C(4)-C(1)-C(3)	113.0(16)
Al(2)-O(2)-Al(1)	99.1(6)	C(2)-C(1)-C(3)	109.0(18)
C(4)-C(1)-C(2)	112.8(19)	C(4)-C(1)-S(1)	111.6(14)
C(2)-C(1)-S(1)	108.3(13)	O(1)-C(5)-C(7)	108.6(15)
C(3)-C(1)-S(1)	101.5(12)	C(8)-C(5)-C(7)	112.5(19)
O(1)-C(5)-C(8)	108.5(16)	O(1)-C(5)-C(6)	108.1(15)
C(8)-C(5)-C(6)	111.1(18)	C(10)-C(9)-C(11)	110.3(2)
C(7)-C(5)-C(6)	107.9(17)	C(12)-C(9)-C(11)	110.5(2)
C(10)-C(9)-C(12)	110.5(22)	C(10)-C(9)-S(2)	110.5(1)

Bond lengths (Å) and angles (°) for $[HAl(S^tBu)(\mu\text{-}O^tBu)]_2$ continued

C(12)-C(9)-S(2)	111.5(17)	O(2)-C(13)-C(15)	107.4(15)
C(11)-C(9)-S(2)	103.4(17)	C(16)-C(13)-C(15)	111.2(20)
O(2)-C(13)-C(16)	107.2(15)	O(2)-C(13)-C(14)	107.4(16)
C(16)-C(13)-C(14)	111.9(19)	C(15)-C(13)-C(14)	111.5(19)

Crystal data for $[Al(S^tBu)_3\{NMe_2Et\}]$

Empirical formula	$C_{16}H_{38}NS_3Al$
Formula weight	367.63
Crystal colour/morphology	Colourless prisms
Crystal size (mm)	0.67 x 0.37 x 0.17
a (Å)	11.6677(6)
b (Å)	16.6259(12)
c (Å)	22.4682(15)
α (°)	90.00
β (°)	90.00
γ (°)	90.00
V ($Å^3$)	4358.5(5)
Z	8
Crystal system	Orthorhombic
Space group	Pbca
Wavelength (Å)	1.54178
Density (calculated) (Mg/m^3)	1.121
Absorption coefficient (mm^{-1})	3.445
Reflections collected	3226
Independent reflections (R_{int})	3226 (0.0000)
Observed reflections [I>2sigma(I)]	2668
R indices (all data)	R1 = 0.0470, wR1 = 0.0848
Final R indices [I>2sigma(I)]	R2 = 0.0342, wR2 = 0.0757
Goodness-of-fit on F^2	1.031
Largest diff. peak and hole ($eÅ^{-3}$)	0.261 and -0.175

Bond lengths (Å) and angles (°) for [Al(S^{t}Bu)$_3${NMe$_2$Et}]

A(l)-N(1)	2.038(2)	A(l)-S(2)	2.2356(8)
A(l)-S(3)	2.2337(8)	A(l)-S(1)	2.2366(8)
S(1)-C(6)	1.852(2)	S(3)-C(14)	1.858(2)
S(2)-C(10)	1.862(2)	N(1)-C(5)	1.482(3)
N(1)-C(4)	1.490(3)	C(2)-C(3)	1.517(4)
N(1)-C(2)	1.500(3)	C(6)-C(7)	1.515(4)
C(6)-C(9)	1.516(3)	C(10)-C(12)	1.518(3)
C(6)-C(8)	1.525(3)	C(10)-C(11)	1.520(3)
C(10)-C(13)	1.529(3)	C(14)-C(16)	1.521(4)
C(14)-C(15)	1.514(3)	C(14)-C(17)	1.535(3)
N(1)-A(l)-S(3)	101.16(6)	S(3)-Al-S(2)	115.68(3)
N(1)-A(l)-S(2)	104.00(6)	N(1)-Al-S(1)	99.83(6)
S(3)-Al-S(1)	116.21(3)	C(6)-S(1)-Al	112.65(7)
S(2)-Al-S(1)	116.17(4)	C(10)-S(2)-Al	112.91(7)
C(14)-S(3)-Al	112.46(8)	C(5)-N(1)-C(2)	110.7(2)
C(5)-N(1)-C(4)	108.3(2)	C(4)-N(1)-C(2)	110.1(2)
C(5)-N(1)-Al	109.29(14)	C(2)-N(1)-Al	109.55(14)
C(4)-N(1)-Al	108.84(15)	N(1)-C(2)-C(3)	116.4(2)
C(7)-C(6)-C(9)	110.0(2)	C(9)-C(6)-C(8)	109.8(2)
C(7)-C(6)-C(8)	110.8(2)	C(7)-C(6)-S(1)	108.4(2)
C(9)-C(6)-S(1)	112.5(2)	C(12)-C(10)-C(11)	110.5(2)
C(8)-C(6)-S(1)	105.3(2)	C(12)-C(10)-C(13)	109.3(2)
C(11)-C(10)-C(13)	109.2(2)	C(11)-C(10)-S(2)	111.7(2)
C(12)-C(10)-S(2)	110.9(2)	C(13)-C(10)-S(2)	105.1(2)
C(15)-C(14)-C(16)	111.2(2)	C(16)-C(14)-C(17)	109.4(2)
C(15)-C(14)-C(17)	109.9(2)	C(15)-C(14)-S(3)	110.7(2)
C(16)-C(14)-S(3)	110.8(2)	C(17)-C(14)-S(3)	104.6(2)

Crystal data for $[Al(SC_6H_3Me_2\text{-}2,6)_3(OEt_2)]$

Empirical formula	$C_{28}H_{37}OS_3Al.Et_2O$
Formula weight	586.86
Crystal colour/morphology	Clear prisms
Crystal size (mm)	0.83 x 0.83 x 0.37
a (Å)	15.946(3)
b (Å)	14.182(2)
c (Å)	14.984(4)
α (°)	90
β (°)	104.128(14)
γ (°)	90
V ($Å^3$)	3286.1(11)
Z	4
Crystal system	Monoclinic
Space group	P21/c
Wavelength (Å)	0.71073
Density (calculated) (Mg/m^3)	1.186
Absorption coefficient (mm^{-1})	0.278
Reflections collected	4218
Independent reflections (R_{int})	6021
Observed reflections [I>2sigma(I)]	5780 (0.0197)
R indices (all data)	R1 = 0.0481, wR2 = 0.1050
Final R indices [I>2sigma(I)]	R1 = 0.0775, wR2 = 0.1216
Goodness-of-fit on F^2	1.044
Largest diff. peak and hole ($eÅ^{-3}$)	0.334 and -0.293

Bond lengths (Å) and angles (°) for $[Al(SC_6H_3Me_2\text{-}2,6)_3(OEt_2)]$

Al-O	1.907(2)	Al-S(3)	2.2336(11)
Al-S(1)	2.2266(11)	Al-S(2)	2.2384(11)
S(1)-C(11)	1.794(3)	S(3)-C(31)	1.796(3)
S(2)-C(21)	1.797(3)	O-C(3)	1.476(4)
O-C(1)	1.479(3)	C(3)-C(4)	1.505(5)
C(1)-C(2)	1.505(4)	C(11)-C(12)	1.407(4)
C(11)-C(16)	1.409(4)	C(12)-C(17)	1.506(4)
C(12)-C(13)	1.392(4)	C(13)-C(14)	1.382(5)
C(14)-C(15)	1.380(5)	C(16)-C(18)	1.507(5)
C(15)-C(16)	1.388(5)	C(21)-C(26)	1.405(4)
C(21)-C(22)	1.407(4)	C(22)-C(27)	1.505(4)
C(22)-C(23)	1.396(4)	C(23)-C(24)	1.379(5)
C(24)-C(25)	1.374(5)	C(26)-C(28)	1.507(4)
C(25)-C(26)	1.397(5)	C(31)-C(32)	1.403(4)
C(31)-C(36)	1.407(4)	C(32)-C(37)	1.503(4)
C(32)-C(33)	1.392(4)	C(33)-C(34)	1.379(5)
C(34)-C(35)	1.370(5)	C(36)-C(38)	1.502(5)
C(35)-C(36)	1.399(4)	O(40)-C(43)	1.340(6)
O(40)-C(41)	1.413(7)	C(43)-C(44)	1.395(9)
C(41)-C(42)	1.394(9)		
O-Al-S(1)	104.03(7)	S(1)-Al-S(3)	112.73(4)
O-Al-S(3)	102.01(7)	O-Al-S(2)	97.34(7)
S(1)-Al-S(2)	120.81(5)	C(11)-S(1)-Al	106.12(9)
S(3)-Al-S(2)	115.61(4)	C(21)-S(2)-Al	107.03(9)
C(31)-S(3)-Al	107.98(9)	C(3)-O-Al	117.8(2)
C(3)-O-C(1)	113.6(2)	C(1)-O-Al	126.1(2)
O-C(1)-C(2)	111.9(2)	C(12)-C(11)-C(16)	120.7(3)
O-C(3)-C(4)	111.4(3)	C(12)-C(11)-S(1)	120.7(2)
C(16)-C(11)-S(1)	118.5(2)	C(13)-C(12)-C(17)	119.5(3)
C(13)-C(12)-C(11)	118.4(3)	C(11)-C(12)-C(17)	122.1(3)

Bond lengths (Å) and angles (°) for $[Al(SC_6H_3Me_2\text{-}2,6)_3(OEt_2)]$ continued

C(14)-C(13)-C(12)	121.3(3)	C(14)-C(15)-C(16)	121.6(3)
C(15)-C(14)-C(13)	119.5(3)	C(15)-C(16)-C(11)	118.3(3)
C(15)-C(16)-C(18)	119.9(3)	C(26)-C(21)-C(22)	120.7(3)
C(11)-C(16)-C(18)	121.8(3)	C(26)-C(21)-S(2)	120.3(2)
C(22)-C(21)-S(2)	118.9(2)	C(23)-C(22)-C(27)	119.4(3)
C(23)-C(22)-C(21)	118.4(3)	C(21)-C(22)-C(27)	122.1(3)
C(24)-C(23)-C(22)	121.1(3)	C(24)-C(25)-C(26)	121.2(3)
C(25)-C(24)-C(23)	120.1(3)	C(25)-C(26)-C(21)	118.4(3)
C(25)-C(26)-C(28)	119.4(3)	C(32)-C(31)-C(36)	120.4(3)
C(21)-C(26)-C(28)	122.2(3)	C(32)-C(31)-S(3)	120.7(2)
C(36)-C(31)-S(3)	118.7(2)	C(33)-C(32)-C(37)	119.4(3)
C(33)-C(32)-C(31)	119.0(3)	C(31)-C(32)-C(37)	121.6(3)
C(34)-C(33)-C(32)	121.0(3)	C(34)-C(35)-C(36)	121.8(3)
C(35)-C(34)-C(33)	119.7(3)	C(35)-C(36)-C(31)	118.0(3)
C(35)-C(36)-C(38)	119.9(3)	C(43)-O(40)-C(41)	112.0(5)
C(31)-C(36)-C(38)	122.0(3)	C(42)-C(41)-O(40)	109.6(5)
O(40)-C(43)-C(44)	113.4(6)		

Crystal data for $[Li(OEt_2)_3][Al(SC_6H_3Me_2\text{-}2,6)_4]$

Empirical formula	$C_{48}H_{76}LiO_4S_4Al$
Formula weight	879.25
Crystal colour/morphology	Colourless tetrahedra
Crystal size (mm)	0.67 x 0.67 x 0.67
a (Å)	12.1858(6)
b (Å)	12.1858(6)
c (Å)	17.693(3)
α (°)	90.00
β (°)	90.00
γ (°)	90.00
V ($Å^3$)	2627.3(4)
Z	2
Crystal system	Tetragonal
Space group	I-4
Wavelength (Å)	1.54178
Density (calculated) (Mg/m^3)	1.111
Absorption coefficient (mm^{-1})	2.108
Reflections collected	1249
Independent reflections (R_{int})	1242 (0.0405)
Observed reflections [I>2sigma(I)]	1130
R indices (all data)	R1 = 0.0480, wR1 = 0.1210
Final R indices [I>2sigma(I)]	R2 = 0.0417, wR2 = 0.1138
Goodness-of-fit on F^2	1.065
Largest diff. peak and hole ($eÅ^{-3}$)	0.211 and -0.154

Bond lengths (Å) and angles (°) for $[Li(OEt_2)_3][Al(SC_6H_3Me_2\text{-}2,6)_4]$

Al-S	2.2534(9)	Al-S(0A)	2.2534(9)
Al-S(0B)	2.2534(9)	Al-S(0C)	2.2534(9)
S-C(1)	1.784(4)	C(1)-C(2)	1.402(6)
C(1)-C(6)	1.394(6)	C(2)-C(3)	1.391(8)
C(2)-C(7)	1.510(8)	C(4)-C(5)	1.345(9)
C(3)-C(4)	1.381(10)	C(5)-C(6)	1.399(6)
C(6)-C(8)	1.498(8)	Li-O(10)	1.921(7)
Li-O(10')	1.841(12)	O(10)-C(11)	1.451(14)
O(10)-C(13)	1.452(13)	C(13)-C(14)	1.50(2)
C(11)-C(12)	1.52(2)	O(10')-C(11')	1.47(2)
O(10')-C(13')	1.47(2)	C(13')-C(14')	1.49(2)
C(11')-C(12')	1.50(2)	O(20)-C(21)	1.42(2)
O(20)-C(23)	1.45(2)	C(23)-C(24)	1.49(2)
C(21)-C(22)	1.49(2)		
S-Al-S(0A)	119.16(6)	S-Al-S(0B)	104.85(3)
S(0A)-Al-S(0B)	104.85(3)	S(0A)-Al-S(0C)	104.85(3)
S-Al-S(0C)	104.85(3)	C(1)-S-Al	107.42(12)
S(0B)-Al-S(0C)	119.16(6)	C(6)-C(1)-C(2)	119.4(4)
C(6)-C(1)-S	122.1(3)	C(3)-C(2)-C(1)	118.5(5)
C(2)-C(1)-S	118.4(3)	C(3)-C(2)-C(7)	120.1(5)
C(1)-C(2)-C(7)	121.4(5)	C(5)-C(4)-C(3)	119.4(5)
C(4)-C(3)-C(2)	121.7(6)	C(4)-C(5)-C(6)	121.4(6)
C(1)-C(6)-C(5)	119.6(5)	C(5)-C(6)-C(8)	119.4(5)
C(1)-C(6)-C(8)	121.0(4)	O(10')-Li-O(10')	91.2(2)
O(10')-Li-O(10')	163.0(11)	O(10)-Li-O(10)	113.2(2)
O(10)-Li-O(10)	102.3(4)	C(11)-O(10)-C(13)	108.2(11)
C(11)-O(10)-Li	127.9(8)	O(10)-C(11)-C(12)	107.5(12)
C(13)-O(10)-Li	123.6(7)	O(10)-C(13)-C(14)	107.4(11)
C(11')-O(10')-C(13')	105.0(15)	C(13')-O(10')-Li	126.7(12)
C(11')-O(10')-Li	128.0(12)	O(10')-C(11')-C(12')	108.1(17)

Bond lengths (Å) and angles (°) for $[Li(OEt_2)_3][Al(SC_6H_3Me_2\text{-}2,6)_4]$ continued

O(10')-C(13')-C(14')	108.2(17)	O(20)-C(21)-C(22)	108.8(18)
C(21)-O(20)-C(23)	111.0(22)	O(20)-C(23)-C(24)	107.4(23)

Crystal data for $[Al(SC_6H_3Me_2\text{-}2,6)_3(HSC_6H_3Me_2\text{-}2,6)]$

Empirical formula	$C_{36}H_{48}NS_4Al$
Formula weight	649.97
Crystal colour/morphology	Colourless blocks
Crystal size (mm)	0.67 x 0.53 x 0.50
a (Å)	11.034(7)
b (Å)	11.485(2)
c (Å)	16.618(2)
α (°)	81.646(12)
β (°)	74.18(2)
γ (°)	62.924(11)
V ($Å^3$)	1803.5(12)
Z	2
Crystal system	Triclinic
Space group	P-1
Wavelength (Å)	1.54178
Density (calculated) (Mg/m^3)	1.197
Absorption coefficient (mm^{-1})	2.832
Reflections collected	5402
Independent reflections (R_{int})	5091 (0.0864)
Observed reflections [I>2sigma(I)]	3658
R indices (all data)	R1 = 0.1233, wR1 = 0.2881
Final R indices [I>2sigma(I)]	R2 = 0.0856, wR2 = 0.2316
Goodness-of-fit on F^2	1.057
Largest diff. peak and hole ($eÅ^{-3}$)	0.720 and -0.698

Bond lengths (Å) and angles (°) for $[Al(SC_6H_3Me_2\text{-}2,6)_3(HSC_6H_3Me_2\text{-}2,6)]$

Al-S(4)	2.250(2)	Al-S(3)	2.254(3)
Al-S(1)	2.250(2)	Al-S(2)	2.275(2)
S(1)-C(11)	1.771(6)	S(3)-C(31)	1.792(6)
S(2)-C(21)	1.790(6)	S(4)-C(41)	1.794(7)
C(11 C16	1.410(9)	C(12)-C(13)	1.374(9)
C11)-C(12)	1.413(9)	C(12)-C(17)	1.498(10)
C(13)-C(14)	1.389(11)	C(15)-C(16)	1.368(10)
C(14)-C(15)	1.371(11)	C(16)-C(18)	1.514(10)
C(21)-C(26)	1.390(8)	C(22)-C(23)	1.395(10)
C(21)-C(22)	1.417(10)	C(22)-C(27)	1.490(10)
C(23)-C(24)	1.371(12)	C(25)-C(26)	1.396(8)
C(24)-C(25)	1.372(12)	C(26)-C(28)	1.496(10)
C(31)-C(36)	1.386(8)	C(32)-C(33)	1.398(11)
C(31)-C(32)	1.424(9)	C(32)-C(37)	1.493(10)
C(33)-C(34)	1.382(14)	C(35)-C(36)	1.383(11)
C(34)-C(35)	1.375(13)	C(36)-C(38)	1.500(11)
C(41)-C(46)	1.384(10)	C(42)-C(43)	1.411(10)
C(41)-C(42)	1.419(9)	C(42)-C(47)	1.504(10)
C(43)-C(44)	1.348(12)	C(45)-C(46)	1.394(10)
C(44)-C(45)	1.378(11)	C(46)-C(48)	1.491(10)
N(50)-C(51)	1.458(11)	N(50)-C(54)	1.559(12)
N(50)-C(53)	1.468(10)	C(51)-C(52)	1.543(15)
S(4)-Al-S(1)	108.28(9)	S(1)-Al-S(3)	119.45(10)
S(4)-Al-S(3)	103.79(9)	S(4)-Al-S(2)	116.49(9)
S(1)-Al-S(2)	104.65(8)	C(11)-S(1)-Al	102.5(2)
S(3)-Al-S(2)	104.78(9)	C(21)-S(2)-Al	103.7(2)
C(31)-S(3)-Al	101.9(2)	C(16)-C(11)-C(12)	118.9(6)
C(41)-S(4)-Al	107.0(2)	C(16)-C(11)-S(1)	121.1(5)
C(12)-C(11)-S(1)	119.9(5)	C(13)-C(12)-C(17)	120.5(7)
C(13)-C(12)-C(11)	119.6(7)	C(11)-C(12)-C(17)	119.9(6)

Bond lengths (Å) and angles (°) for $[Al(SC_6H_3Me_2\text{-}2,6)_3(HSC_6H_3Me_2\text{-}2,6)]$ continued

C(12)-C(13)-C(14)	120.7(7)	C(16)-C(15)-C(14)	121.4(7)
C(15)-C(14)-C(13)	119.7(7)	C(15)-C(16)-C(11)	119.6(7)
C(15)-C(16)-C(18)	120.7(7)	C(26)-C(21)-C(22)	119.6(6)
C(11)-C(16)-C(18)	119.7(6)	C(26)-C(21)-S(2)	120.9(5)
C(22)-C(21)-S(2)	119.5(5)	C(23)-C(22)-C(27)	119.6(7)
C(23)-C(22)-C(21)	118.4(7)	C(21)-C(22)-C(27)	122.0(6)
C(24)-C(23)-C(22)	121.3(8)	C(24)-C(25)-C(26)	120.1(7)
C(23)-C(24)-C(25)	120.5(6)	C(21)-C(26)-C(25)	120.1(7)
C(21)-C(26)-C(28)	121.8(5)	C(36)-C(31)-C(32)	121.7(6)
C(25)-C(26)-C(28)	118.1(6)	C(36)-C(31)-S(3)	120.3(5)
C(32)-C(31)-S(3)	118.0(5)	C(33)-C(32)-C(37)	120.4(7)
C(33)-C(32)-C(31)	117.1(7)	C(31)-C(32)-C(37)	122.5(7)
C(34)-C(33)-C(32)	121.2(8)	C(34)-C(35)-C(36)	121.7(8)
C(35)-C(34)-C(33)	119.8(8)	C(35)-C(36)-C(31)	118.3(7)
C(35)-C(36)-C(38)	119.5(7)	C(46)-C(41)-C(42)	122.0(6)
C(31)-C(36)-C(38)	122.1(6)	C(46)-C(41)-S(4)	120.3(5)
C(42)-C(41)-S(4)	117.7(5)	C(43)-C(42)-C(47)	121.0(7)
C(43)-C(42)-C(41)	115.7(7)	C(41)-C(42)-C(47)	123.3(6)
C(44)-C(43)-C(42)	123.6(7)	C(44)-C(45)-C(46)	122.0(8)
C(43)-C(44)-C(45)	118.7(7)	C(41)-C(46)-C(45)	118.0(7)
C(41)-C(46)-C(48)	121.8(7)	C(51)-N(50)-C(53)	116.1(7)
C(45)-C(46)-C(48)	120.0(7)	C(51)-N(50)-C(54)	106.3(7)
C(53)-N(50)-C(54)	106.4(8)	N(50)-C(51)-C(52)	105.6(9)